

**Critical factors that impact the mechanical properties of robot  
assisted 3D-printed cement based structures**

By

Oluwatimilehin Abdulwahab Disu

BEng (Hons) Mechanical Engineering

School of Physics, Engineering and Computer Science

Submitted

**The University of Hertfordshire in partial fulfilment of the  
requirements of the degree of Doctor of Philosophy**

England, United Kingdom

November 2024

Page Intentionally Left Blank

## **Author's Declaration**

I declare that the work in this dissertation was carried out in accordance with the requirements of the University's Regulations and Code of Practice for Research Degree Programmes and that it has not been submitted for any other academic award. Except where indicated by the specific reference in the text, the work is the candidate's work. Any views expressed in the dissertation are those of the author.

Signed: Oluwatimilehin Disu

Date: 08 November 2024

## **Dedication**

This thesis is solely dedicated to God Almighty and my Parents, Cp Olatunji Disu and Olufunmilola Disu. Your unwavering support, sacrifice, and endless encouragement have been the cornerstone of my achievements. Your belief in me gave me the strength to carry on through the most challenging moments.

To the person I was when I started this journey and to the person I have become through it, resilient and determined. May this work serve as a reminder of how far one can go with consistency, resilience and passion.

Finally, to my brother, Adams Kaka, whose loss I still carry with me, your memory is woven into every step of this journey. Your absence has been deeply felt, but your spirit fuelled my strength in ways I can't fully explain. This work carries your name in every line, and I hope it makes you proud.

## Acknowledgements

As I look back at the year 2020, a year marked by global turmoil and uncertainty. I realise it was also the year I made one of the most important decisions of my life: beginning my PhD journey. In hindsight, I wouldn't change a thing, except perhaps to give even more of myself to this path.

With that, I would like to express my deepest gratitude to **God Almighty** for granting me the strength, perseverance, and guidance to complete this PhD journey. Without His grace, none of this would have been possible.

I extend my heartfelt thanks to my supervisory team: Dr. Sikiru Ismail, Professor Andreas Chrysanthou, Dr. Luke Wood, and Dr. Anthonios Kanellopoulos, for their unwavering patience and guidance throughout my research journey.

To **Dr. Sikiru Ismail**, words cannot adequately express my gratitude for your tireless support and invaluable mentorship. Your wisdom, dedication, and belief in me, even during the most challenging phases, have been a constant source of motivation. You always found time to offer your insights, and your attention to detail has greatly shaped the quality of my work. I am deeply indebted to you not only for your professional guidance but also for the kindness and encouragement that extended far beyond the academic realm. Working with you has been both a privilege and a profound learning experience.

To my office mates at the University of Hertfordshire, Aaqib, Harris, Hemant, David, Reza, Moez, Andrew, Mike, and Ronnie: Thank you for all the lovely memories we created over the last few years. I have grown to enjoy your company and will miss you all dearly. Especially the part where we all pretend to get work done in the office, chat for the next hour, and later realise it's better to work from home (Ha ha). We've had a lot of fun together and there are many moments I will keep close to my heart. Without you, my research journey would not have been what it has been. (I promise I didn't forget you if I didn't mention your name).

I would also like to acknowledge the tremendous support of the lab technicians, Lewis Batt, Emine Dinc, and Vienna Unamba. Your expertise and constant support led to the success of my research. Thanks for always remembering to put the sand in the oven; I promise I do not take that for granted.

To Alex Kingstrom, who served as a lab technician and provided essential support in the early stages of my research, thank you for laying a solid foundation for this work and for all the effort you put into ensuring a smooth start to my experiments. Your contributions were instrumental, and I am grateful for your dedication. Finally, to the proctors, thank you for making the experimental process a seamless one. You guys are the real ones.

To Mike Watkins and Martin Thomas, words truly fail me. Your commitment to manufacturing the essential parts needed for my experiments, along with your unwavering supports and tireless assistance, was a cornerstone of my work. Without your craftsmanship, patience, and dedication, this research would not have reached its potential. Thank you for your constant encouragement and for going above and beyond at every step.

*"It is amazing what you can accomplish if you do not care who gets the credit."*

*Harry S. Truman*

Oluwagbotemi Akinsoji, my amazing, intelligent, and supportive girlfriend. Without you, none of these documents would be written because I was mentally checked out of this degree. We've had such an amazing time in this chapter of our lives, including the privilege of having front-row seats to each other's research journeys. It's been incredibly exciting and rich with memories I'm sure we will both cherish for years to come. Oluwagbotemi, as you complete your own PhD program, my goal is to be as much of a rock for you as you have always been for me. I love you dearly.

Special shout-out to my grandparents, Alhaji Taoreed Alade Disu and Princess Sidikat Ayodele Disu. Mr and Mrs Disu, Mrs Temilolu Soares, Mrs Olufunmilayo Ajayi and Ms Bola Ayanwale. And most of all, I am thankful to the people without whom I would never be where I am today. My parents Mr and Mrs Olatunji. Disu. To my dad, CP Olatunji Disu, your enthusiasm about my work kept me going on the days I almost gave up. Thank you for all the Instagram videos related to my work and for constantly asking me, "How far? Kilo tun ku bayi?" To my mom, your endless prayers and unwavering support have been my constant source of strength throughout this entire journey. Thank you for listening to me whenever I felt down and for all the "Pele Pele." This success is as much yours as it is mine.

My siblings, Fikeyinmi (Mama) and Rahman Disu (Jago), I cannot thank you guys enough. I appreciate your understanding throughout this journey. You have all been there for me, reminding me that there's always light at the end of the tunnel. I am deeply grateful to have

you in my corner. To Yemi Ogundeyi, you met me halfway but still managed to make a huge impact. And to Adams.K and Dapo, thank you for being there every step of the way.

I did not complete this quest alone. It was a journey shared with my inner circle, whose time, energy, love, trust, understanding, and support helped me survive, thrive, and ultimately finish this phase of my life. To my friends-turned-family, Ayomide Sodja, Mubarak, Sadiq, Nabeel, Ayo, Shadow, Shope, Toyosi, Musa, George, Fortunate, Emeka, and Femi, Nelson. I finally made it! Thank you for being my support system through all the highs and lows. Your friendship, encouragement, and unwavering belief in me have meant the world, and I couldn't have asked for a better group of people to share this journey with. With age comes the realisation that nothing compares in importance to the people we have in our lives.

Most importantly, to quote the great Snoop Dogg:

*I WANT TO THANK ME FOR BELIEVING IN ME*

*I WANT TO THANK ME FOR DOING ALL THIS HARDWORK*

*I WANT TO THANK ME FOR HAVING NO DAYS OFF*

*I WANT TO THANK ME FOR NEVER QUITTING*

*"Success is not final, failure is not fatal: It is the courage to continue that counts"*

*Winston Churchill.*

## Abstract

This research was motivated by pressing challenges in the construction industry. These challenges include, but are not limited to, high-cost of materials, labour shortages, safety risks and environmental impact. Despite the significant contribution of the building and construction sector to the global economy, the sector lags in technological adoption, leading to inefficiencies and waste. Robot-assisted 3D printing, particularly for cement-based structures, offers a transformative solution by automating production, reducing material waste and enabling complex designs. This approach eliminates the need for traditional formwork and minimises labour demands, aligning construction practices with sustainability goals through lower CO<sub>2</sub> emissions. This PhD research, therefore, aimed to investigate the critical factors in cement-based Additive Manufacturing (AM) processes that impact the mechanical properties of 3D-printed cement-based structures.

Given these benefits, the study investigated the critical factors in cement-based additive manufacturing processes that impact the mechanical properties of 3D-printed cement-based structures. Through an experimental approach, the research examined layer bonding, print speed, layer height and material composition, focusing on optimising the process parameters to enhance structural integrity. However, despite advancements in printable concrete technology, maintaining high-quality printing remained a challenge. Quality control was closely linked to both geometric and material aspects of the printer nozzle design, especially for small-scale printing applications suited to Small and Medium-sized Enterprises (SMEs). This research also explored the design and development of a robot nozzle system that was optimised for small-scale 3D printing of cement-based structures.

The nozzle design considered key factors, such as weight, nozzle diameter and shape, material compatibility, flow control, mixing mechanisms, temperature resistance, cost-effectiveness, adaptability, safety and ease of maintenance. Iterative designs were developed, focusing on stress concentration mitigation and material flow optimisation. These considerations informed the adoption of an on-demand accelerator spraying system, which overcame challenges associated with integrating mixing mechanisms directly into the nozzle. This method used a micro-peristaltic pump connected to an accelerator tank to spray the accelerator onto the surface of deposited material as the robot moved along its programmed path, thus enhancing layer stability and print quality.

The mechanical performance and microstructural characteristics of 3D-printed cement structures were also examined, focusing on compressive and flexural strengths alongside SEM analysis of interlayer bonding. Finite Element Analysis (FEA) revealed high-stress concentrations at edges under compression and at mid-span under flexural loads, correlating with observed crack patterns. SEM analysis highlighted the effects of aluminium sulphate on interlayer bond strength, with early ettringite formation improving initial adhesion but excessive sulphate leading to expansive crystal growth, reduced bond strength, and premature cracking over time.

From the experimental results, mechanical testing demonstrated that 3D-printed structures gained strength over time, with compressive strength increasing from 2 MPa on day 1 to 22 MPa on day 28, although this remained lower than the 39.4 MPa achieved by traditional monolithic structures. Early flexural strength in 3D-printed samples benefited from the use of aluminium sulphate additive that was introduced as an accelerator, reaching 0.25 MPa on day 28, nearly matching the 0.27 MPa of monolithic samples, though initial benefits diminished with curing. Split tensile testing showed that interlayer bond strength improved, with tensile strength increasing from 0.35 MPa on day 1 to 3.65 MPa on day 28. However, excessive aluminium sulphate was observed to reduce bond strength due to the formation of ettringite, highlighting the importance of controlled accelerator integration.

Importantly, the optimal printing parameters emerged as crucial to achieving buildable structures, with speeds up to 20 mm/s supporting up to 10 stable layers with a thickness of 40 mm. Higher speeds, such as 80 mm/s, reduced layer thickness to 13 mm, but compromised interlayer bonding, resulting in early structural collapse. An optimal layer height of 10 mm proved effective, enabling stability for up to 10 layers, whereas larger layer heights led to reduced adhesion. Aluminium sulphate significantly enhanced early setting and enabled up to 14 stable layers at a 45% concentration, although higher concentrations were detrimental to long-term tensile strength.

This research provides valuable insights into additive manufacturing in construction, showcasing that robotic 3D printing can produce sustainable, viable structures by optimising printing parameters, thereby addressing environmental and labour challenges. The study also highlights the role of aluminium sulphate in accelerating setting time and early strength development, though initial integration faced challenges. Early attempts with direct mixing led to some issues, including backpressure and mixing inefficiencies, which were later mitigated

by using a peristaltic pump and auger, though these modifications introduced new challenges, such as peristaltic pump nozzle blockages. This can be attributed to insufficient dissolution of powder solute/accelerator in the solvent/distilled water. Ultimately, surface spraying of the accelerator on each layer proved effective, significantly improving layer stability and surface finish.

**Keywords:** 3D printing, Cement-based structures, Additive manufacturing, Aluminium Sulphate, Buildability, Structural stability, Nozzle design, Mechanical Properties, Robot-assisted construction.

# TABLE OF CONTENTS

Author’s Declaration.....	iii
Dedication.....	iv
Acknowledgements.....	v
Abstract .....	viii
TABLE OF CONTENTS .....	xi
List of Figures .....	xviii
List of Tables .....	xxv
CHAPTER ONE .....	28
INTRODUCTION.....	28
1. Background .....	28
1.1. Motivation.....	29
1.1.1. Accidents and injuries.....	32
1.1.2. Work-related ill health.....	32
1.1.3. Fatal Injuries.....	32
1.1.4. Non-Fatal Injuries.....	33
1.1.5. Lung Disorders and Occupational Cancer .....	34
1.1.6. Economic Costs .....	34
1.1.7. Working Days Lost.....	34
1.2. Statement of Problems .....	35
1.3. Research questions.....	36
1.4. Research scope.....	37
1.4.1. Project Aim.....	37
1.4.2. Project Objectives .....	38
1.5. Relevance of 3D printing to the national economy and global relevance .....	38
1.6. Contribution to Knowledge (Research Novelty).....	39
1.7. Thesis Structure .....	42
1.8. Summary .....	43
Chapter 2: Literature Review .....	1
2. Introduction.....	1
2.1. Additive Manufacturing .....	1
2.1.1. 3D printing methods.....	4
2.1.2. Contour Crafting (CC).....	4
2.1.3. Fused Deposition Modelling .....	7

2.1.4.	Ink Jet Printing.....	8
2.1.5.	Stereolithography (SLA).....	9
2.1.6.	Powder Bed Fusion (PBF).....	10
2.1.7.	Directed Energy Deposition (DED) .....	11
2.1.8.	Laminated Object Manufacturing .....	12
2.2.	3D Printing Materials .....	17
2.2.1.	Overview of cement-based 3D printing Materials .....	17
2.2.2.	Cement-based materials.....	17
2.2.3.	Cement mix design.....	18
2.3.	Fresh properties of cement-based materials .....	26
2.3.1.	Flowability.....	26
2.3.2.	Extrudability .....	27
2.3.3.	Buildability .....	29
2.3.4.	Open time .....	31
2.4.	Hardened properties of 3D printed cementitious structures .....	31
2.4.1.	Compressive strength.....	32
2.4.2.	Flexural strength .....	35
2.4.3.	Tensile bond strength.....	37
2.5.	Shrinkage and Cracking.....	40
2.5.1.	Chemical shrinkage.....	40
2.5.2.	Plastic shrinkage.....	41
2.5.3.	Autogenous shrinkage .....	41
2.5.4.	Drying shrinkage.....	41
2.5.5.	Thermal shrinkage.....	42
2.5.6.	Carbonation shrinkage.....	42
2.6.	Advantages of 3D printing.....	43
2.6.1.	Structural Complexibility .....	45
2.6.2.	Sustainability.....	46
2.7.	Limitations of 3D printing of cement-based materials in construction .....	47
2.8.	Application of robots for 3D printing of cement-based materials .....	48
2.8.1.	Historical development of robots .....	50
2.9.	Robotic 3D printing systems.....	55
2.9.1.	Gantry .....	57
2.9.1.1	Mini-builders.....	58
2.9.1.2	Cable suspended platforms .....	59

2.10.	Printing parameter using material extrusion and a robotic arm.....	60
2.10.1.	3D printing orientation .....	60
2.10.2.	Thickness of deposited layers .....	60
2.10.3.	Air gap.....	60
2.10.4.	Raster angle/width .....	61
2.10.5.	Nozzle design .....	62
2.10.6.	Flow rate .....	63
2.11.	Effect of nozzle parameters on fresh and hardened properties of cement-based materials	63
2.11.1.	Extrudability .....	64
2.11.2.	Flowability.....	64
2.11.3.	Buildability .....	65
2.11.4.	Shape stability .....	65
2.11.5.	Interlayer bonding.....	66
2.11.6.	Nozzle speed .....	67
2.12.	Summary .....	68
Chapter 3: Materials and Methods .....		70
3.	Introduction.....	70
3.1.	Materials .....	70
3.1.1.	Raw material .....	70
3.1.2.	Chemical accelerator .....	71
3.1.3.	Mixture design and preparation methods.....	71
3.2.	Material preparation and printing procedure.....	72
3.2.1.	Accelerator.....	72
3.2.2.	Dry/raw material .....	73
3.3.	Development and optimisation of set-up .....	74
3.3.1.	Steel table (Stage 1).....	74
3.3.2.	Marine plywood (Stage 2).....	75
3.3.3.	Polycarbonate sheet and Polyvinyl Chloride (PVC) (Stage 3).....	76
3.3.4.	Aluminium angle and steel (Stage 4).....	76
3.3.5.	Micro switches (Stage 5).....	77
3.3.6.	Emergency stop (Stage 6) .....	78
3.3.7.	Electrical wiring and trunking (Stage 7).....	79
3.3.8.	Gantry system (Stage 8).....	79
3.4.	3D printing robot configuration .....	80
3.4.1.	Robot controller technical specifications .....	85

3.4.2.	Robot software.....	86
3.4.3.	Programming .....	87
3.4.4.	3D Viewer .....	89
3.4.5.	Software maintenance function.....	89
3.5.	Design and development of small-scale robot extrusion nozzle.....	89
3.6.	Design requirement.....	89
3.6.1.	Design process .....	91
3.6.2.	Nozzle design 1.....	92
3.6.3.	Nozzle design 2.....	94
3.6.4.	Nozzle design 3.....	96
3.6.5.	Nozzle design 4.....	96
3.7.	3D printing process.....	98
3.7.1.	Cement mixer.....	98
3.7.2.	Cement mixer technical specifications .....	99
3.7.3.	Transformer .....	99
3.7.4.	Mortar pump.....	100
3.7.5.	Mortar pump technical specification .....	102
3.7.6.	Material-conveying pipe.....	102
3.7.7.	Pressure gauge .....	103
3.7.8.	Pinch valve .....	103
3.7.9.	Solenoid valve .....	104
3.7.10.	Air compressor .....	105
3.7.11.	Air compressor technical specifications .....	106
3.8.	Optimised 3D printing process.....	106
3.9.	Experimental parameters .....	109
3.9.1.	Printing speeds.....	109
3.9.2.	Layer height .....	110
3.9.3.	Pump pressure .....	110
3.9.4.	Accelerator dosage.....	111
3.10.	Casting procedure.....	111
3.11.	Evaluation methods.....	113
3.11.1.	Flowability test.....	113
3.11.2.	Extrudability test .....	114
3.11.3.	Buildability test .....	115
3.12.	Mechanical testing.....	116
3.12.1.	Penetration resistance test.....	118

3.12.2.	Scanning Electron Microscopy (SEM) .....	119
3.13.	Finite Element Analysis .....	121
3.13.1.	Material properties .....	121
3.14.	Compressive test model description .....	122
3.14.1.	Contact Conditions .....	123
3.14.2.	Mesh Configuration.....	123
3.14.3.	Boundary Conditions and Loading .....	124
3.15.	Flexural test model description.....	124
3.15.1.	Geometry and Loading Assembly.....	124
3.15.2.	Material Properties .....	125
3.15.3.	Mesh configuration .....	125
3.15.4.	Solver and Boundary Conditions .....	126
3.16.	Summary .....	127
Chapter 4: Results .....		129
4.	Introduction.....	129
4.1.	Flowability .....	129
4.2.	Penetration resistance .....	130
4.3.	Preliminary printing .....	132
4.3.1.	Performance analysis of preliminary cement mixes .....	139
4.4.	Preliminary robot 3D printing .....	140
4.5.	Nozzle Optimisation.....	141
4.6.	Process optimisation.....	149
4.6.1.	Processes parameter .....	162
4.7.	Effect of printing speed on buildability of 3D-printed small-scale structures.....	164
4.8.	Effect of layer height on 3D-printed small-scale structures.....	170
4.9.	Effect of aluminium sulphate on buildability of 3D-printed structures.....	174
4.9.1.	Structural failure .....	179
4.10.	Mechanical properties of 3D-printed structures.....	181
4.11.	Compressive strength .....	181
4.11.1.	Analysis of 3D-Printed Structures .....	181
4.11.2.	Analysis of monolithic structures .....	183
4.11.3.	Comparative Analysis .....	184
4.11.4.	Failure mode analysis .....	184
4.11.5.	Finite Element Analysis.....	186
4.11.6.	Analysis of 3D-Printed Structures .....	188
4.11.7.	Analysis of Monolithic Structures .....	190

4.11.8.	Comparative Analysis .....	191
4.11.9.	Fracture mode of concrete .....	191
4.11.10.	Finite Element Analysis.....	193
4.11.11.	Failure mode analysis.....	194
4.11.12.	Effect of layer-by-layer deposition.....	196
4.12.	Split tensile test .....	197
4.12.1.	Analysis of Split Tensile Strength Results for CTRL_ST00 .....	198
4.12.2.	Comparative analysis of control sample <i>versus</i> accelerated samples.....	199
4.12.3.	Effect of aluminium sulphate on the interlayer bond strength .....	202
4.12.4.	Reaction between water and cement .....	206
4.12.5.	Reaction between aluminium sulphate and cement .....	207
4.13.	Summary .....	211
CHAPTER FIVE.....		214
Conclusions .....		214
5.	Introduction.....	214
5.1.	Process optimisation.....	214
5.2.	Effect of printing speed on buildability of 3D-printed small-scale structures.....	215
5.3.	Effect of layer height on 3D-printed small-scale structures.....	216
5.4.	Effect of aluminium sulphate on buildability of 3D-printed structures .....	217
5.5.	Mechanical properties of 3D-printed structures.....	218
5.5.1.	Compressive strength.....	218
5.5.2.	Flexural strength .....	218
5.5.3.	Split tensile test.....	219
5.6.	RECOMMENDATIONS FOR FUTURE WORKS .....	221
References .....		223
APPENDICES .....		245
APPENDICES A.....		245
A1.	Robot mass capacity .....	245
A2.	Technical instruction for wiring the external emergency stop connection .....	246
A3.	Cost analysis of materials.....	247
APPENDIX B.....		248
B1.	Mitsubishi electric certifications.....	248
APPENDIX C.....		251
Standard Operating Procedure .....		251
Robot System .....		251
C1.	Safe Start Procedure .....	251

C2. Safe Working Procedure .....	252
C3. Safe Stopping Procedure.....	252
C4. Accident / injury response .....	252
C5. Equipment Malfunction .....	253
APPENDIX C2.....	254
Standard Operating Procedure .....	254
3D Printed Cement Robotic Arm Rig .....	254
C2.1 Initial steps .....	254
<b>C2.2. Checklist:</b> .....	254
<b>C2.2.1 Cement Pump</b> .....	254
<b>C2.2.2 Robotic arm</b> .....	255
C2.3 Standard Operating Procedure.....	255
APPENDIX D.....	258
Risk assessment.....	258

## List of Figures

Figure 1.1. Conventional construction vs 3D printing construction process [9].....	30
Figure 1.2. (a) Percentage of fatal injuries by accident kind in construction, (b) Percentage of non-fatal injuries by accident kind in construction [28] .....	33
Figure 2.1 Overall printing process of material [15] .....	3
Figure 2.2 Building construction using a gantry robot system and CC technique [61].....	5
Figure 2.3. Trowel mechanism to shape different geometry [43] .....	6
Figure 2.4. 3D printed projects based on the extrusion-based 3D printing technique. <b>(a)</b> House Zero in USA, <b>(b)</b> Humanity Central in USA, <b>(c)</b> Hobrobero House in Denmark (2021), <b>(d)</b> Serendix in Japan, <b>(e)</b> Beckum House in Germany, and <b>(f)</b> Milestone House in the Netherlands [70].....	7
Figure 2.5. Schematic diagram of Fused Deposition Modelling (FDM) [44].....	8
Figure 2.6. Schematic diagram of IJP technology and 3D printed parts with IJP technology [44].....	9
Figure 2.7. schematic diagram of SLA technology and 3D printed systems using SLA technology [44].....	10
Figure 2.8.schematic diagram of SLS technology and 3D printed systems using SLS technology [44].....	11
Figure 2.9. 3D-printed parts with DED [44] .....	12
Figure 2.10. Schematic illustration of vertical and horizontal deformation of deposited filaments through a circular nozzle, showing (a) theoretical and (b) practical geometry [114] .....	29
Figure 2.11. Buildability test: (a) stacking plate test, (b) printing on layers method and(c) cylinder stability test [106].....	30
Figure 2.12. linear voids between filaments (namely inter-filament voids) in (a) transverse and (b) side view [114].....	32
Figure 2.13. Testing in different directions for comprehensive strength: (a) perpendicular, (b) longitudinal and (c) lateral to the layer orientation. The dashed lines represent the printing path, and the x and z axes are parallel to dashed lines and the gravitational direction respectively. The printed layers locate in the x-y plane [114].....	34
Figure 2.14. Different testing directions for flexural strength of printed prism specimen: (a) & (b) perpendicular, (c) & (d) longitudinal and (e) & (f) lateral to the layer orientation [114] .	36

Figure 2.15. Schematic representation of fibre alignment inside the printing nozzle during the 3D printing process [114].....	37
Figure 2.16. Testing set-up for measurement of inter-layer bonding strength [29].....	38
Figure 2.17. Schematic illustration of the mechanism of interlayer bonding [114] .....	39
Figure 2.18. Scanning electron microscopy (SEM) images depicting: (a) cold joints along filaments, (b) development of cavities between filaments and (c) silt-like separation filled by calcite and ettringite [201].....	40
Figure 2.19. (a) XtreeE pillar built in Aix-en-provence, France and (b) section of the pillar [209] .....	43
Figure 2.20. (a) Schematic of the nozzle with the cable extruder system (b) Top view of cable extruder [212].....	44
Figure 2.21. Mesh mould reinforcement approach [211].....	45
Figure 2.22. 3D printed concrete columns mimicking the anatomy of a bone by Siam Cement Group (SCG)(left) and the inner bone structure (right) [106] .....	46
Figure 2.23. (a) Completion time and (b) Construction cost of a 3D printed wall [36] .....	47
Figure 2.24. Industrial robots: (A) welding robots, (B) assembly robots, (C) pick and place robots and (D) 3D printing robots (IFR 2019) .....	50
Figure 2.25. Evolution of robots .....	51
Figure 2.26. Evolution of robots .....	54
Figure 2.27. The Tangential Continuity Method (TCM) [115] .....	56
Figure 2.28. Gantry system [244] .....	57
Figure 2.29. Mini builder grip robots [64] .....	58
Figure 2.30. WASP-Big Delta project. Full size 12m building built from clay and mud [64] .....	59
Figure 2.31. The effect of air gap on the surface quality of parts [247] .....	61
Figure 2.32. Overall material extrusion printing parameter [247].....	62
Figure 2.33. Models for nozzle outlet shapes [248].....	62
Figure 3.1. Table used to support the setup.....	74
Figure 3.2. Marine plywood used to provide the total working area for robot system.....	76
Figure 3.3. Aluminium angle to reinforce the corners of the polycarbonate sheets .....	77
Figure 3.4. Micro switches, activator, and electrical trunk .....	78
Figure 3.5. Schneider Electric emergency stop button .....	78
Figure 3.6. Gantry system to reduce the weight on the robot arm.....	80
Figure 3.7. Names of each part of the robot [268].....	81
Figure 3.8. Robot controller design and specifications [268].....	82

Figure 3.9. a) Stainless material used on the tip of the robot, b) Chemical resistant coating to chassis, c) Special hexagon flange bolt [268].....	83
Figure 3.10. Robot controller and teaching pendant.....	85
Figure 3.11. RT Toolbox 3 Operation screen [268].....	86
Figure 3.12. Robot programming and operation panel .....	88
Figure 3.13. 3d printing path .....	88
Figure 3.14. Process of 3D printing robot nozzle .....	91
Figure 3.15. Nozzle design 1 .....	92
Figure 3.16. Comparison between filleted corner stress and sharp corner [269] .....	93
Figure 3.17. (a) Material flow view of second nozzle prototype showing the point of high stress concentration and (b) 3D-printed prototype of the nozzle.....	95
Figure 3.18. Nozzle design 3 .....	96
Figure 3.19. (a) CAD view showing labelled features, (b) Cross sectional view/ section cut view of the fourth design showing a smooth flow of material across the print nozzle and (c) 3D-printed prototype of the nozzle .....	97
Figure 3.20. Process of 3D printing .....	98
Figure 3.21. Cement mixer (SOROTO forced action mixer).....	99
Figure 3.22. Transformer from RS component .....	100
Figure 3.23. Markham mortar pump.....	101
Figure 3.24. Illustration of progressive cavity pump [272].....	101
Figure 3.25. Material conveying pipe, T-piece, and pinch valve .....	103
Figure 3.26. Pinch valve illustration [273].....	104
Figure 3.27. Solenoid valve.....	105
Figure 3.28. Ranger air compressor used alongside the pinch valve.....	105
Figure 3.29 Flowchart of 3D printing process.....	106
Figure 3.30 Overall 3D printing process .....	107
Figure 3.31. (a) cast mould and (b) monolithic structures .....	112
Figure 3.32. Flow table test .....	113
Figure 3.33. Extrudability test sample .....	114
Figure 3.34. Hand-squeezed buildability test.....	115
Figure 3.35. Vertical deposition of layers to test buildability .....	116
Figure 3.36 (a) Compressive, (b) flexural and (c) split tensile test set-ups.....	117
Figure 3.37. Split tensile test .....	118
Figure 3.38 Penetration resistance test machine.....	119

Figure 3.39. FEA model for compression test .....	122
Figure 3.40. Mesh visualisation for compressive model.....	123
Figure 3.41. FEA model of four-point bending test with explicit dynamics setup and contacts .....	125
Figure 3.42. Mesh visualisation.....	126
Figure 4.1. Penetration dept vs time.....	131
Figure 4.2. a) Test 1 - Extrusion level after first extrudability test, b) Test 2 - Extrusion level after the addition of 250 g of cement and 50 g of water. ....	132
Figure 4.3. a) 3D printed material immediately after printing, b) 3D printed material after one day. ....	134
Figure 4.4. Extrusion levels of second batch of printing .....	135
Figure 4.5. Failed printing due to low viscosity .....	136
Figure 4.6. Test 3 .....	136
Figure 4.7. Buildability test using materials from test 3b showing slump on the bottom layers .....	137
Figure 4.8. Test 4 material print .....	138
Figure 4.9.a) Material extrusion form nozzle, b) Failed system due to pressure build up....	141
Figure 4.10. a) Force acting downwards on nozzle inlet, b) fractured nozzle.....	142
Figure 4.11. Technical drawing of extrusion nozzle.....	144
Figure 4.12. Nozzle design with threaded grove .....	145
Figure 4.13. Robot 3D printed material (a and b showing 6 consecutive printed layers, and c showing material accumulation at corners and collapse). ....	146
Figure 4.14. List of MELFA-BASIC V commands [268] .....	147
Figure 4.15. 3D-printed structure with uniform extrusion on all sides. ....	148
Figure 4.16. Key guide to 3D printing equipment.....	150
Figure 4.17 3D printing process stage 1 and 2 .....	150
Figure 4.18. Extrusion auger .....	151
Figure 4.19. Back pressure of material through the proposed accelerator inlet .....	152
Figure 4.20. Propeller-like mixer.....	153
Figure 4.21. Optimised process (stage 3).....	154
Figure 4.22. (a) 3D-printed structure with undermixed material and excess aluminium sulphate. (b) Massive void between the structure.....	155
Figure 4.23. 3D-printed structure by manual on-demand spraying of accelerator .....	157
Figure 4.24. Micro nozzle attached to robot extrusion nozzle .....	158

Figure 4.25. setup of cement and accelerator extrusion .....	159
Figure 4.26. 3D-printed structure by automated on-demand spraying of accelerator .....	160
Figure 4.27. Graphical illustration of number of layers achieved versus printing speeds ....	165
Figure 4.28. Buildability test with varying printing speeds .....	166
Figure 4.29. Examples of surface contact between 3D-printed structures.....	168
Figure 4.30. Printing limits, showing the effects of pump pressure and printing speed on the 3D-printed layers .....	168
Figure 4.31. Schematic showing layer height, thickness, and width in 3D concrete printing .....	170
Figure 4.32. Buildability test with varying layer heights .....	171
Figure 4.33. No of layers versus layer height.....	172
Figure 4.34. Uncontrolled nozzle extrusion .....	174
Figure 4.35. Buildability test with varying accelerator concentration.....	175
Figure 4.36. Influence of accelerator concentration on layer height of the 3D-printed structures.....	176
Figure 4.37. Reduction in height with varying accelerator concentrations.....	177
Figure 4.38. Penetration of aluminium sulphate.....	179
Figure 4.39. Graph of compressive strength of 3D-printed versus monolithic structure.....	181
Figure 4.40. Microstructure defect.....	182
Figure 4.41. Failed structure after 1 day of (a) 3D-printed and (b) monolithic structures....	185
Figure 4.42. Failed structure after 28 days of (a) 3D-printed and (b) monolithic structures	186
Figure 4.43. (a) Total deformation and (b) Von mises stress .....	187
Figure 4.44. Flexural strength of 3D-printed structure versus monolithic structure .....	189
Figure 4.45. Failed structures of (a, b) 3D-printed and (c, d) monolithic structures at 1 and 28 days .....	192
Figure 4.46. Deformation and stress contour of cement block.....	194
Figure 4.47. Failure modes in (a) FEA, (b) 3D-printed and (c) monolithic structures .....	195
Figure 4.48. cross section of monolithic structure <i>versus</i> 3D-printed structure.....	196
Figure 4.49. Microscopic analysis showing void .....	197
Figure 4.50. Split tensile strength of cement-based material with varying accelerator concentration.....	198
Figure 4.51. Split tensile failure of concrete with varying accelerator dosages .....	204
Figure 4.52. Microstructure of 3D-printed structure.....	206

Figure 4.53. Micro-structure of 3D-printed material, (a)1 day, (b)7 days, (c)14 days, d) 28 days ..... 207

Figure 4.54. Cold joints and sulphate attach on3D-printed structure ..... 209

## Appendices

A 1. Position of center of gravity for loads [268] .....	245
A 2. Internal circuit structure [268] .....	246
B 1. Mitsubishi electric training on robot programming.....	249
B 2. Mitsubishi electric training on robot maintenance .....	250
D 1. Risk assessment 1 of 16.....	259
D 2. Risk assessment 2 of 16.....	260
D 3. Risk assessment 3 of 16.....	261
D 4. Risk assessment 4 of 16.....	262
D 5. Risk assessment 5 of 16.....	263
D 6. Risk assessment 6 of 16.....	264
D 7. Risk assessment 7 of 16.....	265
D 8. Risk assessment 8 of 16.....	266
D 9. Risk assessment 9 of 16.....	267
D 10. Risk assessment 10 of 16 .....	268
D 11. Risk assessment 11 of 16 .....	269
D 12. Risk assessment 12 of 16 .....	270
D 13. Risk assessment 13 of 16.....	271
D 14. Risk assessment 14 of 16.....	272
D 15. Risk assessment 16 of 16 .....	273
D 16. Risk assessment 16 of 16.....	274

## List of Tables

Table 1.1. Structure of the thesis .....	42
Table 2.1. Classification of AM processes .....	13
Table 2.2. Advantages and limitations of additive manufacturing processes. ....	15
Table 2.3. Mix design and descriptions.....	19
Table 2.4 Timelines of robot evolution.....	52
Table 3.1. Mixture design.....	71
Table 3.2. Robot safety specification.....	83
Table 3.3. Robot standard specification .....	83
Table 3.4. Robot controller specifications.....	85
Table 3.5. Properties of PLA material.....	92
Table 3.6. Size of the simplified extrusion nozzle.....	97
Table 3.7. Technical specification of cement mixer. ....	99
Table 3.8. Technical specifications of mortar pump.....	102
Table 3.9. Technical specification of air compressor. ....	106
Table 3.10. 3D printing parameters with varying print speeds .....	109
Table 3.11. 3D printing parameters with varying layer heights .....	110
Table 3.12. 3D printing parameters with varying accelerator dosage .....	111
Table 3.13: Material Properties Assigned in ANSYS.....	121
Table 3.14. Mesh parameters.....	124
Table 3.15. Mesh parameters.....	126
Table 4.1. Material composition.....	129
Table 4.2. Summary of Preliminary Mix Designs and Performance Outcomes .....	140
Table 4.3. Material properties of test 1. ....	140
Table 4.4. Material properties.....	145
Table 4.5. Effect of printing speed on layer thickness of the 3D-printed structures. ....	164
Table 4.6. Effect of layer height on layer thickness of the 3D-printed structures. ....	170
Table 4.7. Effect of aluminium sulphate on buildability.....	174
Table 4.8. Structural modes of failure.....	179
Table 4.9. Compressive strength of 3D printed structure.....	182
Table 4.10. Strength of Monolithic Structure.....	183

Table 4.11. Flexural strength of 3D-printed structure.....	189
Table 4.12. Flexural strength of Monolithic structure .....	190
Table 4.13. Crack propagation and stress distribution. ....	195
Table 4.14. Split tensile test of CTRL_00.....	200
Table 4.15. Split tensile test of AL_ST15 .....	200
Table 4.16. Split tensile test of AL_ST25 .....	201
Table 4.17. Split tensile test of AL_ST35 .....	201
Table 4.18. Split tensile test of AL_ST45 .....	202

#### Appendices

A3. 1. Cost analysis of materials used to manufacture the robot security enclosure.....	247
---	-----

# **CHAPTER 1: INTRODUCTION**

---

## **Introduction**

# CHAPTER ONE

## INTRODUCTION

### 1. Background

Additive manufacturing, with particular emphasis on 3D printing of cement-based materials, is emerging as a transformative innovation within the construction sector [1-5]. Distinguished by its potential to revolutionise traditional building practices, 3D printing of cement-based materials offers several compelling advantages. These include reduced reliance on manual labour, enhanced construction site safety, shortened project timelines, and the capacity to produce architecturally complex forms while minimising material waste [6, 7]. The rise of high-tech construction tools, along with the need to build more sustainably, has made 3D concrete printing an exciting and promising way to solve some of the construction industry's biggest ongoing problems[8].

However, despite these prospects, the widespread implementation of 3D printing of cement-based materials remains constrained [7, 9]. A major barrier lies in the performance of printable concrete mixtures, particularly the challenge of achieving an optimal balance among pumpability, extrudability, buildability, and early-age strength [10]. The interdependence of these properties necessitates rigorous formulation strategies and novel process control methods to ensure the structural viability of printed elements during and immediately following deposition.

To fully realise the potential of 3D printing in cement-based construction, there is a pressing need to deepen our understanding of how material formulation and process parameters influence print quality and mechanical performance. Addressing these challenges is essential for the development of robust, scalable, and economically viable solutions. This research, therefore, seeks to bridge these knowledge gaps by investigating critical factors affecting the mechanical properties of 3D-printed cement-based structures, with the ultimate goal of advancing the adoption of additive manufacturing in mainstream construction practices.

## 1.1. Motivation

The building and construction industry plays a vital role in the economic development of countries, accounting for approximately 9% of the GDP and employing a significant portion of the global workforce [11, 12]. The fast growing industry is also a huge economic contributor and is expected to increase the total widespread spending in construction from \$11.4 trillion in 2018 to \$14 trillion by 2025 [13]. However, the industry is still characterised by low technological innovation with low productivity and low use of automation [9]. This sector can be referred to as a conservative sector, with its basic principles being constant over the years. The lack of technological innovation in the building and construction industry has then led to the low sustainability index [9], hence why the introduction of three-dimensional (3D) printing is germane. This will help to improve worker safety [6], speed up building processes and is less labour intensive when compared with the conventional method of casting or bricklaying used in the building and construction industry [6]. In the U.S, the construction industry has invested a mere 1.5% of value added on technology, which is significantly lower than the manufacturing industry's investment of 3.3% and the economy's overall average of 3.6 % [9]. Several analyses indicate that the productivity of the construction industry has remained stagnant over the past few decades, while the productivity of the manufacturing industry has almost doubled [14]. The building and construction industry has great potential for improvement in comparison to its current state, which makes use of human labour, putting workers at a high level of risk, attracting high costs and taking a longer time to complete [9]. The conventional construction method requires utilising human resources at various stages, which is costly and time-consuming. In addition, the final product generates a substantial amount of construction waste [9]. In contrast, modern 3D printing technology uses an autonomous system that prints structures using Computer-Aided Design (3D-CAD), which requires less human labour and less flexible tooling, resulting in multiple reductions in labour requirements, manual process and material waste [2]. The use of formwork in conventional construction is one of the main causes of significant spending, which leads to higher material and equipment costs, high material waste and higher labour [15-17]. Formwork is time consuming and accounts for 25-35% of the total cost of the structural work [18]. The use of formwork is also adversely affected by the complexity of the geometry. Contrary to that, 3D printing of cement-based materials has not affected any complexity in the construction geometry [19, 20]. In addition, sustainability is a significant issue in the current construction industry [1]. The production of cement, a key component of concrete, is highly energy-intensive due to the burning of slag in a kiln. As a

result, concrete production contributes significantly to global CO2 emissions. Estimates and calculation methods may vary, but the cement industry has approximated that cement production accounts for about 5% of global CO2 emissions [21]. Efforts to mitigate this impact have been made by introducing cement replacers like fly ash, a by-product of blast furnaces, which has helped reduce the average CO2 output associated with concrete. However, the overall CO2 footprint of concrete remains substantial. Despite the affordability of concrete's raw materials, the lack of economic incentives for CO2 reduction poses challenges in achieving significant emissions reductions [1]

A report by Markets and Markets suggests that 3D Concrete Printing (3DCP) has the potential to reduce construction time by 50-70%, waste by 30-60% and cost of labour by 50-80% [9]. However, more research is needed to understand these savings fully. A study by Allouzi et al. [22] in Jordan found that 3D printing could decrease material costs by 65% compared to conventional construction methods but did not consider other factors, such as equipment and labour costs. In addition, Agustí-Juan and Habert [23] reported that 3DCP is more environmentally friendly when compared with the conventional method. The comparison between the conventional method and 3DCP can be observed in Figure 1.1.

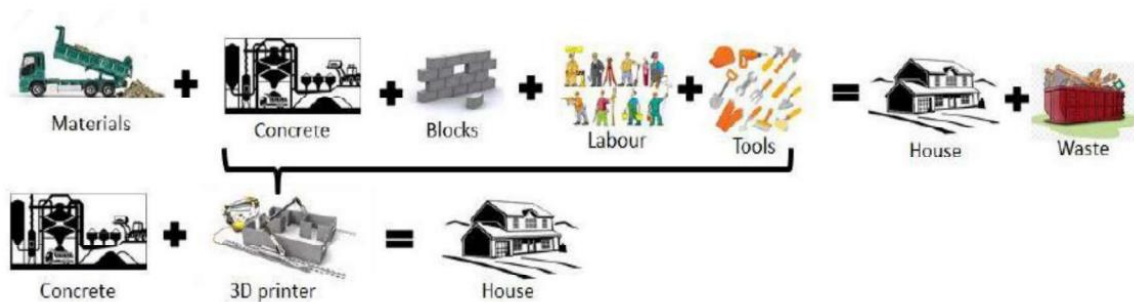


Figure 1.1. Conventional construction vs 3D printing construction process [9]

There are several challenges involved in the process of 3D printing. Research is still ongoing to ensure that 3D-printed structures outperform their conventionally manufactured counterparts in terms of mechanical performance, cost efficiency, and environmental sustainability. Since cement is the most used construction material, the industry faces several challenges, which the high cost of production is a major one [24]. Boral Innovation Factory conducted research in Sydney Central Business District (CBD) and stated that about 80% of the total cost of concrete

is being used by the formwork [24]. The speed of construction is another major issue due to the number of steps involved. These include, but are not limited to, material production and transportation, which are all time consuming [24]. Factors, including safety issues and labour intensity, especially for in-situ cast concrete, amongst others, are also challenges faced by the current concrete construction industry [1]. The requirements for Bespoke geometries involve intense labour in the assembly of reinforcements and erection of moulds [1]. These factors hinder the health of construction workers, especially with the ageing workforce.

The current building and construction industry faces the following challenges:

- Aging workforce and Lack of skilled workers - This has been a major issue in the construction industry for many years now, with the highest proportions of workers aged between 45-54 years [25]. The next age group with high proportion of workers were between 35- 45 years [25]. This means that many of the older age group are retiring, and the younger ones are not taking over these jobs. This opens up a wide gap in the industry, leading to the industry being short-staffed. According to Manpower [25], the overall interest in the construction industry by the younger age group has fallen to about 4 out of 10 amongst the age group of 14 to 19. This leads to a major challenge as essential skill trades are lost as older employees retire due to the lack of interest from the younger age groups [25].
- Slow Technology Adoption - Many firms have been slow to adopt emerging technologies such as Building Information Modelling (BIM), robotics, and automation. This is often due to high implementation costs and a lack of skilled personnel to operate advanced systems [26].
- Health and safety - According to Health and Safety Executive [27], the construction sector has the highest number of health and safety related accidents in the United Kingdom (UK). This is a result of a lack of training, safety processes and equipment compliance [25].
- Gender diversity – There is a general stereotype that the construction industry is not meant for women. Hence, they will not thrive in the sector. The industry is dominated by mostly men, resulting in about 99% of all construction workers [25]. This is generally not true, as there is a huge variety of opportunities in the industry, such as; architecture, surveying, and construction design, amongst others [25].
- Design and Documentation Errors - Errors and omissions in design and engineering drawings are frequent, leading to costly rework and project delays [26]. These issues

often stem from poor coordination between design teams and a lack of constructability reviews during preconstruction phases [26].

- Regulatory Pressures - Navigating complex and evolving regulations remains a challenge. Firms face difficulties complying with varying standards at the federal, state, and local levels, which can lead to delays, inefficiencies, and legal risks [26].

#### 1.1.1. Accidents and injuries

The Construction Statistics for Great Britain [28] Provided an insightful analysis of workplace health and safety within the construction sector. The data, collected up until March 2023, covers various aspects, including work-related ill health, workplace injuries, and the economic impacts of health issues and injuries in the industry.

#### 1.1.2. Work-related ill health

An estimated 69,000 workers in the construction sector were affected by work-related ill health between 2020/21 and 2022/23. Musculoskeletal disorders emerged as the most prevalent issue, accounting for 54% of the cases. These disorders are a significant concern in construction due to the physical nature of the work. Stress, depression, or anxiety impacted 16,000 workers during the same period, representing 24% of all health-related cases. However, compared to other industries, the overall rate of work-related ill health in construction, at 3.3%, was lower than the all-industry average of 4.1%.

#### 1.1.3. Fatal Injuries

Fatal injuries remain a critical concern in the construction industry. In 2022/23, there were 45 fatalities, which is higher than the five-year annual average of 37. Falls from height accounted for more than half of these fatalities, highlighting the persistent risk of working at heights in the sector. The fatal injury rate in construction was calculated at 1.72 per 100,000 workers, which is more than four times higher than the rate observed across all industries. Figure 1.2a shows the graph of fatal injuries by accident kind in construction.

#### 1.1.4. Non-Fatal Injuries

Non-fatal injuries in the construction sector also present a significant issue, with an estimated 53,000 workers sustaining injuries in the three-year period from 2020/21 to 2022/23. Of these injuries, 28% resulted in workers being absent for more than seven days. The rate of non-fatal injuries in construction, at 2.6%, is considerably higher than the all-industry average of 1.5%. The types of injuries varied, with falls, slips, and trips being among the most common causes. Figure 1.2b shows the graph of non-fatal injuries by accident kind in construction.

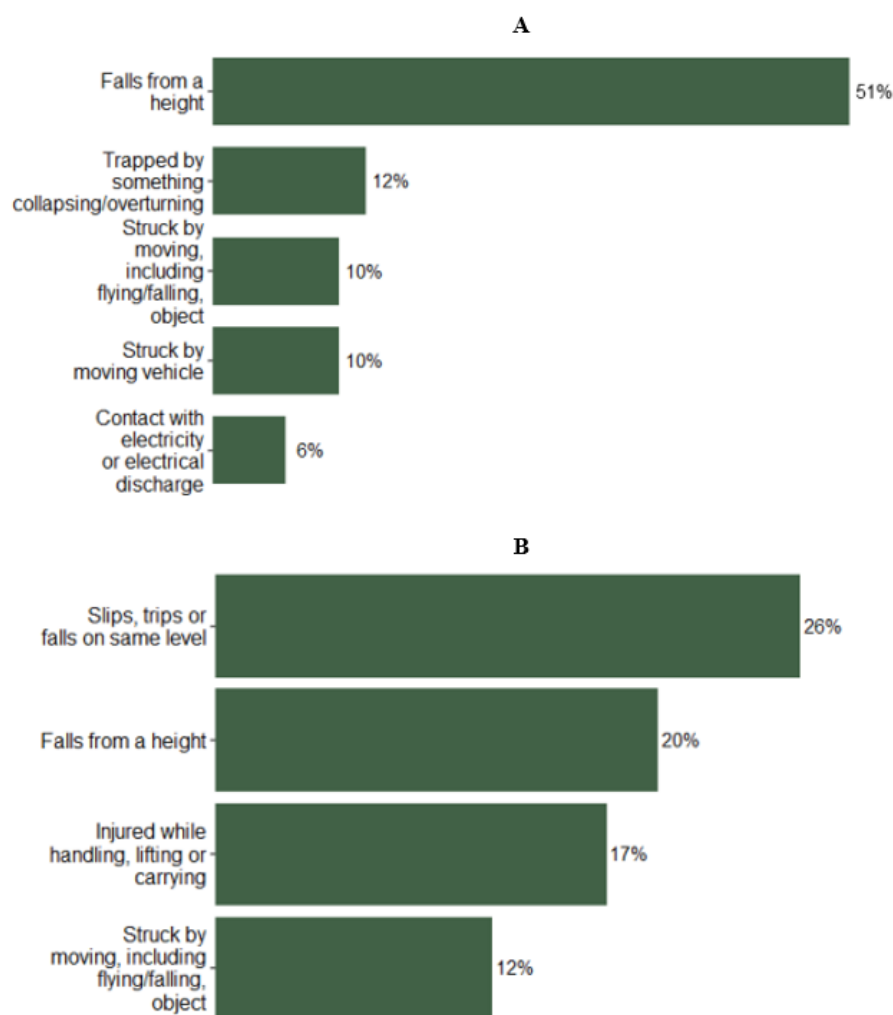


Figure 1.2. (a) Percentage of fatal injuries by accident kind in construction, (b) Percentage of non-fatal injuries by accident kind in construction [28]

### 1.1.5. Lung Disorders and Occupational Cancer

Lung disorders are another health concern in the construction sector. An estimated 4,000 workers were affected by work-related breathing or lung problems during the period. The construction sector saw a statistically higher rate of lung problems compared to the all-industry average, particularly due to exposure to hazardous substances like asbestos. The issue of occupational cancer also looms large, with around 3,700 deaths per year linked to past work in construction. The majority of these cases are attributed to asbestos exposure, with smaller contributions from silica and solar radiation. The long-term health impacts from exposure to these materials continue to affect many workers, particularly those involved in tasks like carpentry, plumbing, and electrical work.

### 1.1.6. Economic Costs

The total economic cost of work-related ill health and injuries in the construction sector was estimated to be £1.3 billion for 2021/22. This accounts for 6% of the total cost of all work-related ill health and injuries across all sectors in Great Britain. The cost includes both financial impacts, such as lost output and healthcare expenses, as well as non-financial impacts, such as the loss of quality of life and fatalities.

### 1.1.7. Working Days Lost

In terms of productivity, around 2.6 million working days were lost in the construction sector each year due to workplace injuries and ill health. The majority of these losses, 80%, were attributed to work-related ill health, while the remaining 20% were due to injuries. On average, this results in approximately 1.3 working days lost per worker, which is comparable to the all-industry average of 1.1 days.

In light of these challenges, 3D printing offers a transformative solution for the construction sector by significantly reducing waste from formworks, construction time, and labour costs. 3D printing aligns with the goals of the sector to improve efficiency, sustainability, and worker safety. In addition to the industry facing an ageing workforce, illnesses and skill shortages, 3D printing provides a modern, sustainable solution that not only enhances productivity but also

helps bridge the gap in labour demands. In essence, 3D printing offers a pathway to sustainable transformation, positioning the construction sector for a future that balances innovation with environmental and economic responsibility.

## **1.2. Statement of Problems**

AM of concrete is an innovative and rapidly emerging technology within the construction industry. Despite its promising potential, it is still in its early stages and faces several significant challenges [29]. In recent years, researchers have increasingly focused on exploring the application of AM to the construction of buildings, identifying key areas for improvement. One of the primary issues is the weak interlayer bonding between deposited layers, where the time gap between successive depositions compromises the structure's integrity. 3D-printed concrete structures often exhibit weaker mechanical properties, such as tensile and compressive strengths, largely due to the inability to incorporate conventional reinforcement techniques effectively [29]. In addition to hardware challenges, the role of mix design in determining the fresh properties of cement-based 3D-printed materials is another critical issue. An inappropriate mix design can result to poor flowability, extrudability and buildability, causing difficulties, such as nozzle clogging, instability of printed layers and compromised structural shape retention. Ensuring the right balance of materials in the mix is crucial to achieving optimal printing performance and avoiding construction failures.

The design and development of a suitable 3D printing extrusion nozzle presents another challenge. Specifically, there is a lack of commercially available small-scale 3D printing robot extrusion nozzles optimised for cement-based materials. This limitation poses a problem as the success of 3D-printed structures heavily depends on precise material deposition and layer bonding. In this research, a significant contribution has been made by designing a custom small-scale robot extrusion nozzle tailored for cement-based 3D printing. This design addresses the limitations of existing nozzles by considering the specific requirements of material flow, extrusion pressure and layer formation in cement-based structures.

Furthermore, while there has been extensive research into 3D printing technology, only a few studies have directly examined key aspects, such as mechanical strength, accelerated durability performance, and porosity in comparisons between 3D-printed structures and conventionally cast, monolithic ones. This limited comparative data makes it challenging to fully assess the overall performance and feasibility of 3D printing as a viable construction method, leaving

some uncertainty as to whether 3D-printed structures can achieve or exceed the critical properties of traditionally built structures.

Therefore, this research addresses these pressing challenges by investigating into the effects of mix design on the fresh properties and buildability of 3D-printed structures, as well as by designing a small-scale extrusion nozzle to improve printing precision. Additionally, the study provides a much-needed direct comparison between 3D-printed and monolithic concrete structures, offering insights into their respective mechanical properties and helping to assess the true potential of 3D printing in construction. By tackling these critical issues, the research aims to advance the understanding and application of AM in the construction industry.

### **1.3. Research questions**

The purpose of this research is to investigate critical factors in cement-based additive manufacturing processes that impact the mechanical properties and buildability of 3D-printed cement-based structures. To address this, the following primary research questions will be examined in this thesis.

#### **RQ-1: How do nozzle geometry and material choices influence flow behaviour and structural performance in cement-based 3D printing?**

This question investigates how design elements such as inlet angle, edge fillets, and material selection affect flow consistency, extrusion efficiency, and mechanical suitability of the nozzle. The study is carried out in the context of a lightweight robotic arm with a 2 kg payload, where nozzle weight and geometry must be optimised to ensure compatibility. While basic structural considerations were addressed, the primary focus was on print quality and operational feasibility within the system's physical constraints.

#### **RQ-2: How does the use of aluminium sulphate as a chemical accelerator influence interlayer bond strength in cement-based 3D-printed structures?**

This question examines the effect of aluminium sulphate on the mechanical bonding between successive layers in 3D-printed cementitious materials. Since interlayer adhesion is critical to the structural performance and long-term durability of printed elements, understanding how this admixture alters setting time and bond formation will offer key insights into enhancing build quality and reducing delamination in additive manufacturing.

**RQ-3: How do the mechanical properties, specifically the compressive and flexural strength of 3D-printed cement-based structures, compare to those of conventionally cast counterparts?**

This question seeks to evaluate whether 3D-printed cementitious elements can achieve equivalent or superior structural performance relative to traditional casting methods. By comparing mechanical strengths, the research aims to assess the viability of 3D printing as a reliable alternative for structural applications, particularly in contexts where durability and load-bearing capacity are critical.

**RQ-4: How do process parameters, such as printing speed, layer height, and the inclusion of aluminium sulphate admixtures, affect the buildability and mechanical performance of cement-based 3D-printed structures?**

This question investigates how variations in key printing parameters influence both the geometric stability (buildability) and mechanical integrity of printed structures. Understanding the interaction between these factors is vital for optimising the additive manufacturing process, ensuring print consistency, minimising defects, and achieving the desired strength characteristics in final components.

## **1.4. Research scope**

After thoroughly evaluating the current state of the art, the present study investigates the critical factors in cement-based additive manufacturing processes that influence the mechanical properties of 3D-printed cement-based structures.

This shall be attained by satisfying the following aim and objectives.

### **1.4.1. Project Aim**

This project aims to identify and analyse the critical factors influencing the mechanical behaviour of 3D-printed cement-based structures using a small-scale printing system, with the goal of optimising process parameters and material selection to enhance structural performance and support the broader adoption of additive manufacturing in construction.

#### 1.4.2. Project Objectives

The following objectives are carefully formulated and carried out in order to achieve the afore-stated aim of this study:

1. Design and development of a small-scale cement-based 3D printing system, especially with a lightweight robot nozzle and optimised printing process.
2. Investigation of key process parameters, including printing speed, layer height and aluminium sulphate additive, impacts the buildability and mechanical properties of 3D-printed cement-based structures. This includes analysing the effects of these parameters on structural stability, layer adhesion, and failure modes to optimise printing quality and strength.
3. 3D printing, mechanical testing and comparative analysis of cement-based structures to assess and compare the mechanical properties, such as compressive and tensile strength, of 3D-printed versus conventionally cast structures, highlighting differences and advantages.

#### **1.5. Relevance of 3D printing to the national economy and global relevance**

The implementation of 3D printing in construction is a technological way to improve the sustainability of cementitious structures by adopting the use of waste products, recyclable materials and eliminating the need for traditional formwork [30]. Due to the global demand for reducing carbon emissions, it is important to adopt innovative building technologies to pave the way for a sustainable building future. Proponents of 3DCP argue that the technology can significantly reduce material usage and waste, such as the reduced usage of formwork [31], increase productivity and address the shortage of skilled workers in the construction industry [32]. 3D printing technology can help to save up to 40% of the total budget for cementitious work in construction [33], by the reduction of formwork, labourers, and building materials, amongst many other factors. While the initial capital investment in 3D printing systems such as robotic arms and extrusion units can be high, the significant cost savings in labour, material use, and formwork contribute to a faster return on investment. These efficiencies make 3D printing of cement-based materials economically viable, especially for large-scale or repetitive construction projects [1, 34]. Moreover, worker safety, particularly in extreme or hazardous

environments, serves as a key motivation for implementing AM in construction [35]. Harsh environments inevitably raise difficulties and risks, leading to adverse effects on construction quality and human well-being. For instance, freezing temperatures can create challenges in excavation and concrete pouring, while high-temperature environments may cause dehydration among construction workers. Sites exposed to chemical or nuclear contamination pose significant health risks [36]. Off-site fabrication has emerged as a solution to address these challenges by delivering pre-fabricated parts and assemblies to be assembled on-site. This approach reduces on-site labour requirements, enhances construction quality, and ensures consistency.

AM has the potential to contribute to the construction industry by reducing on-site worker exposure to harsh environments and automating certain construction tasks [37]. Furthermore, the use of 3D printing reduces the need for global transportation because the manufacturing sites can be made closer to the end destination which helps to save time, energy, and cost of transportation.

## **1.6. Contribution to Knowledge (Research Novelty)**

This PhD study makes several significant contributions to knowledge in the field of AM of concrete, addressing both technological challenges and gaps in the existing body of research. The following are the key contributions:

- ***Design and development of a lightweight extrusion nozzle for cementitious 3D printing:*** One of the primary contributions is the design and development of a purpose-built extrusion nozzle engineered to operate within the payload constraints of small-scale robotic arms ( $\leq 2$  kg). Existing commercial nozzles are often bulky, generic, or incompatible with the flow dynamics of cement-based materials. This study bridges that gap by designing a nozzle that not only meets structural performance requirements but is also optimised for material flow, reduced stress concentration, and enhanced print consistency.
- ***Investigation of mix design and its impact on fresh properties of cement-based 3D-printed materials:*** The research thoroughly investigates how the composition of the cement mix, such as the ratios of cement, water, aggregates and additives, affects the fresh properties of 3D-printed materials, such as flowability, extrudability and

buildability. It highlights the critical role that mix design plays in the success of 3D printing. The study provides novel insights into optimising mix design for 3D printing to ensure smooth extrusion, proper bonding between layers, and overall structural stability. This is a key area of contribution, as improper mix design can lead to nozzle clogging, poor layer adhesion and even structural collapse.

- ***Formulation of an optimised process for accelerator application:*** Another novel aspect of the research is the development of an optimised process for applying chemical accelerators to the system during the 3D printing process. This advancement allows for controlled integration of accelerators, improving the setting time and overall buildability of the structure without compromising material flow or extrudability. The careful regulation of the accelerator dosage and timing ensures that each printed layer achieves sufficient strength while maintaining the desired fresh properties. This process is especially important for enhancing the mechanical performance and reducing construction times in real-world applications.
- ***Direct comparison between 3D-printed and monolithic structures:*** One of the unique aspects of this research is its direct experimental comparison of the mechanical properties, such as compressive, tensile and flexural strengths of 3D-printed cementitious structures and conventionally cast (monolithic) structures. The results obtained provide valuable information on whether 3D printing can meet or surpass the performance benchmarks of monolithic structures, which is crucial for the wider adoption of 3D printing in construction.
- ***Addressing weak interlayer bonding caused by aluminium sulphate:*** The research explores the impact of aluminium sulphate on the interlayer bond strength of 3D-printed cement-based structures, by analysing how aluminium sulphate impacts the interlayer bond between 2 successive layers. The findings contribute to a better understanding of how aluminium sulphate used as a chemical additives interact with the rheological and mechanical properties of cementitious materials during extrusion-based 3D printing, supporting efforts to optimise mix designs for improved structural adhesion.
- tackles the problem of weak interlayer bonding, a major challenge in 3D printing, where time gaps between the deposition of successive layers weaken the overall structure. By investigating the factors that affect interlayer bonding and analysing the impact of time

gaps, the study offers novel insights into how to improve the structural integrity of 3D-printed materials. The findings help refine the printing process.

- ***Optimisation of printing parameters for enhanced buildability:*** The research also contributes to the optimisation of key printing parameters, including nozzle speed, layer height and extrusion pressure. They all influence the buildability of 3D-printed structures. By analysing how these parameters affect the quality and performance of printed structures, the research offers guidelines for optimising the printing process to achieve more reliable and efficient construction. This optimisation is crucial for ensuring that printed structures maintain their intended shapes and are structurally sound.
- ***Application of finite element analysis to evaluate damage mode and mechanism of the printed structures:*** The use of finite element analysis (FEA) in this research adds a computational dimension to the evaluation of 3D-printed structures. The research applies FEA to simulate the stress distribution, failure modes and mechanical behaviours of 3D-printed concrete structures under various load conditions. This computational approach complements the experimental results, offering a deeper understanding of how printed structures perform in real-world scenarios and providing a tool for further refinement of the printing process.

## 1.7. Thesis Structure

This thesis is structured into five main chapters, some of which are further divided into parts to reflect the flow and focus of the research. Table 1.1 outlines the organisation of each chapter and its corresponding parts for clarity and ease of reference.

Table 1.1. Structure of the thesis

<b>Chapter 1</b>	INTRODUCTION
	LITERATURE REVIEW
<b>Chapter 2</b>	Part A: Additive manufacturing Part B: Robot 3D printing systems
	MATERIALS AND METHODOLOGY
<b>Chapter 3</b>	Part A: Materials Part B: 3D Printing set-up Part C: 3D Printing Processing Parameters Part D: Performance Evaluation Part E: Finite Element Analysis
	RESULTS AND DISCUSSION
<b>Chapter 4</b>	Part A: Assessment of fresh-state performance of mortar mixes Part B: Preliminary testing and nozzle optimisation Part C: Printing process Optimisation and accelerator administration Part D: Performance Evaluation of experimental works
<b>Chapter 5</b>	CONCLUSION AND FUTURE WORKS
	References
	Appendices

## **1.8. Summary**

The first chapter began by introducing the research and providing background information on the topic of 3D printing, particularly in the context of construction. The motivation for the research was then discussed, highlighting real-world challenges in the construction sector, such as accidents, injuries, and inefficiencies, that 3D printing could help address. The chapter proceeded to present a clear statement of the research problem, followed by the formulation of the research aims and objectives. The scope of the study was defined to outline its boundaries and focus areas. Key advantages of 3D printing in construction, including its potential to improve efficiency, reduce waste, and enhance safety, were also discussed. Importantly, the chapter acknowledged the existing limitations and challenges associated with implementing 3D printing technologies in the field. The original contributions of the research were outlined, highlighting the study's novelty and relevance to the existing body of knowledge. Finally, the chapter concluded by presenting the structure of the thesis, offering an overview of how each subsequent chapter contributes to the development of the research.

## **CHAPTER 2: LITERATURE REVIEW**

---

**Additive Manufacturing**

**And**

**Application of Robots for 3D Printing of Cement-Based Materials**

# Chapter 2: Literature Review

## 2. Introduction

This chapter presents a comprehensive literature review on additive manufacturing (AM) in the construction industry, with a particular focus on the use of 3D printing for cement-based materials. It explores both the material and technological aspects of the process, beginning with an overview of the fresh and hardened properties of cementitious materials, which are critical to achieving successful printability, buildability, and long-term performance. The chapter also discusses the role of robotic systems such as robotic arms, gantry setups, and cable-suspended platforms in enhancing automation, precision, and efficiency in 3D construction printing. Key elements such as nozzle design and printing parameters, including layer height, speed, and orientation, are examined for their influence on the quality and mechanical behaviour of printed structures. The literature review was continuously updated throughout the course of the research, allowing for the incorporation of the most recent advancements and ensuring that the analysis remained current, relevant, and reflective of the evolving state of the field.

### 2.1. Additive Manufacturing

Additive manufacturing (AM), also known as three-dimensional (3D) printing, is the process of creating three-dimensional objects from Computer-Aided Design (CAD) models by depositing material layer by layer to achieve the desired shape [38-40]. In recent years, the building and construction industry has experienced rapid interest in the development of 3D printing, from the conception and formation of printable materials to the design and implementation of new printable systems to commercialisation [1-3, 41-43].

A major issue involved in the adoption of AM is the size constraint of printed structures [44]. This technology, still in its infancy, first emerged in the late 1980s under the name rapid prototyping. Initially, it was used to produce conceptual models for discussing design ideas, form and fit applications, and the creation of architectural or anatomical models [15, 45]. At the time, materials were limited to a small selection of polymers, ceramics, and metals [5]. Over time, the technology evolved from rapid prototyping to rapid tooling, enabling the direct or indirect fabrication of tools for applications such as injection moulding, thermoforming,

blow moulding, or even for the production of electrodes for electrical discharge machining [46]. Eventually, AM progressed from its origins in rapid prototyping and rapid tooling to what is now known as rapid manufacturing, allowing for the production of final, fully functional products [47]. Currently, AM encompasses seven distinct, which are capable of processing a wide range of materials, including biological materials like cells and biomolecules, as well as smart and functionally graded materials [48, 49].

The process of 3D printing can be shown in Figure 2.1. The first stage involved in the process includes the design and creation of the computer 3D model with the help of Computer Aided Design (CAD) software [44]. The second stage involves path generation, conversion to a Stereolithography (STL) document before slicing to generate a Toolpath file (G-code). The third stage is a more complicated one, as it involves the manufacture of the 3D model by printing, using one of a various number of techniques, such as fused deposition modelling, Laminated Object Manufacturing, Selective Laser Sintering, stereolithography amongst others [44]. All these printing techniques have their advantages, of which some of them include:

- (i) Flexibility to the design process that would have been difficult to manufacture using the traditional method for manufacturing. A company named General Electric (GE) Aviation once used AM to improve the airflow of blade edges with complex designs. This would have been difficult to manufacture using the traditional method of manufacturing that involves the production of various parts and then coupling them up to form one piece without causing a spike in the price and increase in time [44, 50].
- (ii) Reduction in the rate of energy consumption and material usage. The traditional methods of construction use human resources, which is expensive and time consuming. The final product also comes with a lot of construction waste, unlike 3D printing which is mostly automated and involves fewer human resources. 3D printing reduces several manual processes, such as the need for formwork, tooling and labour requirement [44, 50].

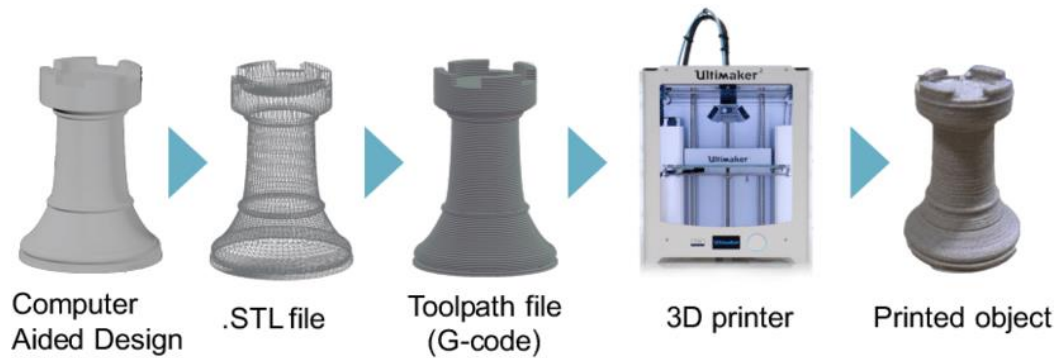


Figure 2.1 Overall printing process of material [15]

In recent times, the aerospace industry and the military fields have constructed several parts using expensive materials, including diamonds and titanium. The use of 3D printing has helped to reduce material usage and energy consumption, as they are more accurate. During the manufacturing process, the traditional method is subtractive, therefore losing up to 80 - 90% of the original billet as when compared to that of 3D printing which is more efficient [50]. Also, AM helps to reduce the number of parts that can be produced at once, which means multiple parts can be produced into a single element that can be easy to substitute and change unlike if the system consists of multiple sections. For example, a fuel pump manufactured by GE Aviation was integrated into one piece using the method of 3D printing which would have otherwise been required 20 separate components, using the traditional method [44]

AM has been successfully incorporated into numerous industries, such as the automotive, aerospace, building and construction, and the healthcare sectors. NASA has conducted tests on the International Space Station to explore the feasibility of 3D printing, enabling astronauts to manufacture tools on-demand within the station [44]. The Boeing Company has successfully printed 22,000 components for various aircraft applications, while European Aeronautic Defence and Space utilised 3D printing to create optimised brackets for use in the Airbus A320. Beyond aerospace, 3D printing finds applications in diverse sectors such as biomedical industry [51] automotive [52], construction and architecture [53], and even food processing [54]. Notably, 3D printing stands out from other prototyping technologies due to its cost reduction potential [55] and its reliance on computer-based technology.

### 2.1.1.3D printing methods

The technology of 3D printing has experienced further interest by several sectors, such as the automobile industry, biomedical, food and processing, construction and architectural fields [44]. Some key aspects that differentiate 3D printing from other technologies that use prototyping are cost-effectiveness and its computer based. Due to the high demand for printing of high quality complex structures, several AM techniques have been invented to meet this criterion. There are several factors that have influenced the development of 3D printing, including the power/ability to print huge structures while taking into consideration a reduced defect and enhanced mechanical property [56, 57]. Fused Deposition Modelling (FDM) is the most common method of AM that primarily uses polymer filaments. However, the main methods of AM are Selective Laser Melting (SLM) or liquid binding in 3D printing, Selective Laser Sintering (SLS), Direct Energy Deposition (DED), Inkjet Printing (IJP), Laminated Object Manufacturing (LOM), Contour Crafting (CC) and stereolithography [44, 58]. This research uses CC to extrude cement based materials for 3D printing.

### 2.1.2. Contour Crafting (CC)

Currently, 3D printing of cement-based materials has developed into four main techniques, with the most prominent being extrusion-based 3D printing, pioneered by Khoshnevis et al. [59], where a robot deposits concrete layer by layer. CC is a form of material extrusion. It is an innovative layered fabrication technology introduced by Khoshnevis for automating the construction of civil structures [60, 61]. CC has the potential to revolutionise the construction industry by allowing for the rapid construction of buildings with complex designs. The primary goal of CC is to enhance building construction in terms of speed, safety, quality, and cost-effectiveness. Similar to other layered fabrication methods like rapid prototyping and stereolithography, CC employs a computer-controlled process to build structures layer by layer in a precise manner [43, 62, 63]. However, CC distinguishes itself by being specifically designed for the construction of large-scale structures ranging from single-family homes to housing complexes and office buildings [61]. The process involves the deposition of strips or beads of material, typically a thick concrete or paste-like substance, using an extrusion method. A nozzle (depicted in yellow in Figure 2.2) extrudes the material at the specified locations. In the original system, the x–y–z position of the nozzle is controlled by a Cartesian gantry manipulator. As the nozzle moves along the walls of the structure, the construction material is

extruded and troweled using a set of actuated, computer-controlled trowels. These trowels enable the production of smooth and accurate surfaces [60]. Figure 2.3 shows a close-up view of the extrusion/troweling tool in a small-scale prototype CC system developed by Koshnevis (from [1]). The use of these automated trowels is critical to achieving the precise finishes that make CC a viable option for large-scale 3D printing applications. Overall, CC is an innovative technology that has the potential to transform the way buildings are constructed, making the process faster, more cost-effective, and more flexible in design. This research utilised CC as a method of extrusion using a 6-axis articulated robot system. One major limitation of CC is its restriction to vertical extrusion, which results in 2.5D typologies rather than true 3D forms. This means that CC creates vertical extensions of a planar shape. It also poses a significant drawback when printing cantilevered structures, where horizontal extensions are needed [64]. Such structures create weak interfacial zones between the printed layers, leading to reduced structural integrity in those areas [64].

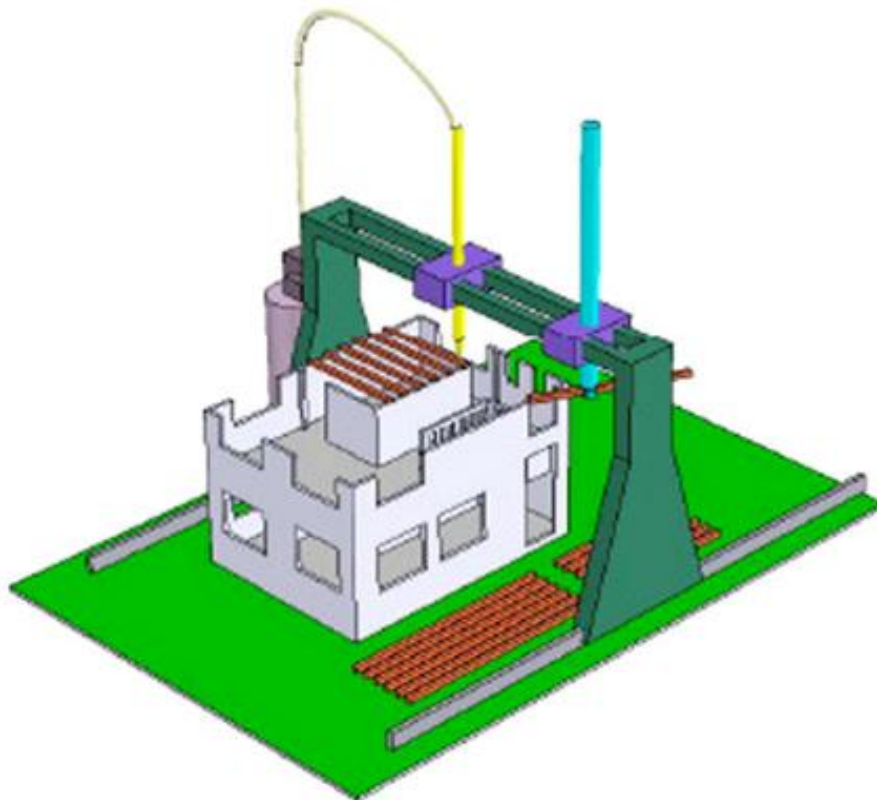


Figure 2.2 Building construction using a gantry robot system and CC technique [61]

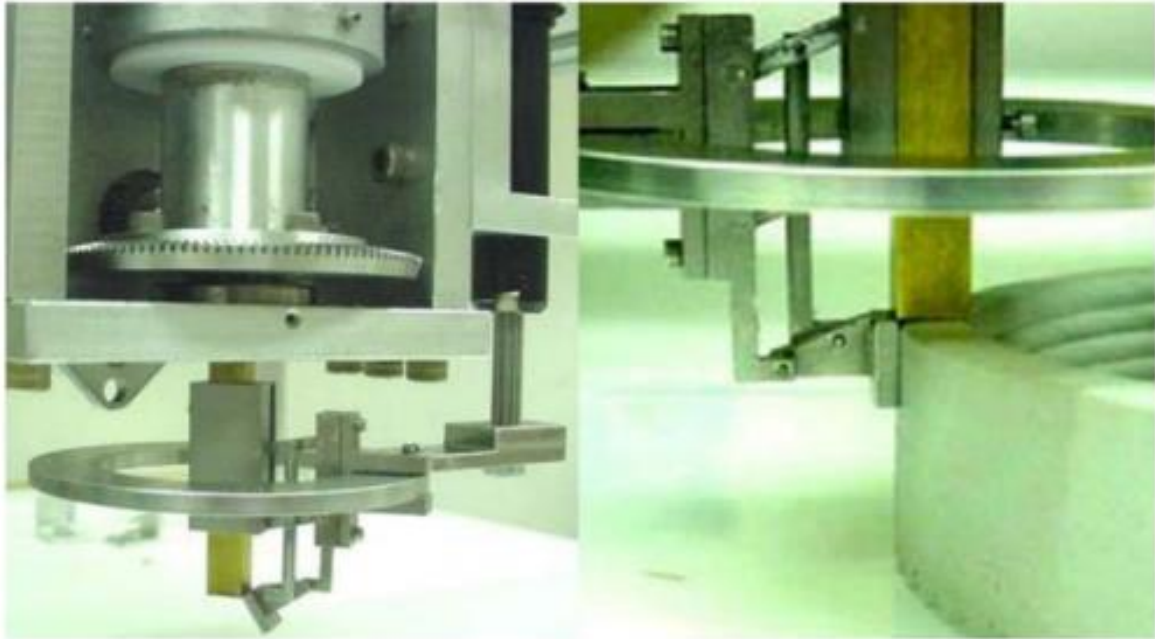


Figure 2.3. Trowel mechanism to shape different geometry [43]

Another key technique is particle-based 3D printing, which involves the selective deposition of binder liquid into a bed of powder or aggregates to bond the particles. A third method, the Digital Casting System, was initially developed by ETH Zurich and involved casting concrete with a short setting time into weak formworks [8] or a moving mould using the slip-forming method [65]. Additionally, Technische Universität Braunschweig developed Shotcrete 3D Printing (SC3DP) [66, 67], which sprays accelerated concrete using compressed air controlled at the printhead nozzle to build layers [68]. Among these techniques, CC is regarded as the most promising for large-scale structures and has already been applied in real construction projects [69]. Figure 2.4 shows some recent projects completed using this technique.



Figure 2.4. 3D printed projects based on the extrusion-based 3D printing technique. **(a)** House Zero in USA, **(b)** Humanity Central in USA, **(c)** Hobrobero House in Denmark (2021), **(d)** Serendix in Japan, **(e)** Beckum House in Germany, and **(f)** Milestone House in the Netherlands [70]

### 2.1.3. Fused Deposition Modelling

Fused Deposition Modelling (FDM) is the most commonly used technique for fabricating polymer-based materials, was first described in Crump's patent [44]. In this process, the thermoplastic polymer is extruded from a movable FDM head, deposited layer by layer, and solidified into the final part. Common materials include PC, PLA, and ABS. The polymer is heated to  $1^{\circ}\text{C}$  above its melting point and solidifies immediately upon deposition. The quality of printed parts is controlled by various parameters, such as layer thickness, printing

orientation, raster angle, velocity, pressure, temperature, and air gap. Sood et al. [56] and Chacon et al. [71] studied the effects of these parameters on the physical behaviour of composites, showing that part quality depends heavily on these process variables. Figure 2.5 shows the schematic diagram of FDM

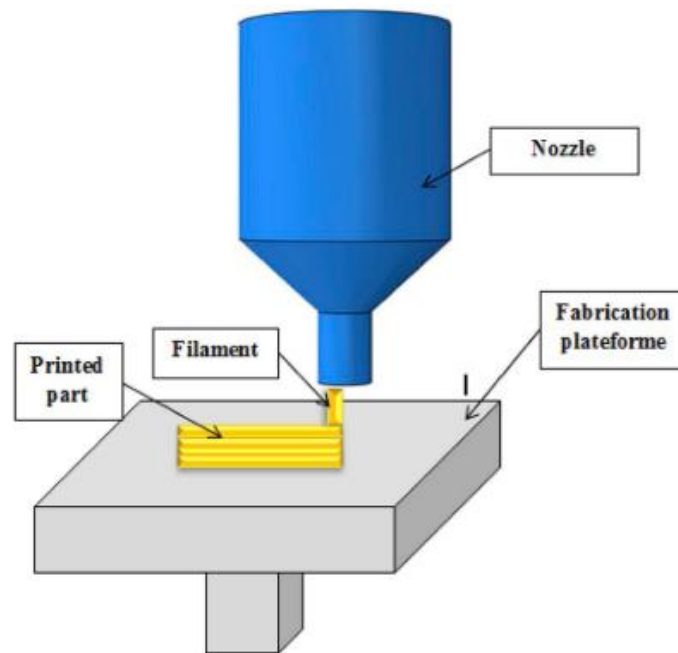


Figure 2.5. Schematic diagram of Fused Deposition Modelling (FDM) [44]

#### 2.1.4. Ink Jet Printing

The first patent for Ink Jet Printing (IJP) was awarded in 1951[44], and the technology was later developed at the Massachusetts Institute of Technology in 1993, transforming it into a rapid prototyping process. IJP involves the precise deposition of liquid materials through a nozzle, with ink droplets ejected by piezoelectric or thermal actuation. It has applications in printing complex composites, ceramic components, and scaffolds for tissue engineering [5, 72-74]. There are two main types of ceramic inks used in IJP: wax-based inks, which solidify on a cold substrate, and liquid suspensions, which solidify through evaporation. Factors such as particle size distribution, ink viscosity, solid content, nozzle size, and printing speed influence the quality of the printed parts [75]. However, limitations like fragile print heads, expensive ink cartridges, coarse resolution, and weak interlayer adhesion remain challenges [5].

Ongoing efforts aim to improve these limitations and advance ceramic AM using IJP technology. Figure 2.6 shows the schematic diagram of IJP technology.

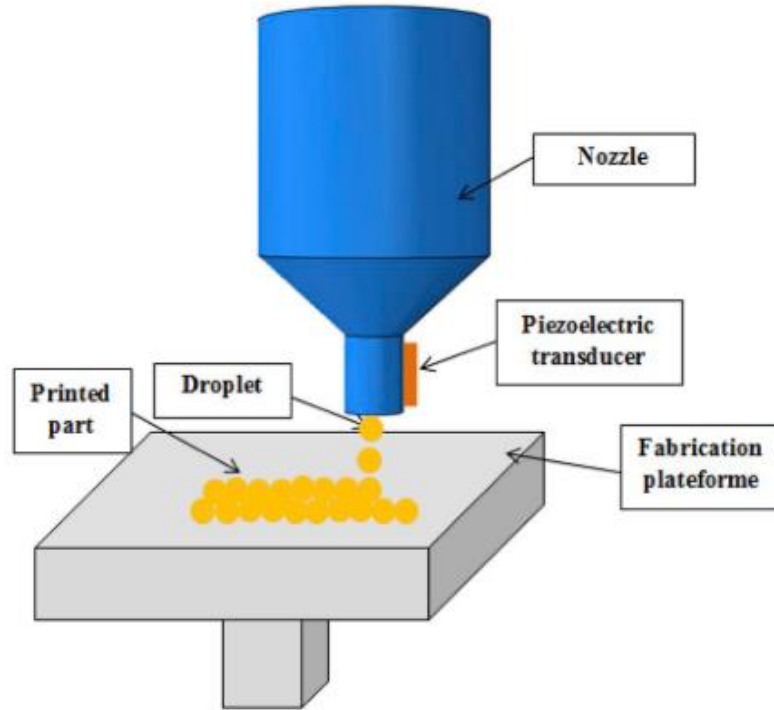


Figure 2.6. Schematic diagram of IJP technology and 3D printed parts with IJP technology [44]

#### 2.1.5. Stereolithography (SLA)

Stereolithography (SLA) is one of the earliest AM methods. It was developed in 1986 [44] and employs UV light or an electron beam to initiate a polymerisation chain reaction in a layer of polymeric resin or monomer solution. This process predominantly uses UV-active monomers, such as acrylic or epoxy, which solidify into polymer chains, enabling the layer-by-layer printing of parts [5, 75]. Ceramic-polymer composites can also be printed using ceramic particle dispersions in monomers, and polymer-derived ceramifiable monomers like silicon oxycarbide are sometimes used [75, 76]. SLA enables high-quality parts with fine resolutions as low as 10  $\mu\text{m}$ , though the size of printed parts is typically limited to 2 cubic feet [75-78]. Post-treatments, such as heating or photo-curing, are often required to enhance the mechanical properties of SLA-printed parts [5]. However, SLA has several limitations, including slow

processing speeds, high costs, and a restricted range of materials. The kinetics of the curing process, which depend on factors such as light energy and exposure, control layer thickness [79]. Despite these challenges and the high cost of photopolymers, SLA remains effective for producing complex nanocomposites [32], though mechanical property issues may persist in the final components [5]. An example of printed materials using the SLA technique is depicted in Figure 2.7.

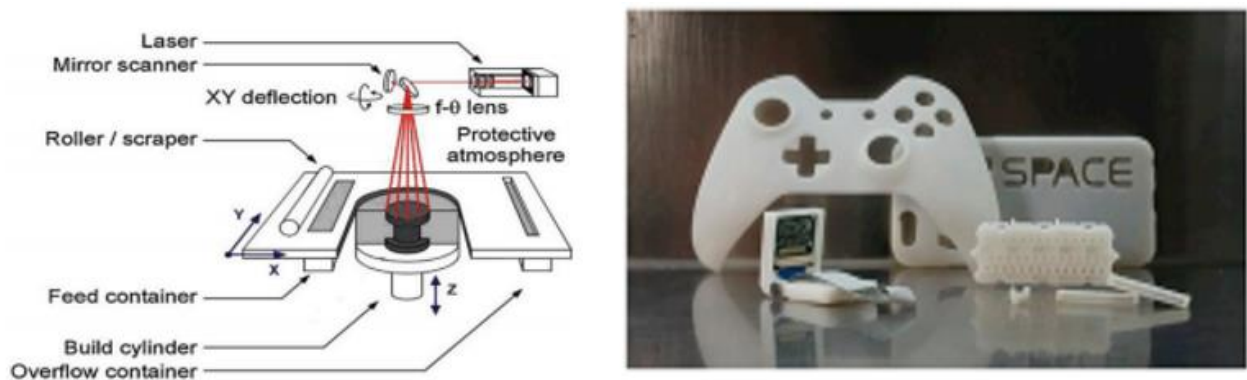


Figure 2.7. schematic diagram of SLA technology and 3D printed systems using SLA technology [44]

### 2.1.6. Powder Bed Fusion (PBF)

Powder Bed Fusion (PBF) involves the layer-by-layer fusion of fine powders to create 3D parts. A laser beam or binder fuses each layer of powder spread on a platform, with excess powder removed after fusion. Additional steps like coating, sintering, or infiltration may be required to enhance part quality. The effectiveness of PBF depends on factors like powder size distribution and packing, which affect the density of the printed part [5]. Two main variations of PBF are Selective Laser Sintering (SLS) and Selective Laser Melting (SLM). SLS works with various polymers, metals, and alloy powders by raising the local temperature to facilitate molecular fusion, without fully melting the powders. SLM, on the other hand, fully melts the powders, resulting in better mechanical properties, but is typically limited to metals like steel and aluminium [5, 80]. Key parameters in the sintering process include laser power and scanning speed [80]. Figure 2.8 shows the schematic diagram of SLS.

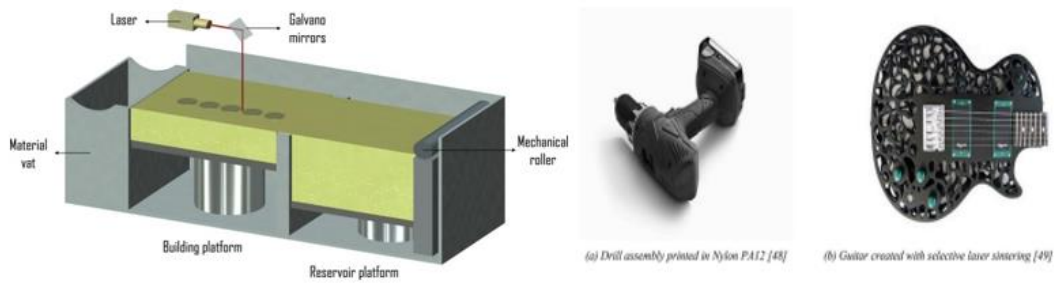


Figure 2.8. schematic diagram of SLS technology and 3D printed systems using SLS technology [44]

### 2.1.7. Directed Energy Deposition (DED)

Directed Energy Deposition (DED), also known as laser solid forming (LSF), Laser Engineered Net Shaping (LENS), Directed Metal Deposition (DMD), Electron Beam AM (EBAM), and Wire + Arc AM (WAAM), is used for manufacturing high-performance super-alloys [5]. It involves using a laser or electron beam to melt feedstock material (powder or wire) while depositing it onto a substrate to create solidified layers [81]. DED systems can use either powder or wire feedstock [82]. Powder-based DED typically uses a coaxial nozzle to deliver metal powder into the melt pool created by a laser, while wire-fed DED (such as WAAM) feeds a continuous metal wire into the heat source, which is often an electric arc or laser [82]. Wire-fed systems generally offer higher deposition rates and lower material waste, whereas powder-based systems provide better precision and are more common in aerospace applications [82].

Unlike powder bed methods, DED does not require a powder bed and melts the material before deposition, making it suitable for retrofitting parts and filling cracks. DED supports multiple-axis deposition, allows the use of multiple materials, and can be combined with subtractive processes. It is commonly employed with materials like titanium, Inconel, stainless steel, and aluminium alloys, particularly in aerospace applications. While DED is known for its high speeds and ability to handle large components, it has lower accuracy and surface quality compared to methods like Selective Laser Sintering (SLS) or Selective Laser Melting (SLM). DED is ideal for large, low-complexity components and repairing larger parts [81]. The method offers reduced manufacturing time and cost, excellent mechanical properties, controlled microstructure, and accurate composition control, making it valuable in industries such as automotive and aerospace, especially for turbine engine repairs. Figure 2.9 shows 3D-printed partes with DED.



Figure 2.9. 3D-printed parts with DED [44]

#### 2.1.8. Laminated Object Manufacturing

Laminated Object Manufacturing (LOM), one of the earliest AM methods, was developed in 1986 and patented in 1987 [7]. LOM involves the layer-by-layer cutting and lamination of materials such as polymer composites, ceramics, paper, and metal-filled tapes. Successive layers are cut and bonded using thermal bonding, making it applicable in industries like paper manufacturing, foundry, electronics, and smart structures. A subclass of LOM, Ultrasonic AM (UAM), combines ultrasonic metal seam welding with Computer Numerical Control (CNC) milling. While LOM offers advantages such as lower tooling costs and reduced manufacturing time for larger structures [5], it has limitations like lower surface quality, dimensional accuracy, and time-consuming removal of excess material. It is less suited for complex shapes. UAM enables the construction of metal structures at low temperatures and the integration of electronic devices. LOM's potential lies in reducing tooling costs and manufacturing time, making it suitable for larger structures [5]. Tables 2.1 and 2.2 illustrate the classification of AM processes and the advantages and limitations of AM processes, respectively.

Table 2.1. Classification of AM processes

Methods	Material	Technologies	Resolution range	Application	Power source
Material extrusion	Ceramics or clay (CC)	Fused Deposition Modelling	FDM (50-200µm)	Toys Rapid prototyping	Thermal energy (FDM) Mechanical (CC)
	Thermoplastics (FDM)	Contour Crafting	CC (10 -50 mm)	Large structures building	
Inkjet Printing	Ink or paste (e.g., ceramic slurry, photopolymer)	Inkjet	50-200µm	Biomedical industry Automotive industry	Piezoelectric or thermal energy
Vat polymerization	Hybrid polymer ceramics	Stereolithography (SLA)	10µm	Biomedical prototyping	Ultraviolet laser
Powder Bed Fusion	Powder	Selective Laser Sintering	80-250µm	Automotive	Electron Beam
	Metals	Direct Metal Laser Sintering		Aerospace	High powered laser beam
	Alloys	Sintering		Biomedical	
	Polymers ceramics	Selective Laser Melting Electron Beam Melting		Electronics Light weight structures	

Directed Energy Deposition	Metals and Alloys in powdery form Ceramics and polymers	Laser Engineered Net (LENS) Electronic Beam Welding (EBW)	250µm	Aerospace Biomedical Repair Cladding and retrofitting	Laser beam
Sheet lamination	Ceramics Paper Metal rolls Polymer composite Metal-filled tapes.	Laminated Object Manufacturing (LOM)	Dependent on laminate thickness	Manufacturing of paper Electronics Smart structures.	Laser

Table 2.2. Advantages and limitations of additive manufacturing processes.

Methods	Advantages	limitations
Material extrusion (CC)	Cost efficient.	Poor surface finish
	Multi-material printing	Size variance due to expansion
	Post extrusion alteration simple	Layer-by-layer finish
Inkjet Printing	Wide range of colours for printing	Coarse resolution
	Decent range of materials	
	Time efficient	Layer-by-layer finish
Vat polymerisation	High printing quality	Slow printing process
	Good accuracy and decent surface finish	Limitation of material
	Fine resolution	Relatively expensive
	High speed	
Powder Bed Fusion	Low cost	Requires post-processing.
	High accuracy	High power usage
	Wide range of materials	Slow printing process
	Powder recycling	Not cost efficient
Direct Energy Deposition	Reduced material waste.	Low resolution

	<p>Ability to manufacture large components.</p> <p>Time and cost efficient.</p> <p>Can be used for repair and retrofitting.</p>	<p>Low accuracy and surface quality</p> <p>No support structures</p> <p>Capital cost is high</p>
Sheet lamination	<p>Low cost</p> <p>High surface finish</p> <p>Time efficient</p> <p>Wide range of materials</p> <p>Production of large structures</p>	<p>Difficulty in manufacturing complex shapes.</p> <p>Potential for high material waste.</p> <p>Post-processing is required.</p>

## 2.2. 3D Printing Materials

Research on 3D printing materials is crucial for advancing AM technology. Different materials have been developed to meet diverse industry needs. This research investigates the use of cement-based materials for 3D printing. Cement-based material such as concrete has gained significant attention in recent years, as AM technology expands to construction applications. Concrete is the most widely used building material globally, known for its strength, durability, and versatility in shaping [1]. However, adapting this material for 3D printing presents unique challenges and requires the development of specialised mixtures and printing techniques. Various research studies have focused on optimising concrete formulations for 3D printing. The composition of printable concrete typically includes a combination of cementitious materials (such as cement or cement-replacers), aggregates (such as sand or gravel), water, and sometimes admixtures or additives to enhance specific properties [83, 84]. Researchers have explored the use of different cement types, including Portland cement and alternative materials like fly ash or slag, to improve the workability, setting time, and mechanical performance of the printed concrete [10, 85, 86]. The development of suitable printing techniques is another crucial aspect of concrete 3D printing research. Extrusion-based methods, such as robotic arm or gantry systems, are commonly employed, where concrete is deposited layer by layer to form the desired structure. Researchers have focused on optimising the printing parameters, including nozzle design, layer thickness, printing speed, and support strategies, to achieve accurate and stable prints [70, 87-89]. Overall, the research on 3D printing materials is driven by the need for advanced materials with specific properties to meet the expanding applications of AM.

### 2.2.1. Overview of cement-based 3D printing Materials

### 2.2.2. Cement-based materials

Cement-based materials, particularly concrete, are among the most widely used building materials globally due to their availability, affordability, and desirable properties, such as strength in compression, durability, and fire resistance [1]. Concrete is versatile and capable of being moulded into various shapes because of its fluid state during application. It consists of granular materials like sand or gravel, bound by a matrix formed through the hydration of

cementitious materials (such as cement or substitutes like fly ash) and water. By incorporating additives, admixtures, aggregates, and cement-based materials, specific properties such as self-compaction, high strength, low CO<sub>2</sub> emissions, and ductility can be achieved. Despite the widespread use of established compositions, researchers continue to explore alternative variants [1]. However, concrete production faces significant challenges. One major issue is the energy-intensive nature of cement production, particularly the kiln-burning process, which significantly contributes to global CO<sub>2</sub> emissions. Another challenge in the concrete industry is the physical labour required, especially for in situ cast concrete. The erection of moulds and the placement of reinforcement often rely on physically demanding work, which is particularly problematic when constructing complex or customised geometries. This can lead to health issues for construction workers, especially in light of the ageing workforce in many developed countries. The US Department of Labor's Occupational Health and Safety Administration (OSHA) identifies several hazards in the concrete industry, including eye, skin, and respiratory irritation from cement dust, unsafe equipment, inadequate lockout/tagout systems, overexertion, awkward postures, slips, trips, falls, and chemical burns from wet concrete. Moreover, the efficient use of materials is another challenge in the industry. The low cost of raw materials discourages the adoption of structurally optimized geometries, leading to a preference for geometric simplicity over material efficiency. The manufacturing of moulds also contributes to inefficiencies, further complicating efforts to adopt more advanced and sustainable design practices [1]. To successfully 3D print objects using cement-based materials without visible cracks or large pores, it is essential to ensure the right mechanical properties and optimisation of printing parameters. Cement-based materials are widely used due to their high strength, durability, and fire resistance [90]. Their initial fluid state allows them to be moulded into various geometries and shapes, making them suitable for future construction applications [90].

### 2.2.3. Cement mix design

A major challenge in the aspect of 3D printing of cement-based materials lies in the selection of raw materials and the optimisation of mix design to meet essential process-related material properties such as pumpability, extrudability, and buildability. These attributes are crucial for ensuring the success of 3D printing and extend far beyond the conventional requirements specified in concrete codes and guidelines, which are typically defined by consistency classes

and workability tests. Numerous studies have been conducted to identify suitable raw materials and refine mix proportions for 3D printing of cement-based applications [91]. It is important to note that there is no standardised mix design for 3D concrete printing. Various types of binders, such as Portland cement, sulfoaluminate cement, composite cements, and geopolymers, have been used [92-98]. In terms of aggregates, materials such as natural sand, lightweight aggregates, and even solid-waste-based aggregates, such as copper tails, iron tails, and recycled aggregates, have been incorporated into 3D printing applications [87, 99-101]. Furthermore, additives like silica fume, nano-clay, nano-silica, and viscosity-modifying agents (VMAs) have been employed to modify the rheological properties of fresh concrete [102-105]. Table 2.3 presents the mix designs and descriptions of materials used for 3D printed of cement-based materials.

Table 2.3. Mix design and descriptions

Materials	Description
Ordinary Portland cement (OPC)	There are different types of OPC: ASTM 150 type II (American standards), CEM I 52.5, CSA A 3000-08 (Canadian standards) and class H oil well cement. The most commonly used type is CEM I 52.5, because of its pure state.
Fine aggregates	This is a combination of natural sand and crushed stoned. The main size of aggregates used for 3D printing of cement-based material is within the range of 0.5-2 mm. Although in some reports, the particle size used was 0.06 mm, no one has ever reported using over 2 mm aggregate size [106]. The material constituent may include sand, gravel, slag, recycled concrete, crushed stone and geosynthetic aggregates.
Clay	Clay is a naturally occurring crystalline soil mineral. The material develops plasticity when it is wet as a result of the molecular film of water around the clay particles. The hardened properties of clay include brittleness, hardness and non-plastic at the drying point or firing. The grain size are less than 4 $\mu m$ .
Silica Fume	Silica fume can also be called micro-silica and is a by-product of the ferrosilicon industry. It is an ultra-fine powder. It is used to enhance the mechanical and durability properties of concrete.

Fly Ash	Fly ash is often used in most studies. The product is obtained from burning pulverised coal in electric-powered generating plants. It is a supplementary Cementitious Material (SCM) when producing Portland cement concrete [85]. It helps to increase the strength of concrete hereby contributing to the hardened properties of concrete through pozzolanic or hydraulic activity. Fly ash also has the ability to reduce water demands, permeability and shrinkage of the final product whilst improving workability of fresh concrete.
Ground Granulated Blast-Furnace Slag (GGBS)	GGBS is used as a supplementary cementitious material in concrete, often replacing a portion of cement to improve the durability, strength, and sustainability of the concrete.
Fibre	Continuous research on the application of fibres in the 3D printing of concrete is currently ongoing. The common types of fibres used are PVA, HDPE and polypropylene. In most cases, the fibre size is 6 mm.
Admixtures	Several admixtures are used in the 3D printing of concrete. The most common ones are superlatives, viscosity modifying admixtures (VMA) and high range water-reducing agents. Others include corrosion-inhibiting admixtures and acceleration admixtures.

Recent research has focused on developing new materials and methods for 3D printing of cement-based structures. The primary materials used for extrusion-based AM are cement-based composites, which consist of cement, admixtures, fine aggregates, secondary cementitious materials, air, and water. These materials are designed for nozzle extrusion and aim to achieve prolonged workability before extrusion and high early strength to support subsequent layers [106]. To achieve these requirements, the addition of various additives and admixtures to the cement mixture is crucial. Additives, such as limestone, silica fume, fly ash, and nano-silica, are incorporated into the dry mix to enhance both the mechanical and physical properties of the cementitious structures. The mechanical properties that can be improved include compressive strength, tensile strength, and flexural strength [107, 108]. Additionally, admixtures like superplasticisers, air-entraining agents, accelerators, shrinkage-reducing agents, water-reducing agents, and viscosity-modifying agents are mixed with the cement during the preparation process. These admixtures serve various purposes, such as reducing

water content, improving hardening or setting times, enhancing workability, and modifying the rheological properties of the cementitious structures [109].

Le et al. [110] used an extrusion-based methodology, preparing a cement-based mortar with silica fume, cement, sand, polypropylene fibre, and fly ash as key ingredients. The optimal mix design was found to be 83 kg/m<sup>3</sup> of silica fume, 579 kg/m<sup>3</sup> of cement, 1241 kg/m<sup>3</sup> of sand, 165 kg/m<sup>3</sup> of fly ash, and 232 kg/m<sup>3</sup> of water. Using a 9 mm diameter nozzle, the printed samples achieved compressive strengths between 75 and 102 MPa. Similarly, Lim et al. [20] optimised a mix of gypsum and cement for 3D printing, achieving compressive strengths of 100–110 MPa in their tests.

The rheological properties of cement matrices continuously evolve due to the hydration process, which limits the "open time" available for 3D printing. Initially, the fresh cement matrix is relatively easy to extrude; however, as time progresses, the viscosity of the mixture increases, resulting in reduced workability. Eventually, the matrix becomes too rigid to be extruded effectively [111]. Although the stiffening of the cementitious matrix complicates the printing process, this phenomenon is essential for providing sufficient support to the initial layers of the structure. This behaviour is closely linked to the build-up rate of the cement matrix, which can be monitored through the evolution of yield stress over the hydration period. Yield stress is the stress required to initiate flow in the material [112, 113]. For the purpose of 3D printing applications, it is essential to define the terms workability, printability, and buildability. Workability refers to the period when the material remains extrudable after initial contact with water, depending on a suitable rheological state that allows the cement to flow effectively through the printing system. Buildability is the material's capacity to be printed in multiple layers while maintaining a defined geometry, requiring the concrete to be sufficiently mouldable and cohesive so that each new layer adheres properly and supports the subsequent layers without deformation. Printability, or extrudability, pertains to the concrete's ability to pass through the nozzle of the printing head, involving the ease with which the material can be pumped and extruded to form continuous, stable layers. Additionally, printing parameters such as printing speed and pumping pressure play a significant role in achieving the desired workability, printability, and buildability, as they directly impact the extrusion process and the stability of the printed layers

Li et al. [114] investigated various cementitious mixtures and found that the rheological properties, particularly thixotropic behaviour, are key factors affecting the pumpability and

printability of the mixtures. Gosselin et al. [115] developed a method where materials are combined at the printhead just before extrusion. In this process, the printing mortar and the accelerator are pumped through separate tubes and mixed at the printhead, allowing for better control over the rheology of the mortar. This method helps maintain the premixed mortar's properties for a longer period, while ensuring the already printed layers retain their strength, enabling the construction of large, complex structures using a six-axis robotic arm without temporary supports. This innovation allows for precise control over material behaviour during and after extrusion.

To enhance the buildability of 3D-printed structures, Kan [116] reported that when aluminium sulphate exceeds 9%, the cement transitions to a quick-setting state, which also increases the fluidity of the cement mixture. The addition of aluminium sulphate generally increases the compressive strength of cement by approximately 5 MPa at 3 and 7 days. However, the compressive strength at 28 days varies: it increases when the aluminium sulphate content is between 6% and 8% but decreases when the content is around 5% or exceeds 8%. The flexural strength of cement at 1 and 28 days tends to decrease gradually as the aluminium sulphate content increases. Additionally, aluminium sulphate significantly increases the dry shrinkage of cement, with more significant shrinkage observed at higher contents, except when the content is at 5%.

Other studies focused on the spraying of alkali-free setting accelerator at the print head on-demand [117, 118]. A dosage of 2.5% accelerator by weight of the binder increased the Bingham yield strength by sixfolds when compared with the reference paste. This effect was attributed to the fact that the alkali-free accelerator (primarily composed of aluminium sulphate), accelerated the crystallisation of ettringite [117]. Ettringite is a crystalline compound formed when the accelerating admixture is sprayed onto the surface of the 3D-printed cement-based structure [117, 119]. Consequently, the use of accelerators impacted the microstructure, thereby influencing the rheology, as discussed by numerous researchers [117, 120, 121]. Therefore, the addition of an accelerator directly affects the rheological behaviour, setting and hardening of the mix, ultimately impacting buildability.

A study conducted by Bhattacharjee and Santhanam [117] concluded that higher dosages of accelerators significantly reduced the setting time of cement-based materials. An 8% accelerator reduced the setting time to 4.5 minutes, while a 2% dosage decreased it from 3 hours 15 minutes to 2 hours 30 minutes. Penetration resistance tests with 1, 2 and 3%

accelerator dosages showed that the initial resistance was corresponding to 3.43 N/mm<sup>2</sup> and the final setting time to 26.97 N/mm<sup>2</sup>. A 3% accelerator reduced the initial setting time to 3.5 hours and the final setting time to 6.2 hours, with build-up starting after 2 hours. The 1 and 2% dosages also reduced setting times by about 1.5 and 1.0 hour, respectively. Higher dosages accelerated ettringite formation, promoting faster build-up. In another study, Bhattacharjee and Santhanam [122] observed that when aluminium sulphate was used as an accelerating agent and sprayed on-demand on the surface of 3D-printed cement-based structures, it increased flocculation and the rate of hydration, enhancing the yield strength of the outer layer. This strengthened outer layer acted as a sacrificial barrier, preventing plastic deformation under subsequent loads [117]. Furthermore, when the accelerating admixture was sprayed at a distance of 50 mm from the surface, X-ray diffraction tests showed ettringite formation up to a depth of 5–7 mm from the surface, with no ettringite found beyond this depth. Ettringite contributed to the early strength development and stability of the surface layer, but it was not detected beyond this depth, indicating its localised effect.

Tay et al. [123] investigated the time-dependent rheological behaviour of printable materials and linked low bond strength to an increase in the storage modulus ( $G'$ ) of the first layer as the time gap increased between layers. Similarly, Nerella et al. [124, 125] attributed poor bond strength to the formation of micro-pores in the interlayers of 3D printed samples, which resulted from extended time gaps between consecutive layers.

Le et al. [110] emphasised that extrudability and buildability are the most critical fresh properties in cementitious structures. In their study, they developed a high-performance mix with a sand-to-binder ratio of 3:2, which included 20% fly ash, 70% cement, and 10% silica fume, supplemented by 1.2 kg/m<sup>3</sup> of polypropylene fibre, with a length of 12 mm and a diameter of 0.18 mm. The mixture also had a water-to-binder ratio of 0.26 and incorporated 0.5% retarder and 1% superplasticiser by weight of the binder. This optimised mix was capable of smooth extrusion through a 9 mm diameter nozzle, while the resulting layers exhibited the strength to support 61 additional layers without significant deformation at the base. The mixture also demonstrated an open time of 100 minutes. To evaluate the compressive strength, a target of 110 MPa at 28 days was established, and the actual compressive strength surpassed this target upon testing.

Zhong et al. [126] explored the use of 3D printing in developing a strong and conductive geopolymer nanocomposite structure, concluding that graphene, owing to its high mechanical

strength, electrical conductivity, and mechanical stability, could effectively enhance the properties of cementitious materials. For fine resolution in printing, a mix of polyvinyl alcohol (PVA) and rapid-hardening cement was utilised. Despite issues such as the formation of voids and layer delamination, post-curing the samples in water mitigated these faults.

Kazemian et al. [127] identified Portland cement as the most viable material for large-scale use in automated construction processes, citing its unique fresh and hardened properties. The material can also be customised with readily available admixtures to optimise performance. In their study, they focused on a mixture of ASTM C150 type Portland cement and fine aggregate with a maximum particle size of 2.36 mm. The addition of nano-clay and silica fume significantly improved the shape stability of 3D-printed cement paste, where shape stability refers to the printed layers' resistance to settlement and deformation from the weight of subsequent layers [5].

Al Jassmi et al. [64] emphasised the importance of finding a balance between printability and buildability in 3D printing. They highlighted the significance of the time interval between layers, as it affects adhesion and bond strength. It was noted that material properties and the printing process must be carefully designed to ensure that the bottom layers can adequately support the load of the upper layers. They also pointed out that various parameters, such as linear speed, layer thickness, the number of printed layers, part diameter, and output characteristics (like layer height, width, surface roughness, and vertical profile), can be adjusted to improve the printing process.

Jianchao et al. [128] examined the production of mortar using two types of cement: Ordinary Portland Cement (OPC) and Sulphoaluminate Cement (SAC). The key differences between these cements are their plasticizers, setting time controllers, and volume stabilization agents. OPC is characterised by a longer setting time and slower hydration, while SAC has a shorter setting time and higher early strength. SAC was deemed more suitable for 3D printing due to its higher early strength and rapid setting time, which are critical in a layer-by-layer printing process, allowing the lower layers to support subsequent ones [5]. However, the structural performance of 3D-printed elements remains unpredictable due to variability in mechanical properties. This variability arises from both inherent material differences and process-related inconsistencies. The distinct additives and hydration kinetics of OPC and SAC result in differences in early strength and setting behaviour. Some researchers have attempted to enhance strength by incorporating glass fibres into the cementitious mix, but these materials

were found inadequate for horizontal load-bearing components such as staircases and slabs [64]. Nevertheless, 3D printing proved useful in the production of materials, into which conventional cementitious materials could be poured. These moulds, becoming part of the final product, offer the advantage of producing complex shapes that are difficult to achieve through traditional casting methods [64].

Hambach et al. [129] explored mixing Portland cement with short fibres of carbon, glass, and basalt (3–6 mm). The mix design included 61.5% Portland cement, 21% silica fume, 15% water, 2.5% water reducer, and 0.3% of a retarder (Pantarhol 85) to slow down cement thickening during printing. The study found that the mix achieved a flexural strength of 30 MPa and a compressive strength of 80 MPa.

Several studies have been conducted to enhance the interlayer bonding strength of 3D-printed mortar [9–12]. These studies focus on optimising material composition and adjusting printing parameters to improve the adhesion between successive layers of mortar, which is crucial for ensuring the structural integrity and durability of 3D-printed concrete elements. Additionally, the interlayer bonding strength of 3D-printed mortar is affected by curing conditions, as highlighted in several studies [130, 131]. Rashid et al. [130] investigated the influence of different curing environments on the bonding strength between mortar and polymer cement mortar interfaces. Their findings indicated that moisture had an insignificant effect on interlayer bonding strength. In contrast, Weng et al. [131] reported that the interlayer bonding strength was significantly enhanced under water-curing and climate chamber-curing conditions. These contrasting results suggest that the impact of curing conditions on the bonding strength at the interface remains a subject of debate, necessitating further research to clarify these effects.

Wolfs et al. [132] reported similar findings regarding the factors influencing inter-layer bond strength. According to Sanjayan et al. [133], the loss of surface moisture is one of the primary factors affecting inter-layer strength, along with process parameters, evaporation rate, and bleeding rate. Roussel [134] further confirmed the impact of moisture loss by comparing the bond strength of interfaces protected from drying with those exposed to drying. His findings revealed that the interface strength was 90% higher when the material was protected from drying compared to the reference material.

Feng et al. [135] investigated the mechanical behaviour of 3D-printed cementitious elements, revealing how the printing process affects structural performance through mechanical tests,

Finite Element Modelling (FEM), and microscopic observations. They identified a pronounced orthotropic behaviour resulting from the layer-by-layer printing process, which influenced the elastic modulus and compressive strength but not the failure mode. Their results demonstrated that extrusion-based processes yield components with anisotropic properties, significantly impacting load-bearing capacity. FEM analysis further confirmed that the printing direction plays a vital role in the structural load-bearing capacity.

In addition to traditional concrete, researchers have developed various specialised concrete with enhanced properties in their hardened states, including High-Performance Concrete (HPC) [84, 110, 136], strain-hardening cement-based composites (SHCC/ECC) [137-140], and even printable foam concrete [141-143]. With regard to 3DPC mix design, several optimal mixture proportions have been proposed for specific applications [144-146], and empirical methods for mix design have been formulated to guide the development of printable concrete [147, 148].

### **2.3. Fresh properties of cement-based materials**

The fresh properties of concrete, such as flowability, extrudability, buildability and open time, are critical to the success of 3D printing of concrete. These properties determine the material's ability to be extruded smoothly through a printer nozzle, maintain its shape once deposited, and bond adequately between layers. Proper control of these factors ensures precision in printing, structural integrity, and overall durability of the final product. Without optimised fresh properties, 3D printed concrete structures may suffer from defects, poor performance, or failure during construction.

#### **2.3.1. Flowability**

Flowability refers to a material's ability to move smoothly from the mixer to the print nozzle. This property is crucial for evaluating the flow behaviour of fresh material within the pumping system [114]. Flowability can be assessed through both qualitative and quantitative methods. Qualitatively, simple tests like the flow table and slump flow tests are commonly used, while the quantitative approach typically involves rheometer tests that characterise the material's flow by measuring key parameters such as plastic viscosity and yield stress. The flowability of the

material is essential for smooth transportation from the storage tank or concrete mixer to the printing head while ensuring the right consistency for deposition. A key challenge is balancing the high workability needed for easy pumping with the stiffness required for the extruded material to retain its shape once deposited [149].

Flowability depends on several factors, such as the mix design and even the setup of the pump. These include the pumping distance, the pumping method, and the diameter of the hose. Longer pumping distances demand careful control over the material's properties to prevent changes in its consistency during transport [150]. The choice of pumping methodology, such as rotor-stator pumps or piston pumps, also affects how the concrete behaves under pressure. Additionally, the diameter of the hose must be matched to the material's viscosity and aggregate size to prevent blockages [4].

Tay et al. [151] introduced a dimensionless parameter termed the flowability index to estimate the flowability of concrete mixtures. In their study, the weight of the mixture transported through the pump operating at a constant speed of 2890 rpm over a duration of 30 seconds was measured, and the flow rate was determined in terms of volume per second. The flowability index was calculated as the ratio of the flow rate of the concrete mixture to that of water. The results demonstrated that the flowability index is directly proportional to the slump-flow value of the samples, meaning higher slump-flow values correspond to a higher flowability index. Conversely, the index was found to be inversely proportional to the pumping speed required to maintain a consistent flow rate, indicating that as the pumping speed increases, the flowability index decreases. A sliding pipe rheometer [149] measures flowability by establishing a relationship between the concrete flow rate and the pressure exerted at the piston head. Other techniques for assessing pumpability include the use of rheographs, viscometers, tribometers, and rheometers, all of which are commonly employed in practice. These methods provide insights into the rheological behaviour of concrete, helping to evaluate its flow properties under different conditions.

### 2.3.2. Extrudability

Extrudability refers to the ability of the material to pass through the printing nozzle continuously and in an intact filament [84]. Similar to flowability, extrudability can be evaluated through both qualitative and quantitative approaches. Most studies focus on the

qualitative aspect, where a material is deemed "extrudable" if it retains its shape and shows no imperfections along a long extrusion path, usually between 1-2 m [106]. For example, Le et al [110] assessed extrudability by examining the stability and continuity of printed filaments, which extended to a total length of 4500 mm from the nozzle. Quantitatively, extrudability is determined using flow tables and rheometers to measure flow consistency and filament integrity [106]

The nozzle plays a crucial role in the extrusion process, being responsible for shaping the concrete layer and influencing its appearance during the printing process. Various nozzle orifice shapes are utilised, including rectangular, square, circular, and elliptical, with the selection depending on the specific application. Circular nozzles, for instance, facilitate ease of printing at corners or when there are changes in the angle of the structure. However, the reduced contact area between the extruded beads may compromise the stability of the printed layers [152]. Conversely, a square orifice tends to provide better surface finish [63] and offers greater ease in construction [153] compared to circular or elliptical orifices. To prevent twisting of the freshly deposited layer, the nozzle should be oriented tangentially to the tool path [1]. The dimensions of the orifice used in extrusion are also determined by the shape and size of the objects being printed.

The principle of ram extrusion and its application in testing the extrudability of cement mortars has been explored, each contributing unique methodologies for evaluating this key property in 3D printing. Perrot et al. [154] applied the principle of ram extrusion to investigate the extrudability of cement mortars, an essential property for 3D printing applications. Ram extruders are employed to evaluate how well the material can be extruded, focusing on its continuous flow during the printing process. Other methods used to measure extrudability include the Penetration Resistance Method [91] and the Squeezing-Test Method [155], both of which provide alternatives for characterising the ease with which cementitious materials can be extruded. Ma et al. [87] introduced a novel approach to measuring extrudability, focusing on the electric power consumed and the flow rate of the material, which helped to optimise the printing process. Their study identified a close relationship between extrudability, extrusion rate, and printing speed, providing a more holistic view of the factors affecting print quality. Nerella et al. [156] also explored a method to evaluate extrudability using 3D printing, measuring the energy required for extrusion based on the electrical power consumed and the

flow rate, further contributing to the understanding of material behaviour under extrusion conditions.

### 2.3.3. Buildability

Buildability refers to the material's ability to resist deformation under load, particularly during vertical deposition [10, 156]. It directly influences the structural stability of the 3D-printed object [106]. For optimal buildability, the material must have sufficient strength immediately after extrusion to support its own weight and the weight of subsequent layers and withstand the extrusion pressure. If these properties are not adequately met, the structure risks deformation or collapse. Figure 2.10 provides a schematic representation of vertical and horizontal deformation in deposited filaments through a circular nozzle.

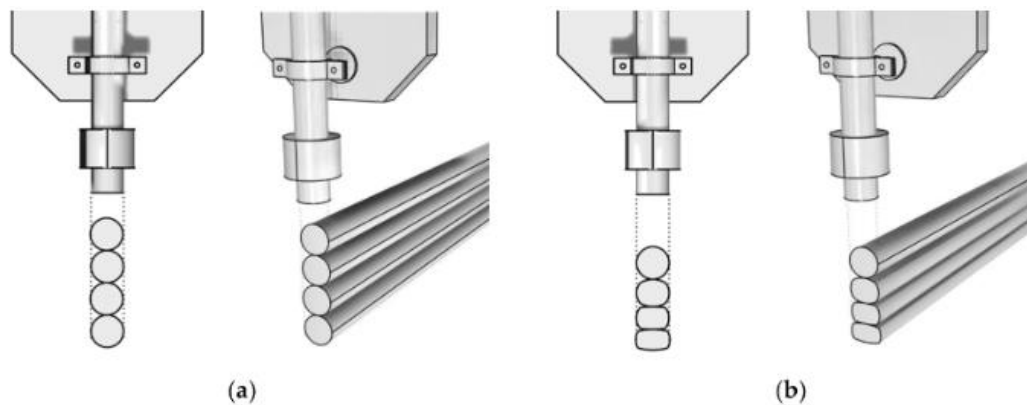


Figure 2.10. Schematic illustration of vertical and horizontal deformation of deposited filaments through a circular nozzle, showing (a) theoretical and (b) practical geometry [114]

As with other 3D printing methods, buildability can be assessed through both qualitative and quantitative approaches. One of the simplest qualitative methods involves printing multiple layers and then measuring the compression of the bottom layer under the weight of the upper layers. However, this approach has a significant drawback: material wastage due to multiple trials. To address this issue, researchers developed the stacking plate method. This experimental apparatus simulates the layer-by-layer structure of 3D printing by applying fixed weights and measuring the height reduction of each layer, thereby simulating real printing conditions without excessive material waste [106]. Another quantitative method is the cylinder stability test, used by Kazemian et al. [127]. This test employs a semi-cylindrical device to measure the height collapse of the filament under constant pressure. It provides a more controlled environment for assessing buildability by monitoring the filament's stability under

uniform load. Figure 2.11 shows the different methods used to test buildability. To improve buildability, Rubio et al. [157] and Rushing et al. [145] have suggested incorporating fibres into the mix. Additionally, Zhang et al. [91] found that the inclusion of silica fumes or nanoclay enhances the yield strength of the material, which in turn improves its buildability. Attapulgite nano-clay has been identified as highly effective in enhancing the buildability of 3D concrete printing (3DCP), and its use is recommended by numerous researchers [158-160]. The incorporation of calcium sulphoaluminate cement in the mix has also been shown to increase hydration and accelerate the rate of structural build-up in the mortar, thereby further improving the buildability of 3DPC mixes [96, 161]. Additionally, the use of accelerators, either added to the mixer or at the print head, has been reported to significantly enhance buildability [118, 162]. For instance, Nerella et al. [118] applied an alkali-free setting accelerator at the print head, while Bhattacharjee et al. [118] used an alkali-free accelerating admixture post-printing by spraying it onto the printed structure. These strategies have proven effective in promoting faster setting and structural stability in 3DCP. Insufficient buildability can lead to vertical and horizontal deformation of deposited layers, causing significant changes to the filaments' structure [114]. This problem can arise from various factors, such as inadequate printing speed in the height direction, resulting in a short time interval between layer depositions. Additionally, the mix design properties, such as a slow setting time, can further contribute to these deformations.

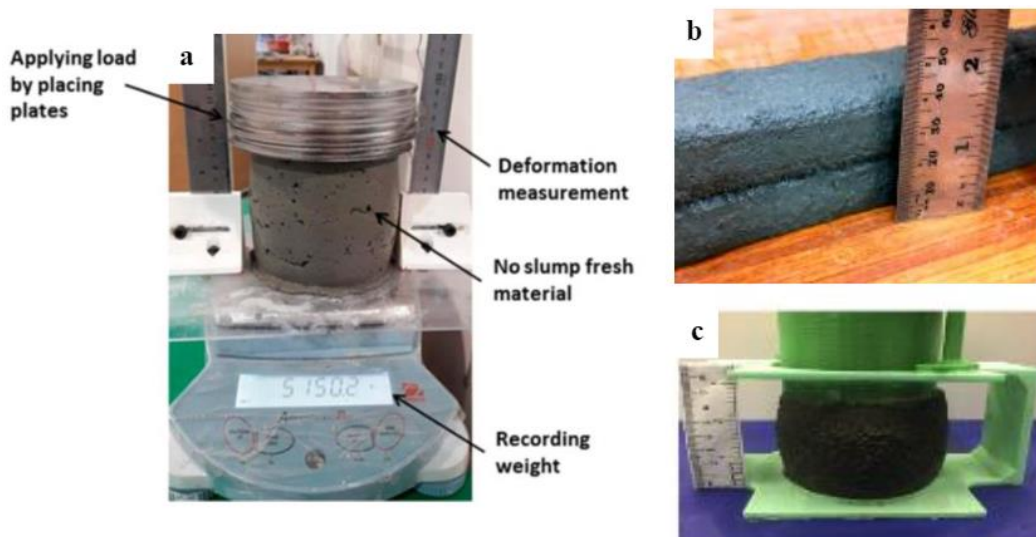


Figure 2.11. Buildability test: (a) stacking plate test, (b) printing on layers method and (c) cylinder stability test [106]

#### 2.3.4. Open time

Open time is the period during which freshly mixed concrete or mortar remains workable, allowing it to be placed, extruded, or manipulated before it begins to set [114]. Time plays a crucial role in influencing the properties of 3DCP, as concrete exhibits a thixotropic nature. This means that the application of shear stress can influence the setting time of the material, which is largely dependent on the workability of the mix design [106]. As viscosity increases with time, the longer a material is allowed to set, the higher its viscosity will become. This behaviour has a direct impact on both extrudability and buildability, making it critical to monitor. It is important to distinguish between open time and setting time. Kazemian et al. [127] referred to open time as the "printing window," which has two key limits: the printing limit and the blockage limit. The printing limit refers to the duration during which the material is printable after mixing, whereas the blockage limit is the point at which the material becomes too viscous to be extruded through the nozzle. To determine the printing window, equipment such as the stacking plate apparatus and the Vicat setting time machine are employed. These tools allow for precise measurement of the point at which the material reaches its printing limit, helping ensure the successful 3D printing of cementitious materials while avoiding nozzle blockages or other flow-related issues.

#### **2.4. Hardened properties of 3D printed cementitious structures**

3D printing operates through the layer-by-layer deposition of material. In the absence of vibrators for further densification or compaction, small linear voids are likely to form between extruded filaments due to the layer-by-layer extrusion method [10, 97, 163]. This leads to anisotropic behaviour in the printed structure as illustrated in Figure 2.12. These voids, also referred to as intra-filament voids, negatively impact the hardened properties of the 3D-printed material [114]. However, certain printing parameters, such as pump pressure, can play a crucial role in minimising the size and number of these voids. A higher pump pressure enhances the compaction of the material, which in turn improves the microstructure of the printed object. The overall print quality is highly dependent on both the fresh material properties and the

printing parameters [114], making careful optimisation of these factors essential for achieving strong, durable 3D-printed structures. [10, 97, 114, 163]

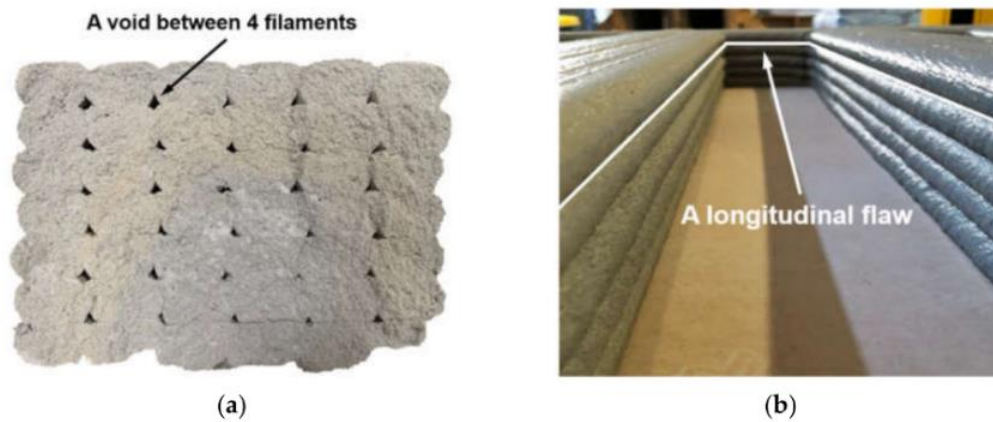


Figure 2.12. linear voids between filaments (namely inter-filament voids) in (a) transverse and (b) side view [114]

In most literature, two main approaches are used to investigate the hardened properties of 3D-printed cementitious materials. The first approach examines the differences between printed and mould-cast specimens from the same material batch. Printed specimens are prepared either by extraction through sawing or coring [87, 88, 110, 115, 133, 162, 164-166], direct printing [129, 167, 168], or casting in moulds simulating the layer-by-layer extrusion process [169-171]. The second approach assesses the hardened properties using only mould-cast samples [98, 127]. The first approach provides insight into how 3D printing affects the properties of printed products compared to traditional methods, while the second is useful for optimising mix proportions. Due to the unique challenges of 3D printing, such as anisotropy, this review focuses on studies using the first approach, with a primary emphasis on mechanical strengths like compressive, flexural, and tensile bond strength. Other properties, such as density, shrinkage, cracking, and reinforcement methods, are covered in later sections.

#### 2.4.1. Compressive strength

Compressive strength refers to a material's resistance to breaking under compression, and it is the most critical test for evaluating the performance of cementitious structures [172]. This test provides essential insights into the structural characteristics of 3D-printed cementitious components. According to research by Li et al. [114], the mechanical performance of a single

layer of extruded material is often superior to that of traditionally cast specimens. This improvement is attributed to the influence of pump pressure during printing, which enhances the material's density and strength. However, when considering multi-layer extruded components, the influence of pump pressure becomes less significant, as other factors, such as print quality, play a more critical role in determining the mechanical properties of the printed structure [114]. There is ongoing debate regarding the compressive strength of cast specimens versus 3D-printed specimens.

The anisotropic nature of 3D-printed materials also influences compressive strength, with the loading direction playing a pivotal role. Li et al. [114] investigated the compressive strength of saw-cut tube specimens tested in three different loading directions: perpendicular, longitudinal, and lateral direction as shown in Figure 2.13. Among the three loading directions, the longitudinal direction consistently exhibits the highest compressive strength values in most previous studies [86, 97, 133, 173-177]. This can be attributed to several factors. Firstly, the highest pressure is applied in the longitudinal direction during the extrusion process. Secondly, during the setting process, the fresh materials are able to expand freely in the lateral direction, where the pressure is minimal due to the absence of formwork [133, 164]. Lastly, in the perpendicular direction, the materials experience a medium level of pressure despite the weight of the layers. From a compaction perspective, the longitudinal direction benefits from a high degree of compaction, the perpendicular direction from a medium level, and the lateral direction from the least, which results in the highest compressive strength being found in the

longitudinal direction, while more voids or weaknesses occur in the perpendicular and lateral directions.

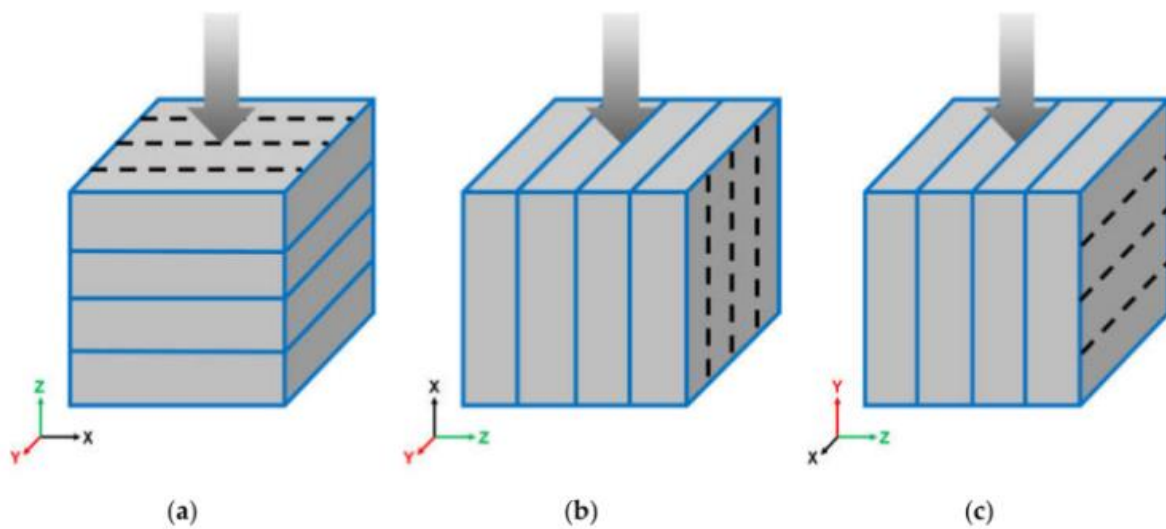


Figure 2.13. Testing in different directions for comprehensive strength: (a) perpendicular, (b) longitudinal and (c) lateral to the layer orientation. The dashed lines represent the printing path, and the x and z axes are parallel to dashed lines and the gravitational direction respectively. The printed layers locate in the x-y plane [114]

Panda et al. [97] offered another explanation, focusing on the micromechanics of stress transfer. They proposed that loading in the longitudinal direction facilitates efficient stress transfer, whereas loading in the perpendicular or lateral directions leads to interfacial slip between the filaments, further weakening those directions. On the contrary, Hambach and Volkmer [129] and Zhang et al. [165] reported a significant decrease in compressive strength in the longitudinal direction compared to the perpendicular direction. Similarly, Panda et al. [164] found that printed samples exhibited the lowest strength in the longitudinal direction and the highest in the lateral direction. These contradictory findings highlight the need for further research and experimental data to better understand the compressive behaviour of 3D-printed materials under different loading directions and to develop more comprehensive explanations for these variations. Asprone et al. [168] tested a set of printed hollow cylinders under compression to explore the geometrical effect of solid *versus* hollow shapes, demonstrating that the compressive strength of hollow cylinders is 16% lower than that of solid ones. Sanjayan et al. [133] found that compressive strength varies with the time gap between printed layers, with specimens having a 20-minute gap exhibiting higher strength than those with 10- or 30-

minute gaps. This change may relate to bond behaviour influenced by moisture content. Hambach and Volkmer [129] studied fibre types, printing paths, and loading directions, concluding that fibre type and path had minimal effect on compressive strength, while loading direction was the key influencing factor. Shakor et al. [178] reported that adding 1% glass fibre increased the compressive strength of printed cement mortar. However, Panda et al. [164] found that increasing glass fibre content from 0.25% to 1% slightly reduced the strength of fly ash-based geopolymer mortar due to the introduction of entrapped air [179-183].

#### 2.4.2. Flexural strength

Flexural strength refers to the stress at failure during bending and is also known as the modulus of rupture, bending strength, or transverse rupture strength. Similar to compressive strength, the loading direction plays a crucial role in determining flexural strength, especially in 3D-printed structures due to their anisotropic nature. Li et al. [114] investigated the anisotropic flexural bending behaviour of printed prisms by considering six different directions [10, 132, 164, 184], though most studies typically only account for three directions [115, 129, 133, 171], with some focusing on just one or two.

Most researchers have only evaluated three of the six possible testing directions for 3D-printed specimens, often without detailed descriptions of their chosen directions. Typically, the highest flexural strength is observed in the longitudinal direction (Figure 2.14a), where the maximum tensile stress occurs along the extruded filament at the bottom centre of the prism specimen. This area benefits from better compaction and a lower water-to-binder ratio due to the weight of the upper layers and the bleeding phenomenon, contributing to higher flexural strength [114]. The mechanical properties are also influenced by the position where the specimens are extracted, highlighting the importance of considering anisotropic behaviour. Additionally, factors like joints contribute to anisotropy. Horizontal joints between longitudinal filaments (Figure 2.14b,d) and vertical joints between layers (Figure 2.14c,e) can create defects in the peak-stress region, significantly reducing flexural strength.

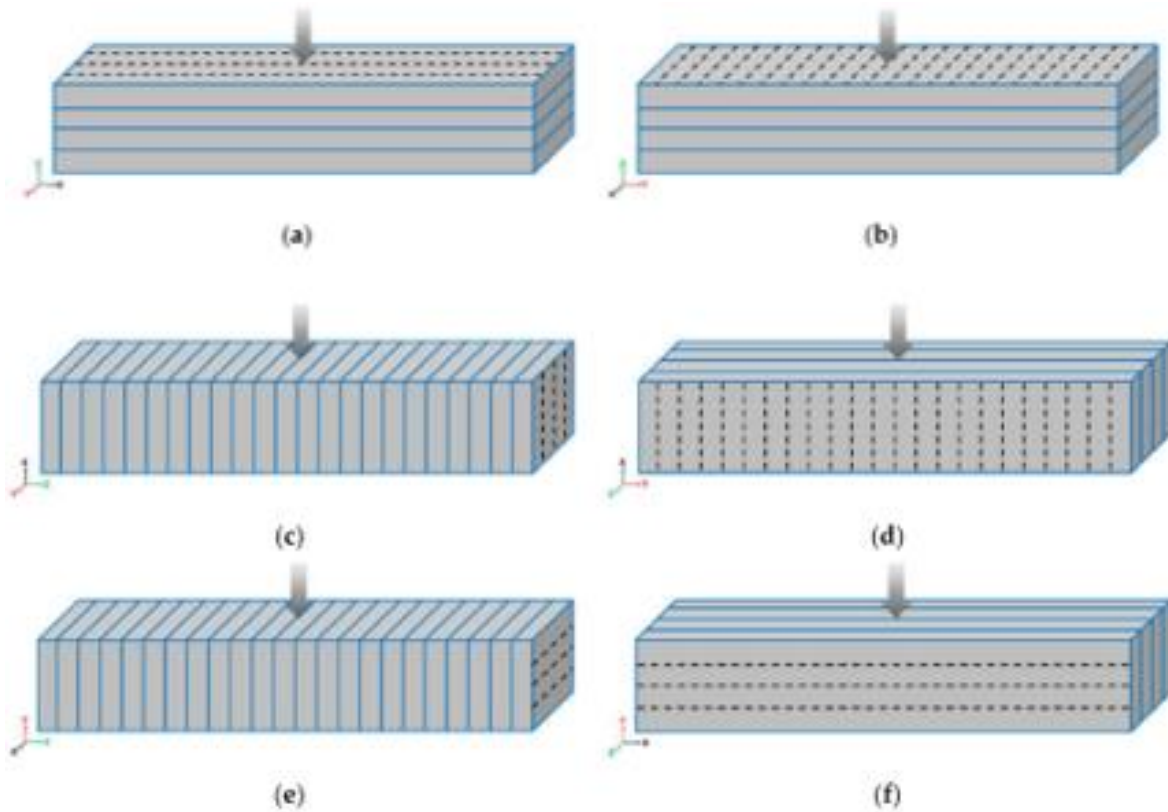


Figure 2.14. Different testing directions for flexural strength of printed prism specimen: (a) & (b) perpendicular, (c) & (d) longitudinal and (e) & (f) lateral to the layer orientation [114]

Le et al. [114], similar to their study on compressive strength, compared the flexural strength of specimens taken from straight-line printed slabs and a trial curvy-shaped bench. They found that samples from the curvy component exhibited higher flexural strength than the cast control, but lower than those cut from the straight slabs. This difference was attributed to variations in print quality along different printing paths. Additionally, the high coefficients of variation in the results highlight the instability and inconsistency in the print quality of the curvy-shaped printing path. Sanjayan et al. [133] observed that the flexural strength of printed specimens initially increases and then decreases as the printing time gap grows, mirroring the pattern seen in compressive strength. However, Al-Qutaifi et al. [171] found that flexural strength decreases with an increasing time gap due to the weakening of the interlayer bond. It's important to note that Sanjayan et al. [133] did not offer an explanation for their results, while Al-Qutaifi et al.'s [171] specimens were produced using a specific layering process with a self-made mould, not an automated printing process. Panda et al. [163] showed that increasing the glass fibre content from 0.25% to 1% in fly ash-based geopolymer mortar enhances the flexural strength of printed

samples, regardless of fibre lengths (3 mm, 6 mm, and 8 mm). A similar trend was seen in research involving 18-mm basalt fibres, with content ranging from 0% to 0.7% by weight [185].

Given the successful application of fibre alignment in extrusion processes [186, 187], Hambach and Volkmer [129], Ma et al. [185], and Shakor et al. [178] capitalised on this phenomenon to improve the hardened performance of 3D-printed cementitious materials. A high degree of fibre alignment is achieved when the diameter of the printing nozzle is smaller than the average fibre length [129, 187], as shown in Figure 2.15. Fibre reinforcement through aligned fibres offers significant advantages, such as increased flexural strength, reduced reinforcement steel content, and spatially controllable mechanical properties, making it a promising approach for fully automated construction processes.

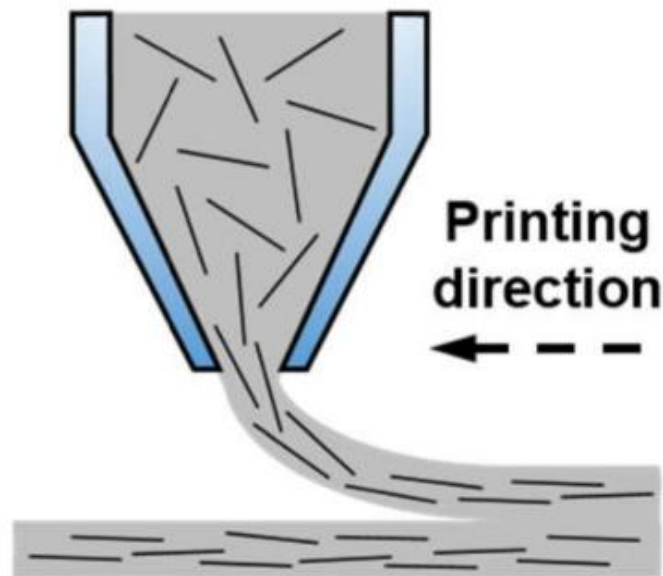


Figure 2.15. Schematic representation of fibre alignment inside the printing nozzle during the 3D printing process [114]

#### 2.4.3. Tensile bond strength

The bond behaviour between new and old cementitious structures has been a key area of investigation for several decades, particularly in the field of repairing, maintaining, and strengthening these structures [188-192]. Recently, with the advent of 3D printing, attention has turned toward understanding the bond behaviour between successfully deposited filaments,

which is crucial in determining the anisotropic mechanical properties of 3D-printed parts. For large-scale 3D printing, it is essential to consider these factors carefully [114]. Comprehensive reviews and comparisons of these test methods have been extensively presented in the literature [43, 193-198]. However, in the context of 3D concrete printing, the application of these test methods is significantly limited. Tensile tests are commonly used to assess the bond strength of printed structures. The bond strength is influenced by the time gap between the extrusion of successive layers and is also a function of the structure's size [88, 123]. Most studies have shown that an increase in the printing time gap leads to a reduction in tensile bond strength, which results in the formation of cold joints [106, 199]. For example, Panda et al. [88] found that reducing nozzle travel speed or height increased the tensile bond strength of 3D-printed geopolymer mortar. Bos et al. [1] proposed improving compaction and adhesion by pressing layers together with the nozzle slightly embedded in the filament, but Panda et al. [88] warned that this approach could compromise the geometric accuracy of the printed structures. Putten and Schutter [200] tested interlayer bond strength using saw-cut samples of 3D-printed filaments. These samples were adhered to a metallic bracket with epoxy, and a tensile force was applied, as shown in Figure 2.16. Similarly, Marchment et al. [29] conducted bond strength tests on saw-cut printed filaments using a custom-made clamp with two centrally loaded pins that pulled in opposite directions, effectively measuring the interlayer tensile strength. These studies highlight the importance of optimising the interlayer bonding in 3D-printed structures, as the mechanical integrity of the printed object can be compromised if the bond strength between layers is insufficient.

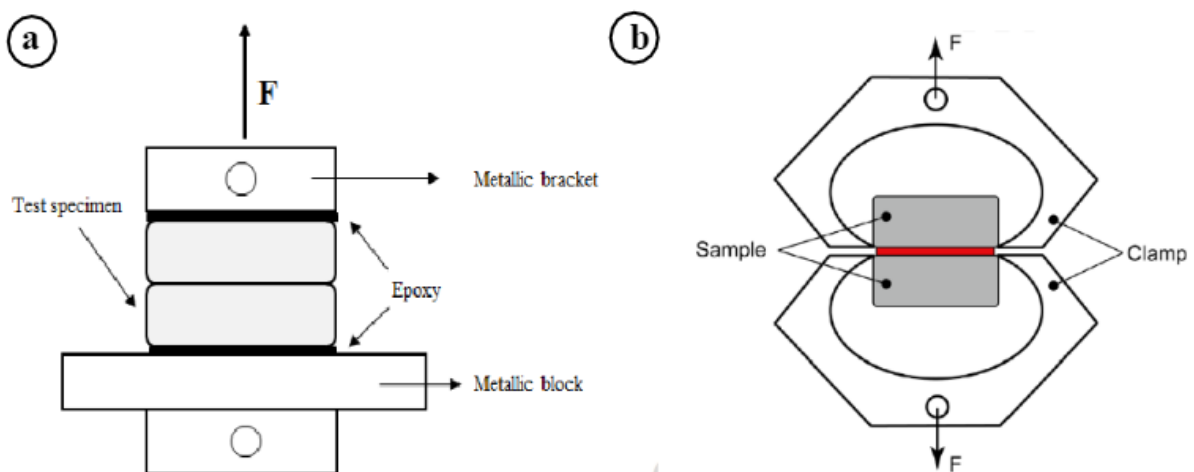


Figure 2.16. Testing set-up for measurement of inter-layer bonding strength [29]

According to Le et al. [110] the reduction in strength between layers is primarily caused by a decrease in interlayer adhesion and the non-uniform shrinkage between the new and old layers. As the printing time gap increases, larger voids tend to form in the cross-section, further weakening the bond. After the initial layers are deposited, the filaments begin to stiffen over time. When subsequent layers are printed, the energy from the extrusion process becomes insufficient to realign or rearrange the interface between the new and old layers. This results in an incompatibility of shear stress between the layers, leading to poor bond strength [123].

Figure 2.17. provides a schematic illustration of the interlayer bonding mechanism, demonstrating how the interaction between the newly deposited material and the hardened filament can lead to weakened adhesion and the development of voids. Addressing these issues is critical for improving the mechanical integrity and long-term durability of 3D-printed cementitious structures.

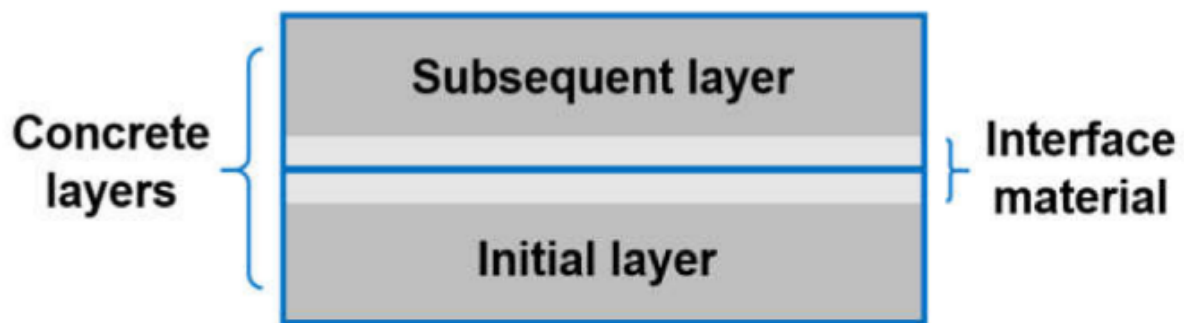


Figure 2.17. Schematic illustration of the mechanism of interlayer bonding [114]

The interface material is a thin film that acts as a lubricant in the pumping hose prior to extrusion and plays a crucial role in determining the tensile bond strength between deposited filaments after extrusion. Mechtcherine [201] examined two filaments with varying time gaps, focusing on the interface between them. The study revealed that a time gap of just 1 minute led to a 9.9% decrease in interlayer bonding strength, while a 10-minute gap resulted in a 14.1% decrease, and a gap of one day caused a 23.1% decrease. This reduction in bond strength is largely due to the formation of cavities caused by air voids and the presence of cold joints along the layers. Figures 2.18a,b, and c illustrate these phenomena, showing cold joints along the filaments, cavities between filaments, and a silt-like separation filled by calcite and ettringite.

Notably, self-healing was observed in some areas where no bonding occurred initially between the filaments. Over time, these silt-like separations were filled with ettringite and/or calcite, which naturally repaired the gaps [201].

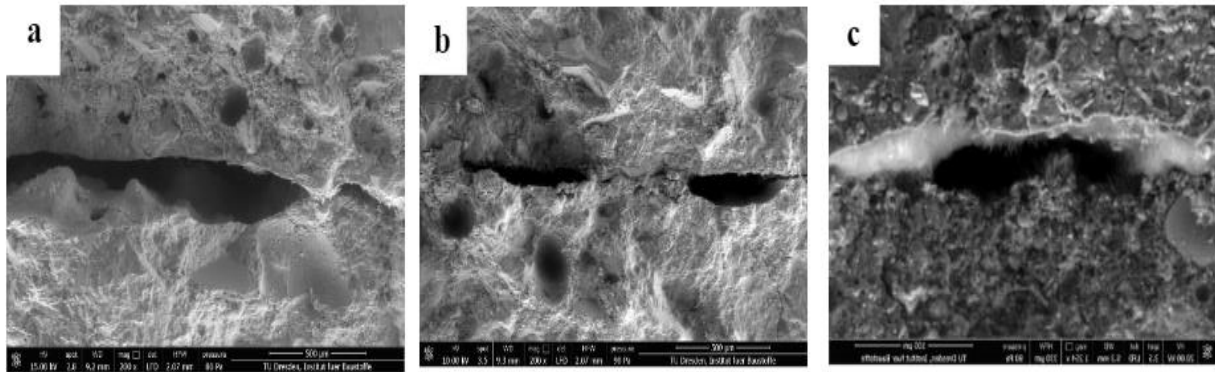


Figure 2.18. Scanning electron microscopy (SEM) images depicting: (a) cold joints along filaments, (b) development of cavities between filaments and (c) silt-like separation filled by calcite and ettringite [201]

## 2.5. Shrinkage and Cracking

Shrinkage in cementitious structures refers to the contraction caused by the loss of moisture during the drying process [202]. Several factors influence the rate of drying shrinkage, including material curing, mixture proportions, restraint, and the environmental conditions during drying [202-207]. Factors such as these play a significant role in the overall shrinkage behaviour of cementitious materials, with environmental factors like humidity and temperature affecting the drying process and mass-related factors like self-desiccation and hydration heat contributing to further shrinkage [208].

### 2.5.1. Chemical shrinkage

Shrinkage in cementitious structures occurs due to a reduction in the volume of the cement paste as a result of the chemical binding of water during the cement hydration process. Once cementitious material is deposited, it begins to harden [208]. During this hardening process, various chemical transformations occur within the cement paste. The stiffness of the chemically bound water increases compared to the free water in the mixture prior to hydration, resulting

in a reduction in the volume of the cement paste compared to the original volume of the water and cement. As the material hardens, shrinkage of the cement paste takes place progressively. This shrinkage leads to the development of empty pores, which contribute to the overall joint pore volume within the cement paste. These pores play a crucial role in autogenous shrinkage, as the ongoing hydration process consumes water, creating internal stresses that further shrink the cement paste [208].

#### 2.5.2. Plastic shrinkage

This type of shrinkage develops on the surface of cement that has freshly been deposited. It occurs as a result of absorption in the cementitious form or the evaporation of water from the surface of cementitious structures. Plastic shrinkage can be easily eliminated by intensive cementitious curing such as wetting the cementitious elements to increase hydration whilst also preventing evaporation [114].

#### 2.5.3. Autogenous shrinkage

Autogenous shrinkage, also known as hydration shrinkage, occurs during the process of self-desiccation within the pores of cement stones, which is the result of water being consumed during cement hydration. Autogenous shrinkage is closely related to chemical shrinkage, and it can be challenging to distinguish between the two. Typically, chemical shrinkage leads to the formation of additional pores as hydration progresses. As self-desiccation occurs within these pores, autogenous shrinkage takes place [208]. This shrinkage, driven by the depletion of water within the pores, can result in significant volume loss or even cracks in the cementitious structure. Autogenous shrinkage is most prevalent during the first month after the cementitious material is deposited

#### 2.5.4. Drying shrinkage

Drying shrinkage is the opposite of autogenous shrinkage, as it results from the reduction in the volume of concrete due to the loss of water from the concrete paste. This type of shrinkage occurs from the surface of the concrete and progresses inward toward the internal mass. The

initial phase involves a phenomenon called bleeding, where water escapes from the surface of the concrete. Once the bleed water has dispersed, the excess water from the internal concrete mass is consumed, leading to shrinkage. Several factors influence drying shrinkage, including the volume of paste, thickness of the element, binder fineness, porosity, temperature, and humidity [208]. These factors collectively determine the rate and extent of shrinkage

#### 2.5.5. Thermal shrinkage

This type of shrinkage occurs when strains develop in concrete during the first few days due to temperature changes caused by the hydration process. When cement is mixed with water, a chemical reaction known as hydration takes place, releasing heat and causing the concrete to expand [208]. The extent of temperature change in the concrete is influenced by several factors, including the concrete composition and the environmental conditions. Proper understanding of the concrete's characteristics before use is crucial, especially in chemically aggressive environments. In such conditions, parameters such as low hydration, early strength development, and improved resistance should be carefully considered to ensure the concrete's long-term durability and performance.

#### 2.5.6. Carbonation shrinkage

This type of shrinkage occurs in hardened concrete and is driven by a chemical reaction between carbon dioxide ( $\text{CO}_2$ ) from the environment and the cement stone. When carbon dioxide reacts with water, it forms carbonic acid, which then reacts with calcium hydroxide ( $\text{Ca}(\text{OH})_2$ ) present in the cement stone. This reaction produces calcium carbonate ( $\text{CaCO}_3$ ), leading to the degradation of other components within the cement stone [208]. This process is known as carbonation shrinkage and can contribute to the deterioration of concrete over time.

## 2.6. Advantages of 3D printing

### 2.5.1 Multi-material design

The ability to manufacture multi-material and multifunctional structures is a significant advantage in the realm of large-scale 3D printing. Some 3D printers are equipped with multiple print heads, allowing them to print different materials simultaneously at separate locations [106]. This capability facilitates the creation of complex structures with varying material properties, optimized for specific functional and aesthetic purposes. A prime example of this technology is demonstrated by the French company XtreeE, which used this method to construct a truss-shaped pillar. This pillar was built with two distinct types of concrete: ultra-high-performance concrete (UHPC) for the core and 3D-printed concrete for the outer shell. UHPC offers exceptional structural stability, serving as a strong alternative to steel reinforcement, while the 3D concrete enhances the pillar's aesthetic qualities and optimizes its topology [106, 115, 209]. Figure 2.19. shows the XtreeE pillar constructed in Aix-en-Provence, France, showcasing the innovative use of multi-material 3D printing in architecture

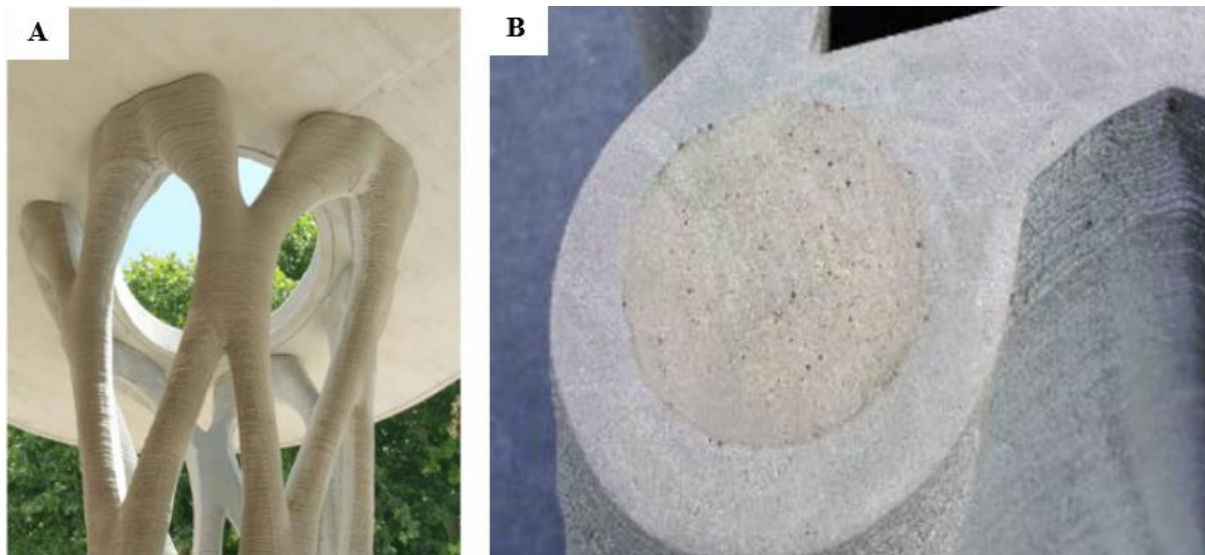


Figure 2.19. (a) XtreeE pillar built in Aix-en-provence, France and (b) section of the pillar [209]

For the XtreeE pillar, Ultra-High-Performance Concrete (UHPC) functions as the structural reinforcement. UHPC is composed of polymer fibres, a mixture of concrete, and steel,

providing enhanced tensile strength and durability. In the broader field of 3D-printed concrete reinforcement, several approaches have emerged, with extrusion guns and mesh mould systems being the most prominent.

- This method involves attaching an extrusion gun to the back of the print head nozzle (as shown in Figure 2.20). During the printing process, as the print head deposits material, the extrusion gun simultaneously extrudes fibres. The primary goal of this technique is to enhance tensile strength in the vertical direction. One notable example of this approach is the hybrid reinforcement printing system at Nanyang Technological University in Singapore, which combines short polyvinyl alcohol (PVA) fibres and continuous steel cables for hybrid 3D-printed geopolymers structures [2, 210, 211]. However, this method has limitations, as further research is necessary to improve both vertical and horizontal reinforcement in the 3D printing of cementitious elements, which remains unsatisfactory at present (Michalopoulos, 2020).

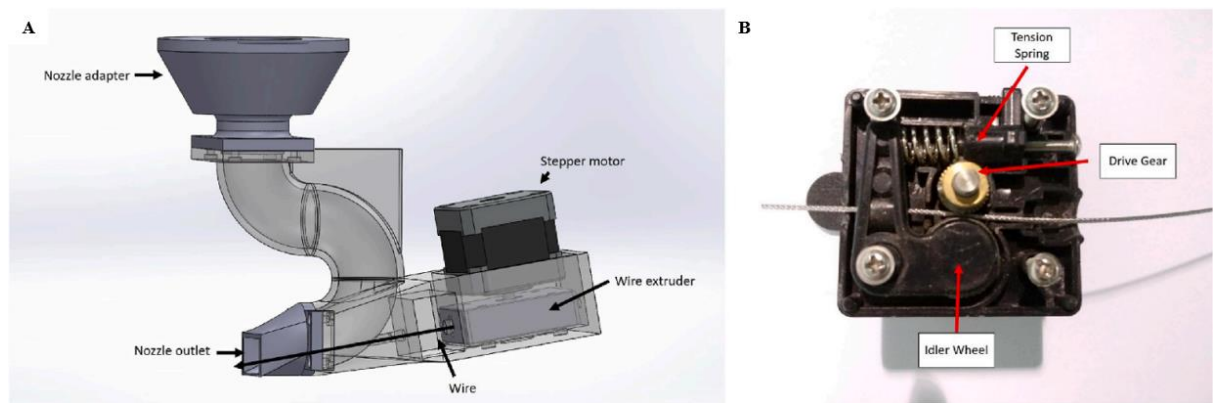


Figure 2.20. (a) Schematic of the nozzle with the cable extruder system, and (b) Top view of cable extruder [212]

**Mesh Mould Method:** This technique involves creating a complex reinforcement mesh that serves as the structural framework. The mesh can be made from either metallic materials or polymers, depending on the requirements of the project. Once the mesh is in place, self-compacting concrete is poured or placed around it to form the complete structure. This method allows for intricate reinforcement patterns and provides greater structural integrity to the 3D-printed element [106]. Figure 2.21 illustrates the complex reinforcement mesh approach, showcasing how the mesh is integrated within the concrete to enhance both durability and stability.

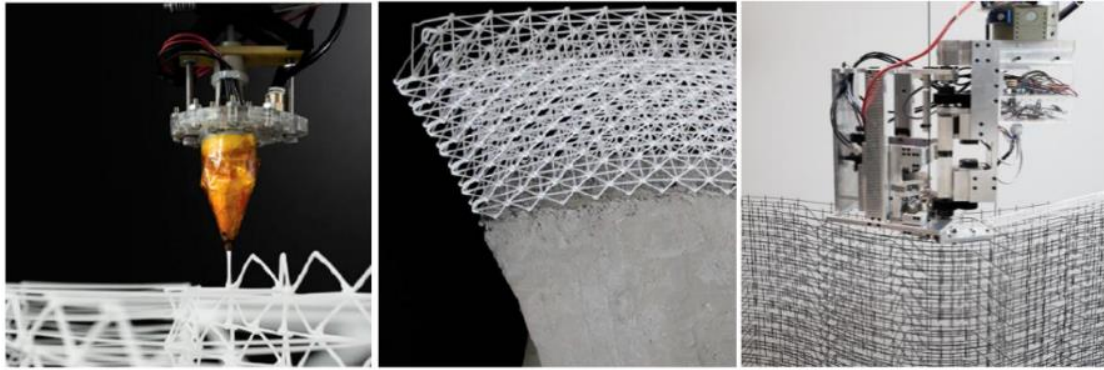


Figure 2.21. Mesh mould reinforcement approach [211]

### 2.6.1. Structural Complexibility

A few years ago, the manufacture of complex shape objects was prohibitive and difficult, meaning the cost of producing complex moulds was very high. Today, the recent advancement in technology in various industries has made it possible to create complex 3D structures, and they are being widely used. Some printing patterns are complicated, ranging in size from a few  $\mu\text{m}$  to cm. They have the ability to give new physical (multi-physics topology optimisation) and mechanical properties (stress-based topology optimisation) to objects such as mechanical meta-materials [106]. These patterns of printing reflect topologies based on biological structures, such as biomimicry, natural structures, such as material lattices, and any structure that provides unique properties to the object.

In recent times, the building and construction industry has seen various needs to construct complex geometry. Figure 2.22 shows a construction of beams and columns that mimic the anatomy of a bone. The structure was constructed using a cable-suspended platform that deposits cementitious materials and fibre. The outer shell of these structural elements is dense while the inner shell displays a spongy and hollow topology. This makes 3D printing of concrete better than the traditional methods of construction because their structural elements are more resilient and self-reinforced [3].

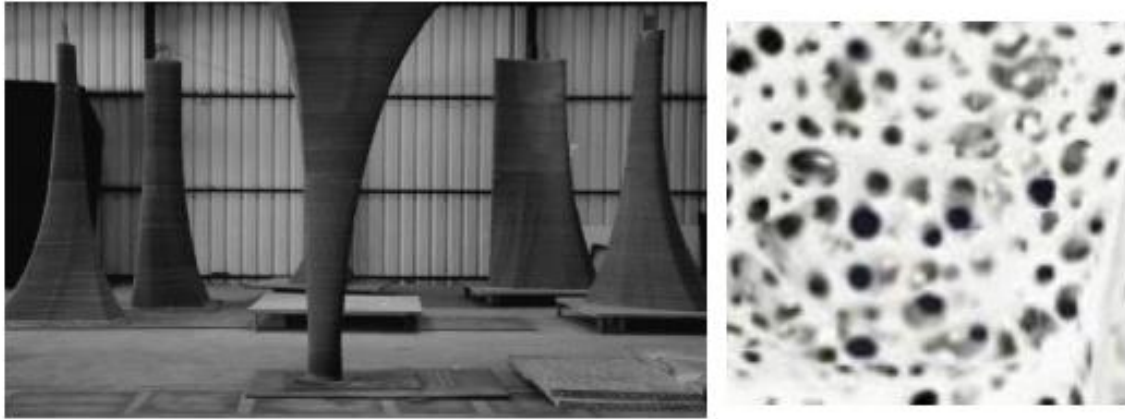


Figure 2.22. 3D printed concrete columns mimicking the anatomy of a bone by Siam Cement Group (SCG)(left) and the inner bone structure (right) [106]

### 2.6.2. Sustainability

A few years ago, manufacturing complex-shaped objects was both prohibitive and challenging, largely due to the high costs associated with producing intricate moulds. However, recent technological advancements across various industries have made it possible to create complex 3D structures, which are now widely used. These 3D printing patterns can be highly intricate, ranging in size from a few micrometres to centimetres. They offer new physical properties through multi-physics topology optimisation and enhanced mechanical properties through stress-based topology optimisation, enabling the creation of advanced mechanical meta-materials [106]. These sophisticated printing patterns are inspired by biological structures, natural lattices, and biomimicry, allowing the production of objects with unique and highly optimised properties. In recent years, the construction industry has increasingly adopted these techniques to meet the growing demand for complex geometries. For instance, Figure 2.23 depicts the construction of beams and columns that mimic the anatomy of bone, achieved using a cable-suspended platform to deposit cementitious materials and fibres. The outer shell of these structural elements is dense, while the inner core features a spongy, hollow topology. This construction method highlights the advantages of 3D printing over traditional methods, as it allows for more resilient and self-reinforcing structural elements [3].

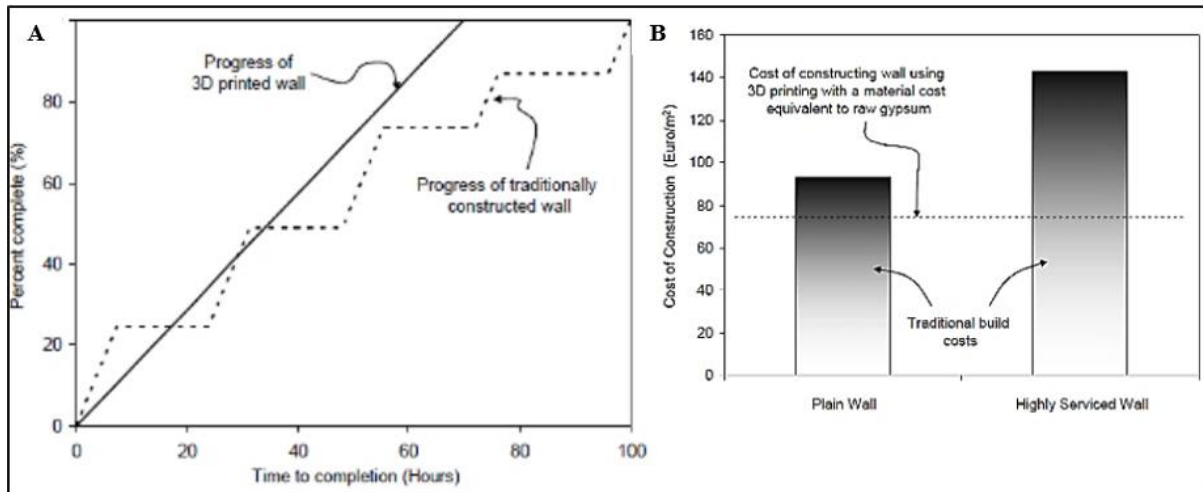


Figure 2.23. (a) Completion time and (b) Construction cost of a 3D printed wall [36]

## 2.7. Limitations of 3D printing of cement-based materials in construction

One of the primary limitations in the 3D printing of cement-based materials is the challenge of controlling the time interval between successive layer depositions [213]. The structural performance of printed elements is highly dependent on this timing. If layers are applied too soon, the lower layer may not have developed sufficient strength to support the subsequent layer, resulting in deformation or collapse. On the other hand, if the interval is too long, the bond between layers weakens due to drying and the formation of cold joints, which compromises the mechanical integrity of the structure [213].

The geometry and orientation of the extrusion nozzle further influence the printing quality. For instance, downward-facing round nozzles can over-compress underlying layers, resulting in dimensional inaccuracies and inconsistent material distribution [214, 215]. This makes the optimisation of nozzle design critical for maintaining uniform layer deposition and build quality.

Architectural and structural design limitations also affect the process. Sharp corners or tight curvatures can disrupt flow and create stress concentrations, leading to potential cracking or structural deformation. Therefore, maintaining a minimum turning radius is essential to ensure consistent material placement and geometric accuracy [216]. Unsupported overhangs present another major limitation due to the low tensile strength of freshly extruded concrete. Without auxiliary supports or rapid-setting strategies, these elements are prone to collapse or distortion during fabrication [1, 217].

The physical size of 3D printers also imposes constraints on build volume. Large-scale construction using current systems may require segmentation and post-assembly of components, which introduces logistical and structural challenges [218].

These limitations highlight the importance of continued interdisciplinary research that consists of process automation, material development, and structural optimisation to fully realise the potential of 3D concrete printing in practical construction applications.

## **2.8. Application of robots for 3D printing of cement-based materials**

The dynamics of manufacturing activities, coupled with the advent of industrial revolutions, have led to increasing complexity in production processes driven by ever-changing customer demands. A robot is an automatic machine that is programmed to execute tasks robotically [219]. In some cases, adequate supervision is needed. As a result, robotic solutions play a crucial role in addressing these challenges by enhancing automation, operational efficiency, productivity, and safety [220, 221]. These technologies offer manufacturers a competitive advantage in their industries. Robotic solutions are available in various configurations, depending on the degree of automation required. Fully autonomous systems are typically used for high-volume, dedicated, and repetitive tasks, with pre-programmed paths and motions that control the robot [219, 222, 223]. In contrast, semi-autonomous systems require a degree of human involvement and offer greater flexibility. These robotic systems help manufacturers carry out operations with a high level of accuracy and precision, reducing errors and minimising the need for rework. Robotic solutions can be employed in a wide range of manufacturing tasks, including handling, assembly or disassembly, machining, and inspection [224, 225]. They are particularly valuable in complex, hazardous, or hard-to-reach environments, where they help maximise operational efficiency or are deemed dangerous for human exploration [226, 227].

The speed and dexterity of robots are essential for manufacturers to stay competitive, especially in areas with labour shortages, where robots can fill the skills gap and reduce costs. Robots excel in repetitive tasks like lifting and placing workpieces [228]. Additionally, they help create flexible, customisable manufacturing systems with advanced sensors for better interaction [229]. Optimising robotic design and process parameters is crucial to enhance performance and prevent inefficiency, with modelling and simulation during the design phase ensuring

operational effectiveness [230, 231]. Improper configuration of robots can lead to inefficiencies and counterproductive results. Therefore, modelling and simulation during the design phase are essential for optimising the robotic system for operational efficiency. Robotic axes are typically designed to reach any point in a plane or space, and for effective control of the robotic manipulator, additional axes such as yaw, pitch, and roll may be required to enhance precision and functionality. Several studies have focused on the modelling and simulation of robotic systems for industrial applications. Brüning et al. [232] examined simulation-based planning for machining processes with industrial robots, while Denkena et al. [233] focused on the design and optimisation of machining robots. Papakostas et al. [234] integrated digital manufacturing and simulation tools for assembly design with cooperating robot cells, and Tsarouhia et al. [235] developed a robotised assembly process using a dual-arm robot. Makris et al. [236] and Michalos et al. [237] studied the design and challenges of cooperating robots in reconfigurable assembly.

During the process of implementation, the robots get their commands from a programmed software. In previous years, robot programming can be complex and difficult unlike now, where there is the availability of several programming software packages with necessary tutorials. Today, the importance of robots cannot be overstated. Robots are mostly used for the application of repetitive tasks [219]. Overall, robots can be divided into two main areas: service and industrial robots. Some examples of industrial robots include welding, assembly, 3D printing, pick and place robots, to mention but a few. Figure 2.24 shows the different types of industrial robots.

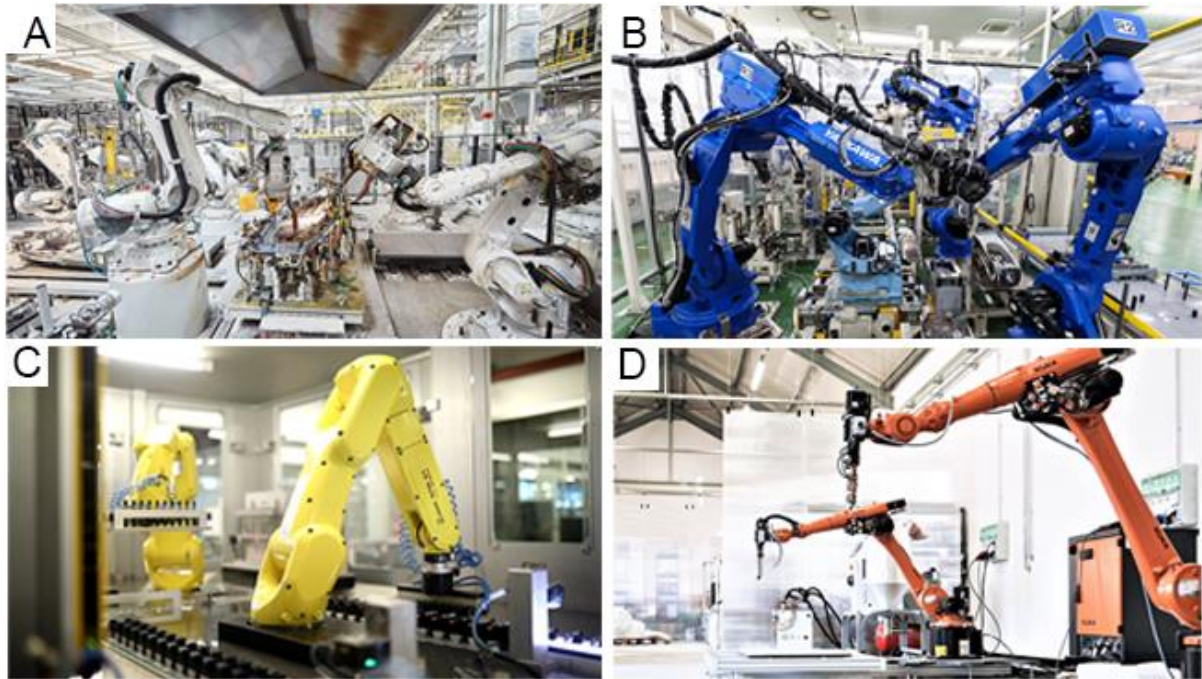


Figure 2.24. Industrial robots: (A) welding robots, (B) assembly robots, (C) pick and place robots and (D) 3D printing robots (IFR 2019)

### 2.8.1. Historical development of robots

The historical development of robotics has played a crucial role in shaping modern automation and manufacturing. Understanding the evolution of robotic systems provides insight into how these technologies have advanced from simple automated machines to sophisticated tools capable of complex tasks in various industries, including construction and 3D printing. Figures 2.25 and 2.25 showcase key milestones and technological advancements in robotics over the years, and Table 2.4 illustrates the timeline of significant developments that have influenced the growth of robotics, highlighting their increasing impact on efficiency, precision, and adaptability in industrial applications.

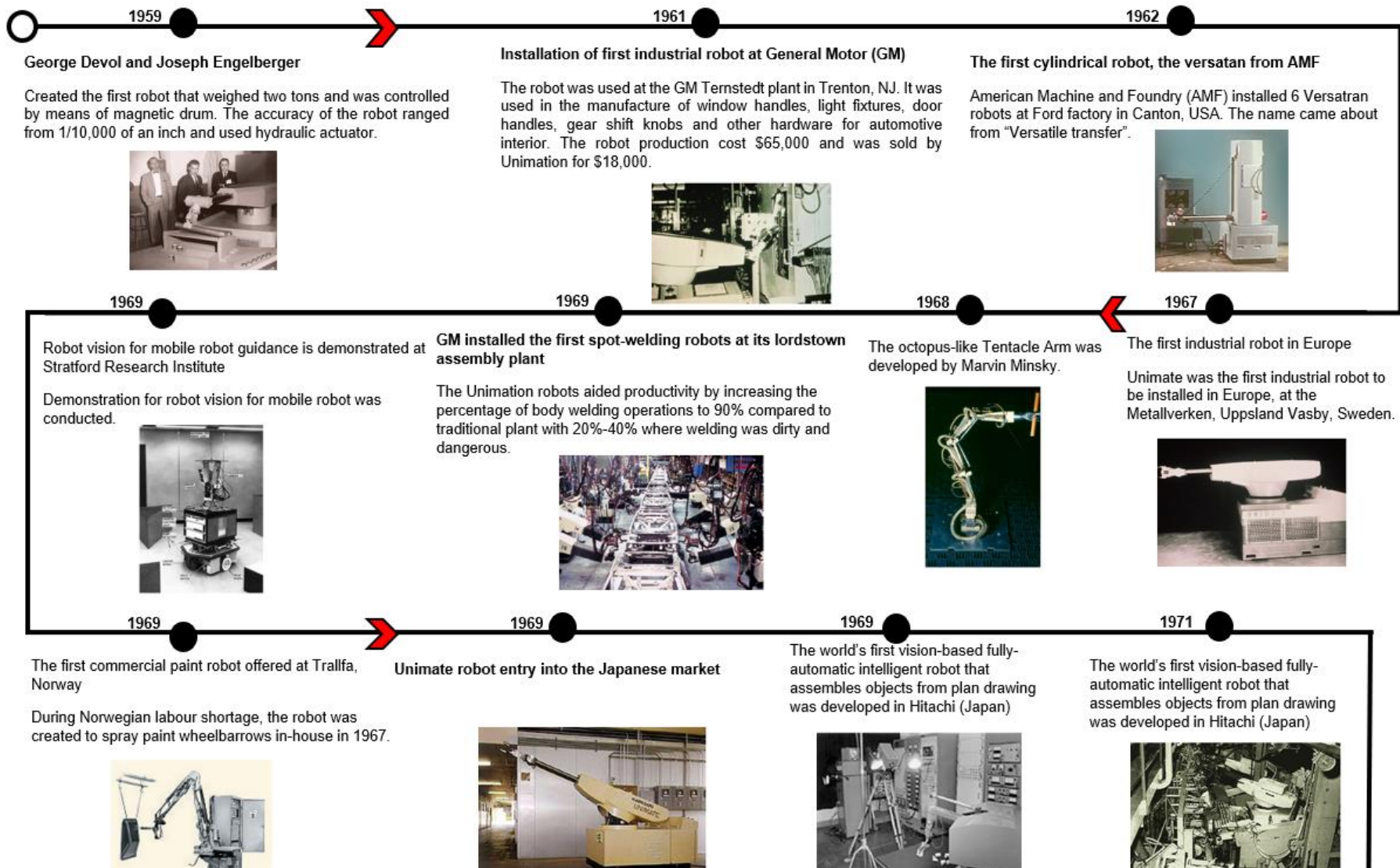


Figure 2.25. Evolution of robots

Table 2.4 Timelines of robot evolution

Year	Description
1971	Establishment of Japanese Robot Association (JIRA). It later became JARA.
1972	Robot production lines installed in Europe.
1973	First electromechanically driven axes robot was manufactured. Production of Vacarm/Stanford arm bat Vicam Inc, USA by Scheinemann An automatic bolting robot for concrete pile and pole industry was developed in Hitachi, Japan.
1974	The first minicomputer-controlled industrial robot was introduced. Japan introduces the first arc welding robots. ASEA introduced the first fully electric microprocessor-controlled industrial robot, IRB 6. The first precision insertion control robot “HI-T-HAND Expert” was developed on Hitachi, Japan.
1975	The first robot used in assembly application was the Olivetti “SIGMA” cartesian-coordinate robot. A robot with a payload of up to 60kg was developed by ABB. The first sensor-based arc welding robot was developed in Japan by “Mr. AROS”.
1976	Robots in space
1977	An assembly cell was developed in Hitachi (Japan) to assemble vacuum cleaners with the use of 2 robot arms and 8 TV cameras.
1978	Unimation/Vicarm developed a Programmable Universal Machine for Assembly (PUMA) in the USA with support from General Motors (GM). SCARA-Robot was developed in Hiroshi Makino, University of yamanashi, Japan. SCARA means selective compliance assembly robot arm.
1979	Reis, Obernburg, Germany introduced the first six-axis robot with own control system RE 15. The first motor-driven robots were developed in Nachi, Japan.
1980	Introduction of Machine vision.
1981	Installation of machine vision system “CONSIGHT” by GM First industrial gantry robot was introduced by PaR Systems, USA.
1982	Robot programming language (AML) was developed by IBM.
1983	Introduction of flexible Automated Assembly Lines.
1984	The first direct drive SCARA robot (AdeptOne) was introduced by Adept, USA. The fastest assembly robot (IRB 1000) was produced by ABB, Sweden
1992	The CAN-Bus control of robots was introduced by Wittmann, Austria. Launching of open control system (S4) by ABB, Sweden. First sales of Delta robot packaging application to Roland by Demarex, Switzerland.
1994	Introduction of first robot control system (MRC) by Motoman. The robots provided the synchronized control for two robots.
1996	First PC-based robot control system was launched by KUKA in Germany.

1998	<p>The 5-robot control generation ROBOTstar V was launched by Reis Robotics. It was launched in a short interpolation cycle times for robot controls.</p> <p>The world's fastest picking robot (FlexPicker) was developed by ABB in Sweden. The robot was based on the delta robots developed in the Federal Institute of Technology, Lausanna (EPFL) by Reymond Clavel.</p> <p>The only curved-track gantry and transfer system "RoboLoop" was launched in Gudel, Switzerland.</p>
1999	<p>KUKA, Germany developed the first remote diagnosis via internet.</p> <p>Introduction of integrated laser beams guiding within the robotic arm by Reis.</p>
2003	<p>Robots to Mars.</p> <p>The first entertainment robot (Robocoaster) was introduced by KUKA Germany. The robot was based on an articulated robot.</p>
2004	<p>An improved robot system (NW100) was introduced by Motoman, Japan.</p> <p>The robot provided the synchronized of four robots, up to 38 axis.</p>
2006	<p>The first Wireless Teach Pendant (WITP) was introduced in Comau, Italy.</p> <p>Presentation of first Light Weight Robot by KUKA, Germany.</p> <p>Human sized single armed (7 axis) and dual armed robot (13 axis) robot was launched by Motoman, Japan. The robot had all supply cables hidden in the robot arm.</p>
2007	<p>A super speed arc welding robot was launched by Motoman in Japan. The robot reduced welding time cycle by 15%, which made it the fastest welding robots in existence in 2007.</p> <p>The first long range robot was launched by KUKA in Germany. They also launched a heavy-duty robot with a payload of about 1,000kg.</p> <p>Reis Robotics became the market leader for photovoltaic module production lines with the first system realised in 2006.</p>
2008	<p>A new heavy-duty robot with a payload of almost 1,200kg was launched in Japan by FANUC.</p>
2009	<p>The smallest multipurpose industrial robot was launched (IRB120) by Abb, Sweden.</p> <p>Control system that could sync about 8 robots was introduced by Yaskawa Motoman, Japan.</p>
2010	<p>A new series of self-mounted robots (Quantec) was launched by KUKA (Germany) including a new controller KR C4</p>
2011	<p>First humanoid robot in space</p>

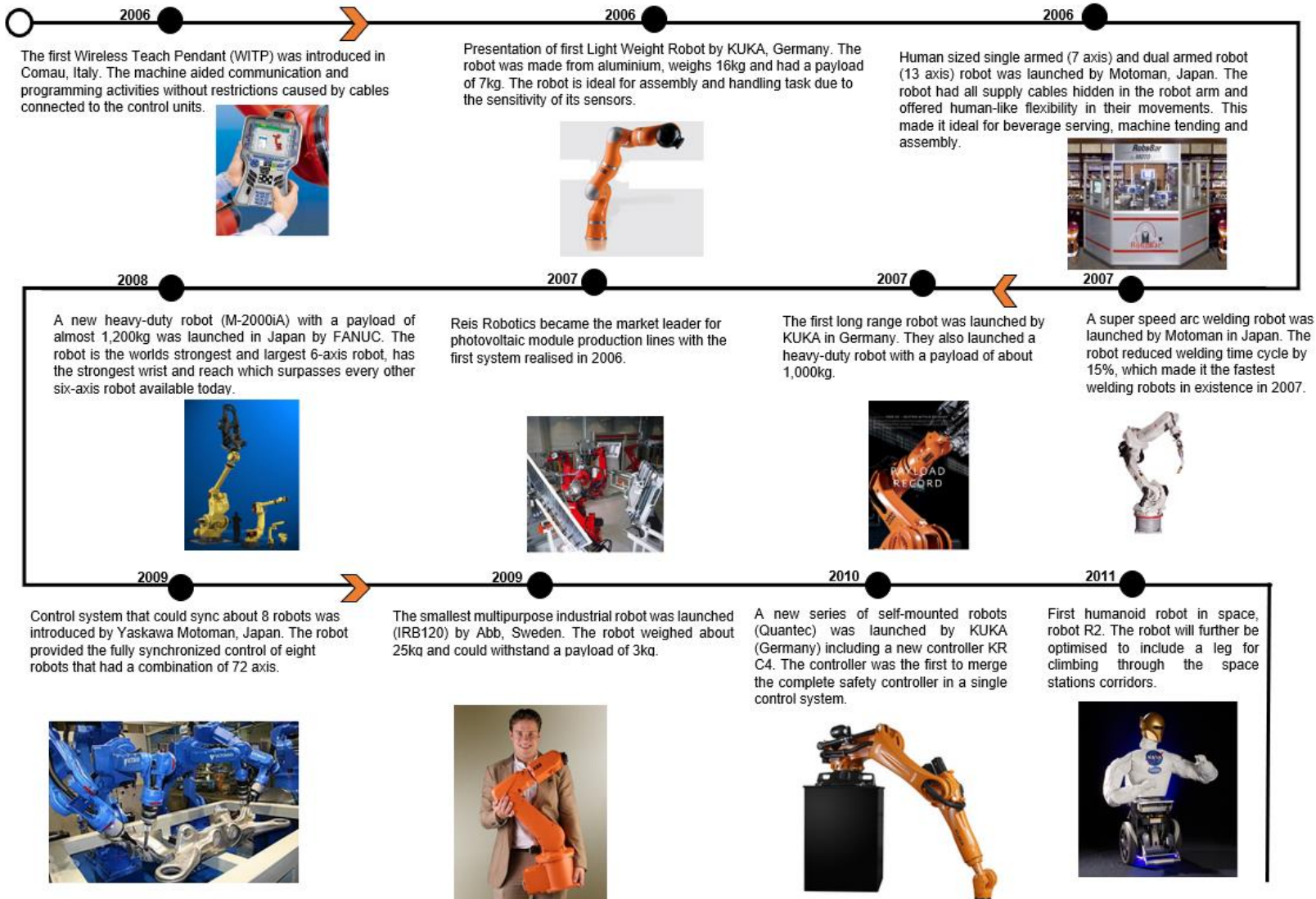


Figure 2.26. Evolution of robots

## 2.9. Robotic 3D printing systems

3D printing of cement-based materials using a robotic arm is a highly promising approach for driving digital evolution in the construction industry, and it has made significant advancements in recent years [70, 152, 168, 238-240]. Robotic arms offer additional roll, yaw, and pitch control over the print nozzle, enabling greater accuracy and more intricate designs, including the application of techniques such as the Tangential Continuity Method (TCM) [6, 64, 241]. These robots can range from custom-built arms to commercially available six-axis robotic arms. A notable example of a custom-made arm is Apis Cor's cylindrical coordinate arm, which provides enhanced mobility and transportability to remote locations, as well as reduced assembly time compared to cable robots [242]. The introduction of this method addresses the limitations posed by earlier technology like cable robots. While cable robots and gantry systems are limited to three degrees of freedom, robotic arms with six degrees of freedom offer greater versatility, allowing a single robot to perform multiple functions such as concrete deposition, component embedding, and post-processing. CC is criticised for being restricted to vertical extrusion, leading to 2.5D typologies rather than true 3D forms. This method relies on slicing software to convert 3D designs into 2D layers for extrusion, much like smaller-scale 3D printing techniques [64].

Robotic arms equipped with sensors to control feedback loops significantly improve printing accuracy. Each layer is filled using patterns such as Hilbert or Peano curves or honeycomb structures, with modifiable filling densities based on design requirements [115]. While this approach has proven effective in small-scale AM with metals or polymers, it faces challenges in large-scale projects, particularly with objects that require performance-driven design considerations or involve complex shapes, such as cantilevered structures [64]. The Tangential Continuity Method helps to overcome these limitations by eliminating weak interface zones between printed layers, as illustrated in Figure 2.27 (left), with red weak zones between grey printed layers.

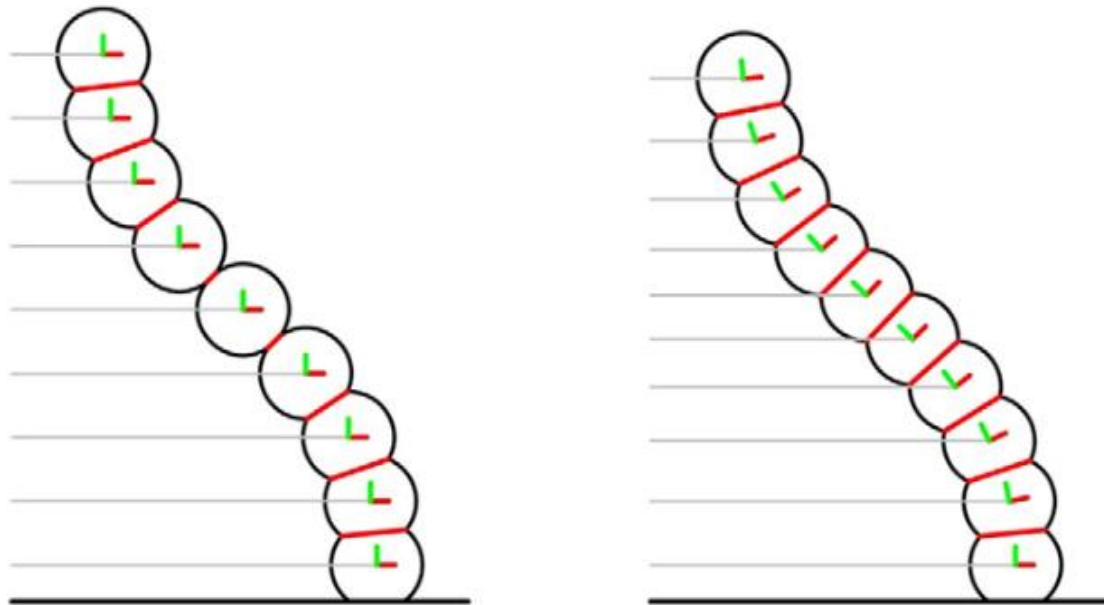


Figure 2.27. The Tangential Continuity Method (TCM) [115]

TCM is particularly well-suited for large-scale 3D printing due to its use of six-axis robotic arms, which enable the generation of truly three-dimensional building paths. Unlike traditional 3D printing, TCM utilises non-planar layers with locally varying thickness (grey), allowing for a more dynamic construction process [64]. The primary goal of this method is to maintain consistent contact surfaces between layers (red), thereby enhancing surface adhesion and eliminating geometrical gaps that could otherwise compromise structural integrity. These gaps are a frequent issue in powder-bed-based processes and fused deposition modelling [115]. From a structural mechanics perspective, TCM has been shown to produce more efficient and mechanically robust constructions. The increased degrees of freedom provided by six-axis robotic arms have been pivotal in the development and success of TCM. Several factors have contributed to the growing use of robotic arms in large-scale 3D printing, making them a dominant tool in both research and industrial applications. Key advantages include the flexibility and versatility of their software and hardware. Industrial robots such as KUKA, ABB, and Mitsubishi, commonly used in 3D printing applications, offer accessible scripting languages and user-friendly software, which simplify robotic trajectory control and planning [64]. However, a significant limitation of the robotic arm technique is its restricted reach. For projects that exceed the arm's range, the robot must be repositioned, which can add complexity and time to the printing process [242]. Despite this limitation, the use of robotic arms remains

a powerful and adaptable approach in the evolution of large-scale 3D printing. Other 3d printing systems include;

### 2.9.1. Gantry

The gantry system is a widely used technology in 3D printing, often referred to as a "giant 3D printer". This system utilises a gantry with an actuator to position the print nozzle across the x, y, and z axes in Cartesian coordinates [243]. Notable examples of gantry-based systems include D-Shape and CC, each utilising different printing techniques. CC employs a material extrusion method similar to fused deposition modelling, whereas D-Shape utilises binder jetting to deposit materials. D-Shape, in particular, is a large gantry-based 3D printer capable of constructing architectural structures with dimensions of up to 6 x 6 x 6 meters [243]. These systems have advanced the capability to print large-scale structures with precision and efficiency. Figure 2.28 shows a gantry system in action using CC as a method of extrusion.



Figure 2.28. Gantry system [244]

### 2.9.1.1 Mini-builders

Mini-builders offer a distinct approach to 3DCP, designed to implement AM in construction environments where transportation and human presence may pose significant risks [64]. A key feature of this technique is the ability of the robot to climb, which allows it to print vertically. However, the system's success hinges on the robots' ability to communicate and coordinate within a swarm, a process made possible by sensors that provide feedback and facilitate algorithmic decision-making [64]. The system comprises three specialised robots: the foundation robot, the grip robot, and the vacuum robot. The foundation robot, equipped with sensors, moves along tracks to build the concrete foundation. The grip robot attaches itself to the structure using four rollers and prints successive layers of concrete until the desired height is reached. Finally, the vacuum robot uses pressurised air and suction cups to print on the vertical surfaces of the structure while reinforcing it with horizontal layers. Together, these robots create an automated, multi-robot construction system that can efficiently build complex structures. Figure 2.29. shows mini-builders robots during the process of 3D printing.



Figure 2.29. Mini builder grip robots [64]

### 2.9.1.2 Cable suspended platforms

Cable-suspended platforms (Figure 2.30), also referred to as cable-driven robots, tendon-driven robots, or simply cable robots, have gained significant attention for large-scale 3D printing and manipulation tasks [61]. This system involves a printer head suspended by cables connected to an external frame. Motors control the extension and retraction of the cables, enabling automated movement of the printer head [61]. The main advantages of this technique include a larger workspace, increased flexibility, and efficient material transfer. An example of this technology in practice is the World Advanced Saving Project (WASP), an Italian company that has explored low-cost additive construction. WASP has successfully implemented cable robots using both natural and cementitious materials to build large-scale structures [245]. This approach offers a promising solution for sustainable and scalable construction.



Figure 2.30. WASP-Big Delta project. Full size 12m building built from clay and mud [64]

## **2.10. Printing parameter using material extrusion and a robotic arm**

The printing parameters need to be altered to control the quality of 3D-printed parts; these parameters include:

### **2.10.1. 3D printing orientation**

The build orientation is one of the most influential factors affecting the mechanical properties of 3D-printed parts. It impacts a range of printing characteristics, including overall printing time, cost, accuracy, mechanical strength, surface roughness, and material usage [243]. Of these, the effect on mechanical properties is the most critical, as it directly influences the performance and functionality of the printed parts, rather than merely affecting their appearance [243]

### **2.10.2. Thickness of deposited layers**

This parameter refers to the height of each layer after the successful deposition of subsequent layers during the 3D printing process. Layer thickness plays a vital role in determining the accuracy and surface quality of the printed part. Thicker layers lead to reduced forming accuracy and increased surface roughness, while thinner layers improve accuracy but increase printing time and reduce efficiency [246]. The optimal layer thickness depends on the material properties, nozzle diameter, and the required moulding precision [246].

### **2.10.3. Air gap**

Also known as the raster-to-raster air gap, this is the distance between two adjacent layers during the printing process. The air gap can significantly influence the surface quality of the printed parts. Figure 2.31, as shown in the study by Gebisa, [247].

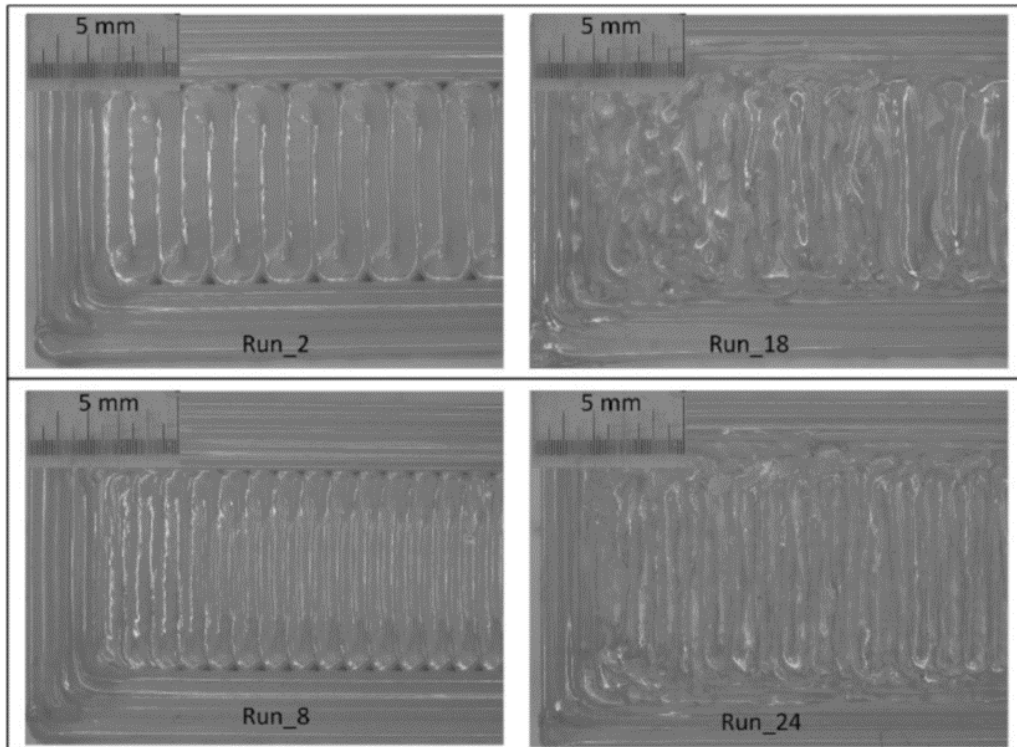


Figure 2.31. The effect of air gap on the surface quality of parts [247]

#### 2.10.4. Raster angle/width

Also referred to as infill orientation, the raster angle is the angle between the x-axis of the printing platform and the nozzle path during material extrusion [246]. The angle can vary between  $0^\circ$  and  $90^\circ$ , and it significantly impacts the mechanical performance and forming accuracy of the printed parts [246]. A higher or lower raster angle can influence how stress is distributed across the part, thus affecting its strength and durability. Raster width, on the other hand, refers to the width of the material bead extruded during the raster process [247]. This width plays a crucial role in the precision and quality of the 3D print, influencing the surface finish and structural integrity. Figure 2.32 shows several key parameters related to material extrusion during 3D printing.

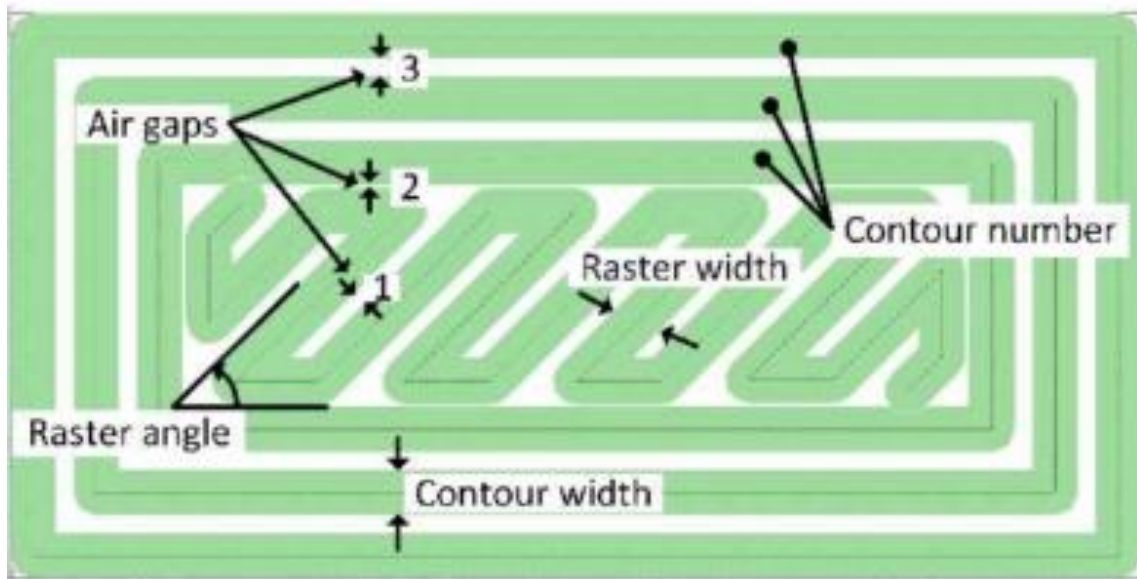


Figure 2.32. Overall material extrusion printing parameter [247]

#### 2.10.5. Nozzle design

The nozzle shape significantly influences the geometry and mechanical properties of 3D-printed structures. Lao et al. [248] concluded that using a rectangular nozzle resulted in better compactness and compressive strength in the printed part compared to a round nozzle. This significant improvement in both compactness and mechanical strength is critical for the goal of constructing safe accommodation structures. The higher mechanical strength contributes to raising the safety factor of this technology, which is essential for its application in real-world construction. Figure 2.33, shows models of different nozzle outlet shapes

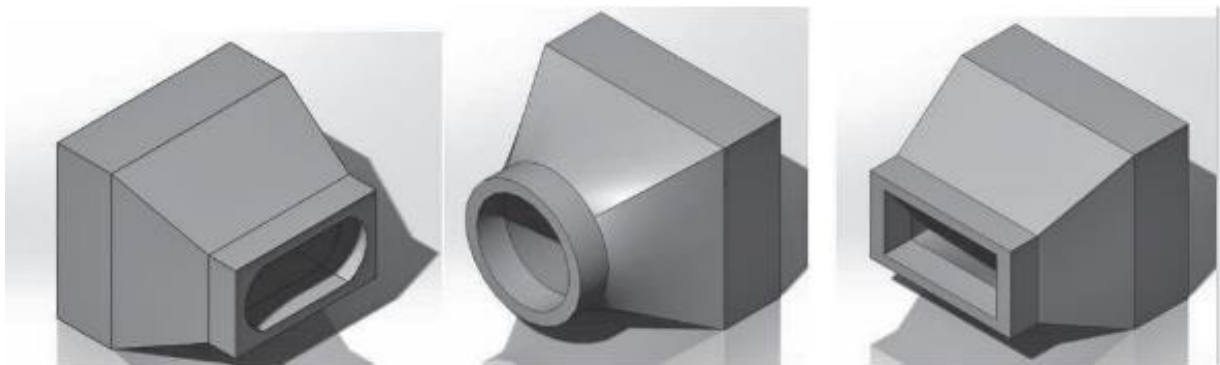


Figure 2.33. Models for nozzle outlet shapes [248]

#### 2.10.6. Flow rate

Flow rate in 3D printing of cement based materials refers to the volume of cement material extruded per unit time [151]. An optimal flow rate is crucial because if the rate is too high, the extruded filament may lose its shape or deform under its own weight, while a rate that is too low can interrupt the continuous deposition process, resulting in weak interlayer bonds. Factors such as pump pressure, nozzle dimensions, and the material's rheological properties determine the optimal flow rate [140, 249, 250]

### **2.11. Effect of nozzle parameters on fresh and hardened properties of cement-based materials**

The design of the nozzle plays a crucial role in the success of 3D printing of cement-based materials, as it directly impacts the quality, precision, and efficiency of the printing process. The shape, size, and configuration of the nozzle influence material flow, layer adhesion, and the overall structural integrity of the printed concrete [70, 251]. Proper nozzle design ensures consistent extrusion, enhances buildability and allows for better control over the geometric accuracy of the printed components. As 3D printing of cement-based structures scales up for real world construction projects, optimising nozzle design becomes essential for achieving high-quality, large-scale structures. Zhang et al. [70] concluded that the relationship between nozzle dimensions and print parameters is crucial for achieving high-quality 3D printing. They found that maintaining nozzle lift height equal to the layer thickness is essential for dimensional consistency and defect-free surfaces. Furthermore, they observed that reducing the printing speed increases the printable layer thickness and that layer width increases linearly with extrusion velocity, regardless of printing speed. Additionally, Zhang et al. [70] noted that the extrusion resistance is influenced by the length of the nozzle and cone angle and suggested that lowering extrusion velocity or the yield stress of the concrete can help reduce this resistance in fixed nozzle designs.

Manikandan et al. [252] discovered that the surface roughness of the printed constructs highlights the importance of selecting the appropriate nozzle geometry before printing. They observed that cylindrical constructs exhibited greater contour deviation when printed with a square nozzle compared to a circular one. Although using a square nozzle improves compression strength by increasing the density of the constructs, this benefit comes at the

expense of the external surface finish, which cannot be overlooked. Another study highlights that achieving buildable layers and the desired shape requires the use of an appropriately designed nozzle [1, 4]. Kwon [63] concluded that a square nozzle provides a better surface finish compared to an elliptical type. In another study, Lim et al. [20] used circular nozzles with varying diameters between 4–22 mm and determined that the optimum diameter for their study was 9 mm.

Building on the importance of nozzle geometry and configuration, it is essential to consider how these design choices interact with material behaviour during extrusion.

#### 2.11.1. Extrudability

Extrudability as stated earlier is the ability of a material to be smoothly pushed through a nozzle to form continuous and stable layers in 3D printing. It ensures consistent material flow, shape retention, and proper layer support. Extrudability measures include both flowability and shape stability, which are important considerations when the material is pumped through a nozzle [152, 253, 254].

#### 2.11.2. Flowability

Maintaining a balance between nozzle travel speed and extrusion rate is essential for ensuring reliable flowability during extrusion [255]. An excessive extrusion rate can generate compression stresses near the nozzle, leading to localised buckling of the filament [256]. On the other hand, a higher nozzle travel speed induces tensile stress in the filament, potentially causing deformation, cracking, or tearing [255]. Guowei et al. [87] also noted that if the extrusion speed is slower than the hydro-conductivity of the filament, liquid phase seepage may result in filament blockage. Furthermore, if the speed of the nozzle at corners is too slow while the extrusion rate remains constant, included angle errors may occur, distorting subsequent filaments. Therefore, proper adjustments to nozzle movement speed and extrusion rate are necessary, especially for different nozzle turning radii [257]. Studies indicate that flowability is influenced by the nozzle's size, shape, height, and movement path [257-259]. Shakor et al. [260] found that nozzle shapes impact the severity of these shocks, with rectangular nozzles experiencing higher interception due to their corners. Avoiding such

interceptions remains a challenge that requires further research. Roussel et al. [255] Concluded that the distance between the nozzle outlet and the printed filament affects flowability, with smaller distances causing localised compression and filament deformation. To minimise intercepting shocks, adjustments to nozzle size, shape, travel speed, and the distance between the nozzle exit and the filament are needed [178, 261]. Given the uncertainties surrounding slurry flowability, it is especially crucial in 3D concrete printing (3DCP) compared to traditional construction methods with formworks.

### 2.11.3. Buildability

Several studies have shown that buildability is influenced by factors such as nozzle size, shape, movement path, travel speed, and height. Le et al. [262] concluded that filaments extruded through smaller nozzles experience lower pressures compared to those from larger nozzles [260]. Similarly, Rahul et al. [146] found that material extruded through a smaller nozzle exhibited significantly lower yield stress than material extruded through a larger nozzle. Jie et al. [263] noted that low nozzle rotation speeds could cause angular errors and twisting filaments during turns, especially with rectangular nozzles where material deposition rates differ between the inner and outer radius [257]. No research has quantitatively examined material extrusion rate variations during turns, even though uneven extrusion rates can lead to cracking and inconsistent layer thickness [264]. However, deformation caused by nozzle turning can be mitigated by increasing nozzle travel speed and adjusting the corner radius [257]. Shakor et al. [178] found that surface cracks appear when nozzle speed exceeds 45 mm/s or falls below 35 mm/s, potentially increasing stress inhomogeneity and reducing the filament's load-bearing capacity. Additionally, increasing the nozzle's distance from the build exacerbates stress inhomogeneity [255, 265].

### 2.11.4. Shape stability

Shape stability in 3D printing is influenced by the nozzle's height and shape. Rob et al. [259] found that increasing the nozzle height causes curling between layers, while decreasing the distance leads to surface squeezing, potentially adding load to the unhardened mortar and destabilising the printed filaments. Shakor et al. [260] observed that filaments printed with a

rectangular nozzle were slightly wider than the nozzle itself, and similar results were seen with circular nozzles, which is due to varying internal load distribution and squeeze flow. The nozzle's deposition location also affects shape stability, as positioning errors can cause uneven extrusion and filament deformation [178].

Other factors, such as nozzle size, travel speed, and movement path, also impact shape stability. Larger nozzles can cause collapse due to insufficient filament support, while smaller nozzles can lead to mortar separation [89]. Nicolas et al. [255] noted that filament deformation is strongly linked to compressive stresses, which result from slower nozzle speeds generating stress within the filament and causing buckling. Conversely, higher speeds can tear or break filaments [29]. Filament swelling and corner rounding often occur during corner deposition, and increasing nozzle speed and reducing material flow at corners can mitigate this issue [257]. Zhixin et al. [258] further explained that deceleration, shearing, and warp occur near the nozzle exit, but there are still no studies on filament anisotropy near the nozzle.

#### 2.11.5. Interlayer bonding

Various studies have demonstrated that nozzle geometry affects interlayer bonding, nozzle-to-surface distance, and nozzle travel speed [146, 214, 216, 266]. Le et al. [110] found that nozzle size and shape significantly influence void formation, which can impact the contact areas between layers and interface pressure distribution. Rectangular nozzles create fewer voids compared to circular ones during extrusion [248]. There are mixed conclusions regarding the relationship between nozzle-to-build distance and interlayer adhesion strength. Panda et al. [88] observed that the highest bond strength occurs when the nozzle distance matches the printed layer height, while increased distance can cause inaccurate filament deposition and uneven pressure distribution [216]. However, Yu et al. [214] found that nozzle distance variations of 0, 5, and 10 mm had minimal effect on interlayer bonding. Additionally, slower nozzle travel speeds increase printing time, leading to drier printed layers as surface moisture evaporates. This drying can cause the printed filament to absorb moisture from newly deposited layers [132], while gas escaping from the filament's surface results in poor adhesion strength [88].

#### 2.11.6. Nozzle speed

The travel speed of the nozzle plays an important role in determining key factors such as bond strength [199], filament width [88, 89], tensile strength [132], and the maximum number of printed layers [89]. Increasing nozzle speed can lead to reduced filament width or even filament breakage while decreasing travel speed can result in excessive material deposition and larger deformations. Panda et al. [88] investigated the impact of varying nozzle speeds on the properties of fresh concrete used in 3D printing and showed that an optimal printing speed supported a consistent layer bead width throughout the process. However, it was also observed that the bonding strength of the printed layers slightly decreased with increasing nozzle speed. Similarly, Kruger et al. [136] developed a design model for 3D concrete printing that predicted the optimal printing speed to prevent structural failure under specific conditions. Weng et al. [71] explored the effect of various nozzle travel speeds (14.5 mm/s, 29 mm/s, 58 mm/s, 92 mm/s, and 116 mm/s) on bond strength and recommended a speed of 116 mm/s and a pump rotational speed of 1200 r/m to achieve optimal bond strength (3 MPa), which is about 1.5 times higher than the bond strength at 14.5 mm/s (1.9 MPa). Yiwei et al. [131] examined the relationship between nozzle speed and interlayer adhesion strength, showing that increasing the nozzle speed from 14.5 mm/s to 116 mm/s resulted in a significant 57.9% increase in adhesion strength. Shakor et al. [178] recommended a nozzle speed between 34.99 mm/s and 46.56 mm/s for mortar mixes but noted that the quality of the printed filament is influenced by the type and proportion of superplasticisers, retarders, and accelerators used, warranting further research on the interaction between chemical admixtures and nozzle travel speed. Jie et al. [263] examined the impact of nozzle travel speed and volumetric flow rate on print quality using four square nozzles of different sizes (10 mm, 15 mm, 20 mm, and 24 mm). The authors found that nozzle speeds of 50-60 mm/s, combined with appropriate flow rates, produced the best quality prints, and this optimal speed range appeared independent of nozzle size.

Changbin et al. [89] found that increasing the nozzle travel speed from 80 mm/s to 100 mm/s reduced the number of maximum deposited layers by approximately 60%. This reduction is likely related to variations in layer cycle time due to increased speed, though further investigation is needed to quantify this effect. Tay et al. [216] studied the effect of nozzle travel speeds on extrudability, concluding that speeds between 80 mm/s and 100 mm/s yield optimal filament width and surface quality. Below 80 mm/s, filaments become significantly wider,

while speeds above 120 mm/s can lead to filament cracking. These findings provide guidelines for defining optimal nozzle travel speeds. Hanzhao et al. [114] noted that inconsistencies between nozzle and pumping hose geometry could cause blockages, although the exact impact of this inconsistency on print quality remains unclear. Liu et al. [257] conducted a numerical simulation and found that reducing the nozzle aspect ratio improves mass distribution within filaments, particularly during turns. Jie et al. [263] tested four nozzles (10 mm, 15 mm, 20 mm, and 24 mm) with different volumetric flow rates, concluding that a 15 mm nozzle size produces the best filament quality. They also discovered that once the nozzle size exceeds 20 mm, the growth rate of optimal nozzle size slows as volumetric flow rate increases. Interestingly, when the volumetric flow rate decreases, the optimal nozzle size rises, with the 15 mm nozzle even requiring a smaller flow rate than the 10 mm nozzle.

## **2.12. Summary**

The chapter provided a comprehensive review of 3D printing in the construction industry, with a particular focus on cement-based materials and the integration of robotic systems. It highlighted the benefits of 3D printing, such as enhanced design flexibility, reduced labour costs, and faster construction timelines, while also addressing key challenges, including shrinkage, cracking, and weak interlayer bonding. The use of robots, especially multi-axis robotic arms, was shown to significantly improve automation, precision, and efficiency in the printing process, enabling the realisation of more complex geometries. Different printing systems, such as gantry setups, swarm robotics, and cable-suspended platforms, were explored for their applicability in large-scale projects. The chapter also emphasised the importance of optimising mix designs to achieve desirable properties like flowability, extrudability, and buildability and discussed the critical role of nozzle design and printing parameters, including layer orientation, height, thickness, and speed, in influencing the quality and mechanical performance of printed structures. The use of accelerators was noted for their ability to improve buildability and early-age strength. Overall, the chapter offered valuable insights into the relationship between materials, robotics, and process optimisation for more efficient and sustainable 3D concrete printing.

# **CHAPTER 3: MATERIALS AND METHODOLOGY**

---

**Part A: Materials**

**Part B: 3D Printing Set-Up**

**Part C: 3d Printing Processing Parameters**

**Part D: Performance Evaluation Methods**

**Part E: Finite Element Analysis**

## **Chapter 3: Materials and Methods**

### **Part A: Materials**

#### **3. Introduction**

This chapter outlines the materials, equipment, and experimental procedures used in this study to develop and evaluate 3D-printed cement-based structures. It is divided into five main parts: materials, printing setup, processing parameters, evaluation methods, and finite element analysis. The materials section introduces the raw components and chemical admixtures used in the mix design, while the printing setup covers the development and configuration of the robotic extrusion system. Detailed descriptions of the printing process, including nozzle and pump design, are provided to support repeatability. The chapter also presents the methods used to assess workability, buildability, mechanical performance, and structural stability. Together, these methodologies establish a comprehensive framework for investigating the influence of mix composition and printing parameters on the performance of 3D-printed structures.

#### **3.1. Materials**

##### **3.1.1. Raw material**

This study utilised Portland-limestone mastercrete cement (CEM II/A-L) produced by the Tarmac company. It was an enhanced Portland-limestone cement, which conformed to the BS EN 197-1 CEM II/A-L standard. The properties included, but are not limited to, lower water demand, enhanced resistance to thaw attack and freeze, and reduced likelihood of water segregation and bleeding. Fly ash 450-N that was produced according to the BS EN 450-1 standard was used as an additive to enhance the mechanical properties of the 3D-printed structures. The fly ash conformed to the normal fineness (N) Category of BS EN 450-1:2005 and met the requirements for Loss on Ignition Category B (2-7%). Although, the maximum permitted residue on a 45 $\mu$  sieve was 40%, test results for the product typically fell well within the limit. The powder had a bulk density ranged from 800 to 1000 kg/m<sup>3</sup>. Another additive used was Ground Granulated Blast-furnace Slag (GGBS), according to the BS EN 15167-

1:2006. This product was an environmentally friendly high quality, low carbon dioxide ( $CO_2$ ) material that was a by-product from the production of iron. Building sand was used as a fine aggregate. The particle size had a maximum particle size of 1 mm. An optimum water/binder ratio of 0.45 was used to ensure workability.

### 3.1.2. Chemical accelerator

The chemical accelerator was aluminium sulphate, a chemical compound with the formula  $Al_2(SO_4)_3$ . Aluminium sulphate acted as an accelerator during the 3D printing process, promoting faster setting times [117, 122]. The specific product used was aluminium sulphate octa-decahydrate, which was available in a highly pure form.

### 3.1.3. Mixture design and preparation methods

Table 3.1 presents the mixture design used to conduct this research. The binder-to-sand ratio was 1.5:2. Additives, such as fly ash and GGBS were added to the mixture to improve the cement properties. The binder mixture consisted of 20, 30 and 50% of fly ash, GGBS, and cement, respectively. These proportions are consistent with established mix design practices in 3D concrete printing, where 20–30% fly ash and GGBS [85, 108] are commonly used to enhance workability and durability without compromising early strength, while 50% cement ensures adequate reactivity for structural performance [84].

Table 3.1. Mixture design.

Material	Quantity ( $kg/m^3$ )	Technical properties
Fine building sand	40	$\leq 1.0$ mm Chlorides $\leq 0.01\%$ Acid soluble sulphates $\leq 0.8$ Total Sulphur $\leq 1\%$ Drying shrinkage $< 0.01\%$
Mastercrete cement	15	Conforming to BS EN 197-1 CEM II/A-L
Fly ash	6	Conforming to BS EN 450-1 Finess category N LOI Category B

		Loss of ignition < 7%
		Density 800-1000 kg/m <sup>3</sup>
		Silica 50%, Alumina 26%
Ground Granulated Blast-furnace Slag (GGBS)	9	Conforming to BS EN 15167-1:2006
Water.	45% of binder weight.	Hydrating substance.

## 3.2. Material preparation and printing procedure

### 3.2.1. Accelerator

The required amount of aluminium sulphate was measured using a measuring cup and a weight scale. Deionised water (DI water) was then added to a container, followed by the mixing of the aluminium sulphate. Deionised water, also known as demineralised water, is water that has had its ions removed. Ions are electrically charged particles, and the deionisation process removes these charged particles, including minerals and salts, from the water [267]. This process results in water that is highly pure and free from impurities, minerals, and ions.

Deionisation typically involves passing water through specialised ion exchange resins or membranes. These materials selectively remove positive ions (cations) and negative ions (anions) from the water, replacing them with hydrogen ions (H<sup>+</sup>) and hydroxide ions (OH<sup>-</sup>), which combine to form pure water [267]. In contrast, tap water contains ions that come from various sources, including the natural environment, pipes, and other channels. These ions may include Sodium (Na), Calcium (Ca), Iron (Fe), and Copper (Cu) [267].

It is crucial to add the aluminium sulphate (Al<sub>2</sub>(SO<sub>4</sub>)<sub>3</sub>) to the DI water rather than the reverse to avoid triggering an exothermic reaction. An exothermic reaction is a chemical process that releases energy in the form of heat. During such a reaction, the system loses energy to the surroundings, typically leading to an increase in temperature (ACS, 2023). Additionally, the choice of container is a critical consideration, as using a metal container could result in an undesirable chemical reaction with the aluminium sulphate. Using correct personal protective

equipment, the aluminium sulphate was thoroughly dissolved in the DI water through stirring, followed by a settling period to ensure complete dissolution.

Other accelerators were also considered, such as calcium sulphate, sodium aluminate, lithium carbonate, and calcium chloride, but each had drawbacks, ranging from higher costs and corrosion risks to compatibility issues, that made them less suitable for the specific requirements. Aluminium sulphate was therefore chosen for its rapid setting performance, moderate cost, and manageable downsides, making it the most practical option.

### 3.2.2. Dry/raw material

The study utilised cement-based materials, including sand (BS EN 933-1), mastercrete cement (BS EN 197-1 CEM II/A-L), fly ash, GGBS and aluminium sulphate. Fly ash 450-N (BS EN 450-1 2005) and GGBS (BS EN 15167-1:2006) substituted part of the cement on a mass-for-mass basis. Sand particles were sieved according to the BS EN 933-1, using a metallic sieve. This was carried out due to the restriction on maximum grain particle size of 1.5 mm, considering the capacity of the cement pump used. A sieve analysis was conducted after drying the sand in an oven at 100-120 °C for 48 hours to remove moisture. This was crucial to determine the water/binder ratio. Dry materials (sand, cement, fly ash and GGBS) were weighed and mixed, using a cement mixer. The mixer was inspected for cleanliness and set up on a stable surface. The mixing sequence included sand, cement, fly ash and GGBS, followed by 5 minutes of machine mixing, 2 minutes of manual mixing and another 5 minutes of machine mixing. An optimum water/cement ratio of 0.45 was obtained to ensure workability and extrudability. Water was added slowly in one-go into the mixer, followed by 4 minutes of machine mixing and 2 minutes of manual mixing and a final 4 minutes of machine mixing, totalling 10 minutes. The prepared material was then transferred to the cement pump for 3D printing.

## Part B: 3D printing set-up

### 3.3. Development and optimisation of set-up

To ensure the safe operation of the robot system, the manufacturing of a security enclosure was essential to safeguard users from potential injuries and simultaneously prevent damage to the robot. The conceptual framework for the design of the robot's security enclosure was derived from the specifications outlined in Table 2. The robot's maximum reach, which is 502 mm, was utilised as the primary reference dimension for the enclosure design. This measurement ensured that the enclosure adequately contained the robot's movements while maintaining a secure boundary for user interaction.

#### 3.3.1. Steel table (Stage 1)

A rectangular steel table measuring 141 cm by 65 cm was utilised as the base of the structure to support the weight of the robot. The table featured a flat surface with an approximate weight of 15 kg, making it suitable for bearing the payload necessary to construct the robot's security enclosure. Figure 3.1 shows the red table.



Figure 3.1. Table used to support the setup

### 3.3.2. Marine plywood (Stage 2)

Two pieces of marine plywood, each cut to the dimensions of 70.5 by 141.0 cm, were affixed to the metal table using bolts and Nyloc nuts to securely hold the plywood in position. This modification was intended to increase the total surface area required for the robot during full operation. Given that the robot was positioned centrally on the table and had a maximum reach of 502 mm, an additional 200 mm of tolerance was provided on each side to prevent potential collisions or accidents. The robot was bolted through both the plywood and the steel table to ensure maximum support and structural integrity. Wooden beams were fastened along the edges of the marine plywood to further enhance the structural strength of the setup. Marine plywood, a high-quality wooden material, was selected due to its inherent structural strength derived from cross-lamination and its ability to resist moisture and water pressure, owing to the application of waterproof adhesive. As the name suggests, "plywood" consists of thin sheets of wood veneer, commonly referred to as plies. Other materials considered for this application included standard plywood and oak wood, however, marine plywood was ultimately chosen because it offered enhanced structural strength and moisture resistance. While standard plywood lacked the durability needed in moist or high-pressure conditions, and oak wood, despite its strength, proved less cost-effective and practical for the required dimensions, marine plywood's cross-laminated construction and waterproof adhesive provided the optimal balance of performance and reliability for the application.

Additionally, a layer of Polyvinyl Chloride (PVC) was applied to the surface of the marine plywood to prevent cement from adhering to it. PVC was selected for its waterproof properties, high tensile and mechanical strength, and significant chemical resistance. The choice of PVC was also influenced by its lower cost compared to polycarbonate sheets, making it a more economical option for this specific purpose.

Figure 3.2 shows the marine plywood utilised in the construction of the robot security enclosure.

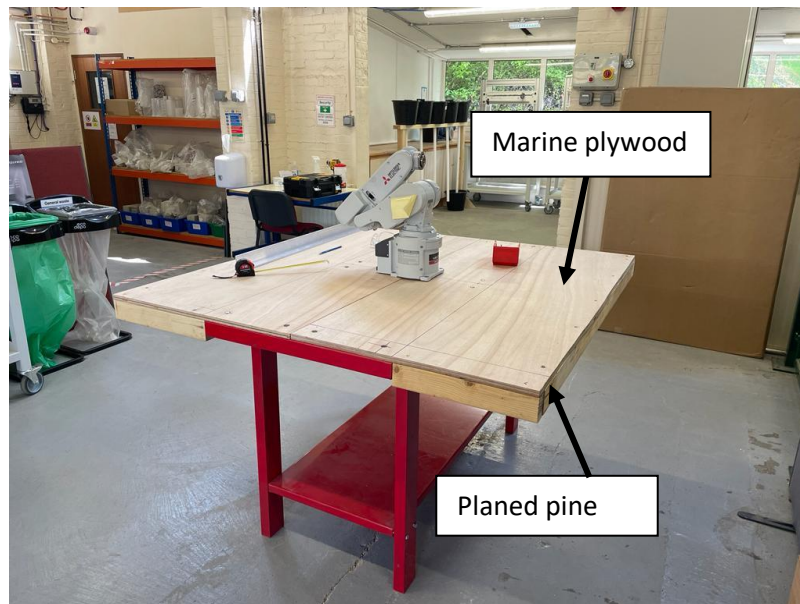


Figure 3.2. Marine plywood used to provide the total working area for robot system

### 3.3.3. Polycarbonate sheet and Polyvinyl Chloride (PVC) (Stage 3)

A polycarbonate sheet with a thickness of 6 mm was utilised to secure the sides of the security enclosure. Holes with a diameter of 5.2 mm were drilled into the sheets, which were then firmly fastened to the aluminium angles using 5 mm bolts and nuts. Polymer expansion was considered during the design. Hence, a 0.2 mm tolerance was included to prevent cracking. The primary purpose of the polycarbonate sheets was to protect against cement splashes, and their transparent nature allowed the operator to observe the printing process. This material was chosen for its durability, impact resistance, water resistance, transparency, toughness, and low moisture absorption. Other materials considered for this application included acrylic and glass; however, they were not used because they did not offer the required impact resistance and durability.

### 3.3.4. Aluminium angle and steel (Stage 4)

Aluminium angles, each measuring 1 metre in length and 5 mm in thickness, were employed to reinforce the corners of the polycarbonate sheets, as depicted in Figure 3.3. The structural aluminium angles were selected due to their favourable properties, including low density, lightweight nature, non-toxicity, workability, corrosion resistance, and recyclability. In addition to providing reinforcement, the angles were used to conceal gaps between the polycarbonate sheets and to cover any rough edges. Zinc-plated

steel hinges were utilised to secure the door of the robot security enclosure, ensuring both functionality and durability.

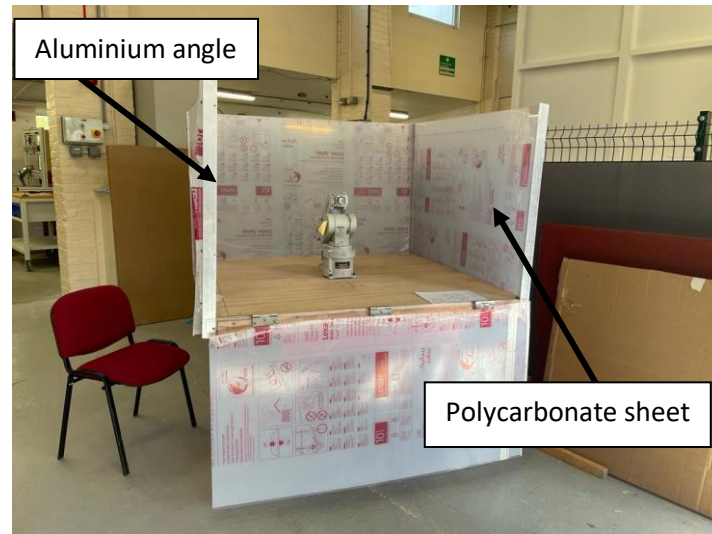


Figure 3.3. Aluminium angle to reinforce the corners of the polycarbonate sheets

### 3.3.5. Micro switches (Stage 5)

According to the robot specifications, two micro switches, commonly referred to as the door switch function, were required to be installed on either side of the security enclosure door to ensure safe operation. These switches monitor the status of the security door and halt the robot's movements when the door is opened [268]. Unlike an emergency stop, the servo motor is deactivated when the door is opened, but no error is triggered [268]. In automatic mode, the servo powers down and the robot ceases operation upon the door being opened. Figure 3.4 illustrates the micro switches used in this research. The micro switch selected for this purpose was the Honeywell micro switch, chosen for its ease of use, durability, lightweight nature, and superior performance. The switches were securely fastened to both sides of the door using bolts and nuts, ensuring reliable functionality.

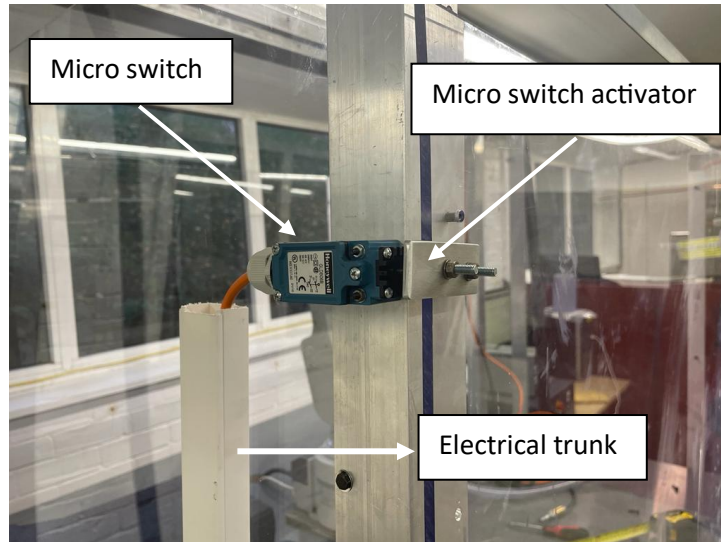


Figure 3.4. Micro switches, activator, and electrical trunk

### 3.3.6. Emergency stop (Stage 6)

For the safe operation of the robot, an emergency stop button was installed. The primary function of this button was to forcibly stop the robot's operation in the event of an emergency, with the intent of preventing harm or minimising the risk of injury to individuals or damage to the machine. To reset the system after the emergency stop had been triggered, the procedure involved releasing the button, resetting the alarm, turning the servo back on, and pressing the reset button. Screws were used to securely fasten the emergency stop button in place. Figure 3.5 shows the installed emergency stop button.



Figure 3.5. Schneider Electric emergency stop button

### 3.3.7. Electrical wiring and trunking (Stage 7)

To ensure the robot operated under safe conditions, electrical wiring was required to install the micro switches, and the emergency stop button. The wiring was conducted in accordance with the standard specifications outlined in the robot's manual. Screws were used to secure both the emergency stop button and the micro switches on either side of the door, after which the electrical connections were made. The wires were directly connected from the micro switches to the controller, as was the case with the emergency stop button. For health and safety considerations, Polyvinyl Chloride (PVC) electrical trunking was installed to shield the wires from potential hazards, such as water exposure, which could otherwise pose risks of electric shocks or fire. The trunking also contributed to improving the aesthetic layout of the system, reducing injury risks, and offering protection for the cables. Additionally, plastic P-clips were used to mechanically secure the cables beneath the table (enclosure). Following the installation, the micro switches and the emergency stop button were thoroughly tested to confirm their proper functioning and ensure they operated under ideal conditions.

### 3.3.8. Gantry system (Stage 8)

According to the robot specifications, the maximum allowable load for the robot was 2 kg, necessitating the introduction of a gantry system. The purpose of this system was to support the weight of the concrete feed pipe by suspending it, thereby relieving the robot of excessive load. Additionally, the gantry was designed to house other critical components, including the return feed pipe, pressure gauge, pinch valve, and the printing supply pipe.

Various materials were considered for constructing the gantry, with aluminium ultimately selected due to its favourable properties, such as low density, lightweight, non-toxicity, workability, corrosion resistance, and recyclability. Metal drills were used to create holes in the aluminium structure, which was then securely fastened to the red metallic table using bolts and Nyloc nuts. Nyloc nuts were specifically chosen for their ability to securely lock the bolts in place. Figure 3.6 shows the gantry system.

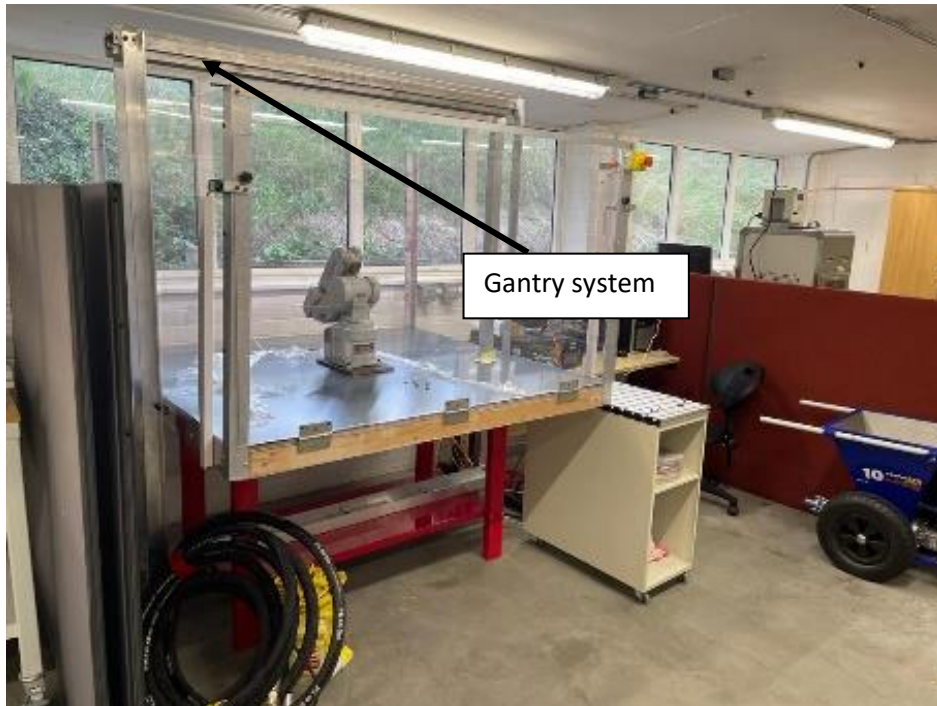


Figure 3.6. Gantry system to reduce the weight on the robot arm

### 3.4. 3D printing robot configuration

The Mitsubishi RV-2F-D robot was utilised for this project. It operated with a CR-750 controller and a teaching pendant 35 model, which allowed for manual control of the robot. This robot is a vertical 6-axis, multiple-jointed type, featuring an optimised arm length designed to offer a wider range of movement, thereby supporting complex assemblies and various process operations, as illustrated in Figure 3.7. The robot has a maximum load capacity of 3 kg (rated for 2 kg) and is equipped with slender arms and a compact body, enabling it to reach a distance of 504 mm as shown in Figure 3.8. It can operate in both automatic and manual modes [268] and is versatile in terms of installation, as it can be wall-mounted or placed on a flat surface. The full standard specifications for the robot are detailed in Table 5.2. This robot is suitable for a wide range of applications, from assembling electrical components and transporting machine parts to performing pick-and-place tasks. Its environmentally friendly design makes it ideal for installation in various settings [268]. Mitsubishi has incorporated intelligent technologies such as highly accurate force and vision sensors, which allow the robot to control the intensity of the force it applies. This innovation has enabled robots to work in adverse environments and perform highly complex tasks that were previously beyond the

capabilities of automation. Other advanced technologies integrated into the system include 2D vision sensors, tracking capabilities, and multi-function grippers, among [268].

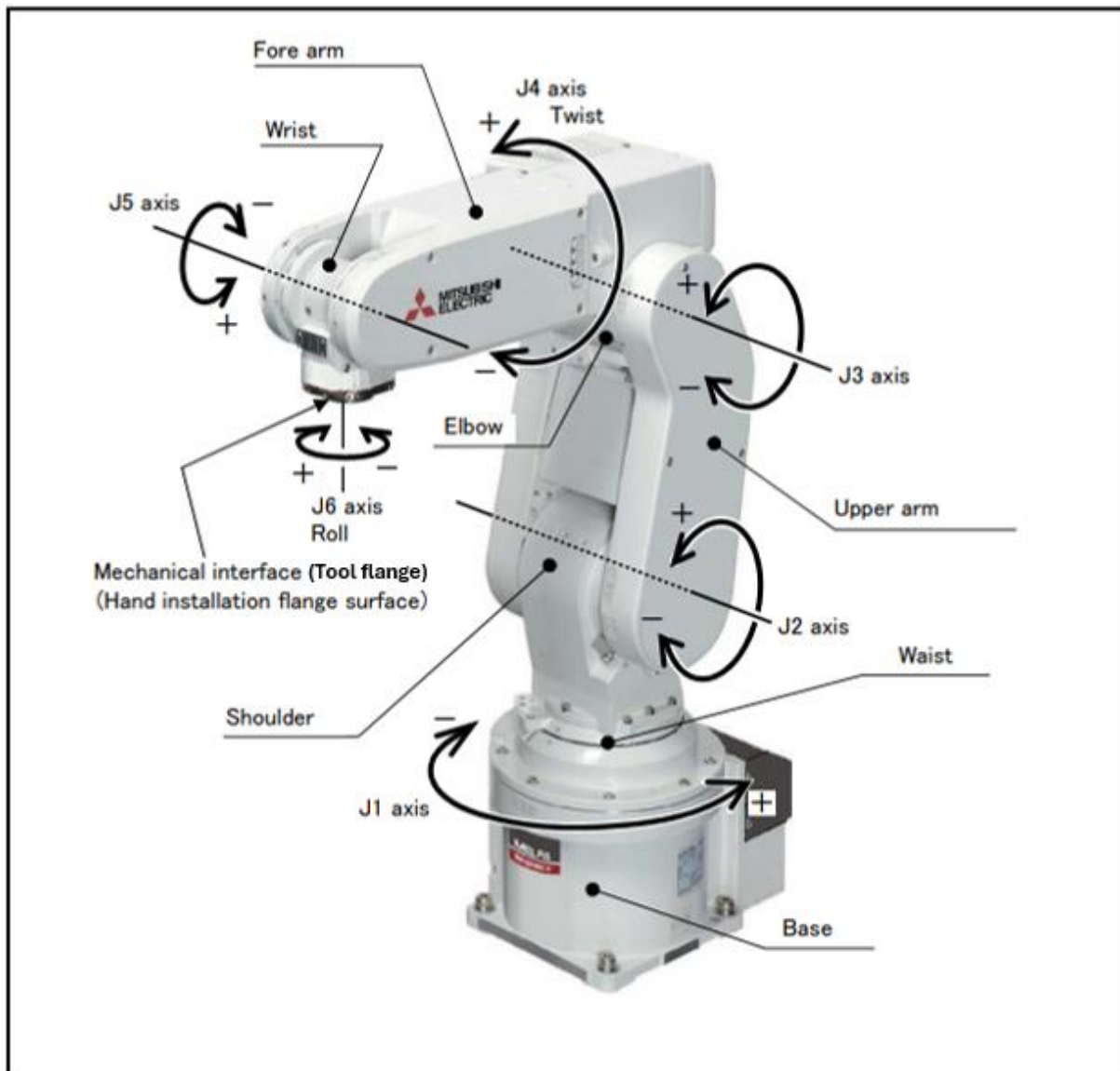


Figure 3.7. Names of each part of the robot [268]

The design of the robot ensures resistance to corrosion caused by chemical cleaning agents [268]. In earlier models, the tool flange was plated, but more recent designs have incorporated stainless steel to further enhance corrosion resistance. This improvement promotes better cleanliness and detergency, making the robot suitable for tasks such as conveying or processing medicinal products [268].



illustrates the various materials used to ensure the safe and hygienic manufacturing of the robot system.

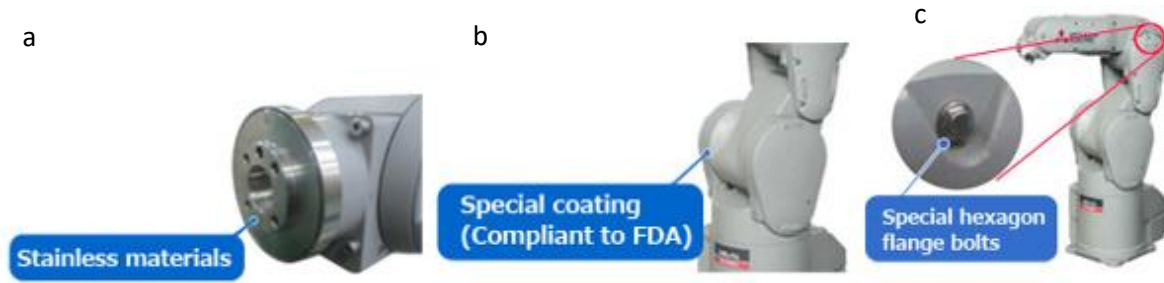


Figure 3.9. a) Stainless material used on the tip of the robot, b) Chemical resistant coating to chassis, c) Special hexagon flange bolt [268]

The robot arm is protected according to specifications that comply with the International Electrotechnical Commission (IEC) [268]. Tables 3.2 and 3.3 present the safety specifications and standard specifications for the robot respectively.

Table 3.2. Robot safety specification

Type	Protection specification (IEC Standards value)	Applicable field	Classification
RV-2F series	Robot arm, Ingress Protection 30 (IP30) on all axes	Can be used in a slightly dusted environment and for assembly applications	General environment specifications

The IEC IP symbol defines a degree of protection against solids and liquids and does not indicate a degree of protection against oil or water ingress [268]. Liquids such as water and oil may cause the robot to corrode or rust.

Table 3.3. Robot standard specification

Item	Unit	Specification
Type		RV-2F
Degree of freedom		6

Structure			Vertical, multiple joint type
Arm length	Forearm	mm	270
	Upper arm		230
mass		kg	19
Arm reachable radius front p-axis centre point		Mm	504
Load	Maximum	Kg	3
	Rating		2
Operating range	Waist (J1)	Degree	480 (-240 to +240)
	Shoulder (J2)		240 (-120 to +120)
	Elbow (J3)		160 (0 to +160)
	Wrist twist (J4)		400 (-200 to +200)
	Wrist pitch (J5)		240 (-120 to +120)
	Wrist roll (J6)		720 (-360 to +360)
Maximum resultant velocity		mm/sec	4,950
Speed of motion	Waist (J1)	Degree/s	300
	Shoulder (J2)		150
	Elbow (J3)		300
	Wrist twist (J4)		450
	Wrist pitch (J5)		450
	Wrist roll (J6)		720
	Waist (J1)		

The robot uses a standalone controller (CR750D) which is similar to the existing models and is shown in Figure 3.10. The robot controller uses a control nucleus which enables the construction of cells [268]. This is a standard interface that allows the development of systems optimised for their applications. It can be connected to the simple (R32TB) or highly efficient (R56TB) Teaching Pendant (TB).



Figure 3.10. Robot controller and teaching pendant

### 3.4.1. Robot controller technical specifications

Table 3.4 presents the robot's standard specifications

Table 3.4. Robot controller specifications

Item	Unit	Specification
Controller type		CR750-02VD-1
Number of control axis		6 simultaneously
Robot language		MELFA-BASIC V
Mass	g	approximately 16
Outline dimension		CR750: 430(W) x 425(D) x 174(H)
Operating temperature	Degree Celsius	0 to 40
Ambient humidity	%RH	45 to 85

### 3.4.2. Robot software

The software used in this project was the latest version of Mitsubishi RT ToolBox3, a next-generation program creation software that offers significant improvements over its predecessor, RT ToolBox 2. Key features of RT ToolBox3 include an output window, docking plane, and a ribbon bar, which enhance usability by making information easier to view and the software more intuitive to navigate [268]. The 3D monitor screen has also been upgraded, providing a more user-friendly interface, as illustrated in Figure 3.11. The software is compatible with Windows operating systems and supports a range of robot controllers, including the CR750-Q/D series, CR800-R/D series, CRnQ/D-700 series, and CRn-500 series.

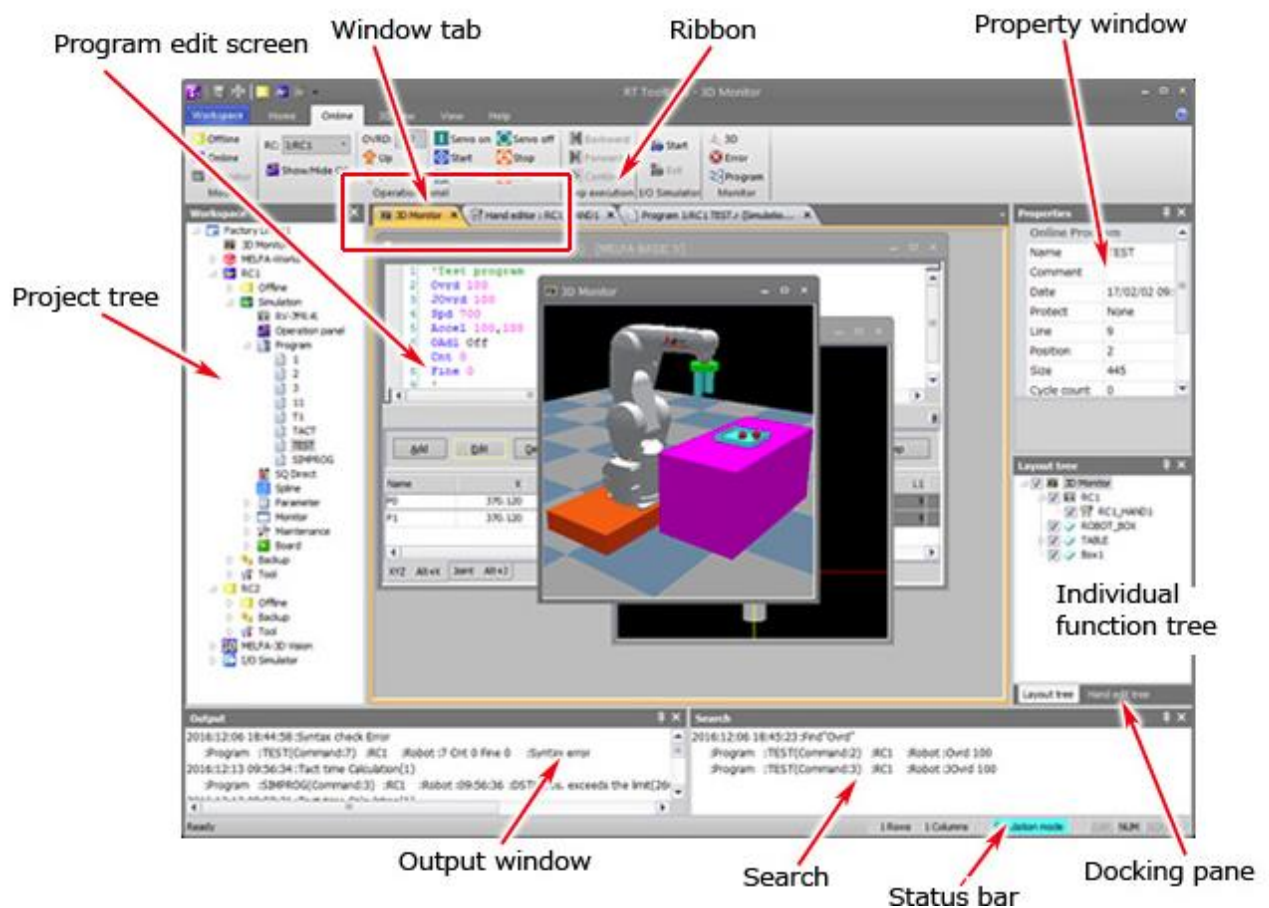


Figure 3.11. RT Toolbox 3 Operation screen [268]

### 3.4.3. Programming

The software employs a programming language called MELFA-BASIC, which comes in several versions, including MELFA-BASIC IV, V, and VI [268]. For this project, MELFA-BASIC VI was used, as it expands and enhances the command set that the robot can interpret. Layout shown in Figure 3.12. This version enables a more comprehensive programming experience, facilitating the robot's operation with greater precision. Structured programming principles were applied to achieve a high level of code reusability and readability [268]. Figure 3.13 illustrates the programming process involved in 3D printing a rectangular structure. The first step involved defining the speed (using the command "ovrd 20"), followed by capturing the coordinates of the robot at specific points. For this rectangular structure, six positions were defined, labelled P0 through P5. P0 marked the robot's starting position, P1 to P4 corresponded to the four corners of the rectangle, and P5 acted as the finishing point, where material deposition occurred. The command "mov" was used to move the robot to a designated position using joint interpolation, while "Mvs" was employed to move the robot with linear interpolation. Single or double quotes (‘ or “) were used to separate printing layers, indicating that characters were being written directly into the code. At the end of the programme, the command "End" was used to signal the completion of the printing process.

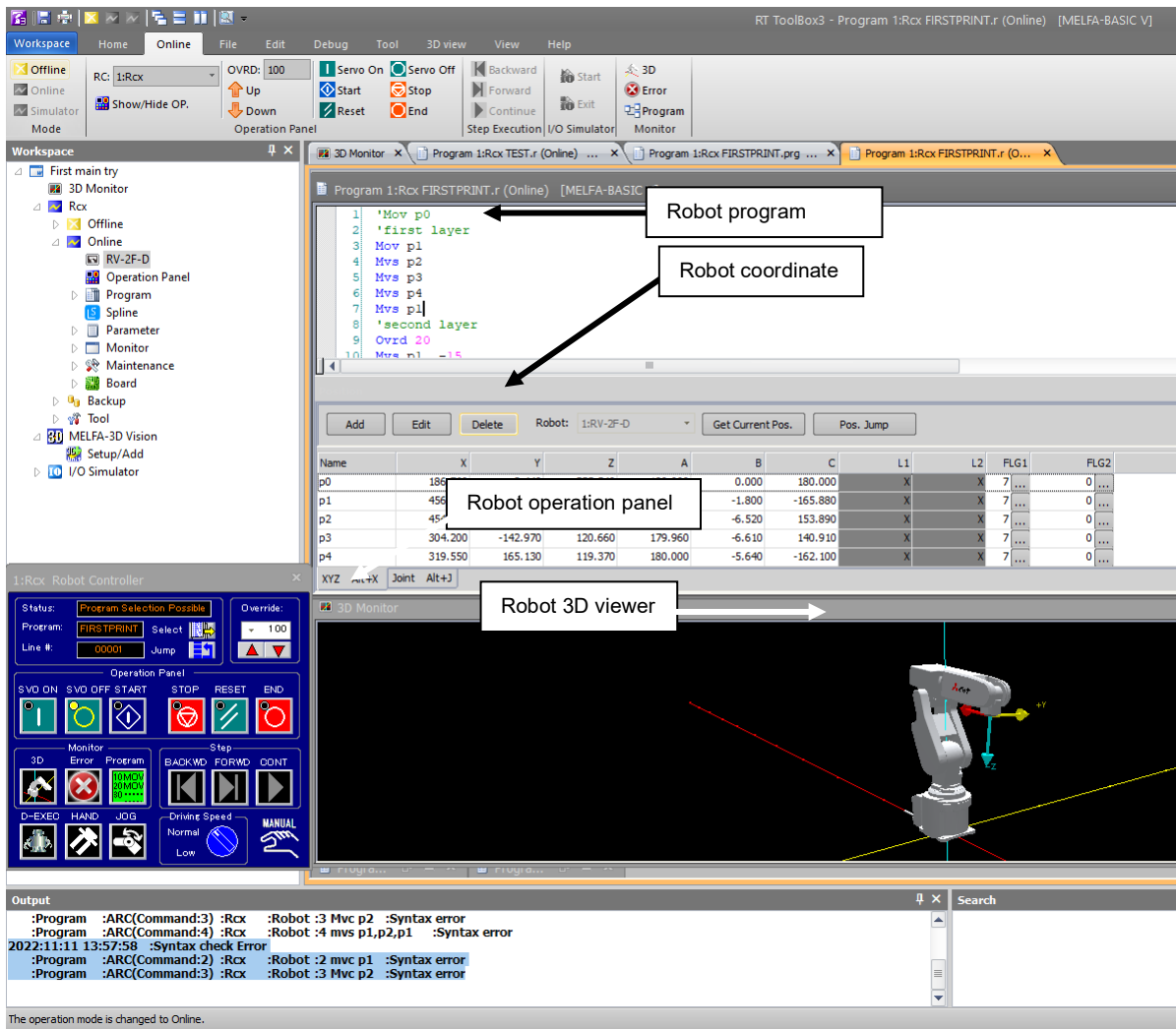


Figure 3.12. Robot programming and operation panel

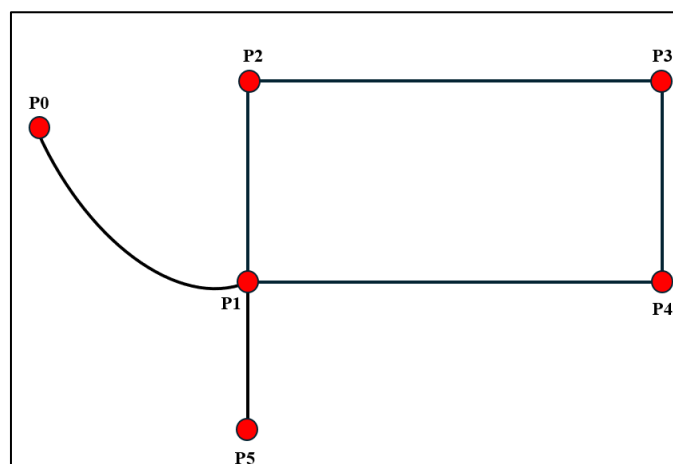


Figure 3.13. 3d printing path

#### 3.4.4. 3D Viewer

The 3D viewer is a powerful tool that allows users to easily verify robot poses and movements, as well as limit values of user-defined parameters. It also enables the virtual placement of peripheral devices by basic objects. In addition, the tool can identify potential interferences between the robot and peripheral devices. Users can also take advantage of distance measuring functions that are available on the screen. Overall, the 3D viewer is a highly useful feature that can greatly enhance the robot programming and verification process.

#### 3.4.5. Software maintenance function

Maintaining a robot is crucial for ensuring its longevity and optimal performance. There are various ways to maintain a robot, such as setting origin data and initialising different information. Some of the functions that aid in maintenance include maintenance forecasting, position recovery support, and parameter management. With maintenance forecasting, operators can reference the timing of parts replacement, such as greasing, battery, and belt replacement, from operation data collected so far in the robot controller. Additionally, there are other useful functions like position repair and servo monitoring that can help ensure the smooth operation of the robot.

### **3.5. Design and development of small-scale robot extrusion nozzle**

#### **3.6. Design requirement**

The design of the nozzle for cement-based 3D printing must carefully balance multiple technical requirements to ensure its effectiveness, durability, and compatibility with the robot system. One of the key considerations is weight, as the robot has a payload capacity of 2 kg. It is essential to ensure that the nozzle, along with any additional components like the cement feed pipe, does not exceed this limit. Exceeding the payload can lead to malfunctions or even damage to the robotic arm.

To reduce the overall load, lightweight but durable materials, such as plastic or aluminium, are often preferred. The diameter and shape of the nozzle are also crucial for controlling the extrusion flow and achieving the desired layer resolution. Material compatibility is another important factor. Cement-based mixtures are abrasive, so the nozzle needs to be made from materials that can withstand continuous wear and tear. Flow control must be considered in the nozzle design, as the viscosity of cement-based materials can vary, affecting how the material is extruded.

The nozzle geometry should be optimised to prevent clogging and ensure consistent material flow, which is essential for producing uniform layers and reducing defects. Proper flow control also helps improve layer adhesion and overall print quality. For cases where additives or accelerators are mixed with the cement, the nozzle may need an internal mixing mechanism to ensure homogeneity. The design must account for potential issues like backpressure, which can disrupt material flow. A well-integrated mixing mechanism ensures that the material is consistently mixed and deposited which is critical for maintaining structural integrity.

Adaptability is another key aspect of the nozzle design. It should be flexible enough to accommodate different printing conditions and materials. For example, variations in cement mixtures or changes in flow rates may require adjustments to the nozzle's geometry. An adaptable design increases versatility and allows the nozzle to be used in a wide range of applications, making it more practical for scaling up or experimenting with different materials.

Safety is paramount in the design of the nozzle, especially when dealing with high temperatures, pressures, or chemical interactions. The nozzle must comply with safety standards such as Control of Substances Hazardous (COSHH) Regulations, Ease of cleaning and maintenance (BS EN 1672), and EN ISO 12100, amongst others, to prevent hazards such as burns, chemical exposure, or mechanical failures. Incorporating safety features like proper insulation, safety valves, and pressure relief mechanisms can help mitigate risks during operation.

### 3.6.1. Design process

The design methodology used within this work includes the different stages as shown in Figure 3.14.

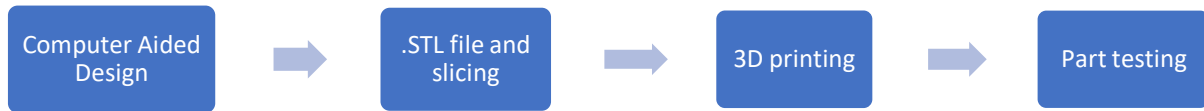


Figure 3.14. Process of 3D printing robot nozzle

Firstly, the nozzle was designed using CATIA, a Computer-Aided Design (CAD) software. The CAD file was then converted into stereolithography (.STL) format before being sent to the slicing software. Slicing refers to the process of converting a 3D computer model into G-code, which a 3D printer can interpret and execute. G-code is a standardised control language used by CNC machines and 3D printers [44]. After the printing process was completed, post-processing was performed to remove all the support structures used during printing and to smooth any sharp edges. The nozzle prototypes were printed using an Adventurer 4 Flashforge 3D printer, utilising Polylactic Acid (PLA), a thermoplastic material derived from renewable sources such as sugarcane or corn starch. Due to its biodegradable nature under appropriate conditions, PLA is one of the most popular bioplastics, making it suitable for a wide range of applications. The material is relatively easy to print with and offers high stiffness compared to other materials such as nylon and Acrylonitrile Butadiene Styrene (ABS). PLA was initially selected to facilitate early-stage design testing due to its excellent printability and low cost, which enabled quick and efficient iteration of multiple nozzle geometries before committing to a more durable material for final use. However, one limitation of PLA is its low heat and chemical resistance. Despite this, PLA was chosen during the initial design phase to simplify the manufacturing of multiple prototypes. Its printability allowed for rapid design iterations and adjustments without the added cost or complexity of machining aluminium components. Table 3.5 presents the key properties of PLA material.

Table 3.5. Properties of PLA material.

Item	Quantity
Density ( $\text{g/m}^3$ )	1.25
Elastic modulus (GPa)	35
Poisson ratio	0.3
Specific heat capacity ( $\text{J}/(\text{Kg}\cdot\text{K})$ )	1200
Thermal conductivity ( $\text{W}/(\text{m}\cdot\text{K})$ )	0.12
Tensile strength (MPa)	65

### 3.6.2. Nozzle design 1

The initial design concept of the nozzle was created to fit seamlessly onto the robot system as shown in Figure 3.15. This design featured a material inlet branch pipe and an outlet pipe intended to facilitate a smooth and consistent flow of material into and out of the nozzle. However, the primary issue with this design was that the material inlet branch pipe was positioned at a  $90^\circ$  angle relative to the material exit pipe.

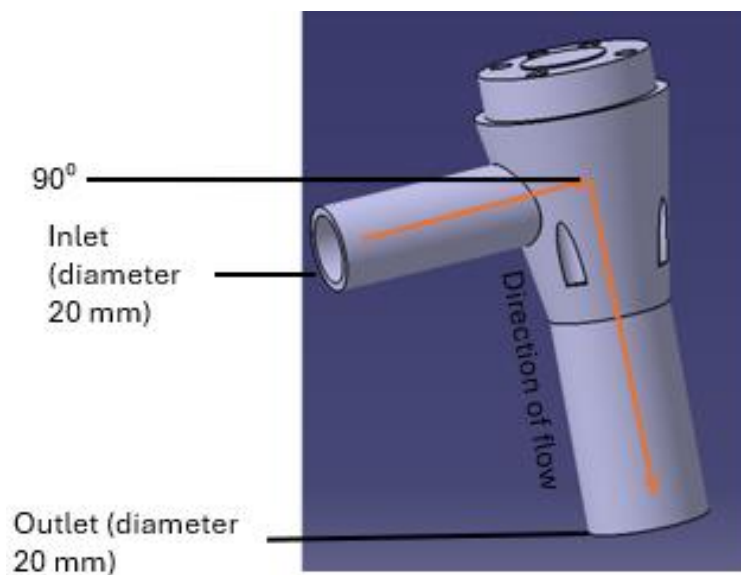


Figure 3.15. Nozzle design 1

According to Cali. [269], this configuration led to a significant concentration of stress on the outlet pipe. The sharp edges of the straight pipes caused the material to collide with the walls of the outlet pipe before abruptly changing direction towards the exit. This high level of stress

concentration could potentially result in cracks or, over time, dramatically shorten the lifespan of the nozzle by weakening its structure. Figure 3.16 illustrates a comparison between the flow of material in sharp corners versus filleted corners, highlighting the impact of design on stress distribution and flow dynamics.

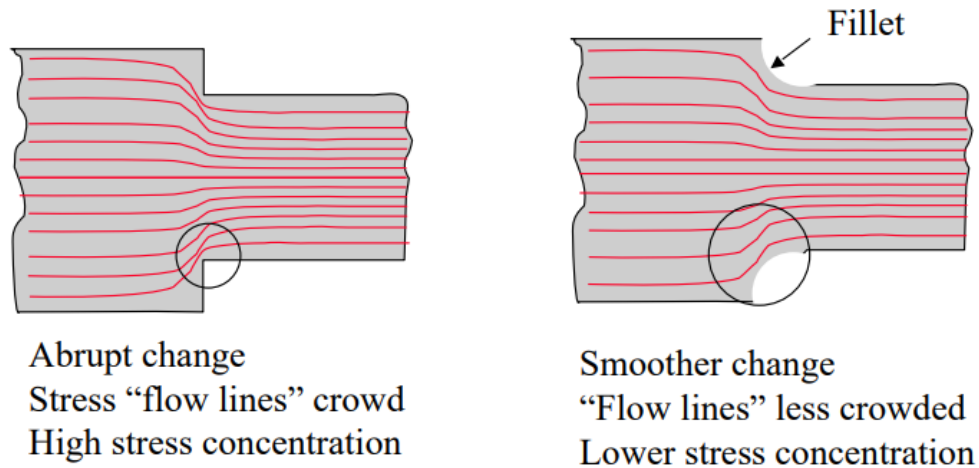


Figure 3.16. Comparison between filleted corner stress and sharp corner [269]

Stress concentration is a critical issue in structural engineering, as it involves localised areas where the material experiences significantly higher stress compared to a uniform configuration. This elevated stress can lead to structural failure, making it crucial to accurately predict, evaluate, and address factors that contribute to stress concentration [269]. As previously discussed, stress concentration typically arises from abrupt changes in geometry, variations in cross-sections, shape discontinuities, and the presence of straight or sharp edges. The severity of stress concentration increases when these geometric alterations are more pronounced and abrupt. For instance, a sudden 90° change in the flow of material, as in the initial nozzle design, should be avoided at all costs. Instead, components should be designed with the smoothest possible geometry to distribute stress more evenly. A practical solution to mitigate stress concentration is the use of fillets, which are curved transitions between adjoining surfaces. Incorporating fillets helps to reduce the value of the Stress Concentration Factor (SCF) by smoothing out sharp transitions, thus improving the durability and performance of the component [269].

A circular extrusion nozzle was chosen for its proven advantages in achieving uniform flow, dimensional stability, and smoother surface finishes in extrusion-based 3D printing of cement-

based materials. Manikandan et al. [252] discovered that round nozzles resulted in lower surface roughness and contour deviations compared to square nozzles. They also found that square nozzle provide higher compressive strength but this introduces more surface defect. Zhang and Sanjayan [70] also mentioned that circular extrusion nozzles decrease extrusion resistance, encouraging steadier material flow and reducing blockages.

### 3.6.3. Nozzle design 2

The second nozzle design was optimised, with the material inlet pipe positioned at a 45° angle to promote a smoother flow of material compared to the initial design. This modification helped to reduce the stress on the outlet pipe, although the concentration of stress remained relatively high. Figure 3.17 illustrates the flow of material through the nozzle in this optimised design, highlighting the improvements made to the material flow and stress distribution over the first version and the 3D-printed prototype.

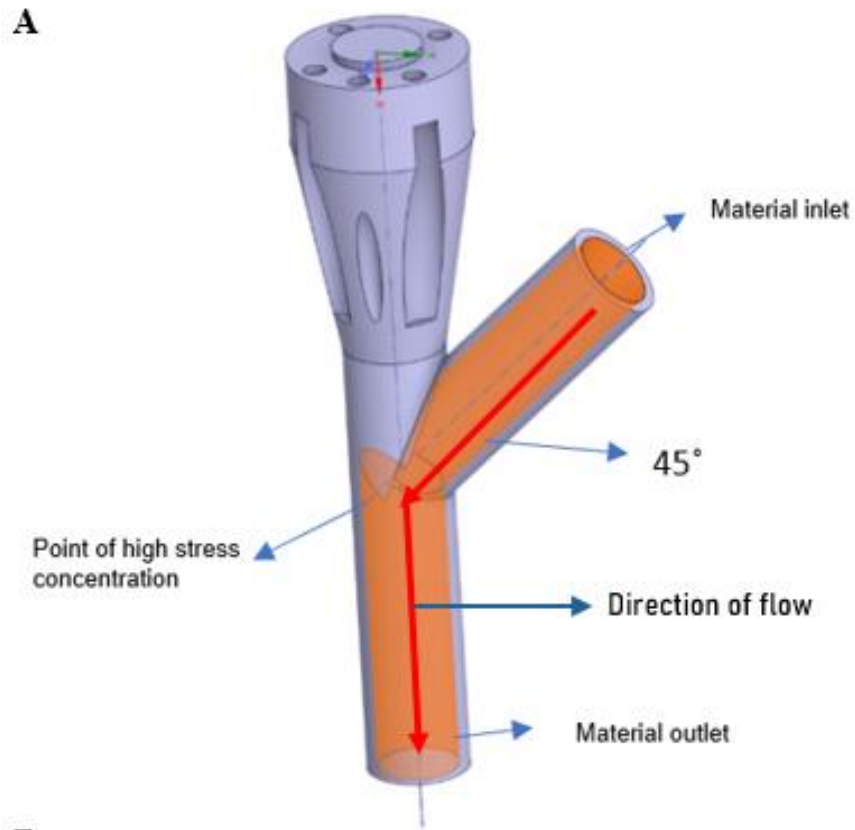


Figure 3.17. (a) Material flow view of second nozzle prototype showing the point of high stress concentration and (b) 3D-printed prototype of the nozzle

### 3.6.4. Nozzle design 3

The third design concept was subsequently developed, as shown in Figure 3.18. In this iteration, a curved pipe was introduced as the material inlet pipe still at an angle of 45°, significantly reducing the stress concentration on the outlet pipe. However, despite the improvement in stress distribution, the design still exhibited issues with stress concentration at the joint due to the presence of sharp edges and the abrupt change in the direction of material flow. This indicates that while the curved inlet improved overall performance, further refinement was needed to address the remaining stress concentration at critical points.

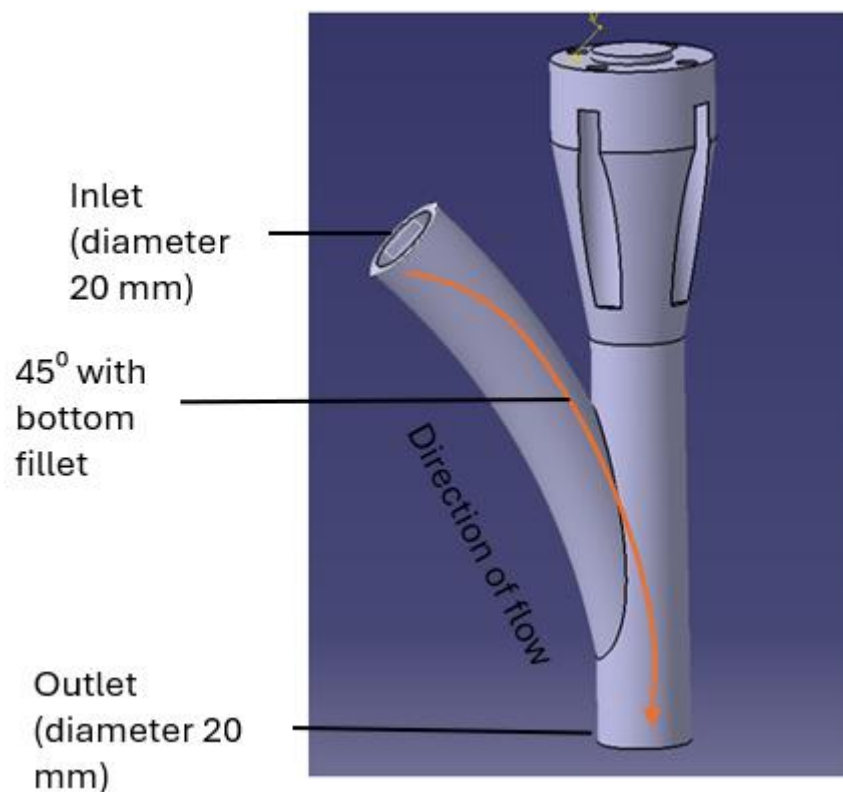


Figure 3.18. Nozzle design 3

### 3.6.5. Nozzle design 4

The fourth design, as shown in Figure 3.19, was a simpler yet more effective solution. The material inlet was positioned at a 45° angle to the material outlet, and additional features, such as a curved material inlet and edge fillets, were incorporated to enhance the flow of material and reduce stress concentration within the pipe. Furthermore, screw holes were precisely engraved onto the nozzle to facilitate a secure and easy connection to the robot

system. The dimensions of the extrusion nozzle are detailed in Table 3.6, ensuring the nozzle's compatibility with the overall system while improving performance and durability.

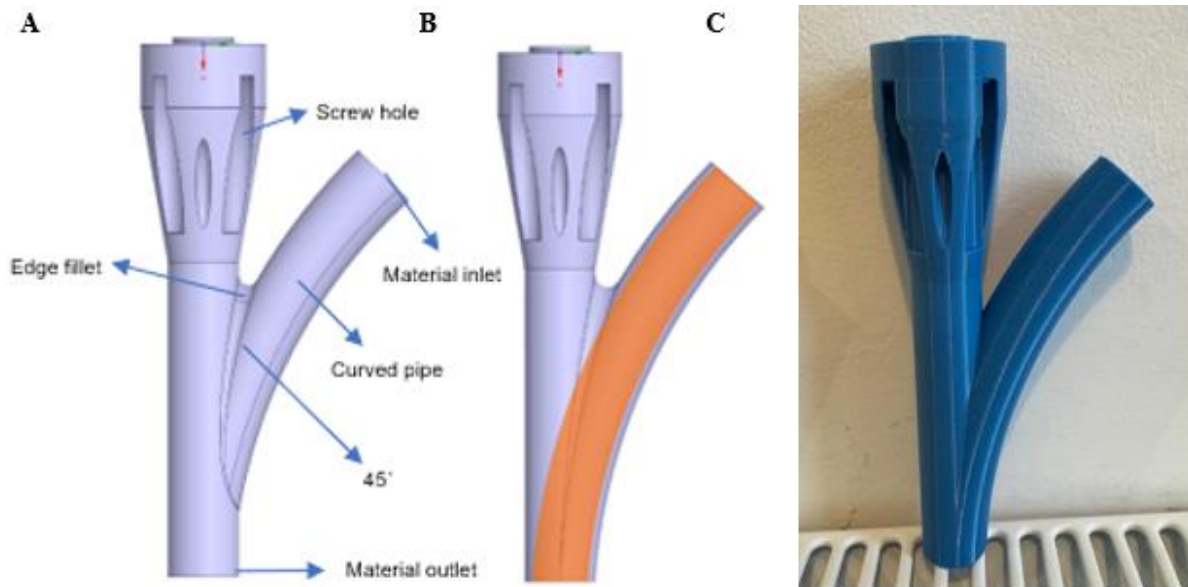


Figure 3.19. (a) CAD view showing labelled features, (b) Cross sectional view/ section cut view of the fourth design showing a smooth flow of material across the print nozzle and (c) 3D-printed prototype of the nozzle

Table 3.6. Size of the simplified extrusion nozzle

Item	Quantity
Branch pipe length (mm)	50
Main pipe length (mm)	100
Branch pipe angle (°)	45
Pipe diameter (mm)	20
Outlet diameter (mm)	20

### 3.7. 3D printing process

This section outlines the key stages of the 3D printing process, exploring the technologies, materials, and parameters essential to achieving high-quality, 3D-printed structures. The specific 3D printing process utilised in this research is depicted in Figure 3.20.

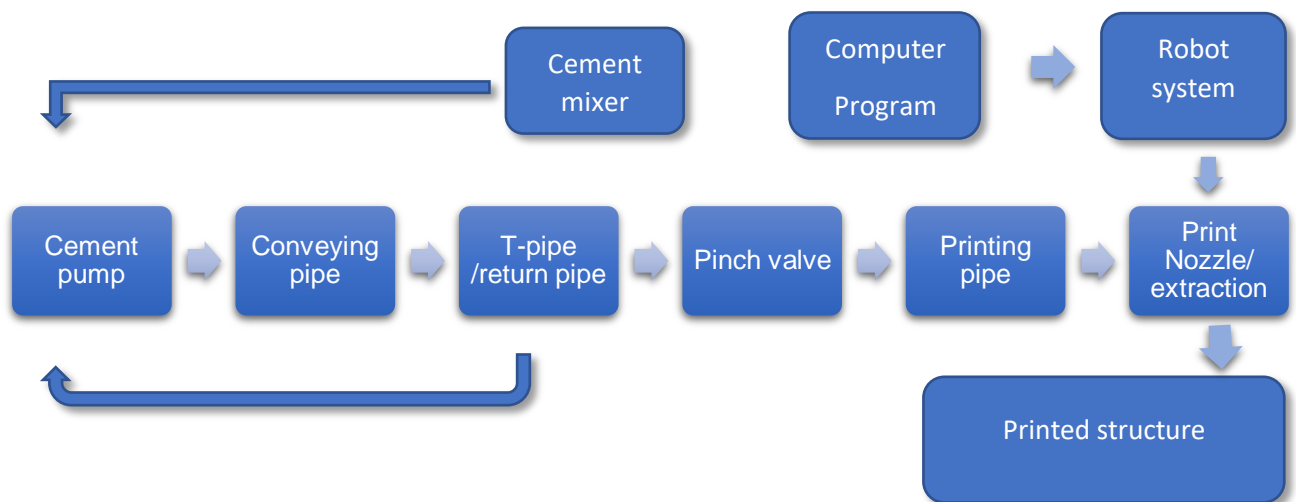


Figure 3.20. Process of 3D printing

#### 3.7.1. Cement mixer

The cement mixer used in this research was the SOROTO forced action 80 L mixer, as shown in Figure 3.21. This mixer proved highly effective, facilitating the quick and efficient mixing of cement mortar. It features a rotating drum and mixer arms that rotate at an angle to ensure thorough mixing of the concrete. The use of removable mixer arms also made cleaning more convenient. The mixer is equipped with a dust controller designed to vacuum dust, removing approximately 80–90% of dust while still allowing the operator an unobstructed view of the mix [270]. The dust controller is easily attachable to the mixer and compatible with most vacuum cleaners, helping to prevent illnesses such as asbestosis and lung cancer [270]. For added safety, the mixer is equipped with an automatic switch that shuts off the pump when the lid is opened. Additionally, the telescopic legs of the mixer are easily adjustable, allowing material to be discharged into a bucket or wheelbarrow through the mixer gate at the bottom of the drum. The compact size of the mixer makes it highly portable and easy to manoeuvre. These mixers are commonly used in small to medium-scale construction projects.

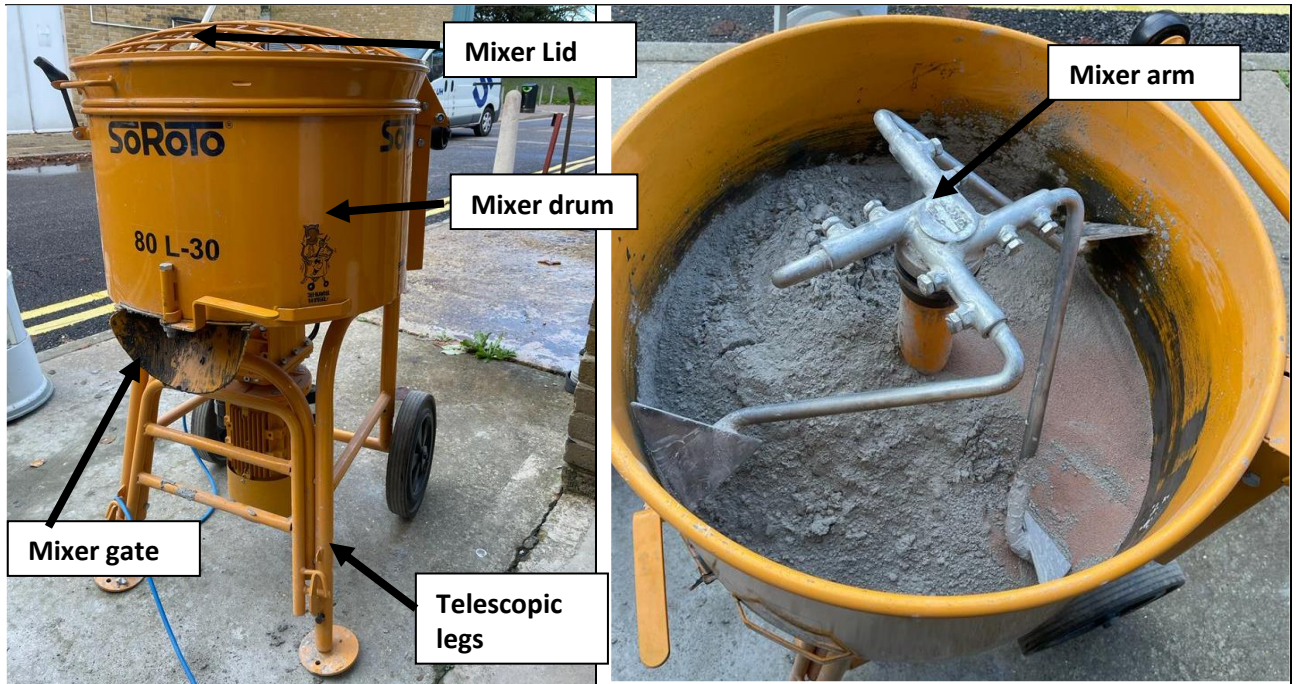


Figure 3.21. Cement mixer (SOROTO forced action mixer)

### 3.7.2. Cement mixer technical specifications

Table 3.7 presents the technical specifications of the cement mixer.

Table 3.7. Technical specification of cement mixer.

Forced action mixer (L)	Motor (V)	Weight (Kg)	Height (cm)	Width/length (cm)	Drum capacity (L)	Mixing capacity (L)	Output (Kw)	RPM	Standard blades
80	240/ 110	86	109- 127	60/75	81	80	11	30	Steel

### 3.7.3. Transformer

The cement pump operates with an input rating of 230 V/16 A/50 & 60 Hz and an output of 110 V. Given that the standard amperage in the laboratory was 13 A, the use of a transformer was necessary. A transformer is an electrical device that either steps up or steps down voltage by transferring electrical energy from one alternating current (AC) circuit to another while

maintaining the frequency of the current. This device was crucial for powering the cement pump during the 3D printing process. Figure 3.22 illustrates the transformer utilised for this purpose.



Figure 3.22. Transformer from RS component

#### 3.7.4. Mortar pump

The mortar pump used for this research is a Markham compact pro-10. It is a powerful machine with an in-line motor. It is light and robust and can easily be transported due to its simple design. The two large diameter wheels and the shaft type handles are the 2 main factors that enhances its ease of transportation [271]. The mechanism used to drive the pump is a progressive cavity pumping system that guarantees maximum performance, as shown in Figure 3.23. It consists of a specially designed metal rotor and an elastomer stator [272]. A metal rotor drives the stator through a chain and begins to fill the cavity with an equal volume of liquid, which is forced out of the pump outlet [272]. The fluid pocket has a fixed volume that determines the volumetric flow rate of the pump, which is directly proportional to the speed of the rotor, resulting in minimal pulse and low levels of shearing. To begin operation, the cement pump is turned on and the rotor begins to rotate. Clean water is used to flush the system down before cement mortar is poured into the cement pump directly from the cement mixer. The cement pump conveys the material through the material conveying pipe. Figure 3.24 shows the compact pro 12 cement pump.



Figure 3.23. Markham mortar pump

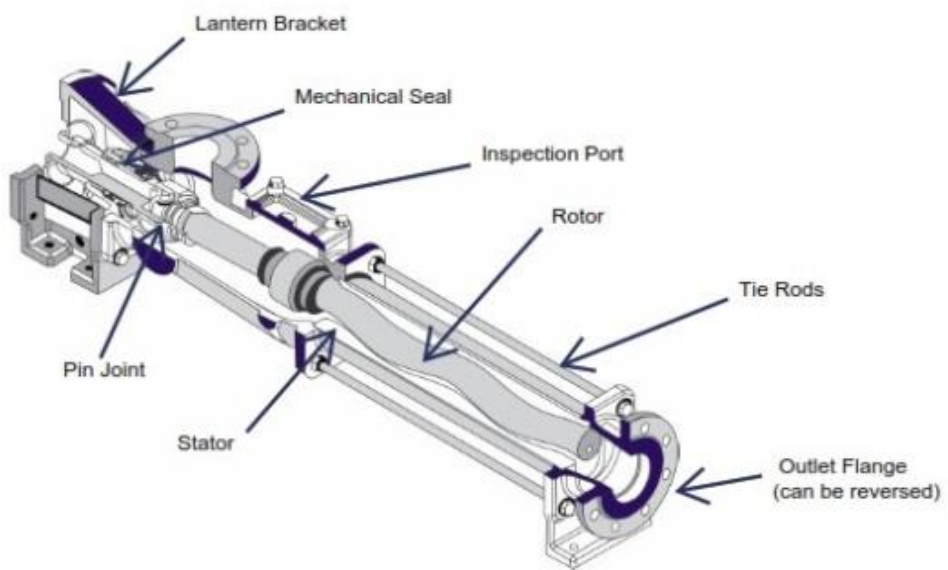


Figure 3.24. Illustration of progressive cavity pump [272]

### 3.7.5. Mortar pump technical specification

The dimensions and technical specifications are presented in Table 3.8.

Table 3.8. Technical specifications of mortar pump.

Technical properties	Quantity
Product pressure	0-20 bar
Product flow rate	0-8 kg/min
Power supply	110v/16A/50 & 60 Hz
Motor power	0.55 kw
Integrated compressor	No
Tank capacity	37 L
Maximum grain size	1.5 mm
Pipe diameter	25 mm
Length	86 cm
Width	48 cm
Height	70 cm
Weight	38 cm

### 3.7.6. Material-conveying pipe

The material-conveying pipe has a length of 8 m, and it is rated at a maximum pressure of 60 bar. As the name implies, it is used to convey material from the cement pump to the robot nozzle. It is also connected to a T- piece that connects to the return feed pipe. The T-piece is a device that allows material to flow through the inlet and then through the outlet which is connected to the return feed pipe. Figure 3.25 shows the material conveying pipe, T-piece, and pinch valve.

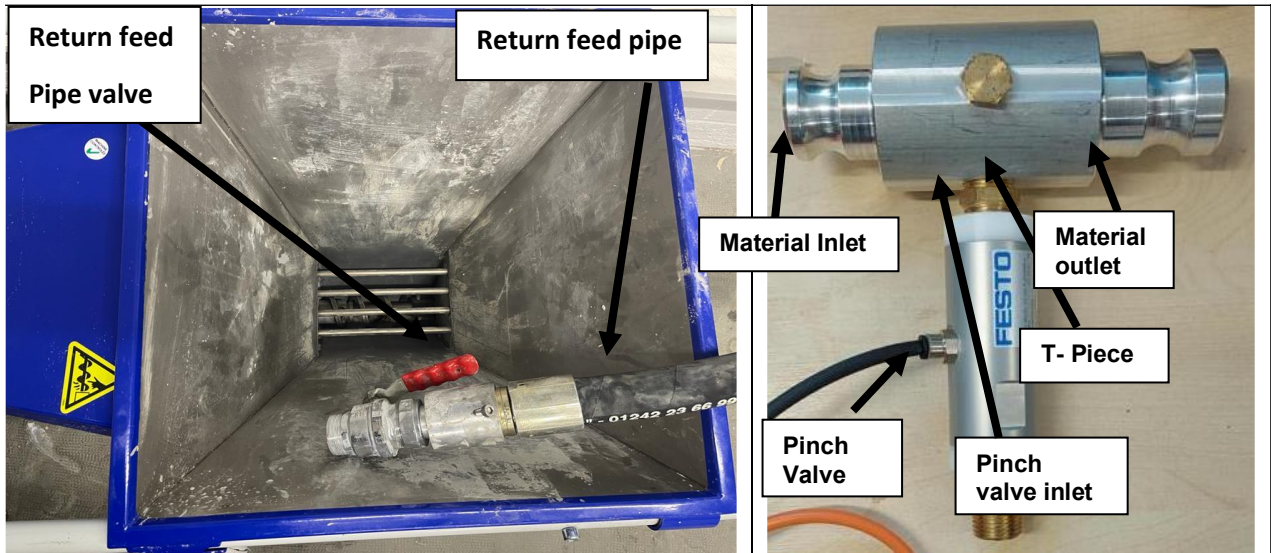


Figure 3.25. Material conveying pipe, T-piece, and pinch valve

The return feed pipe is rated at a maximum pressure of 40 bar. The main purpose of this pipe is to reduce the pressure at the robot print nozzle since the pump has a pumping capacity of 20 bar. When the valve is shut, and the pinch valve is opened, this enables pressure build-up within the return feed pipe, which then escapes through the pinch valve and then to the robot printing nozzle. When the pinch valve is closed, the return feed pipe must be opened to enable the circulation of material within the system. It is important to note that the material conveying pipes could potentially burst, which could lead to cement explosion if both the pinch valve and the return feed pipe are shut simultaneously. This is due to the high pressure build-up within the system.

### 3.7.7. Pressure gauge

A pressure gauge was installed on the return feed to measure the pressure of cement and water passing through the system, and also to ensure that there are no leakages. The SI unit of pressure is Pascal (Pa).

### 3.7.8. Pinch valve

The printing process involves the continuation and discontinuation of printing material, hence why the pinch valve was introduced. The pinch valve used was the pneumatically actuated Festo VZQA-C-M22U which makes it compatible with the robot system. The valve is a 2/2-

way valve with a tubular elastomeric pinch sleeve and uses a pinching effect to obstruct the flow of fluid. The pinch valve is normally open as illustrated in Figure 3.26, to ensure minimum flow resistance and prevent blockage or clogging of the valve. When the valve is pressurised, the pinch sleeve closes and cuts off material flow. The valves open when the pressure is no longer applied as a result of the pressure of the flow medium or the inherent stress in the pinch valve sleeve [273]. The design is also easy to clean.

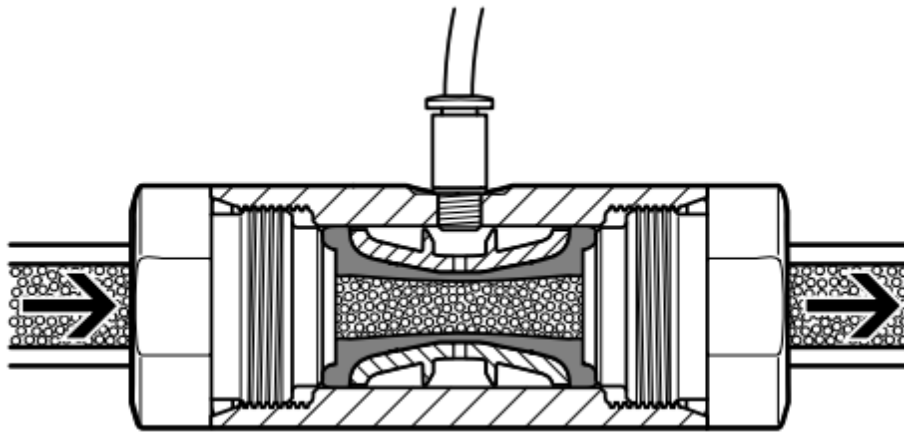


Figure 3.26. Pinch valve illustration [273]

### 3.7.9. Solenoid valve

The solenoid valve connects to the pinch valve. It is operated electromagnetically and converts electrical energy to mechanical energy [274]. The valve used is a 24 v 2-way valve. It consists of an inlet and outlet, an electric coil (solenoid) and a plunger, which is a movable ferromagnetic core in the centre [274]. When an electric current passes through the coil within the solenoid, the plunger goes up or down to open or close the orifice. To eradicate the need for manual operation, the solenoid valve regulates the flow of liquid or gas [274]. Figure 3.27 shows the solenoid valve used in this research.



Figure 3.27. Solenoid valve

### 3.7.10. Air compressor

The air compressor used for this research is the Clarke Ranger oil free air compressor as shown in Figure 3.28. It uses an electric motor to convert power into potential energy stored in pressurised air. It connects to the solenoid valve, which is also connected to the pinch valve. The air compressor pressurises the pinch valve to continue and discontinue the flow of material.



Figure 3.28. Ranger air compressor used alongside the pinch valve

### 3.7.11. Air compressor technical specifications

Table 3.9 presents the technical specifications of the air compressor.

Table 3.9. Technical specification of air compressor.

Motor (HP)	Watts (w)	Input voltage	Air displacement (cfm)	Air tank volume (L)	Maximum pressure (bar)	Wheel mounted
2.0	1500	230	7	24	8	Yes

### 3.8. Optimised 3D printing process

Precise preparatory steps and equipment are essential to ensure consistent and excellent quality of the cement-based materials used in 3D printing. Figures 3.29 and 3.30 shows the flowchart and the overall 3D printing process, respectively.

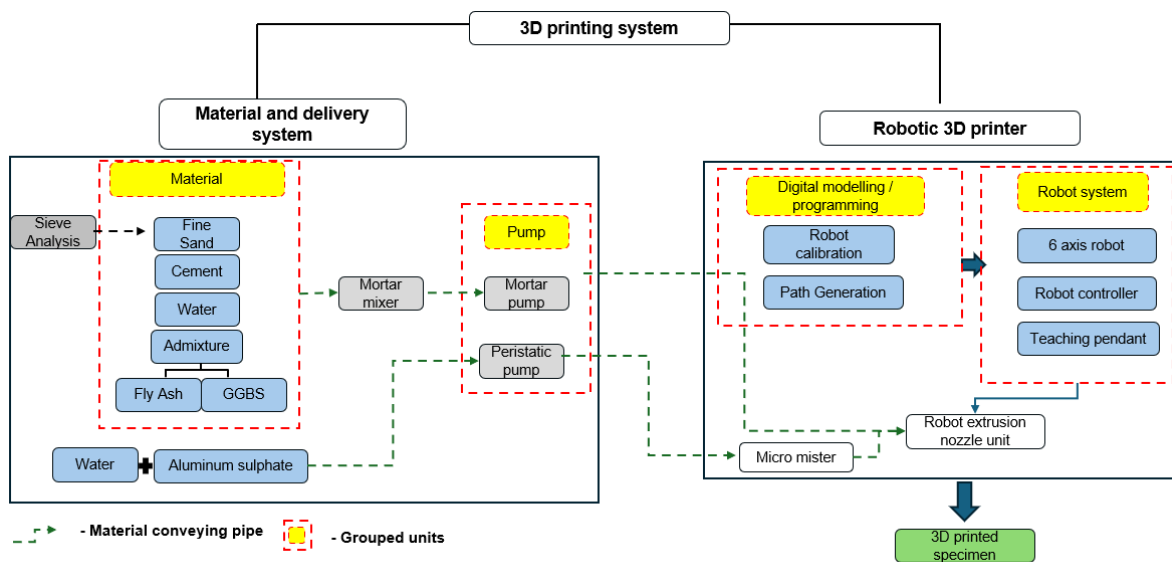


Figure 3.29 Flowchart of 3D printing process

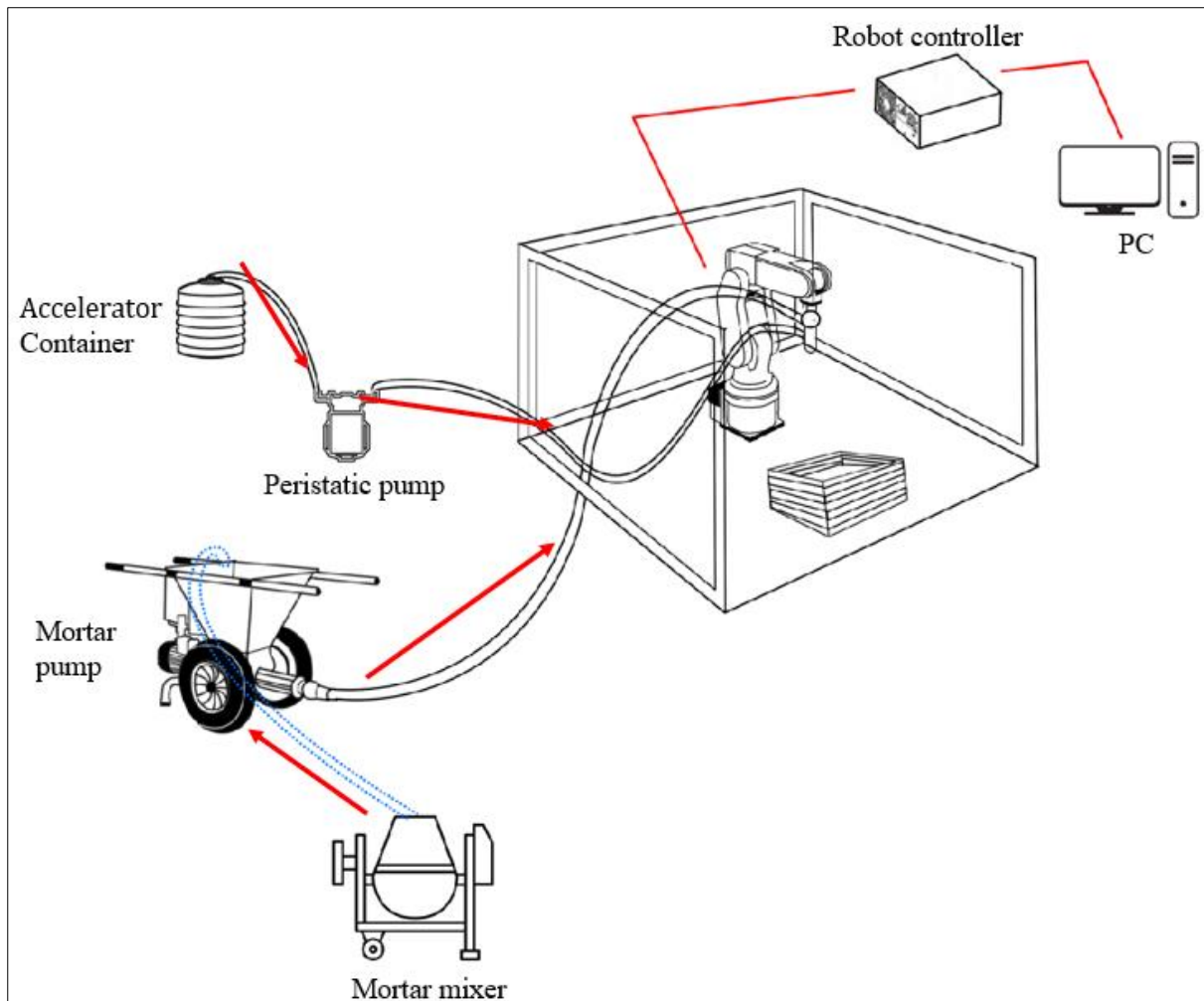


Figure 3.30 Overall 3D printing process

The mortar mixer was used for efficient and precise mixing of the cement-based materials. When the mixing was completed, the cement pump was turned on, and the rotor began to rotate. Clean water was used to flush the system down before the prepared cement mixture was fed into a hopper, which connected to the mortar pump. The hopper acted as a reservoir, ensuring a continuous flow of material during the printing process. The mortar pump pushes the mixture through the material-conveying pipe to the robot extrusion nozzle. The nozzle was a critical component, as it allowed the flow and deposition of the cement material. Before printing started, the system was allowed to extrude the cement-based material, washing away the water within the system and extracting the air bubbles. This step was crucial to get rid of potential voids, blockages or interruptions during the 3D printing process. The formation of air bubbles is an extremely complex phenomenon influenced by various factors, such as mixing process, concrete mixture proportioning, characteristics of cement and aggregates, water content and other chemical admixtures [275].

To begin the 3D printing process, a specialised 6-axis robotic system was used to deposit layers of cement-based material layer by layer. A Cartesian coordinate method was used to take the target point, which the robot system followed along the x, y and z axis, allowing the nozzle to move and create the desired structure layer by layer. During this process, a peristaltic pump also pumped accelerator from an accelerator storage tank to the micro mister that was attached to the nozzle of the robot. The micro mister was a small device that sprayed accelerator on the just deposited layer in form of mist to avoid overflow of the accelerator. The robot system operated with Cartesian motion to ensure accuracy and precision. The movement of the robot nozzle was precisely controlled by the robotic arm. The extrusion process plays a crucial role in 3D printing. The movement of the nozzle was synchronised with the extrusion process to improve the quality of the 3D-printed structure. The quality of the 3D-printed material was highly dependent on the printing speed, pump speed and layer height, among other factors, as subsequently elucidated.

## Part C: 3D Printing Processing Parameters

### 3.9. Experimental parameters

This study tested the mechanical properties of 3 different 3D-printed structures, including compressive strength, split tensile strength, and flexural strength. The printed structures were left to cure for 1 day, after which they were transferred to a controlled water tank for further curing for 7, 14 and 28 days at a temperature of  $20 \pm 2^\circ$ . The same material was used for all specimens. The printing conditions for the compressive and flexural tests included 10 layers of material deposited at a speed of 20 mm/s with a layer height increment of 10 mm. Each structure took approximately 8 minutes to print. For the split tensile test, the conditions were similar, except only 4 layers were printed, taking approximately 3 minutes. The specimens were cut using a concrete cutter to ensure dimensional accuracy for the split tensile test. To minimise the impact of cutting on the internal structure, the cutting process was carried out 20 hours after the printed specimens had fully hardened.

#### 3.9.1. Printing speeds

This study evaluated four different specimens that were 3D-printed with varying printing speeds. The structures were printed with speeds of 10, 20, 40 and 80 mm/s with a layer height increment of 10 mm. A constant pumping pressure of 2 bar was maintained. The environmental temperature and humidity at the time of printing were 11.5 °C and 73%, respectively. One of the objectives of the experiment was to observe how the different printing speeds would affect the buildability of the 3D-printed small-scale structures, while keeping other parameters constant. Table 3.10 presents the 3D printing parameters with varying printing speeds.

Table 3.10. 3D printing parameters with varying print speeds

<b>Samples</b>	<b>Print Speed (mm/s)</b>	<b>Layer Height (mm)</b>	<b>Pumping Pressure (bar)</b>	<b>Temperature (°C)</b>	<b>Humidity (%)</b>
<b>1</b>	<b>10</b>	10	2	11.5	73
<b>2</b>	<b>20</b>	10	2	11.5	73
<b>3</b>	<b>30</b>	10	2	11.5	73
<b>4</b>	<b>40</b>	10	2	11.5	73

### 3.9.2. Layer height

Similar to the previous procedure used for printing speed, four different structures were 3D-printed and evaluated based on a difference in the layer height. The structures were printed with a layer height increment of 5 mm, having samples C1, C2, C3 and C4 at 10, 15, 20 and 25 mm, respectively. The layer thicknesses and the number of layers printed before structural failure were recorded for each sample. The layer thicknesses were adjusted to ensure proper interlayer adhesion, with specific attention to the distance between the nozzle and the previously deposited layer. Both constant pumping pressure and printing speed of 2 bar and 20 mm/s were maintained, respectively. The environmental temperature and humidity at the time of printing remained 11.5 °C and 73%, respectively. Table 3.11 presents 3D printing parameters with varying layer heights.

Table 3.11. 3D printing parameters with varying layer heights

<b>Sample</b>	<b>Print Speed (mm/s)</b>	<b>Layer Height (mm)</b>	<b>Pumping Pressure (bar)</b>	<b>Temperature (°C)</b>	<b>Humidity (%)</b>
<b>1</b>	20	<b>10</b>	2	11.5	73
<b>2</b>	20	<b>15</b>	2	11.5	73
<b>3</b>	20	<b>20</b>	2	11.5	73
<b>4</b>	20	<b>25</b>	2	11.5	73

### 3.9.3. Pump pressure

The study used a constant pump pressure of 2 bar throughout the 3D printing process to ensure a stable and continuous extrusion flow. This pressure was selected to provide consistent material output, supporting layer integrity and adhesion without introducing variability in flow rate. The constant pressure helped to standardise the extrusion process, minimising fluctuations that could impact the uniformity and stability of each printed layer.

### 3.9.4. Accelerator dosage

Buildability was evaluated by the number of deposited layers and the overall layer height. All layers were printed with a consistent time gap of 50 seconds. Accelerator dosages of 10, 15, 25, 35 and 45% were used for the 3D-printed samples AL\_ST15, AL\_ST25, AL\_ST35 and AL\_ST45 respectively. The accelerator was pumped through a small peristaltic pump, operating at a maximum flow rate of 600 ml/m. To ensure an even distribution of the accelerator onto each layer, the accelerator nozzle diameter of 6  $\mu\text{m}$  was attached to a robot nozzle, which then sprayed the mixture onto each deposited layer. The diameter of the extrusion nozzle was 15 mm, and the 3D-printed structure measured 440 x 140 mm with a layer thickness of 40 mm. Continuous printing was conducted until the structure failed to determine the maximum layer height. Environmental factors, such as temperature of 15 °C and humidity of 62%, were closely monitored at the start to the end of 3D printing, providing a comprehensive understanding of the experimental outcomes. Table 3.12 presents 3D printing parameters with varying accelerator dosage.

Table 3.12. 3D printing parameters with varying accelerator dosage

<b>Sample</b>	<b>Accelerator Dosage (%)</b>	<b>Layer Thickness (mm)</b>	<b>Layer Height (mm)</b>	<b>Print Speed (mm/s)</b>	<b>Pumping Pressure (bar)</b>	<b>Temperature (°C)</b>	<b>Humidity (%)</b>
AL_ST15	15	40	10	20	2	15	62
AL_ST25	25	40	10	20	2	15	62
AL_ST35	35	40	10	20	2	15	62
AL_ST45	45	40	10	20	2	15	62

### 3.10. Casting procedure

The same batch of cement-based material used in the 3D printing process was prepared and mixed with identical procedures to ensure consistency in material properties for the traditionally cast structure. A rectangular mould of dimensions 440 mm x 140 mm x 100 mm (length x width x height) was prepared (Figure 3.31a), with its inner surfaces coated in a release agent to facilitate easy de-moulding. A trowel was used to transfer the cement material from

the cement mixer into the mould and uniform distribution was ensured to prevent air void, gaps or segregation. After the mould was filled, it was placed on a vibrating table to compact the cement material and remove any possible entrapped air. The vibrating table facilitated the even distribution of the material, ensuring a dense and uniform structure throughout the specimen. Once the compaction was complete, the top surface was levelled with a trowel to create a smooth, flush finish. Excess material was carefully removed to ensure the final dimensions of the specimen precisely matched the mould.

The filled mould was left undisturbed for initial curing, allowing the cement material to gain sufficient strength to hold its shape. The cast structure was then covered with a plastic sheet to prevent rapid moisture loss, which could lead to cracking. After the initial curing period, the mould was removed carefully to avoid damaging the specimen. The specimen was then carefully transferred to a curing water tank (same as the 3D printed structures), where it remained submerged to promote proper hydration and strength development. This controlled moist environment was crucial for achieving the full potential strength of the material, with the curing process maintained at 1,7,14 and 28 days. Upon final removal, the specimen was inspected for surface quality, dimensional accuracy, and any signs of defects, such as cracks or voids. This traditional casting process provided a reliable basis for comparison with the 3D-printed structures, enabling a comprehensive evaluation of the cement material's performance across different production methods. Figure 3.31 shows the cast mould and the cast monolithic structure.

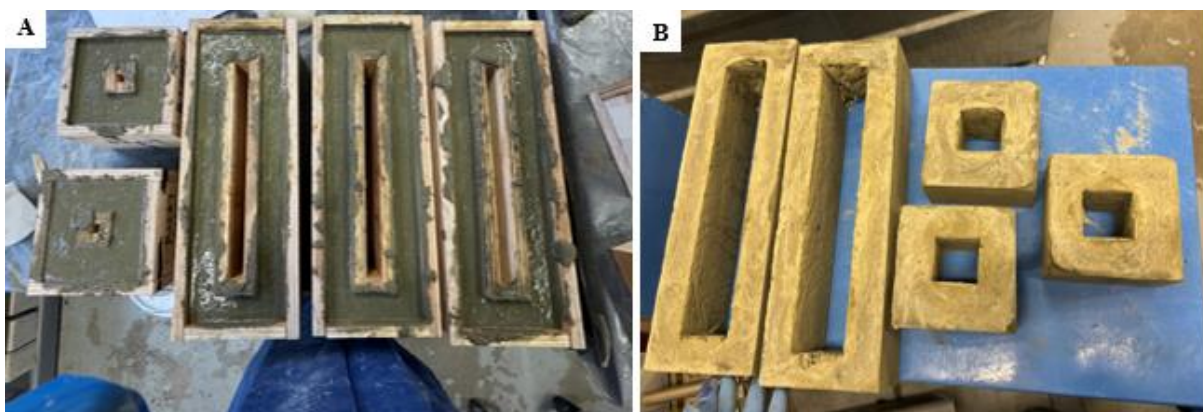


Figure 3.31. (a) cast mould and (b) monolithic structures

## Part D: Performance Evaluation Methods

### 3.11. Evaluation methods

#### 3.11.1. Flowability test

The mortar flow table test was conducted according to British Standards (BS EN 12350-5) to assess the workability of a concrete mix [276]. A specific mortar batch was mixed to achieve the desired flowability and prevent premature stiffening. The flow mould was placed on a stable flow table, filled up and compacted to eliminate air pockets. After carefully lifting the mould, the table was dropped 15 times to spread the mortar. The flow diameter was measured in two perpendicular directions, and the average was recorded to determine workability. Multiple tests were performed for consistency, and equipment was calibrated to ensure accuracy and repeatability, following strict adherence to standards. Figure 3.32 shows the flow table equipment. This method is widely supported in the literature as a valid approach for assessing flow in extrusion-based 3D concrete printing. Li et al. [114] and Krishnaraja and Guru [277] explicitly reference the slump flow test as a standard and accessible method for evaluating flowability of printable concrete.



Figure 3.32. Flow table test

### 3.11.2. Extrudability test

To achieve extrudability, an initial test print was conducted using a single continuous path to ensure uninterrupted and consistent material flow. This preliminary test was essential to confirm that the mix could form a long, uniform filament without signs of tearing, clogging, or deformation. Extrudability refers to the material's ability to pass smoothly through the nozzle while maintaining a coherent and continuous filament upon deposition. A mix is deemed extrudable when it can maintain its shape and create a smooth, defect-free line over an extended distance without interruptions. According to the literature, an extrudable material should show minimal deformation and no breakage throughout the extrusion path. [104].

This approach aligns with the methods presented by Yang et al. [254] and Le et al. [84], who defined extrudability as the ability of a mix to flow through the nozzle smoothly without blockage or deformation, using visual assessment of filament quality as a primary indicator.

The test print in Figure 3.33 shows excellent extrudability. The printed filament remains intact and follows a sharp zig-zag path with well-defined corners, indicating both consistent flow and shape retention.



Figure 3.33. Extrudability test sample

### 3.11.3. Buildability test

Buildability was assessed through a two-stage approach to determine the material's capacity to support successive layers without slumping or collapsing. First, manual preliminary testing was conducted by hand-squeezing the fresh mix through a nozzle and layering it vertically. This enabled a quick evaluation of the mix's early-age structural integrity and assisted in modifying the mix proportions before committing to full-scale 3D printing. The focus was on observing whether each manually applied layer could support the next without excessive spreading or collapse, providing immediate feedback on stiffness and thixotropy behaviour. Figure 3.34 shows the preliminary buildability test conducted by hand squeezing.

In the second stage, automated 3D printing trials were conducted by depositing vertical columns layer-by-layer without any formwork as shown in Figure 3.35. Each layer was printed at 1-minute intervals to simulate realistic printing conditions and allow for partial setting. The maximum number of layers achieved before visible deformation or collapse was recorded as the buildability limit. Columns that maintained structural stability beyond 10 layers (approximately 100 mm in height) were considered to have passed the buildability threshold.

This approach is consistent with Joh. [89] who evaluated buildability based on the maximum number of layers printable before failure. Bhattacharjee and Santhanam. [117] also emphasised the deformation of lower layers and the importance of interlayer time in structural build-up. While their work involved accelerator spraying to enhance buildability, our use of layer stability and maximum height as evaluation criteria aligns with their methodology.



Figure 3.34. Hand-squeezed buildability test



Figure 3.35. Vertical deposition of layers to test buildability

Overall, the two-stage buildability testing in this study is consistent with techniques adopted in the literature and effectively balances practical validation with recognized experimental standards in 3D printable concrete research.

### 3.12. Mechanical testing

The experiments were conducted on two types of hollow cube structures to determine their compressive strength. Both structures, one 3D-printed and the other monolithic, had the same dimensions of 100 x 100 x 100 mm (l x b x h). The tests were carried out in accordance with BS EN 12390-3, which specifies the method for making and curing test specimens and the procedure for compressive strength testing of concrete. The load was applied at a rate of 0.2 MPa/s. For both the 3D-printed and monolithic specimens, the compressive load was applied perpendicular to the layer build direction (Z-orientation) to ensure consistent strength assessment across both methods. Additionally, the flexural strength tests were conducted using a 4-point bending test method in accordance with BS EN 12390-5. This test was applied to a rectangular hollow structure and a rectangular monolithic structure, both with dimensions of 440 x 140 x 100 mm (l x b x h). The specimens were simply supported over a support span of 400 mm, with two concentrated loads applied symmetrically at one-third points along the span, creating a load span of 133 mm between the loading noses. The load was applied at a constant rate of 200 N/s until failure.

$$Strength = stress = \frac{Failure\ Load}{Cross - sectional\ Area} \quad (1)$$

Where the failure load is measured in Newtons (N) and the area in  $mm^2$ . The 4-point bending test was chosen over the 3-point bending test because it provides a more uniform distribution of stress over the central region of the specimen, making it more suitable for concrete. Figure 3.36 shows the different testing methods.

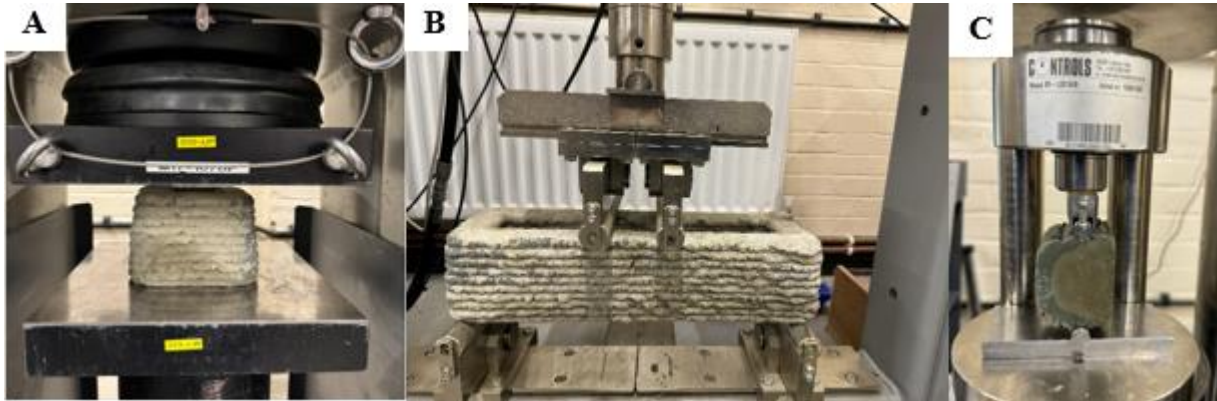


Figure 3.36 (a) Compressive, (b) flexural and (c) split tensile test set-ups

The splitting tensile test was conducted in accordance with BS EN 12390-3 to study the effect of different aluminium sulphate dosages used as an accelerator on the interlayer bond strength of the 3D-printed structure. Interlayer bond strength is a key parameter in 3D-printed concrete as it influences the overall structural integrity and durability of the printed components [169, 278]. For this test, the 3d-printed structure was cut to dimensions of 50 x 40 x 40 (length x width x height) using a concrete cutter after curing to prevent deformation. In the testing apparatus, two rolling pins were strategically placed between the layers of the 3D-printed structure, positioned at the interlayer interface. When force was applied to the pins, they exerted a controlled outward pressure directly between the layers, causing them to separate along the bond line as shown in Figure 3.37. This design specifically tested the tensile strength by directly challenging the interlayer bond between layers. By applying force in this way, the setup allowed for a precise assessment of how effectively the layers were bonded and how the varying aluminium sulphate dosages influenced this bond.

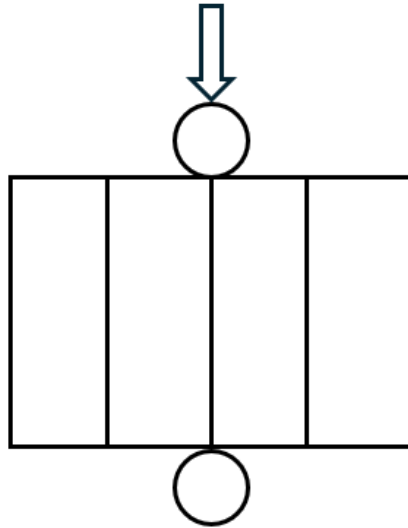


Figure 3.37. Split tensile test

#### 3.12.1. Penetration resistance test

The vicamatic machine was used to test the setting time of the cement material (Figure 3.38). The material was mixed according to the mix proportion in section 2.1. The prepared paste was then placed into a standard conical mould, with the surface levelled flat and even. Aluminium sulphate of different concentrations was then sprayed onto the surface to imitate the on-demand spraying process. Once the mould was filled, it was positioned inside the transparent chamber of the Vicamatic-2 tester, ensuring the cement sample was properly aligned under the Vicat needle. The machine was powered on, and the test parameters were set via the digital control panel, including the penetration interval frequency of 40 s and the maximum penetration depth of 40 mm. After setting the parameters, the machine began its automatic testing process. The Vicat needle penetrated the cement sample at the programmed intervals, and the machine measured and displayed the depth of penetration during each cycle. After the test, the sample was removed from the chamber, the initial and final setting times were recorded, and the Vicat needle and surrounding equipment were cleaned to remove any residual cement.



Figure 3.38 Penetration resistance test machine

### 3.12.2. Scanning Electron Microscopy (SEM)

The SEM procedure began by carefully preparing the sample, ensuring the specimen was clean, dry, and properly mounted on a specimen stub using conductive carbon tape. A thin gold coating was used to prepare the cement-based material for SEM using the sputter coater since the material was non-conductive. The samples were positioned in the chamber while ensuring the valves were properly sealed and the chamber was flushed with argon. Once the desired pressure was reached, plasma was generated, and the gold coating was applied by maintaining the correct beam current. After the coating process, the system was shut down, and the coated sample was removed for SEM imaging. This gold layer reduced surface charging, improving the clarity and quality of the SEM images for examining the microstructure of the concrete.

Once prepared, the sample was placed into the SEM chamber, and the system was allowed to reach the required vacuum level. The beam voltage was set to 20 kV, and the optimal working distance was between 10-15 mm for high-resolution imaging. Secondary electron detection

was used to focus on surface topography, providing detailed surface images. Initial focusing was conducted at low magnification, followed by gradual increases in magnification to observe the sample's microstructural features better. Fine adjustments were made to both focus and astigmatism to ensure image clarity. Contrast and brightness were adjusted to enhance the visibility of surface details, particularly those related to the fine textures present in the microstructure of the specimen. Multiple images were captured at various magnifications. The final step involved carefully removing the sample from the chamber once the pressure returned to atmospheric levels.

## Part E: Finite Element Analysis

### 3.13. Finite Element Analysis

The finite element simulations presented in this study were conducted using ANSYS Workbench 2024 R1, a widely used commercial software package for structural analysis. The simulations aimed to evaluate the deformation and stress distribution in 3D-printed cement-based structures under compressive loading. The simulation was conducted on a monolithic concrete specimen and the analysis focused on determining how internal stresses developed during compression and whether the FEA model could accurately predict the failure-prone zones noted during testing. 3D models were developed in ANSYS DesignModeler to replicate the dimensions of the test specimens used for compression and flexural testing. Two simulation setups were created:

1. A Static Structural Analysis for uniaxial compressive loading
2. An Explicit Dynamic Analysis for four-point flexural bending

#### 3.13.1. Material properties

Material properties for both the concrete and steel components were assigned based on experimental data and standard engineering references. All materials were defined as linearly elastic and isotropic. Table 3.13 presents the material properties used in ANSYS.

Table 3.13: Material Properties Assigned in ANSYS

Property	Concrete	Structural Steel
Density ( $kg/mm^3$ )	$2.3e^{-6}$	$7.85e^{-6}$
Young's Modulus (MPa)	30000	$2e^5$
Poisson's Ratio	0.18	0.3
Bulk Modulus (MPa)	15625	$1.6667e^5$
Shear Modulus (MPa)	12712	76923
Yield Strength (MPa)	-	250

### 3.14. Compressive test model description

The FEA model for compressive strength testing was developed to replicate the experimental loading conditions used in laboratory testing. As shown in Figure 3.39, the model consists of three primary components:

- Cement-based specimen (central body)
- Top steel plate, representing the loading platen of the Universal Testing Machine (UTM) (Green)
- Bottom steel plate, representing the rigid base support (green)

These steel plates were included not as structural components of interest, but to realistically model the interaction surfaces that apply and resist load during the test (see Figure 3.39). Their inclusion ensured accurate boundary condition application and force transfer to the concrete specimen.

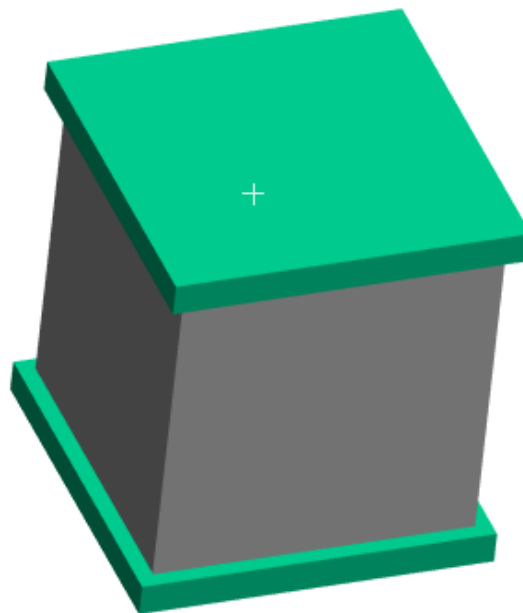


Figure 3.39. FEA model for compression test

### 3.14.1. Contact Conditions

Two types of surface interactions were defined to simulate realistic behaviour at the interfaces:

- Frictional Contact was applied between the bottom plate and the concrete specimen to simulate the rough, stable base contact typically seen in UTM setups. This allowed for some resistance to lateral movement.
- Frictionless Contact was used between the top plate and the specimen, ensuring pure vertical load transmission without shear or lateral force interference. This replicates the smooth contact with the loading head during testing.

These settings allowed for an effective simulation of constrained and unconstrained interfaces in line with real-world mechanical conditions.

### 3.14.2. Mesh Configuration

The entire model was meshed using tetrahedral elements. ANSYS default meshing controls were applied, with a global element size of 5 mm, offering a balance between computational efficiency and model resolution. Figure 3.40 shows the mesh visualisation and Table 3.14 presents the detailed mesh parameters.

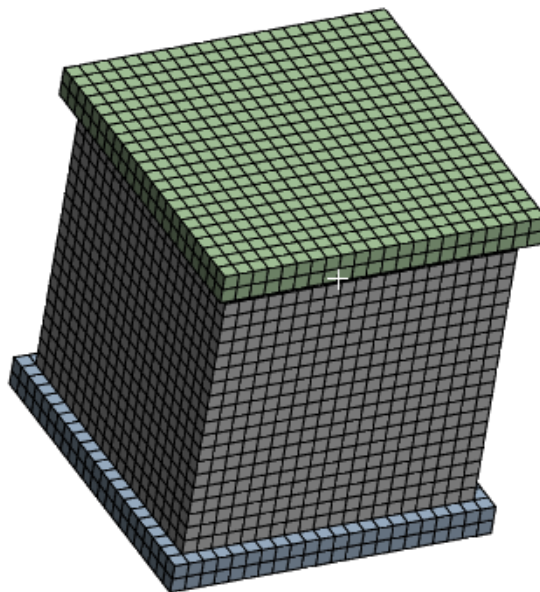


Figure 3.40. Mesh visualisation for compressive model

Table 3.14. Mesh parameters

Setting	Value
Element Type	Tetrahedral
Element Size	5 mm
Element Order	Program Controlled
Physics Preference	Mechanical

### 3.14.3. Boundary Conditions and Loading

**Pressure Load** - A compressive pressure load rate of 0.2 MPa was applied normal to the top face of the upper steel plate. The load was ramped during the solution phase to simulate gradual application of force, as would be experienced during a real compression test.

**Displacement Constraint** - To prevent in-plane motion of the top plate, displacement constraints were applied to restrict movement in both the X and Y directions. Movement in the Z direction (the axis of loading) was left free to enable vertical deformation under the applied load.

**Fixed Support** - The bottom plate was fully constrained using a Fixed Support boundary condition. All six faces in contact with the UTM base were locked in all degrees of freedom, ensuring a completely immovable base reference.

## 3.15. Flexural test model description

This section outlines the explicit dynamic simulation of a monolithic cement-based beam subjected to a four-point bending test. The simulation was performed in ANSYS Workbench using the Explicit Dynamics solver, which is ideal for transient structural simulations involving complex contact interactions and large deformations.

### 3.15.1. Geometry and Loading Assembly

The geometry model consisted of a centrally positioned rectangular concrete beam supported by two hemispherical roller supports at either end, and loaded symmetrically at two points using cylindrical steel load blocks (Figure 3.41). This configuration reflects a standard four-

point bending test setup, widely used to evaluate flexural behaviour and cracking potential in cement-based materials.

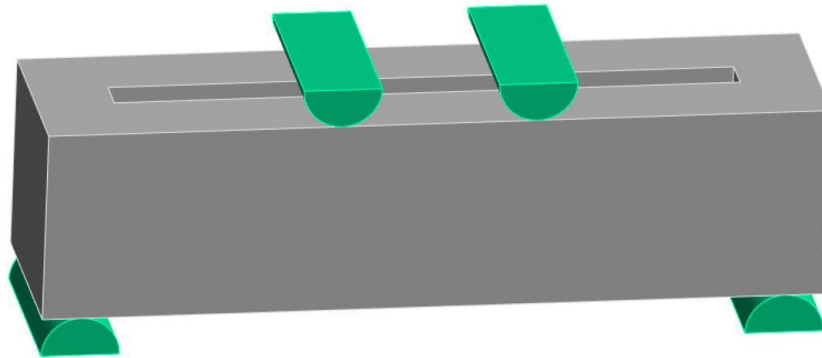


Figure 3.41. FEA model of four-point bending test with explicit dynamics setup and contacts

The support and load blocks were defined as rigid bodies to ensure consistent load transfer and to reduce computational overhead.

### 3.15.2. Material Properties

Two material types were used in the simulation: concrete (for the beam) and structural steel (for the loading and support blocks). The materials were defined using isotropic, linear elastic properties.

### 3.15.3. Mesh configuration

The mesh was generated using adaptive sizing with explicit physics preference and an assigned body element size of 9 mm. The mesh was controlled using the Assembly Initial Size Seed method. Figure 3.42 shows the mesh visualisation, and Table 3.15 presents the mesh visualisation.

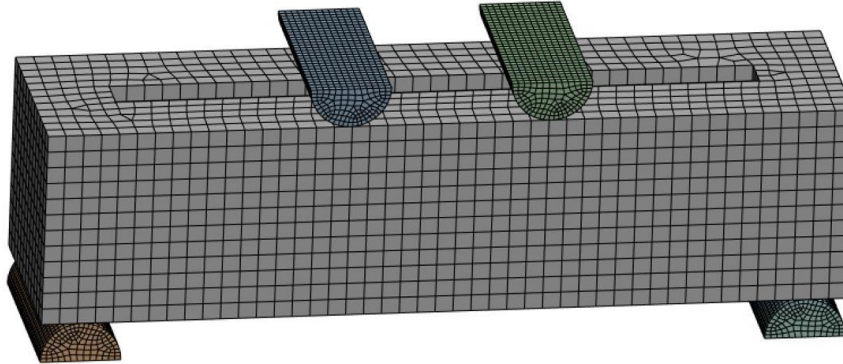


Figure 3.42. Mesh visualisation

Table 3.15. Mesh parameters

Setting	Value
Element Type	Tetrahedral
Element Size	9 mm (Body sizing)
Element Order	Linear
Solver preference	Explicit Dynamics
Adaptive sizing	Enabled
Mesh quality check	Enabled

#### 3.15.4. Solver and Boundary Conditions

The Explicit Dynamics solver was used due to the transient nature of the contact loading and potential for sudden stress wave propagation in the material.

- Supports: Constrained to only allow rotational movement (simulating realistic roller behaviour).
- Loading Blocks: Vertically applied force using dynamic ramping.
- Frictionless, time-controlled contact ensured smooth and accurate force transmission.

### **3.16. Summary**

This chapter presented the materials, equipment, and experimental methods employed in the development and evaluation of 3D-printed cementitious structures. A wide range of raw materials, including binders, aggregates, and chemical accelerators, were characterised and used in tailored mix designs to meet printability requirements. The design and optimisation of the printing system, including the robot setup, extrusion components, and control systems, were described in detail. Printing parameters such as speed, layer height, and accelerator dosage were systematically varied to assess their influence on buildability and structural performance. Standard tests for flowability, extrudability, and setting behaviour were used alongside mechanical testing to evaluate the mixtures under realistic printing conditions. The approaches established in this chapter form the experimental basis for the results and discussion presented in the next chapter, including FEA simulation.

## **CHAPTER 4: Results**

---

**Part A: Assessment of Fresh-State Performance of Mortar Mixtures**

**Part B: Preliminary Testing & Nozzle Optimisation**

**PART C: Printing Process Optimisation and Accelerator Administration**

**Part D: Performance Evaluation of Experimental Works**

## Chapter 4: Results

### Part A: Assessment of Fresh-State Performance of Mortar Mixtures

#### 4. Introduction

This chapter presents the key findings from the experimental investigation, analysing the influence of mix design parameters, printing conditions, and material modifications on the printability and performance of cement-based mixtures. The results are discussed in relation to flowability, extrudability, buildability, and early-age mechanical properties, with particular emphasis on the effect of aluminium sulphate as a setting accelerator. Both visual and quantitative assessments are used to evaluate structural stability, interlayer bonding, and deformation resistance. Where applicable, comparisons are made with existing literature to contextualise the results and highlight the contribution of this study to 3D concrete printing research.

#### 4.1. Flowability

A series of four mortar mixtures were evaluated to investigate the effects of sand type, water-to-binder ratio (W/B), and the presence of supplementary cementitious materials (SCMs) on flowability, using slump and slump-flow tests as indicators of workability. The results, presented in Table 4.1, demonstrate clear trends in how sand gradation and binder composition influence extrudability and potential 3D printability.

Table 4.1. Material composition

	<b>Sand type</b>	<b>W/B</b>	<b>S/B</b>	<b>FA/B</b>	<b>GGBS/B</b>	<b>Slump (mm)</b>	<b>Slump-flow (mm)</b>
<b>Mix 1</b>	Sharp sand	0.40	4.00	-	-	1.8	118
<b>Mix 2</b>	Sharp sand	0.40	3.00	-	-	2.7	127

<b>Mix 3</b>	Fine sand	0.40	1.33	0.20	0.30	3.9	144
<b>Mix 4</b>	Fine sand	0.45	1.33	0.20	0.30	4.5	152

Mixes 1 and 2 were made of sharp sand without SCMs. Both had a W/B of 0.40 but differed in sand-to-binder ratio (S/B): Mix 1 had an S/B of 4.00, while Mix 2 was reduced to 3.00. Mix 1 exhibited the lowest workability, with a slump of 1.8 mm and a slump-flow of 118 mm. The cement content and high sand proportion contributed to this stiff, unworkable mixture. A reduction in S/B in Mix 2 resulted in a little improvement, yielding a slump of 2.7 mm and a slump-flow of 127 mm. This is consistent with findings by Papachristoforou et al. [279], who showed that reducing sand content increases flowability by improving the binder-to-aggregate balance.

Significant improvement in workability was observed with Mixes 3 and 4, both of which utilised fine sand and incorporated SCMs specifically, fly ash-to-binder (FA/B = 0.20) and ground granulated blast-furnace slag-to-binder (GGBS/B = 0.30). Mix 3 maintained the same W/B of 0.40 as the previous mixes but had a lower S/B of 1.33. This resulted in a slump of 3.9 mm and a slump-flow of 144 mm, placing it well within the printable range between 145 mm and 190 mm, according to Wei et al. [151].

Mix 4 built on this design by increasing the W/B ratio slightly to 0.45 while keeping all other proportions constant. This change yielded the highest flowability overall, with a slump of 4.5 mm and slump-flow of 152 mm. The increased water content improved the fluidity of the mix without compromising buildability, which aligns with recommendations by Le et al. [84] for achieving balance between extrudability and structural stability in 3D printable mixes. This mix design was selected to conduct the experiment.

## 4.2. Penetration resistance

The penetration resistance tests were conducted to investigate the effect of aluminium sulphate on the early stage setting time of mortar mixes, using the Vicat apparatus. A total of five mixes were tested: one control sample (CTRL\_ST00) with no accelerator, and four mixes containing varying dosages of aluminium sulphate (AL\_ST15, AL\_ST25, AL\_ST35, and AL\_ST45). Figure 4.1 shows the penetration depth versus time for all samples

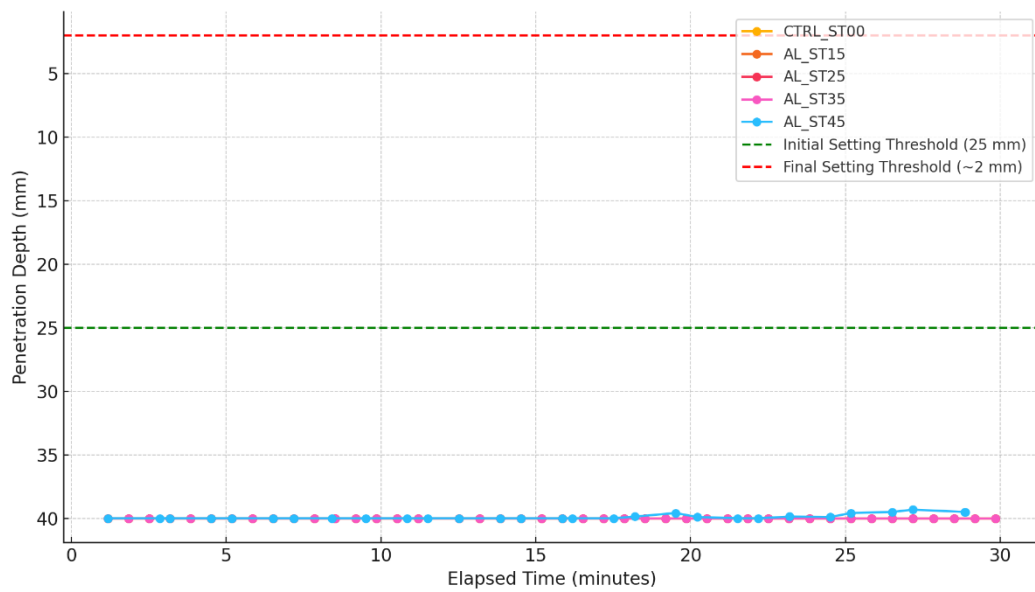


Figure 4.1. Penetration dept vs time

All five samples exhibited consistent penetration depths around 39–40 mm throughout the entire test duration of approximately 30 minutes. None of the mixes reached the initial setting threshold of 25 mm, nor did they approach the final setting criterion (defined at ~2 mm penetration depth) according to BS EN 196-3. This indicates that no observable setting occurred within the time window of testing for any of the mixes. However, a slight reduction in penetration depth was observed in AL\_ST45, 17 min into the test, dropping just below 40 mm (39.8mm). While minor, this suggested the early onset of setting in the highest dosage mix.

## Part B: Preliminary Testing & Nozzle Optimisation

### 4.3. Preliminary printing

The initial cement mixture was prepared at a temperature of 29°C and a humidity level of 44%, utilising a sand-to-cement ratio of 4:1, with a water content equal to 0.40 of the cement content. The cement mortar mixture comprised 2 kg of sand with a grain size ranging between 1.3 and 1.5 mm, 0.5 kg of cement, and 0.2 kg of water. All components were precisely measured using a calibrated weight scale. The dry mixture was thoroughly mixed using a cement mixer for 5 minutes. After achieving a uniform dry mix, water was gradually introduced, and the mixture was mixed for another 6 minutes to ensure homogeneity. A single scoop of the cement mixture was then extracted using a small plastic trowel to manually test its extrudability through a nozzle with a diameter of 14 mm fitted to a plastic bag, as shown in Figure 4.2.

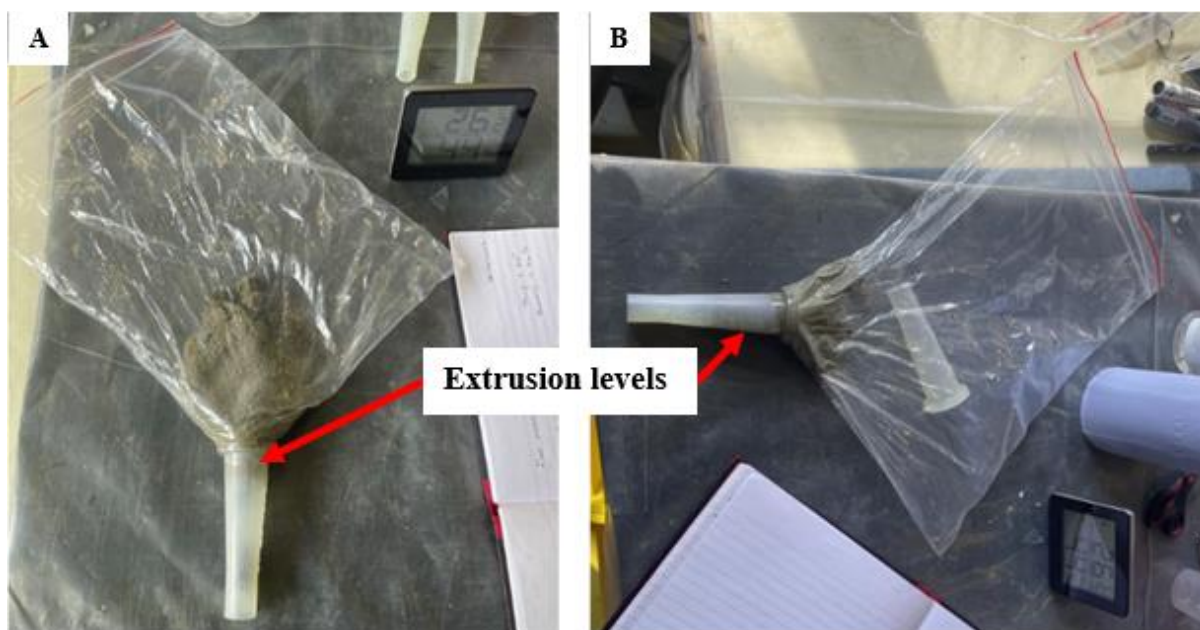


Figure 4.2. a) Test 1 - Extrusion level after first extrudability test, b) Test 2 - Extrusion level after the addition of 250 g of cement and 50 g of water.

This initial extrudability test (test 1) failed due to insufficient water content in the mixture. However, from the physical appearance of the mixture, it was evident that the sand-to-cement ratio was not proportionate, resulting in a suboptimal consistency and insufficient binding

properties. Subsequently, an additional 250 grams of cement and 50 grams of water were incorporated into the remaining mixture (test 2) to enhance its extrudability. A second scoop of mortar was extracted from the adjusted mixture and subjected to another extrudability test. Despite the modification, the experiment failed once again due to the persistent deficiency in water content, although it displayed notable improvements compared to the previous trial, as observed in the extrusion levels illustrated in Figures 4.2a and 4.2b. An additional 200 grams of cement and 100 grams of water were incorporated into the mixture, following which it was subjected to another extrudability test.

From the printed material depicted in Figure 4.3, it was observed that the increase in cement content enhanced the binding capacity and significantly improved the buildability of the mixture. The modified mixture was able to support the printing of three consecutive layers before exhibiting signs of structural failure. The observed structural failure could have been attributed to several factors, including inconsistency in the printing pressure caused by manual squeezing, unstable hand movements during extrusion, irregularities in the printing surface, or the manual nature of the printing process itself. Furthermore, other potential contributing factors might include void formation within the structure, which could be linked to an inadequate material mixture, prolonged open time, and improper extrusion pressure, among various other possibilities. The overall print quality is highly dependent on the properties of the fresh material and the parameters employed during printing. After the first day, it was noted that the printed material possessed a rough surface finish, which was primarily attributed to the quality of the sand used (specifically fine aggregate or sharp sand).



Figure 4.3. a) 3D printed material immediately after printing, b) 3D printed material after one day.

The second cement mixture was prepared (Test 2) following a procedure similar to the one employed in the initial experiment. The temperature and humidity levels during this experiment were 23°C and 56%, respectively. A sand-to-cement ratio of 3:1 was used, with a water content of 0.40% of the cement mass to achieve optimal strength. The cement mortar mix consisted of 1.5 kg of sand, with a grain size ranging between 1.3 and 1.5 mm, 0.5 kg of cement, and 0.2 kg of water. The initial extrudability test failed due to insufficient water content. Moreover, the visual appearance of the mixture suggested an improper sand-to-cement ratio, as illustrated in Figure 4.4a. To address this issue, an additional 50 g of water was incorporated into the remaining mixture. Another scoop of the modified cement paste was then subjected to a second extrudability test. Despite the adjustment, the mixture remained too viscous, resulting in another test failure. However, it performed better compared to the initial mixture, as shown in Figure 4.4b.

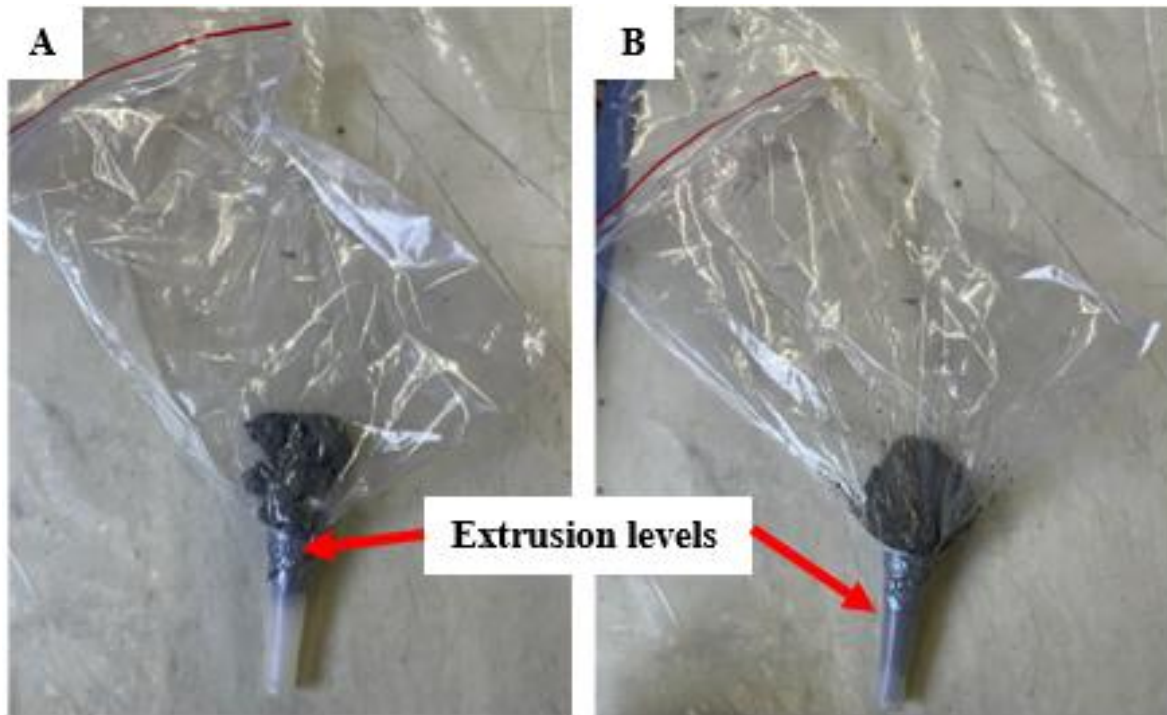


Figure 4.4. Extrusion levels of second batch of printing

Still utilising the rest of the mortar mix, an additional 50 g of water was incorporated, and the mixture was then manually subjected to another extrudability test. On this occasion, the viscosity was found to be excessively low, leading to a failed extrudability test. This failure occurred because the material particles were not adequately bonded together, which was attributed to the low cement content combined with high proportions of sand and water. As a result, the mixture lacked sufficient cohesion and structural integrity. Figure 4.5 illustrates the failed printing outcome due to the low viscosity of the mixture.



Figure 4.5. Failed printing due to low viscosity

The third attempt (Test 3) was carried out using a sand-to-cement ratio of 2:1. A total of 2 kg of sand with a grain size ranging between 1.3 and 1.5 mm, 1 kg of cement, and 0.2 kg of water were utilised to prepare the cement mixture. The extrusion test was conducted following the same procedure as in Test 1 and Test 2. Based on the printing results depicted in Figure 4.6, it was observed that the buildability of the material had significantly improved, as it was able to support four consecutive layers before collapsing after the fifth layer. This collapse could potentially be attributed to the method of printing employed during the test.



Figure 4.6. Test 3

A buildability test was also conducted to evaluate the number of layers the material mixture could withstand without exhibiting deformation, using a sand-to-cement ratio of 2:1. The mixture was prepared with 2 kg of sand, with a grain size ranging between 1.3 and 1.5 mm, 1 kg of cement, and 0.25 kg of water. A total of five distinct layers were deposited sequentially, one on top of the other, and allowed to dry. After one day, the average thickness of each layer was measured, and the results are presented in Figure 4.7. It was clearly demonstrated that as more layers were deposited, the degree of deformation in the bottom layers progressively increased.

The primary distinction between Test 3a and Test 3b was the water content 0.2 kg in Test 3a compared to 0.25 kg in Test 3b. Test 3a was able to support five layers without collapsing, while in Test 3b, compression was observed as the number of deposited layers increased, indicating reduced structural stability due to the higher water content.

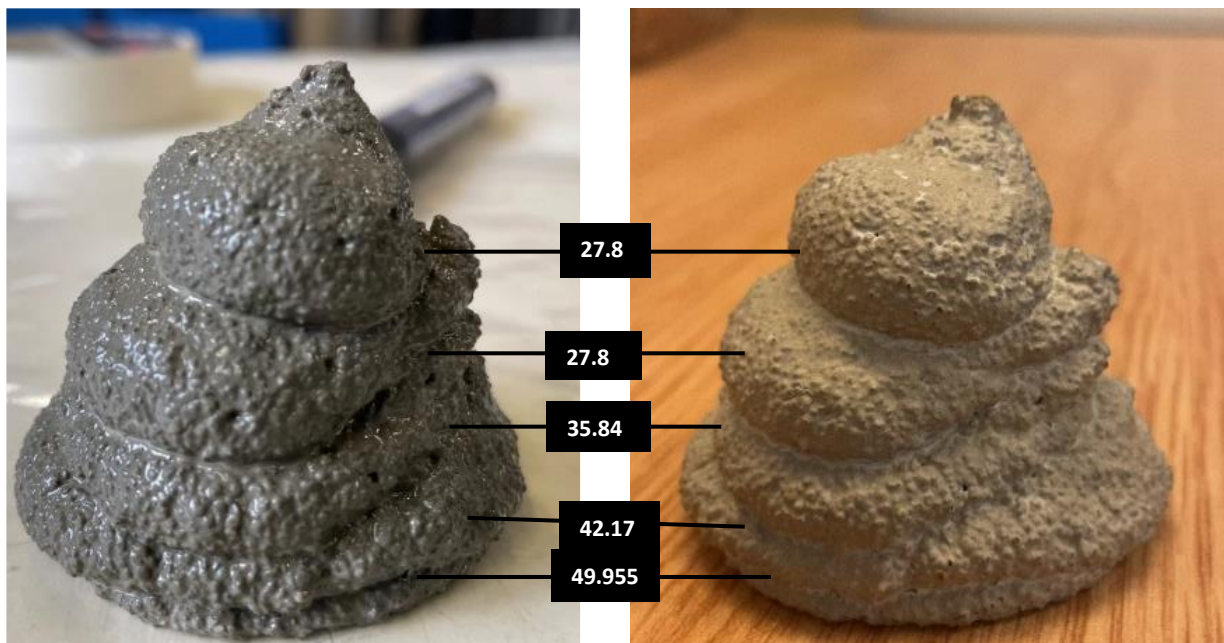


Figure 4.7. Buildability test using materials from test 3b showing slump on the bottom layers

Test 4 was conducted using very fine aggregate sand and cement in a ratio of 2:1, with 0.45 kg of water. The mixture was prepared with 2 kg of sand, with a grain size less than 1 mm, 1 kg of cement, and 0.20 kg of water. The experiment was performed under controlled environmental conditions at a temperature of 27°C and a humidity level of 53%. The extrusion test was executed using the same procedure as in Test 1 and Test 2. Based on the printing results shown in Figure 4.8, it was observed that the material mixture exhibited a much finer surface

finish compared to the outcomes of Tests 1, 2, and 3. The buildability of the material also demonstrated substantial improvement, as it was able to support four consecutive layers without showing any signs of collapse. However, the viscosity of the material was relatively high, which resulted in reduced surface contact between each deposited layer, potentially impacting the tensile strength of the printed structure. Huge void formation was observed within the printed structure compared to the previous tests. The primary factor contributing to the improved surface finish in Test 4, as opposed to Tests 1, 2, and 3, was the quality of the sand used in the mixture.



Figure 4.8. Test 4 material print

#### 4.3.1. Performance analysis of preliminary cement mixes

An extensive evaluation of various cement-based mixtures was conducted to identify optimal parameters for flowability, extrudability, and buildability in 3D printing applications.

In the first test (Test 1), which had a sand-to-cement ratio of 4:1, the performance was poor across all metrics. This was primarily due to insufficient cement and inadequate water content. In the subsequent tests (Test 2), small increases in cement (450g) and water (150g) were made, resulting in little improvements. These adjustments significantly improved extrudability and buildability, allowing the mixture to support three layers before eventually failing due to insufficient bonding.

The performance improved significantly when the sand-to-cement ratio was modified to 2:1 in Tests 3a and 3b. Test 3a, with 0.2 kg water content, displayed improved extrudability, successfully supporting up to four stable layers before collapse occurred at the fifth. Conversely, Test 3b, with a higher water content of 0.25 kg, experienced increased deformation under load, reducing overall structural stability.

Test 4 introduced finer aggregates with a grain size of less than 1 mm while maintaining the 2:1 ratio. This change resulted in a finer surface finish and stable extrusion, successfully supporting four layers. However, the increased viscosity of the mixture slightly compromised interlayer adhesion.

Overall, the analysis confirmed that a sand-to-cement ratio of 2:1, combined with controlled water content and finer aggregates, provided the best balance of performance, optimizing extrudability, buildability, and print surface quality. Table 4.2 presents the mix designs and test outcomes for the preliminary trials.

Table 4.2. Summary of Preliminary Mix Designs and Performance Outcomes

Parameter	Test 1	Test 2	Test 3a	Test 3b	Test 4
Sand (kg)	2	1.5	2	2	2
Cement (kg)	0.5	0.5	1.0	1.0	1.0
Water (kg)	0.2	0.2	0.2	0.25	0.45
Sand-to-Cement Ratio	4:1	3:1	2:1	2:1	2:1
Aggregate Size (mm)	1.3–1.5	1.3–1.5	1.3–1.5	1.3–1.5	<1.0
Temperature (°C)	29	29	23	23	27
Humidity (%)	44	44	56	56	53
Flowability	Failed	Failed	Pass	Pass	Pass
Extrudability	Failed	Failed	Pass	Pass	Pass
Buildability	Fail	Improved but failed	Pass	Pass (limited deformation)	Pass

#### 4.4. Preliminary robot 3D printing

The first 3D printing involved a material formulation as presented in Table 4.3.

Table 4.3. Material properties of test 1.

Cement (kg)	Sand (kg)	Water (kg)	Temperature (°)	Humidity (%)
30	-	10	8	90

The material was mixed using the SOROTO forced-action mixer. As this was the first attempt at printing, the primary objective was to ensure adequate open time, pumpability, and extrudability rather than focusing on buildability. Consequently, a high water content was used without the addition of any chemical additives. The cement pump was activated while the material was being mixed in the cement mixer, and clean water was poured into the system to flush it out. Following this, the mixture was introduced into the pump, and the material conveying pipe successfully transported the mixture through the system to the robot nozzle, as illustrated in Figure 4.9a.

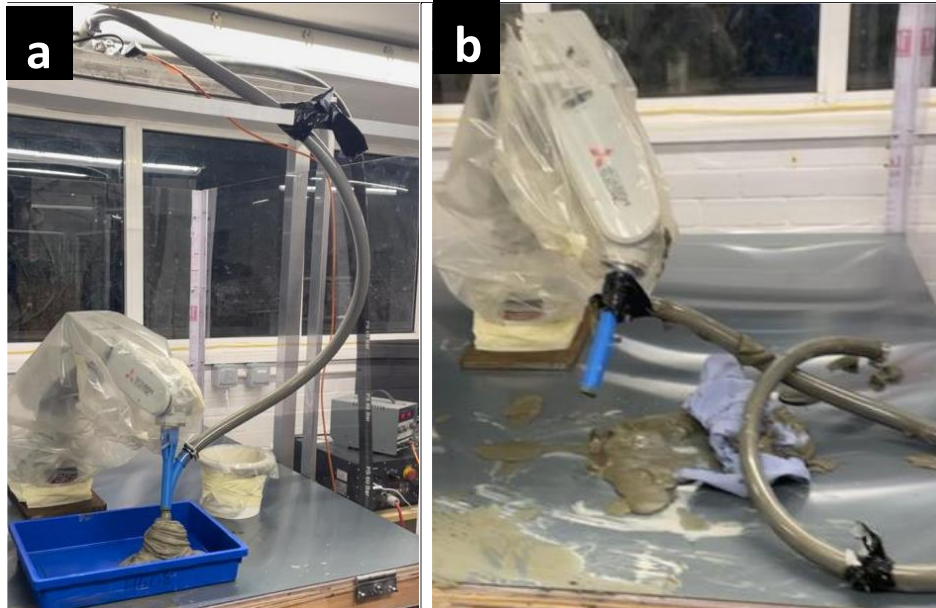


Figure 4.9.a) Material extrusion form nozzle, b) Failed system due to pressure build up

The mixture consisted of a material formulation with a sand-to-cement ratio of 2:1 and a water content amounting to 0.65% of the cement mass. The primary difference between this mixture and the one used in the second test was the water content. The water content was increased specifically to prevent blockages within the pipes and to enhance the pumpability of the material.

#### 4.5. Nozzle Optimisation

The final nozzle design, representing the fifth iteration, was developed in response to a failure observed in the fourth nozzle design (section 3.6.5). During the printing process, a fracture occurred, attributed to the combined effects of pumping pressure, the weight of the cement pipe, and the rotational movement of the robot, as shown in Figures 4.10a and 4.10b. Since the initial setup successfully validated pumpability, open time, and extrudability of the material, the focus shifted towards enhancing structural integrity and component durability. As a result, aluminium was introduced for the next phase of nozzle development.

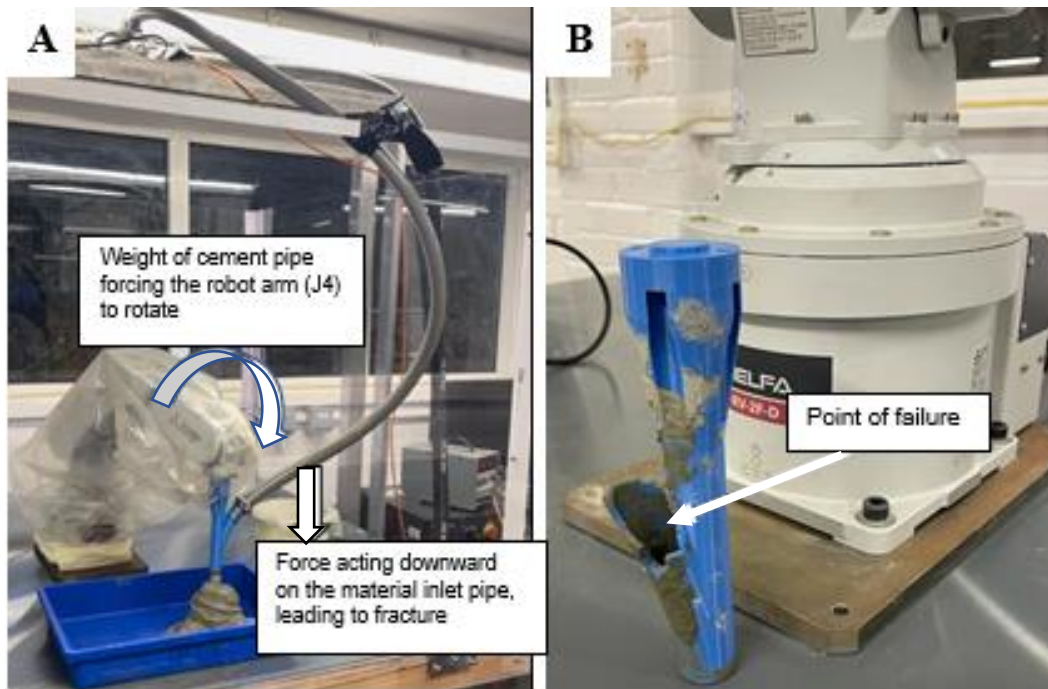


Figure 4.10. a) Force acting downwards on nozzle inlet, b) fractured nozzle

The material selection is a critical factor that can significantly impact both the durability and performance of the printed structure and aluminium was selected for several reasons. First, its high thermal conductivity ensures that the nozzle can withstand the high temperatures generated during the 3D printing process without compromising its performance. This is particularly important when working with cement-based structures, which often require high heat to maintain flow and integrity. Additionally, aluminium's lightweight properties play a key role in improving the overall performance of the robot. Weighing significantly less than materials like steel, the aluminium nozzle reduces strain on the robot's motors and components, ultimately prolonging the lifespan of the machine. This feature aligned with the design goal of minimising load, especially considering that the robot's maximum capacity is 3 kg but operates best within 2 kg. A lighter nozzle not only reduces the risk of overload but also enhances the precision and speed of the printing process, contributing to more accurate and efficient prints. Aluminium's resistance to corrosion and wear further reinforces its suitability for this application, as it ensures that the nozzle can withstand repeated use without losing functionality, a clear advantage over materials like ABS or PLA, which degrade more quickly. Lastly, the machinability of the aluminium allowed the precise manufacturing of the nozzle, including the threaded groove on the inlet pipe, which enhanced the connection between the cement pipe and the nozzle inlet. The ability to machine intricate and functional designs is

essential for this application, where accuracy and strength are important. Overall, the combination of these properties, lightweight, thermal resistance, corrosion resistance, and ease of machining, made aluminium the ideal choice for this nozzle, ensuring functionality, precision, and longevity. Figures 4.11 and 4.12 illustrate the technical drawing and the nozzle connected to the robot, respectively, highlighting the design improvements that make this version superior to previous ones.

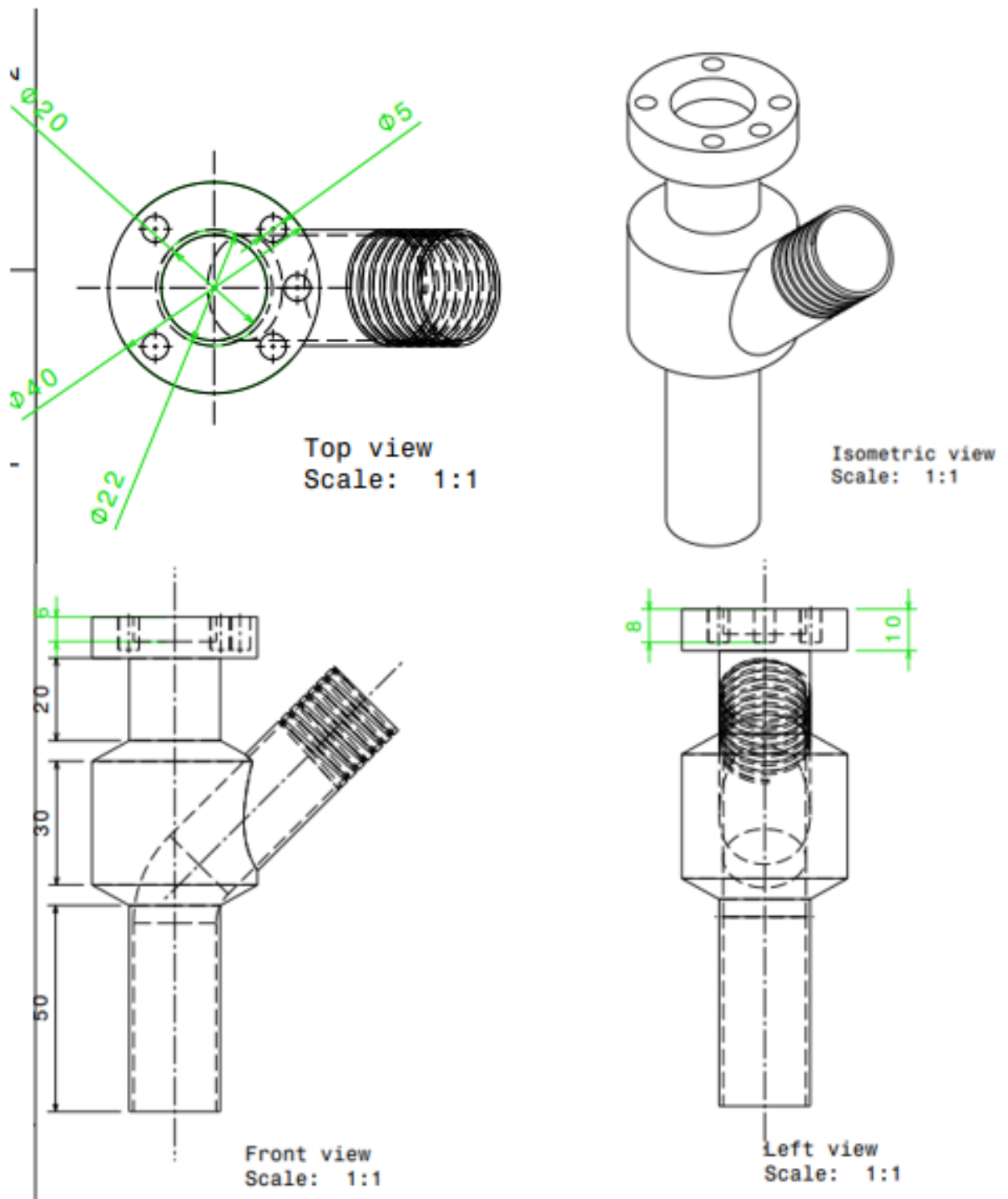


Figure 4.11. Technical drawing of extrusion nozzle

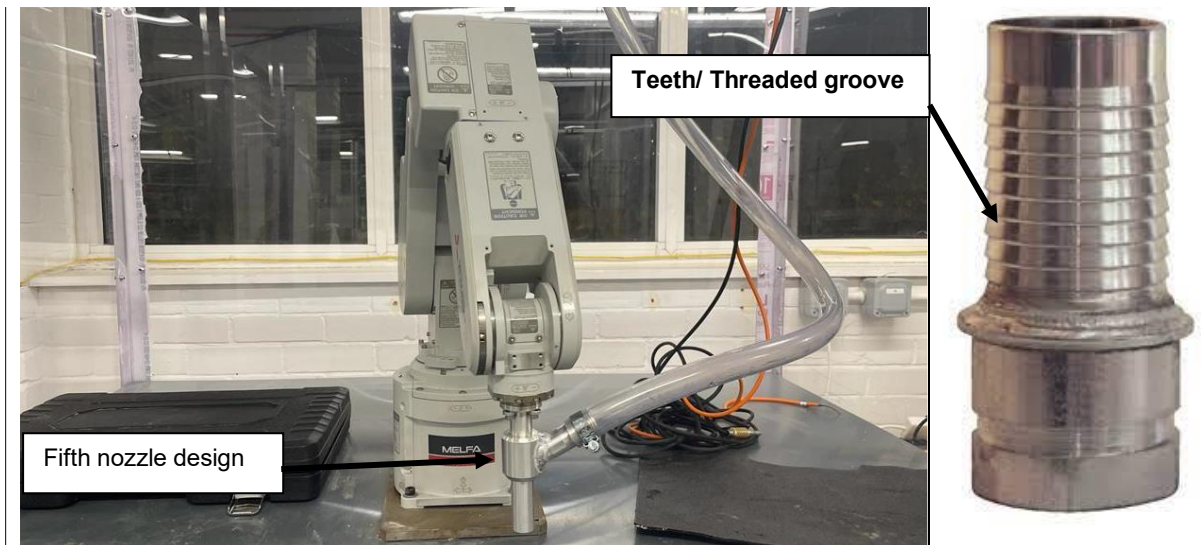


Figure 4.12. Nozzle design with threaded groove

Following the failure of the previous nozzle using ABS and the manufacture of the new robust aluminium nozzle, further 3D printing tests were conducted. The tests were conducted using the same steps as described in the preliminary robot 3d printing Tests 1 and 2. The material was introduced into the cement pump and carefully monitored throughout the procedure. Improved pumpability could be seen, as the material flowed with ease, indicating that the adjustments to the water content was effective. The material continued to flow smoothly through to the robot nozzle, and after a short interval, the 3D printing process commenced successfully. The outcome of the 3D printing is depicted in Figure 4.13. Table 4.4 presents the material properties used to for this print.

Table 4.4. Material properties

Cement (kg)	Sand (kg)	Water (kg)	Temperature (°)	Humidity (%)
6	12	3.9	9	88

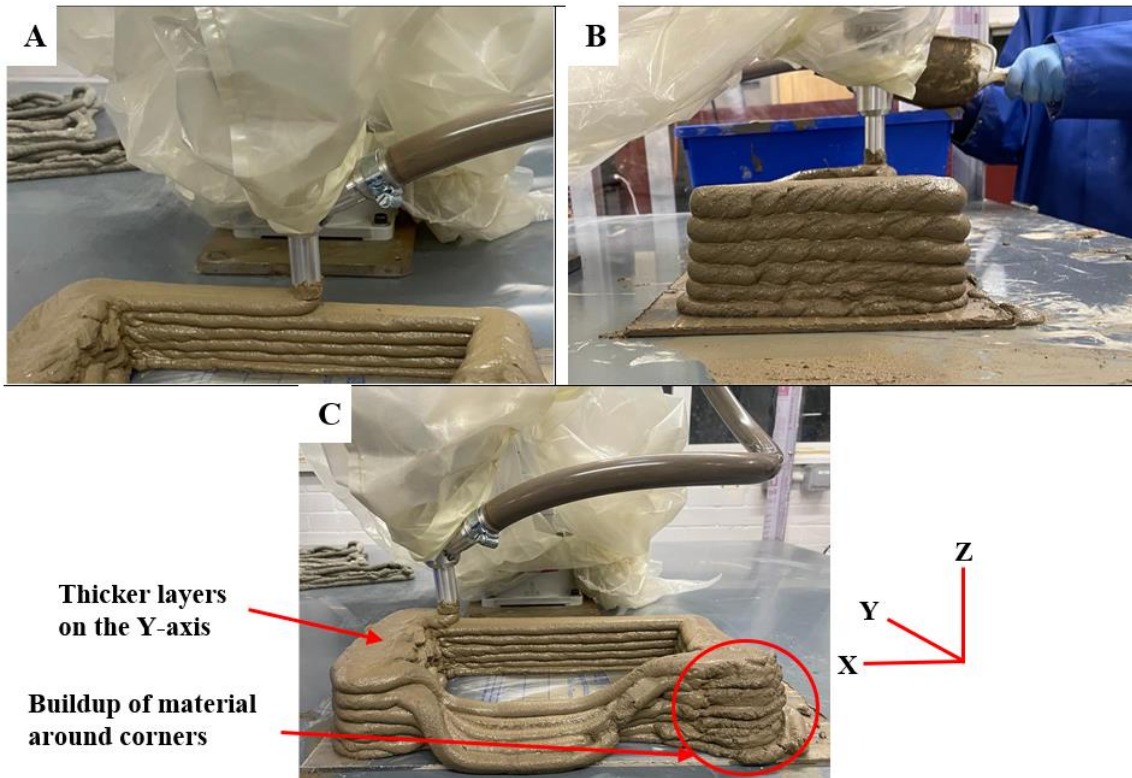


Figure 4.13. Robot 3D printed material (a and b showing 6 consecutive printed layers, and c showing material accumulation at corners and collapse).

The material extruded smoothly, forming clear and distinct layers, yet the stability of the structure became compromised as it reached a certain height. This suggested that, although the material was extrudable, the properties of the cement and its curing time limited the number of layers that could be built before structural failure occurred. A noticeable issue was the inconsistency in layer width between the x-axis and y-axis. The y-axis layers were visibly wider than those on the x-axis, indicating non-uniform deposition. This difference was directly linked to the programming command used during the initial setup, where the OVRD command was employed to control the speed of the robot. This command caused faster movements on the x-axis and slower movements on the y-axis, resulting in uneven layer formation. Furthermore, the structure exhibited noticeable stress concentrations at the edges, particularly where the layers intersected. These stress concentrations were a direct result of non-uniform material deposition and variations in the speed of the robot along different axes. Figure 4.14 shows the list of programming functions used to designate speed on the robot.

Type	Class	Function	Input format (example)
ation control	Joint interpolation	Moves to the designated position with joint interpolation.	Mov P1
	Linear interpolation	Moves to the designated position with linear interpolation.	Mvs P1
	Circular interpolation	Moves along a designated arc (start point → passing point → start point (end point)) with 3-dimensional circular interpolation (360 degrees).	Mvc P1,P2,P1
		Moves along a designated arc (start point → passing point → end point) with 3-dimensional circular interpolation.	Mvr P1,P2,P3
		Moves along the arc on the opposite side of a designated arc (start point → reference point → end point) with 3-dimensional circular interpolation.	Mvr2 P1,P9,P3
		Moves along a set arc (start point → end point) with 3-dimensional circular interpolation.	Mvr3 P1,P9,P3
		Speed designation	Designates the speed for various interpolation operations with a percentage (0.1% unit).
	Designate the speed for joint interpolation operation with a percentage (0.1% unit).	JOvrd 100	
	Designates the speed for linear and circular interpolation with a numerical value (mm/s unit).	Spd 123.5	
	Designates the acceleration/deceleration time as a percentage in respect to the predetermined maximum acceleration/deceleration. (1% unit)	Accel 50,80	
	Automatically adjusts the acceleration/deceleration according to the parameter setting value.	Oadl ON	
Sets the hand and work conditions for automatic adjustment of the acceleration/deceleration.	Loadset 1,1		

Figure 4.14. List of MELFA-BASIC V commands [268]

During the initial trials, the faster movement along the x-axis and slower movement along the y-axis led to excessive material build-up at the corners, causing the edges to experience higher localised stress. This accumulation of material increased the weight at the corners, making these areas more susceptible to deformation and potential cracking. Furthermore, as the height of the structure increased, the weight of the upper layers exerted additional pressure on the lower layers, increasing the stress at the edges. This effect was further magnified by the inherent properties of the cement, such as its relatively low tensile strength and prolonged curing time, which could not adequately support the load distribution at these critical points. The observed structural failure at higher layers indicated that these stress concentrations contributed significantly to the overall instability, particularly at the junctions where the geometry of the material changed.

To address this, the programming was switched to the SPD command, which specified speed in mm/s for both linear and circular paths. This adjustment allowed for a more uniform speed distribution across all axes, potentially mitigating the irregularities observed earlier as show in Figure 4.15. Although the surface finish of the material was rough, we were able to validate the effect of the programming code change on the outcome of the 3D-printed structure.



Figure 4.15. 3D-printed structure with uniform extrusion on all sides.

While the uniform speed improved the layer formation, the printed structure still exhibited instability at higher levels, which highlighted the need for further optimisation of the mix design. To enhance the rheological properties and improve the print quality, two supplementary cementitious materials were incorporated: fly ash and ground granulated blast-furnace slag (GGBS). Fly ash was chosen for its ability to improve workability and reduce shrinkage, while GGBS was selected to enhance the durability and long-term strength of the mix

## **Part C: Printing Process Optimisation and Accelerator Administration**

### **4.6. Process optimisation**

The buildability of a 3D-printed structure is a critical factor in ensuring the successful completion of 3D printing of cement-based materials. This led to the introduction of an accelerator (aluminium sulphate) into the mix to enhance the setting time of the material and improve the buildability. Aluminium sulphate was selected due to its ability to reduce the initial setting time of cement, thereby providing increased early strength and supporting the buildability of the structure. Aluminium sulphate was introduced by feeding it directly into an overhead tank (Figure 4.17, stage 1), which was connected to an inlet at the extrusion nozzle of the 3D printing system. This setup aimed to allow the accelerator to mix directly with the cement as it flowed through the nozzle. However, this method proved problematic due to back pressure caused by the flow of cement through the nozzle. To address the problem of back pressure and improve the consistency of accelerator introduction, a micro pump was incorporated into the system in Figure 4.17, stage 2. The peristaltic pump was chosen for its ability to handle viscous or sensitive fluids without direct contact with the internal components of the pump, making it ideal for transporting the aluminium sulphate without risking chemical degradation or contamination. Additionally, the peristaltic pump offered precise control over the flow rate, which was crucial for maintaining a steady supply of accelerator to the cement mixture. Despite the introduction of the micro pump, the problem of back pressure persisted. Although the micro pump offered some improvement in delivering the accelerator, it was not sufficient enough to achieve the required buildability. This led to the accelerator being released from the nozzle without effectively mixing with the cement. Figure 4.16 shows a key-guided image of the 3D printing process.

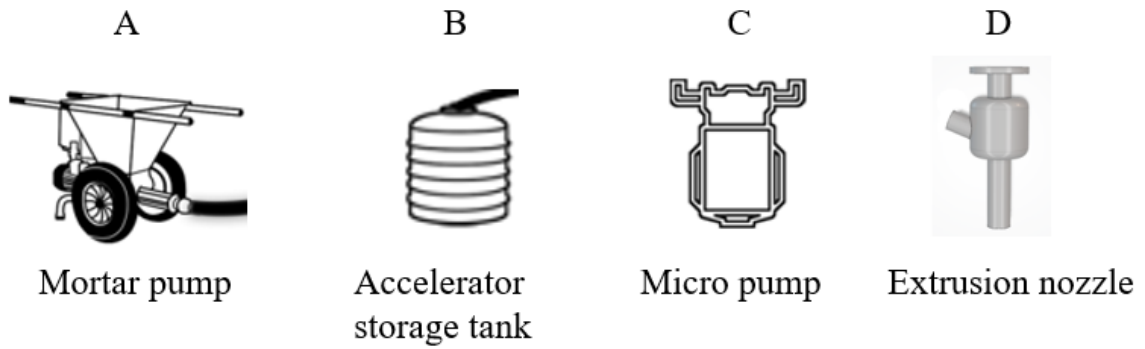


Figure 4.16. Key guide to 3D printing equipment

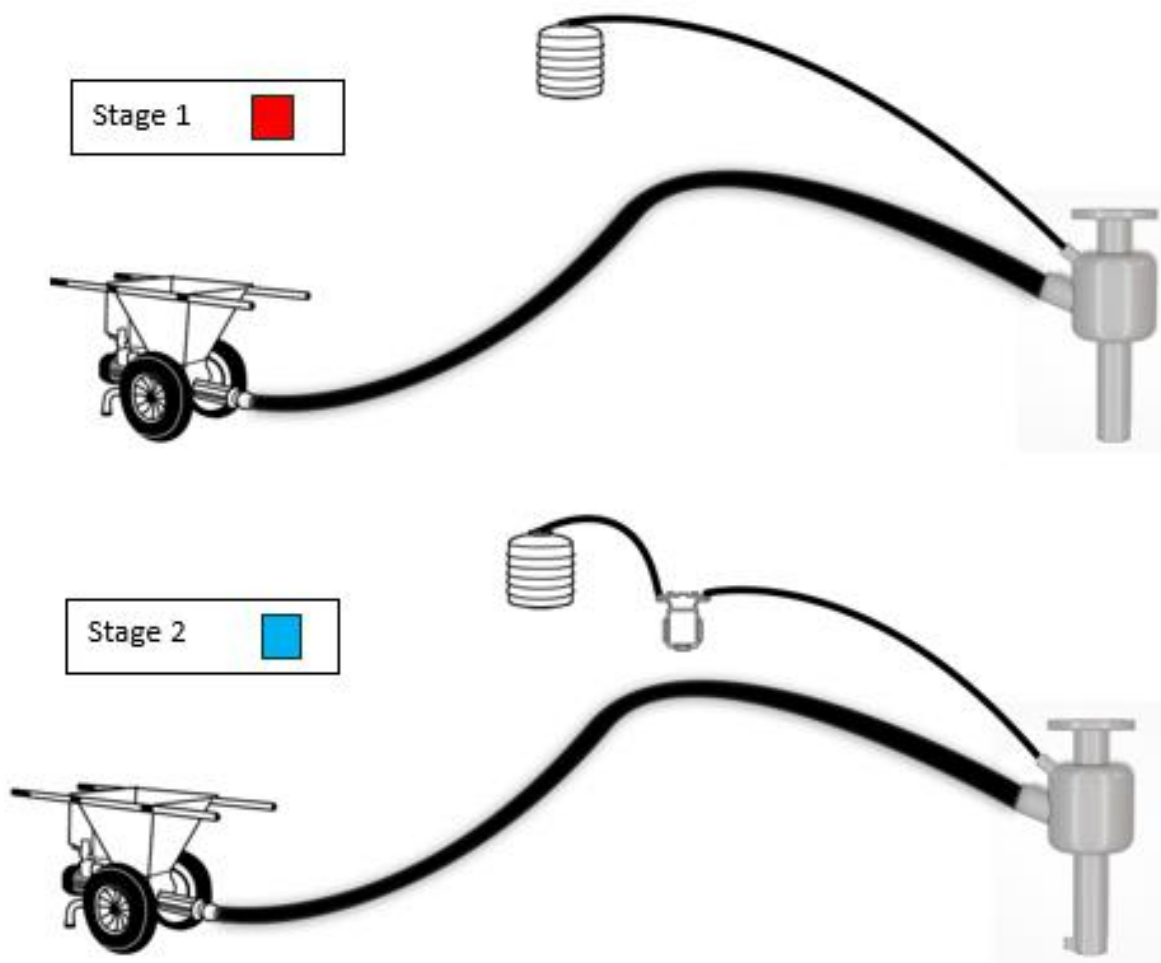


Figure 4.17 3D printing process stage 1 and 2

As a result of the challenges faced in stage 1 and 2, an auger was introduced inside the nozzle to aid a more effective mixing of the accelerator with the cement as shown in Figure 4.18. The auger was driven by an electric motor and was installed to initiate rotational mixing of the

cement-based material and accelerator. While this mechanism was crucial for achieving effective mixing and maintaining a consistent blend throughout the extrusion process, it inadvertently caused another issue. The rotational action of the auger created more back pressure within the nozzle assembly, particularly at the accelerator inlet as shown in Figure 4.19. As the high flow rate of the cement-based material passed through the nozzle, the slow rotation of the auger caused the cement to push against the inlet of the aluminium sulphate. This resulted in the accelerator inlet becoming blocked, and the back pressure forced the cement mortar to flow back up through the intended inlet, disrupting the entire mixing process [280]. The role of the auger was initially designed to serve a dual function: to integrate the accelerator into the cement mixture uniformly and to maintain a consistent composition throughout the print. However, this design led to an unexpected pressure build-up, which ultimately compromised the incorporation of the aluminium sulphate. As a result, the backflow of cement not only prevented effective accelerator mixing but also posed a risk of damaging the nozzle system.



Figure 4.18. Extrusion auger

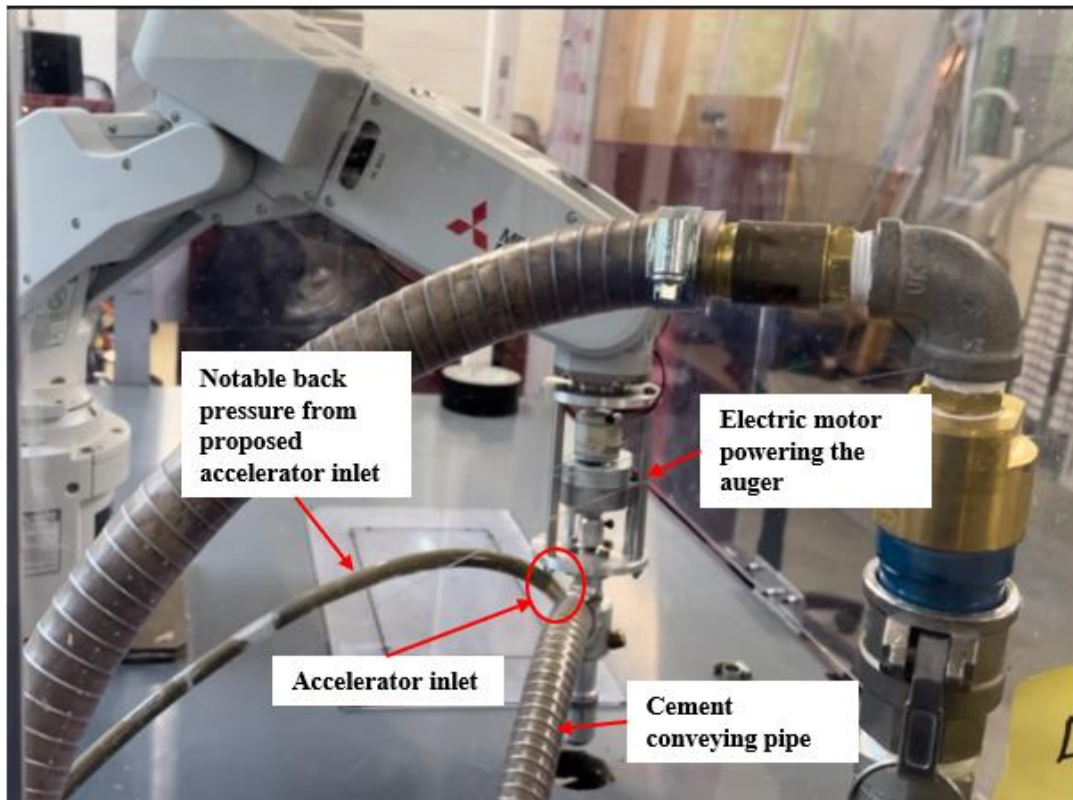


Figure 4.19. Back pressure of material through the proposed accelerator inlet

Further optimisation of the 3D printing nozzle was conducted to address the issues associated with the initial auger design. This optimisation led to the replacement of the auger with a propeller-like mixer inside the nozzle as shown in Figure 4.20. The auger was made from aluminium material. The new propeller-like mixer was designed to operate at a low speed, was introduced to improve the homogeneity of the mixture without generating excessive backpressure. However, this modification presented similar issues. The slower rotation speed of the propeller did not adequately prevent back pressure, leading to the same undesired effect of cement back pressure through the accelerator inlet. Furthermore, the distinct shape of the propeller blades caused the extruded cement to emerge in four separate partitions rather than as a cohesive material. This partitioning compromised the structural uniformity and created flow inconsistencies, highlighting a fundamental flaw in the design.



Figure 4.20. Propeller-like mixer

To resolve these issues, the propeller-like mixer and motor were removed entirely to ensure a smooth and unobstructed flow of the cement-based material through the extrusion nozzle. A novel aluminium device (Figure 4.21) was introduced further down the printing system, featuring a 3 mm diameter accelerator inlet positioned at a 45° angle. This design aimed to mitigate any chance of cement flowing backwards while allowing for a controlled and steady injection of the accelerator into the main cement flow. The placement of the inlet at an angle was strategic, ensuring that the aluminium sulphate could mix effectively without disrupting the natural flow of cement. While this solution resolved the immediate problem of backpressure and provided a more stable integration of the accelerator, it introduced two new challenges. Firstly, increasing the pumping pressure of the accelerator risked rendering the overall cement mix overly viscous, affecting the overall buildability and surface finish, which led to a slumpy and rough layer deposition. Secondly, reducing the pump pressure to avoid such issues made the accelerator inlet more prone to blockages, particularly because of its small diameter. Any slight reduction in flow could cause the cement to solidify and clog the 3 mm inlet, interrupting the steady delivery of the accelerator into the cement stream. Figure 4.22 shows a 3D-printed structure with undermixed material showing excess accelerator and void within the structure.

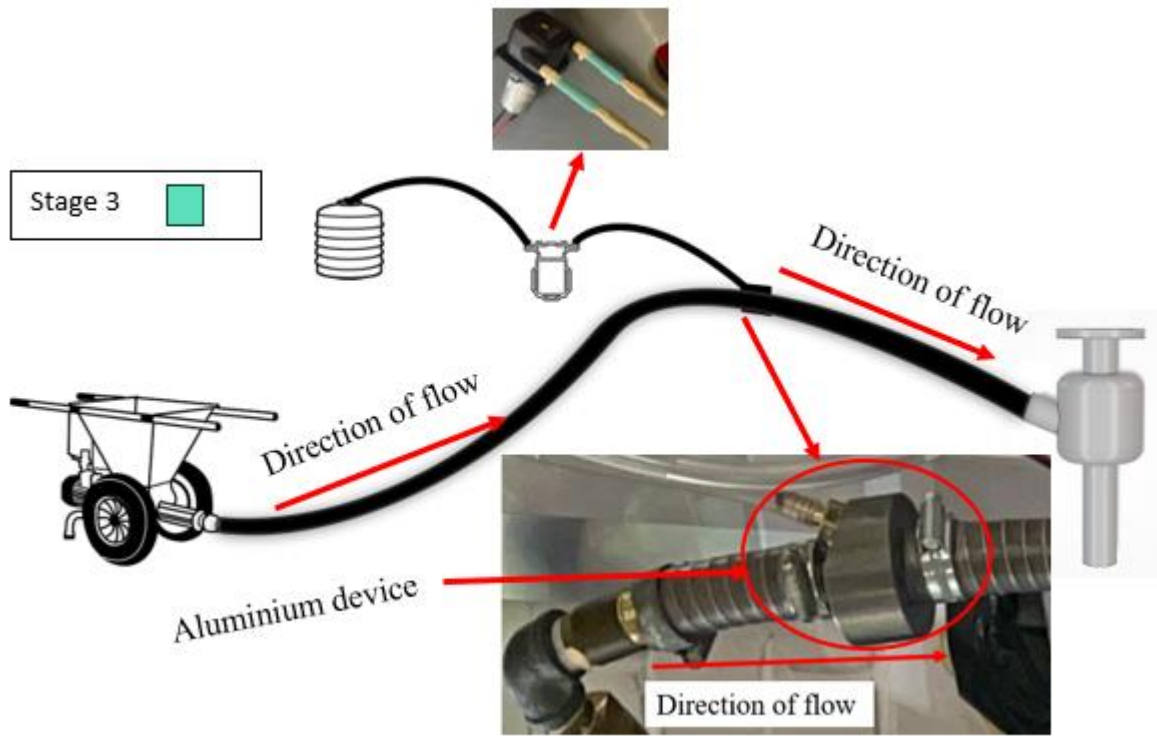


Figure 4.21. Optimised process (stage 3)

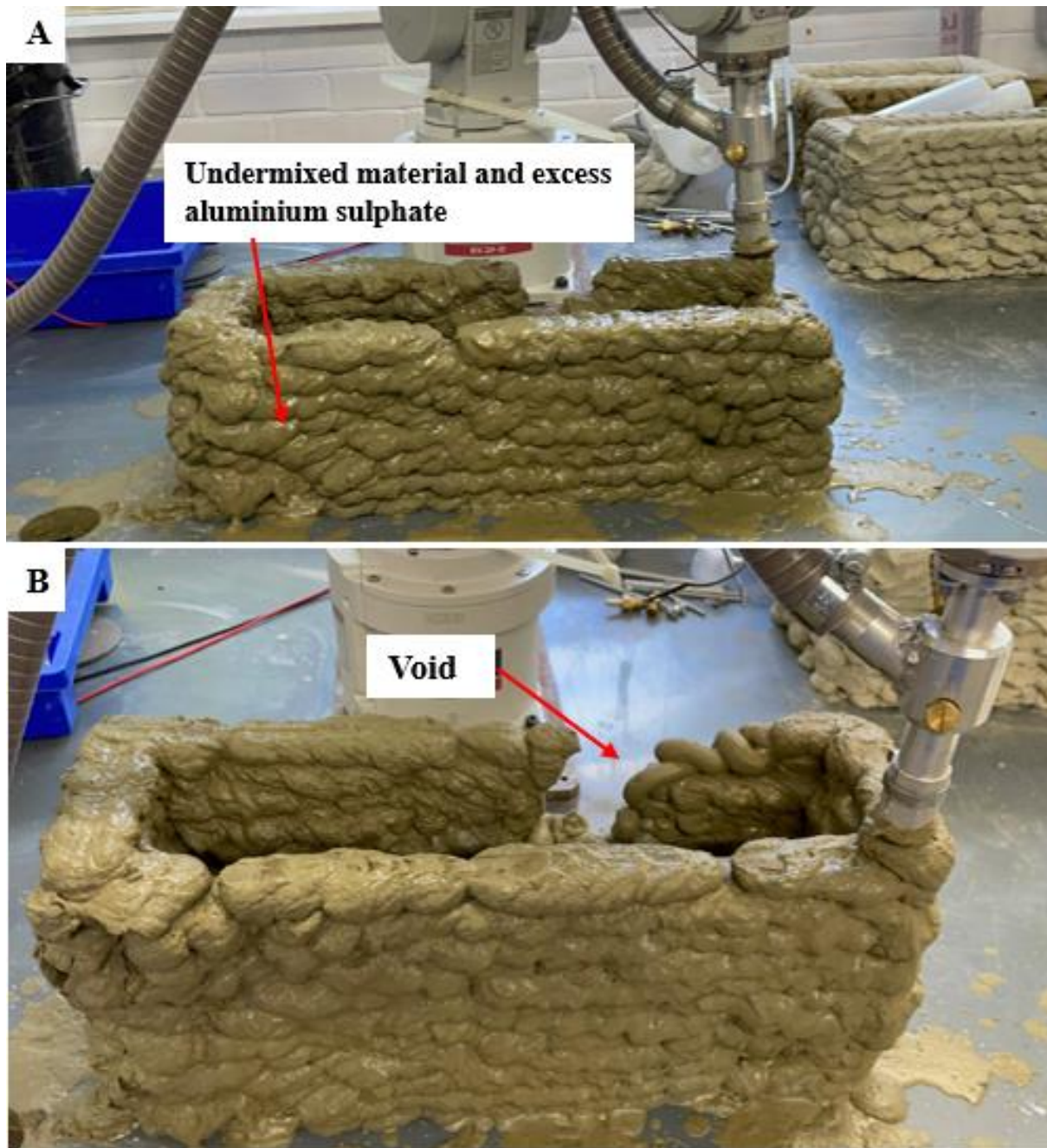


Figure 4.22. (a) 3D-printed structure with undermixed material and excess aluminium sulphate. (b) Massive void between the structure

To address the ongoing complications and backpressure caused by the aluminium device, the aluminium device was completely removed from the system. This change restored the cement flow to its original, smooth state, eliminating the issues of backflow and blockages that were hindering the effective integration of the accelerator. With the removal of the device, the focus shifted towards a more straightforward method of introducing the accelerator into the printing process to evaluate its impact on buildability and layer stability.

Instead of incorporating the accelerator directly into the cement flow, a manual approach was adopted. The accelerator was applied using a hand-held bottle spray, administered on-demand after each layer was deposited. This method allowed the aluminium sulphate to be sprayed onto the surface of each printed layer, enabling real-time control over its application. By spraying the accelerator manually, the amount of accelerator applied could be adjusted based on the observed stability of each newly printed layer, ensuring a more targeted approach as compared to the previous continuous integration attempts.

This surface application aligns with findings from recent studies, where selective accelerator application in 3D printing of cement-based materials has been shown to enhance interlayer adhesion and improve structural integrity without disrupting the internal cement matrix. Lowke et al. [240] demonstrated that surface application of accelerators can effectively target specific layers for improvement, while Mechtcherine et al. [281] observed enhanced bond strength with external application. Additionally, Shao et al. [282] and Bhattacharjee et al. [122] validated that spray-on accelerators can improve yield strength and interfacial properties in 3D-printed structures, supporting this method as a practical alternative to full integration within the mix.

The results from this on-demand application method were promising. Spraying the accelerator directly onto each layer significantly improved the buildability of the structure. The material gained strength more rapidly, allowing additional layers to be deposited without experiencing premature slumping or deformation. Moreover, the surface finish of the printed structure remained smooth, and the layers exhibited proper adhesion, avoiding the segmented flow and irregularities seen in earlier designs. This method also ensured that the accelerator did not interfere with the internal flow of the cement through the nozzle, maintaining a consistent extrusion rate and material quality throughout the printing process. Figure 4.23 shows a 3D-printed structure by manual on-demand spraying of the accelerator.

The new 3D printing process, which combined the standard cement flow with manual on-demand application of the accelerator, proved to be successful. By selectively strengthening each layer as needed, the structure was able to support more layers before experiencing any signs of structural failure. This approach not only enhanced the overall buildability of the cement-based structure but also provided greater flexibility and control during the printing process.



Figure 4.23. 3D-printed structure by manual on-demand spraying of accelerator

The success of the manual, on-demand spraying of the accelerator highlighted the potential of surface application in enhancing the buildability of the 3D-printed cement-based structures. This breakthrough demonstrated that applying the accelerator directly onto the surface of each newly deposited layer significantly improved early strength, enabling more layers to be printed without compromising the stability or surface quality of the structure. Observing these positive results motivated the transition from manual spraying to an automated system as shown in Figure 4.24, stage 4 to ensure consistency and efficiency throughout the printing process.

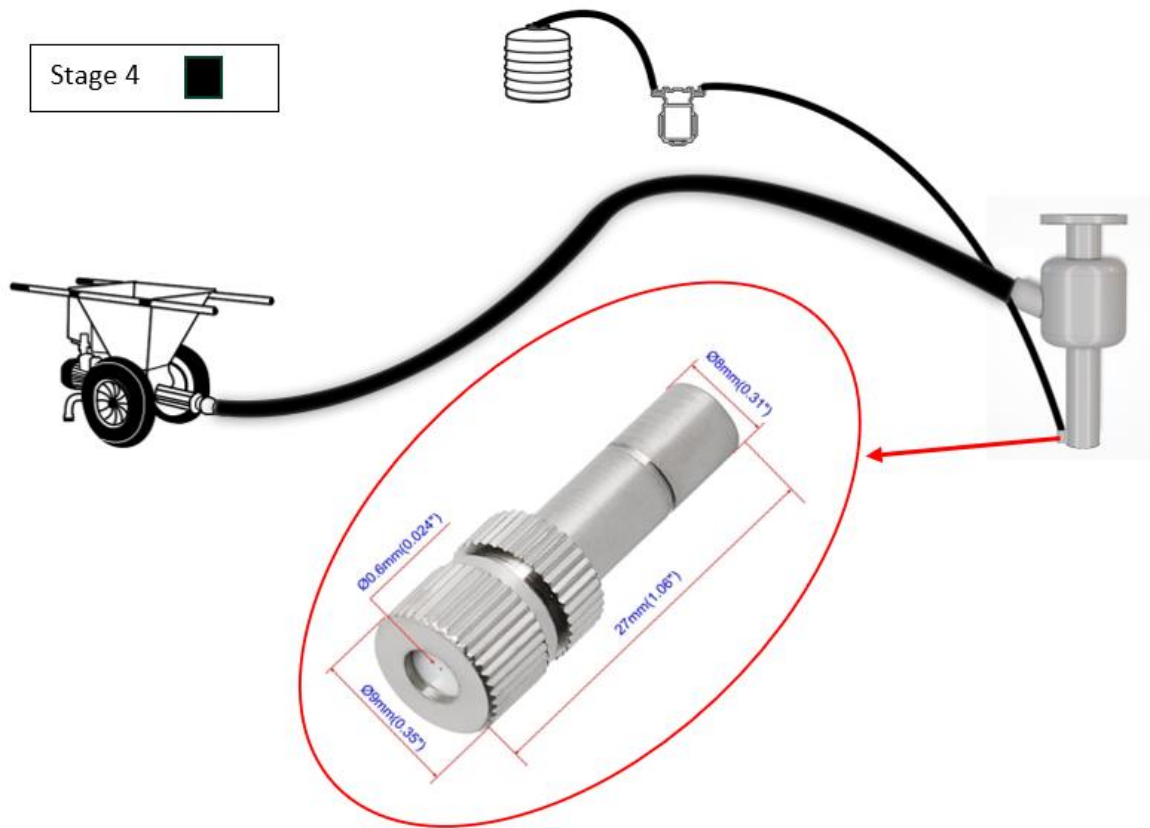


Figure 4.24. Micro nozzle attached to robot extrusion nozzle

To achieve automation, the previously used accelerator storage tank and peristaltic pump were reintroduced into the setup, with a precise flow rate of 20 ml/min to ensure consistent and controlled application. Instead of incorporating the accelerator directly into the cement flow, the new system featured a separate micro-nozzle, with an outlet diameter of 0.6 mm, specifically designed for the surface application of the accelerator. This micro-nozzle was attached to the main extrusion nozzle of the robotic arm and oriented to spray the accelerator directly onto the top surface of each freshly deposited layer as shown in Figure 4.25. The peristaltic pump was then connected to this micro-nozzle through a plastic pipe to control the flow of the accelerator from the storage tank, ensuring precise and consistent delivery as the robot moved along its programmed path.

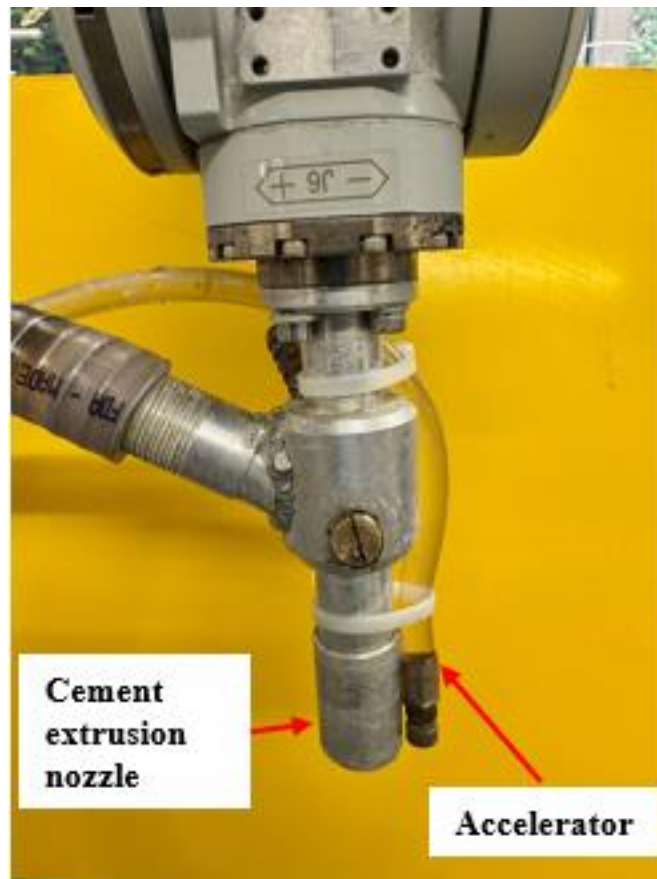


Figure 4.25. setup of cement and accelerator extrusion

With the automated system in place, the accelerator was applied simultaneously with the extrusion process, ensuring that each layer received the optimal amount of accelerator immediately after deposition. This integration eliminated the need for manual intervention, maintaining a uniform application rate and reducing variability between layers. The peristaltic pump, known for its precise flow control, played a key role in conveying the aluminium sulphate from the storage tank to the micro-nozzle without any risk of contamination or degradation. The automated spraying allowed for the accelerator to be dispensed in synchrony with the movement of the robot, making the process more efficient and reducing the chances of human error. This solution preserved the benefits observed during the manual application phase, such as improved early strength and enhanced buildability. The uniform layer-by-layer spraying resulted in a smoother, more cohesive structure, with each layer setting quickly and supporting the weight of subsequent layers. Additionally, the automated application maintained the surface finish quality and interlayer adhesion observed during manual testing, thereby

enhancing both the structural integrity and the overall print quality of the 3D-printed cement-based structures.

The transition to automation signified advancement, demonstrating how a successful manual method could be refined into a scalable, reliable process that could be implemented for small and large-scale 3D printing applications. This development not only streamlined the printing process but also provided a platform for future modifications, such as integrating multiple additives or varying the accelerator application rate to accommodate different print geometries and material properties. Figure 4.26 shows a 3D-printed structure by automatically spraying the accelerator on-demand.



Figure 4.26. 3D-printed structure by automated on-demand spraying of accelerator

The early decision not to incorporate aluminium sulphate into the dry mix was based on several practical and material-related considerations. Aluminium sulphate is known to significantly accelerate the hydration process of cement, which could be highly problematic if the reactions were initiated too early in the 3D printing process. Adding it directly to the dry mix would have caused the cement particles to begin hydrating almost immediately after adding water, resulting in a rapid increase in viscosity and setting rate even before the material reached the extrusion stage. If the accelerator had been part of the initial mix, the cement mortar would become increasingly difficult to pump through the system. The early onset of hydration would cause the cement to thicken prematurely, creating a high risk of clogging within the mortar pump and the material conveying pipes. This would disrupt the smooth flow of the material and cause severe blockages that could potentially damage the pump and other components of the 3D printing system. The resulting high pressure within the pump could lead to mechanical failures. Additionally, if the material managed to flow to the robot extrusion nozzle, the rapid setting of the cement would have prevented the material from flowing uniformly through the extrusion nozzle, making it challenging to achieve a consistent layer deposition. The hardened or partially set material would lose its ability to be extruded in a controlled manner, leading to rough, uneven layers and poor surface finish. Therefore, it was essential to keep the accelerator separate from the dry mix and introduce it at a later stage, allowing the cement to maintain its workable state as it passed through the mortar pump and nozzle. This approach prevented premature setting, ensuring that the mixture remained pumpable and extrudable while still allowing the benefits of aluminium sulphate to be harnessed once the material was deposited. By spraying the accelerator onto the surface of each layer, the buildability could be enhanced without compromising the flowability and integrity of the cement-based mixture during its journey through the system.

#### 4.6.1. Processes parameter

The optimisation process was conducted systematically in four distinct stages. In Stage 1, aluminium sulphate was introduced directly into the cement mixture using a gravity-fed system to enhance early strength and buildability. However, this approach caused persistent backpressure issues, leading to blockage problems. To address these challenges, a peristaltic pump was introduced in Stage 2, providing more precise control over accelerator delivery. While the pump improved flow control, it did not fully resolve the backpressure issue. Consequently, Stage 3 implemented internal mixing mechanisms, first using an followed by a propeller-type mixer to achieve better accelerator integration. However, both internal mixers further increased backpressure and intensified blockage issues. Ultimately, Stage 4 adopted an external, surface-level application of the accelerator, initially through manual spraying and later automated. This final approach effectively eliminated previous issues, significantly enhancing buildability, structural stability, and surface finish without causing internal flow disruptions.

Stage	Process parameter	Material/Method/Value	Justification
1	Accelerator type	Aluminium sulphate	Accelerates cement hydration, improving early strength and buildability
	Accelerator integration method	Overhead tank directly to the nozzle inlet by gravity feed	Simplified direct integration approach; minimal setup required. identified backpressure issues
2	Accelerator delivery system	Peristaltic micro pump	Precise flow control, handles viscous fluids without contamination
	Pump flow rate	20 ml/min	Optimised flow rate aiming for controlled delivery

	Accelerator inlet	Direct inlet connection; 45° to nozzle	Simplified direct inlet; encountered persistent backpressure and blockage
<b>3</b>	Internal mixing mechanism	Auger followed by a propeller mixer	Aimed to improve accelerator integration; both methods led to increased backpressure and nozzle blockage
	Final inlet design	3 mm diameter at 45° angle; connected to an aluminium device further down the system	Reduced backflow and facilitated accelerator injection into cement flow; however, introduced viscosity and blockage challenges
<b>4</b>	Accelerator application method	Surface spraying (manual followed by automated)	Avoided internal blockage issues, precise accelerator control, improved interlayer adhesion and stability.
	Automated spraying nozzle diameter	0.6 mm	Ensured precise, consistent accelerator application.
	Automated spraying slow rate	20 ml/min	Provided consistent surface application, enhancing buildability and adhesion.
	Nozzle attachment position	Adjacent to extrusion nozzle	Ensured correct timing and position for accelerator application.

## Part D: Performance Evaluation of Experimental Works

### 4.7. Effect of printing speed on buildability of 3D-printed small-scale structures

This section presents a comprehensive analysis of how varying concentrations of aluminium sulphate, printing speeds, and layer heights affect the buildability and structural integrity of 3D-printed cement-based structures. Key results highlight the relationship between accelerator dosage and the number of stable layers achieved, the impact of printing speed on layer adhesion and stability, and the influence of layer height on interlayer bonding. This section discusses these findings in detail, providing a comprehensive understanding of the buildability challenges and potential solutions for 3D printing applications in construction

Understanding the critical role of printing speed in 3D printing is essential to optimise the buildability and stability of printed structures. Figure 4.27 shows a graphical illustration of the number of layers before collapse *versus* printing speed. Figure 4.28 shows the results of the investigation, highlighting how varying printing speeds significantly impacted the performance and buildability of small-scale 3D-printed structures. Table 4.5 presents the effect of printing speed on layer thickness of the 3D-printed structures.

Table 4.5. Effect of printing speed on layer thickness of the 3D-printed structures.

Parameters	Samples			
	B1	B2	B3	B4
Printing speed (mm/s)	10	20	40	80
Layer thickness (mm)	70	40	20	13

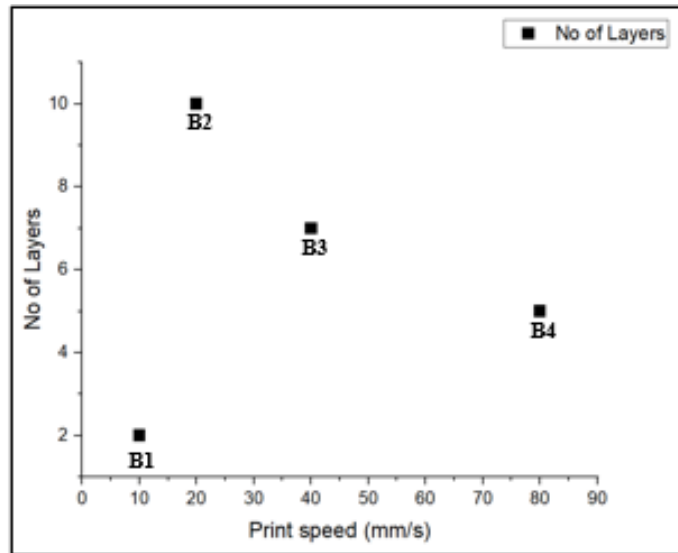


Figure 4.27. Graphical illustration of number of layers achieved versus printing speeds



Figure 4.28. Buildability test with varying printing speeds

The investigation into the effect of printing speed on the buildability of 3D-printed small-scale structures revealed distinct differences in performance across different printing speeds. The volumetric material deposition rate ( $Q$ ) was calculated using the formula:

$$Q = A_{nozzle} \times v \quad (2)$$

Where  $A_{nozzle} = 176.71 \text{ mm}^2$  is the cross-sectional area of a 15 mm diameter nozzle, and  $v$  is the printing speed.

Sample B1, printed at a slow speed of 10 mm/s, resulted in a deposition rate of  $1767.1 \text{ mm}^2/\text{s}$  and a layer thickness of 70 mm. This large filament surface area led to several detrimental

effects, including excess material being forcefully squeezed onto the printed surface leading to localised buckling of the filament [256], as shown in sample B1 (Figure. 4.28). Consequently, this resulted in a poor surface finish and nozzle blockage, due to a combination of slow printing speed and constant pump pressure. The excessive material accumulation caused the system to clog after two layers only, making this speed the least effective in terms of buildability.

In contrast, sample B2, printed at a speed of 20 mm/s, achieved a deposition rate of 3534.2  $mm^2/s$  and a layer thickness of 40 mm. This speed enabled the structure to achieve a maximum of 10 layers before structural failure. The layers maintained good adhesion and stability up to the point of collapse, indicating that 20 mm/s was the most effective speed for achieving high buildability. The balanced interaction between material deposition and setting time at this speed ensured strong inter-layer bonding and structural integrity.

Sample B3, printed at a higher speed of 40 mm/s, had a deposition rate of 7068.4  $mm^2/s$  and managed to produce 7 layers with a layer thickness of 20 mm before reaching structural failure. However, the increased speed resulted in early noticeable deformation and reduced layer adhesion when compared to sample B2. The limited settling time for the material at this speed hindered proper layer bonding, reducing the overall buildability and leading to structural failure after fewer layers when compared with sample B2.

Finally, sample B4, printed at the highest speed of 80 mm/s, resulted in a deposition rate of 14,136.8  $mm^2/s$  and a layer thickness of 13 mm. While this speed allowed for the printing of up to five layers, it induced major inconsistencies and weak inter-layer bonding. The rapid deposition rate at this speed did not allow sufficient time for the material to settle and bond adequately, leading to poor layer adhesion and early structural collapse. Figure 4.29 shows the effect of printing speed and pump pressure on the interlayer bond of 3D-printed structures.

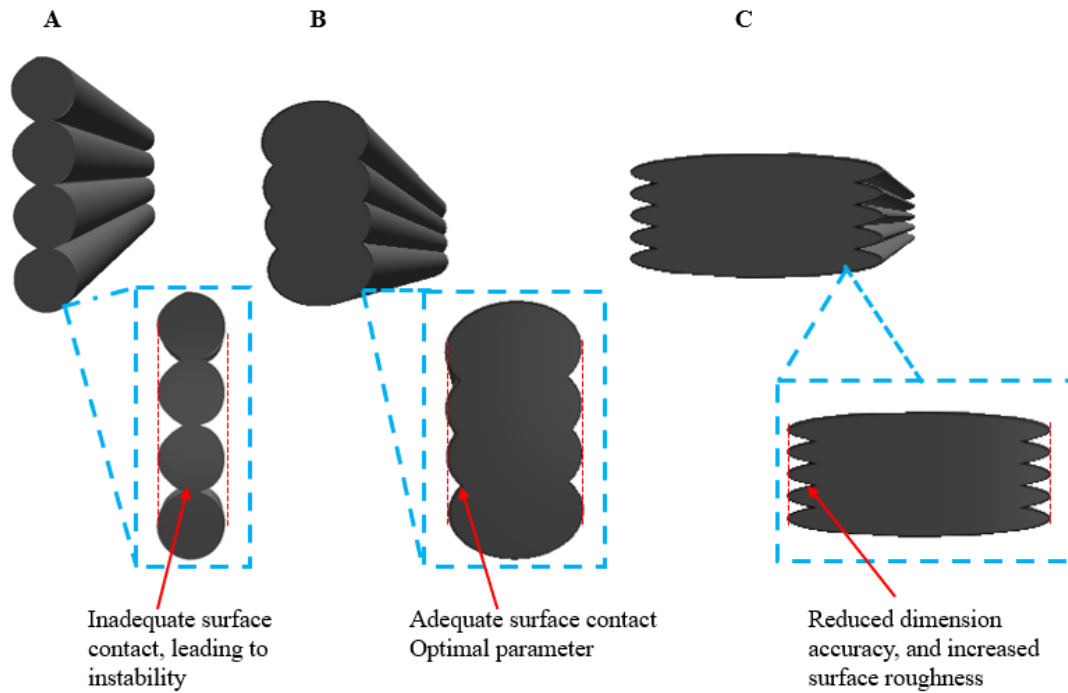


Figure 4.29. Examples of surface contact between 3D-printed structures

The optimal printing speed was identified at the value of 20 mm/s, which allowed for the printing of 10 stable layers with strong inter-layer bonding and stability. Figure 4.30 shows a graphical illustration of the effect of print speed and pump pressure on 3D-printed structures.

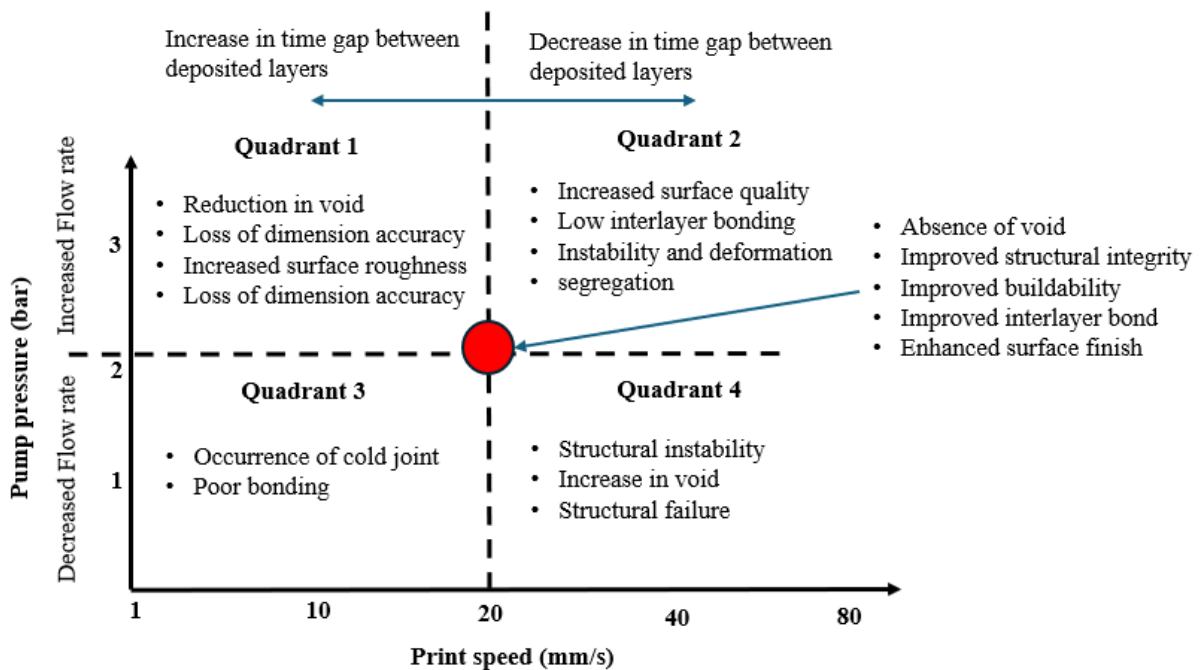


Figure 4.30. Printing limits, showing the effects of pump pressure and printing speed on the 3D-printed layers

Figure 7.4 is divided into 4 quadrants, and it shows how varying print speed, pump pressure, and time gaps between layers affect the build quality and structural stability of 3D-printed concrete. In quadrant 1, a combination of increased pump pressure and decreased print speed results in a reduction of voids but affects the dimensional accuracy and increased surface roughness. This is because the excessive material flow tends to overfill the layers, making it difficult to control the precise placement and leading to poor surface quality. Conversely, quadrant 2, where both pump pressure and print speed are high, shows that the material is deposited too rapidly, reducing surface quality and interlayer bonding. This can cause instability, deformation, and segregation of the material, compromising the structural integrity of the print. Quadrant 3, with low pump pressure and low print speed, results in the occurrence of cold joints and poor bonding between layers. The slow deposition and insufficient material flow create time gaps between layers that prevent proper bonding, leading to weaker connections and potential delamination. On the other hand, in quadrant 4, where low pump pressure is combined with high print speed, risks structural instability and an increase in voids. This imbalance leads to under-extrusion, as the pump is unable to supply enough material to match the high speed of the nozzle, resulting in incomplete layer formation and poor structural strength. At the midpoint, the optimal condition is represented by the red circle, where the pump pressure and print speed are optimised. In this zone, the concrete is deposited evenly, resulting in the absence of voids, improved interlayer bonding, and enhanced surface finish. This central area reflects the ideal operational range for the printing process, where structural integrity and buildability are maximised.

Additionally, the Figure 4.27 highlights the influence of time gaps between deposited layers, as indicated by the horizontal arrows. Increasing the time gap between layers, as shown by the arrow pointing left, can lead to a loss in dimensional accuracy and rougher surfaces, as the material may not properly bond if the previous layer has already begun to set. Conversely, decreasing the time gap, represented by the arrow pointing right, can reduce surface quality and interlayer bonding, leading to instability and deformation if the layers are deposited too quickly without allowing enough time for each layer to settle.

#### 4.8. Effect of layer height on 3D-printed small-scale structures

The influence of layer height on the buildability of 3D-printed structures is crucial to optimise the printing quality and structural stability. Therefore, this study further explored how varying layer heights affected the buildability and performance of 3D-printed small-scale structures. Figures 4.31, 4.20 and 4.33 show the schematics of the 3D nozzle and extruded layers, buildability test with varying layer heights and graphical illustration of number of layers *versus* layer height, respectively. Table 4.6 presents the effect of layer height on layer thickness of the 3D-printed structures.

Table 4.6. Effect of layer height on layer thickness of the 3D-printed structures.

Parameters	Samples			
	C1	C2	C3	C4
Print speed (mm/s)	20	20	20	20
Layer height (mm)	10	15	20	25
No of layers	10	7	4	3
Width (mm)	40	30	28	20

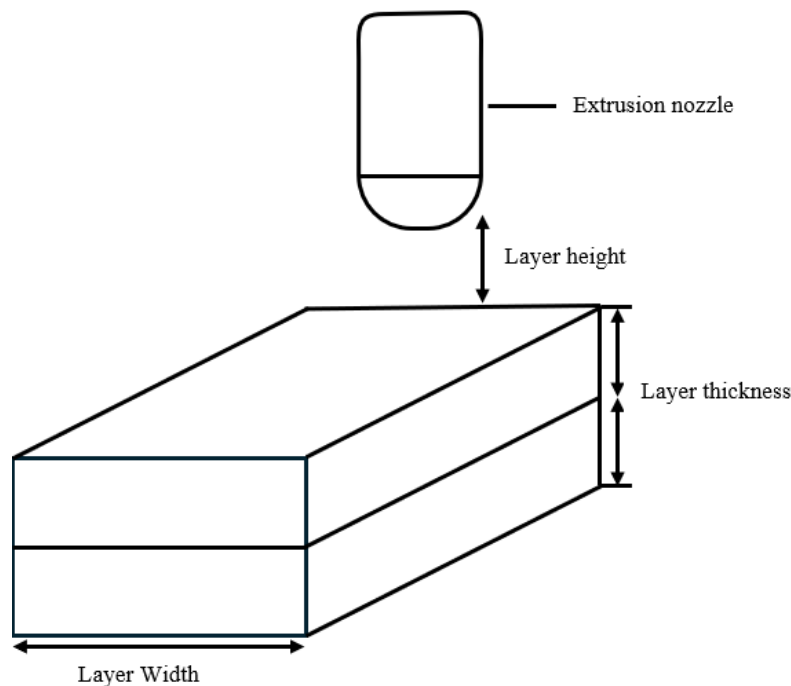


Figure 4.31. Schematic showing layer height, thickness, and width in 3D concrete printing



Sample C1 ( layer height 10 mm)



Sample C2 ( layer height 15 mm)



Sample C3 ( layer height 20 mm)



Sample C4 ( layer height 25 mm)

Figure 4.32. Buildability test with varying layer heights

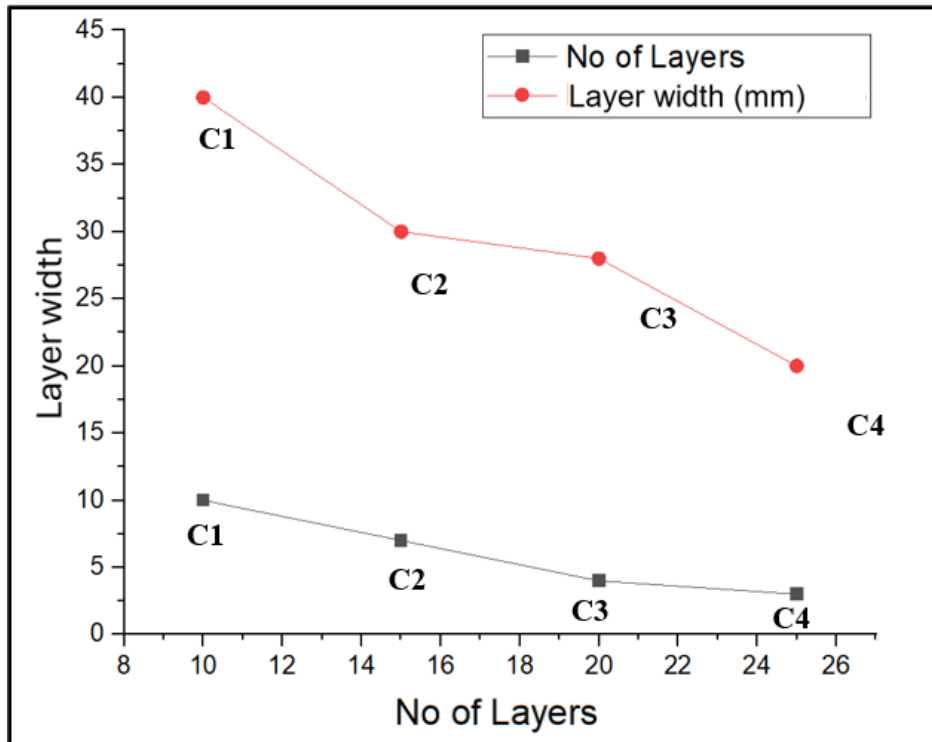


Figure 4.33. No of layers versus layer height

The investigation into the effect of layer height on the buildability of 3D-printed small-scale structures revealed distinct differences in performance primarily attributed to the relationship between layer height, interlayer adhesion and structural stability. To aid a better understanding of the observed results, the interlayer adhesion strength ( $\sigma_{adh}$ ) can be conceptually expressed as:

$$\sigma_{adh} = \alpha \cdot \frac{A_{int}}{h} \quad (3)$$

Where  $\alpha$  is a material-dependent coefficient,  $A_{int}$  is the interfacial contact area and  $h$  is the layer height. This simplified representation helps illustrate that adhesion strength is inversely proportional to layer height. As the layer height increases, the contact area between successive layers decreases, resulting in weaker bonding and reduced buildability.

Sample C1, with a layer height of 10 mm, achieved the highest buildability by printing 10 layers before structural failure. The relatively small layer height of 10 mm facilitated proper interlayer adhesion, contributing to the structural stability of the printed layers. Sample C1 had a layer thickness of 40 mm, indicating that a smaller layer height allowed for better material

adhesion and stronger layer bonding, which in turn enhanced the overall buildability of the structure.

Conversely, sample C2, with a layer height of 15 mm, successfully printed seven layers before experiencing structural failure. While the increase in layer height to 15 mm still allowed for adequate interlayer adhesion, it was less effective when compared with sample C1. Sample C2 exhibited a layer thickness of 30 mm, which implied that the increase in layer height began to compromise the ability of the material to adhere properly between layers, leading to a reduction in buildability.

Sample C3 with a layer thickness of 28 mm managed to print only four layers before failure occurred. The larger layer height of 20 mm contributed to improper interlayer adhesion, resulting to a reduction in the interlayer bond strength. This is due to the reduced interfacial contact area and increased potential for cold joints, which can lead to weaker structural integrity and increased risk of delamination or cracking.

Finally, sample C4 supported a mere three layers before structural failure occurred. The substantial layer height of 25 mm resulted in a nozzle height far from the previously deposited layer, leading to uncontrolled extrusion (Figure 4.34) and significant buildability challenges. This sample exhibited a layer thickness of 20 mm. The excessive distance between the nozzle and the previously deposited layer resulted to weak interlayer bonding and inadequate structural support, culminating to rapid structural failure. Significantly, the optimal layer height was 10 mm, facilitating proper interlayer adhesion and allowing for the printing of ten layers before structural failure. This observation has been supported by similar studies [5, 15] that established that smaller layer heights improved material cohesion and layer bonding, enhancing overall buildability.

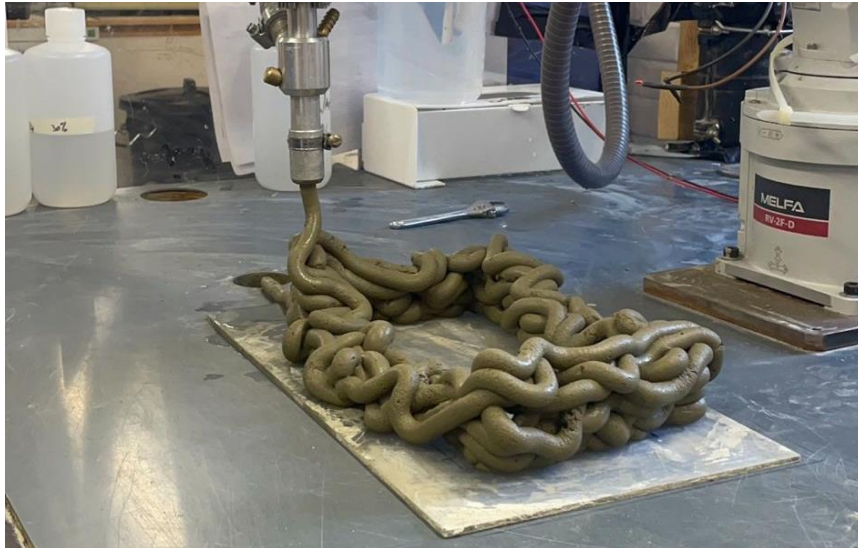


Figure 4.34. Uncontrolled nozzle extrusion

#### 4.9. Effect of aluminium sulphate on buildability of 3D-printed structures

To evaluate the effect of aluminium sulphate on the buildability of 3D-printed cement-based structures, five samples were tested. One sample, labelled CTRL\_ST00, served as the control and contained no aluminium sulphate. The other four samples included varying percentages of aluminium sulphate: 15% (AL\_ST15), 25% (AL\_ST25), 35% (AL\_ST35), and 45% (AL\_ST45). The aim of the study was to assess how different concentrations of aluminium sulphate influenced the structural integrity and the number of layers that could be successfully printed before collapsing, as illustrated in Figure 4.35. The effects of aluminium sulfate on the buildability of the 3D-printed structures are represented in Table 4.7.

Table 4.7. Effect of aluminium sulphate on buildability

	Samples				
	CTRL_ST00	AL_ST15	AL_ST25	AL_ST35	AL_ST45
Aluminium sulphate concentration (%)	0	15	25	35	45
No of layers	10	10	11	13	14

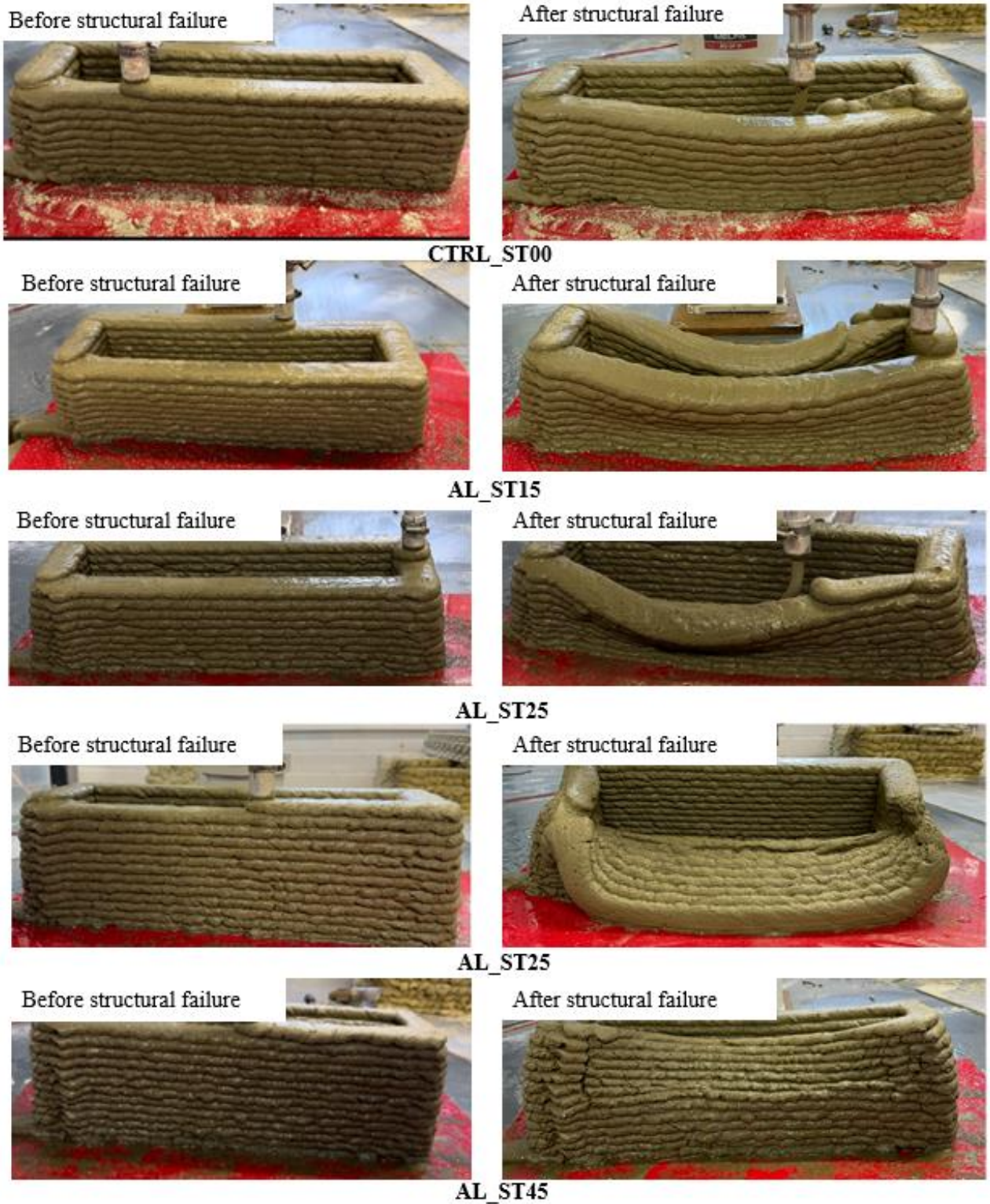


Figure 4.35. Buildability test with varying accelerator concentration

The experimental results revealed a noticeable correlation between the concentration of aluminium sulphate and the buildability of 3D-printed structures. Five different structures were tested, having a percentage of aluminium sulphate concentration of 0, 15, 25, 35 and 45%. The

sample structures printed with 0, 15, 25, 35 and 45% concentrations produced 10, 10, 11, 13 and 14 layers, respectively, before structural failure occurred (Figure 4.36). This progressive increment indicated that the number of 3D-printed layers increased with the concentration of the accelerator, thereby enhancing the buildability of the structures.

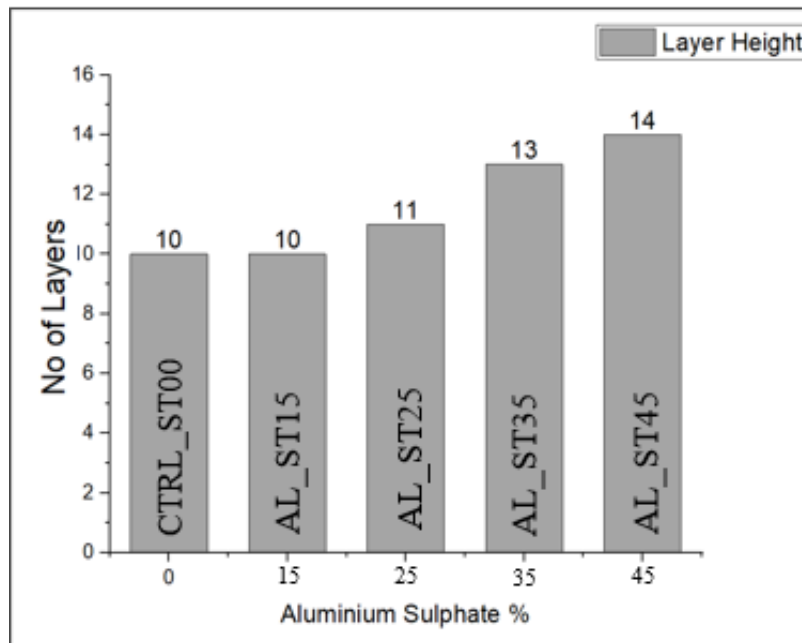


Figure 4.36. Influence of accelerator concentration on layer height of the 3D-printed structures

Moving forward, the number of layers achieved before structural failure demonstrated that higher concentrations of accelerator significantly improved the structural integrity and buildability of the 3D-printed layers. Both the CTRL\_ST00 sample and the AL\_ST15 sample achieved 10 layers before they collapsed. Sample AL\_ST25 achieved 11 layers, indicating a slight improvement. The enhancement became more pronounced with sample AL\_ST35, which achieved 13 layers, and sample AL\_ST45, which achieved 14 layers before failure.

The reduction in height before failure also provided insights into the effects of accelerator dosage on buildability, as shown in Figure 4.37. The CTRL\_ST00 sample experienced an 8% reduction in height, while both AL\_ST15 and AL\_ST25 exhibited a 6% reduction. Sample AL\_ST35 had a minimal reduction of 2%, and the AL\_ST45 sample did not compress before failure. The absence of compression in AL\_ST45 suggested that the lower layers became significantly stiffer under the influence of the accelerator concentration, thereby preventing deformation under the weight of subsequent layers. In contrast, the bottom layer of the

CTRL\_ST00 sample was compressed from 10 to 2 mm, highlighting the benefit of the accelerating admixture to maintain layer integrity.

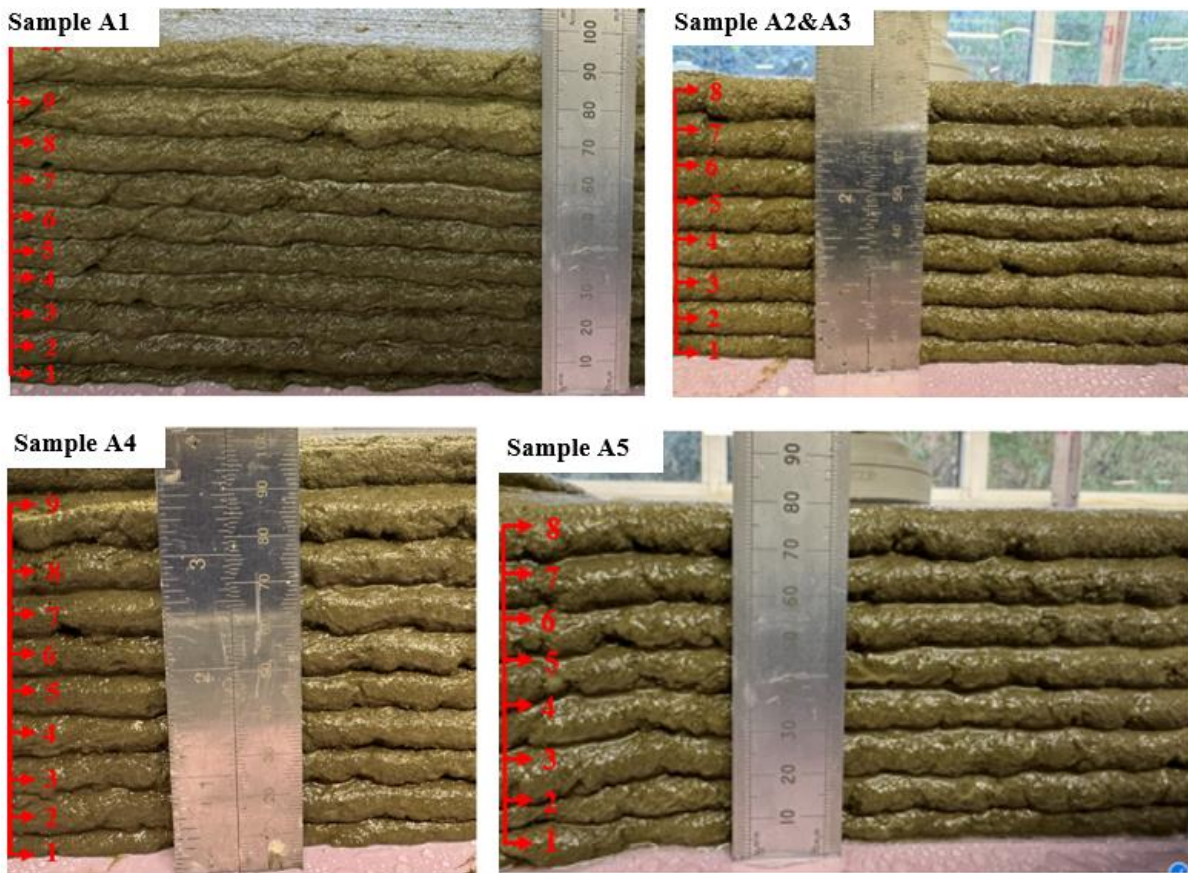


Figure 4.37. Reduction in height with varying accelerator concentrations

This result clearly indicated that the optimum concentration for maximum buildability in this experiment was 45%. At this concentration, the bottom layer of the structure did not compress under the weight of the subsequent layers, unlike the other samples. This phenomenon was significant, as it established that the accelerator/aluminium sulphate not only enhanced the number of layers that could be printed before structural failure, but also improved the stiffness and load-bearing capacity of the 3D-printed layers. Similar findings were reported by Bhattacharjee and Santhanam [117] who printed two large-scale structures, one of which was printed with an accelerator sprayed on the surface. For the first structure, printed in panels, the target height of the lower layer was 15 mm, but the achieved height was only 9 mm, resulting in a compression of 40%. The second structure was printed continuously with simultaneous spraying of the accelerator on the vertical surfaces of the layers, showing higher deformation. The target layer height was 20 mm, and the achieved height was 15 mm, resulting to a

compression of 25%. Therefore, this research can conclude that spraying aluminium sulphate on the 3D-printed layer surfaces enhanced their buildability.

These results align with the role of aluminium sulphate in promoting early surface setting, which is critical in extrusion-based printing. Conversely, this effect was not reflected in standard penetration resistance tests. The penetration depths remained close to 40 mm across all mixes for the duration of the test, including AL\_ST45, which only began to show a slight reduction after 17 min into the test. This can be attributed to the nature of the Vicat test itself, which applies spot pressure through a needle, in contrast to the surface-wide loading experienced during 3D printing.

Summarily, there was a clear positive correlation between the concentration of aluminium sulphate and the buildability of 3d-printed structures. The number of 3D-printed layers before structural failure increased from 10 to 14 by increasing the concentration from 0 to 45%. This result was consistent with previous studies [68, 116, 117, 122, 283-285] that suggested that accelerators, including aluminium sulphate, can enhance the stiffness and load-bearing capacity of 3D-printed layers by accelerating the setting time and improving early-age strength. In addition, it has been similarly reported that higher accelerator dosages significantly reduced setting time, accelerated ettringite formation and improved structural build-up. Figure 4.38 highlights how aluminium sulfate, when applied in controlled amounts, forms a thin, protective layer (red) on the surface of each 3D-printed layer. This surface layer enhances buildability by promoting rapid setting, which stabilises the layer and prevents early deformation during the addition of subsequent layers.

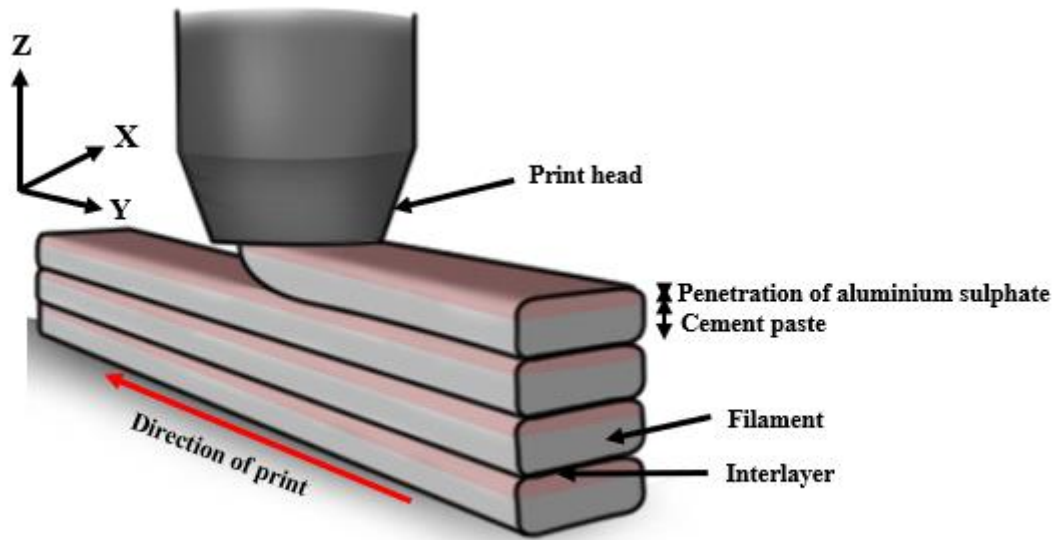
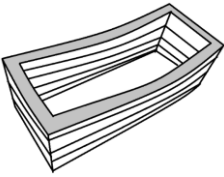
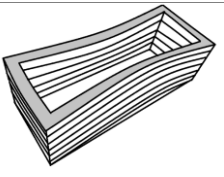


Figure 4.38. Penetration of aluminium sulphate

#### 4.9.1. Structural failure

Table 4.8 presents the different modes of failure from varying the effect of aluminium sulphate on the buildability of 3D-printed structure

Table 4.8. Structural modes of failure.

Sample identification	3D-printed structure	Failure mode	Likely cause of failure
CTRL_ST00 AL_ST15 AL_ST25 AL_ST35		Elastic buckling	<ul style="list-style-type: none"> <li>▪ Weak layer adhesion.</li> <li>▪ Homogeneity of mixture.</li> <li>▪ Insufficient curing time between layers.</li> </ul>
AL_ST45		Plastic collapse	<ul style="list-style-type: none"> <li>▪ Inadequate support / reinforcement.</li> <li>▪ Lower layers experiencing stresses exceeding yield stress.</li> </ul>

The Table 4.8 provides a comprehensive analysis of the structural behaviour of different 3D-printed cement-based samples, highlighting various failure modes and potential causes. Samples A1, A2, A3, and A4 exhibited signs of elastic buckling, where the structures showed lateral deflections. This mode of failure happens when the lower layers of the samples cannot maintain its geometrical stability [286] under the increasing load from the upper layers, causing it to bend sideways. This suggested that the critical buckling load had been reached. This resulted in significant shape distortions whilst the material remained within its elastic limit. Such deformations occurs because the structure's geometry, particularly its height-to-thickness ratio, makes it more susceptible to buckling under vertical loading. The critical load at which a structure will buckle can be calculated using Euler's formula:

$$P_{cr} = \frac{\pi^2 EI}{(KL)^2} \quad (4)$$

here:

$P_{cr}$  is the critical buckling load, E is the Young's modulus of the material,  $I$  is the moment of inertia of the cross-section, L is the effective length of the column and K is the effective length factor. The moment of inertia  $I$  is directly influenced by the thickness of the. For a rectangular cross-section of width b and thickness t, the moment of inertia is given by:

$$I = \frac{bt^3}{12} \quad (5)$$

As the thickness  $t$  decreases, the moment of inertia  $I$  reduces rapidly due to its cubic dependence on t. A lower moment of inertia results in a lower critical buckling load  $P_{cr}$ . On the other hand, the height L appears in the denominator of Euler's formula squared. As the height L increases, the critical buckling load decreases significantly. This indicates that tall and slender structures are more likely to buckle under a smaller compressive load compared to shorter, thicker structures with the same material properties.

In contrast, sample A5 experienced a more severe failure mode known as plastic collapse. This was characterised by a complete structural failure, where the material had yielded and undergone permanent deformation. The large, irreversible changes in shape, with the material spreading outwards and losing its initial form, indicated that the stress levels had exceeded the yield strength of the concrete. Plastic collapse suggested that the structure could no longer carry any load, leading to a complete loss of structural integrity.

## 4.10. Mechanical properties of 3D-printed structures

### 4.11. Compressive strength

The average compressive strength of the 3D-printed structures at 1, 7, 14, and 28 days was found to be 2, 12, 14, and 22 MPa, respectively. In contrast, the monolithic structures exhibited higher average compressive strengths of 2.1 MPa, 22.8 MPa, 29.9 MPa, and 39.4 MPa at the same respective curing times. Figure 4.39 shows the graphical illustration of both strengths.

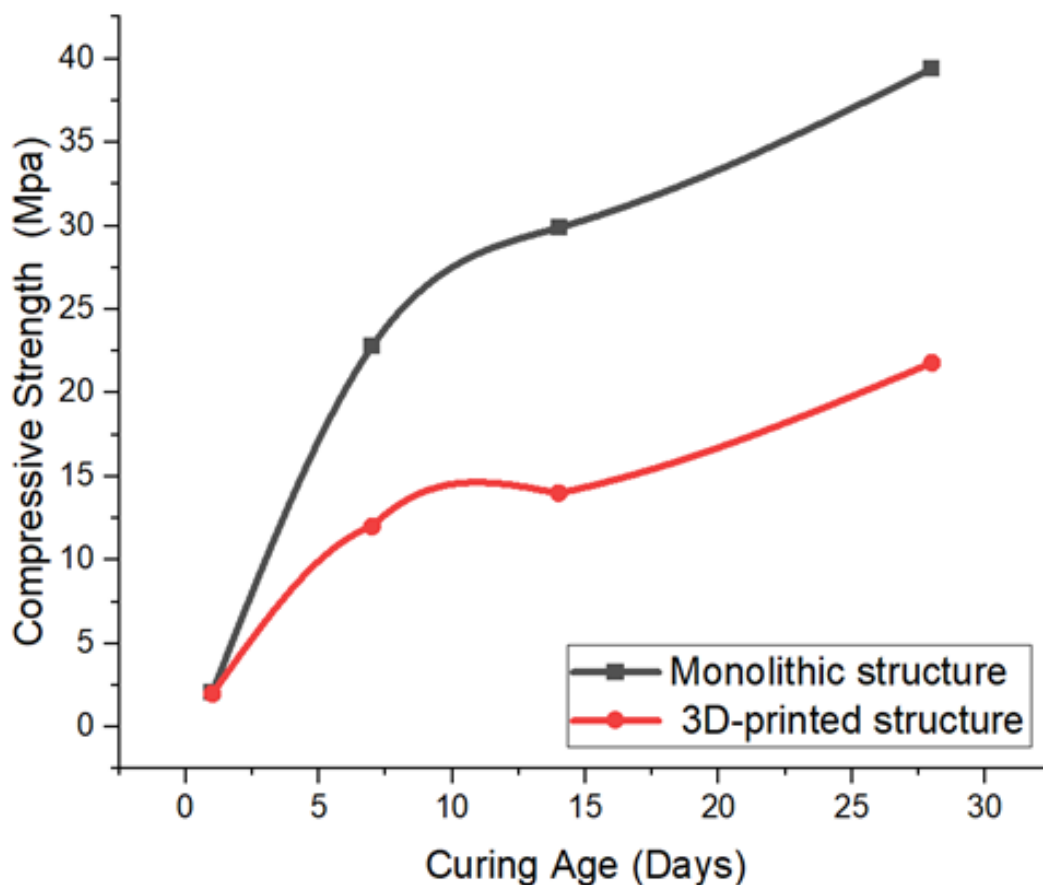


Figure 4.39. Graph of compressive strength of 3D-printed versus monolithic structure

#### 4.11.1. Analysis of 3D-Printed Structures

The compressive strength of the 3D-printed structures increased significantly over the curing period, starting at 2 MPa on day 1 and reaching 22 MPa at 28 days. This improvement showed that the hardened properties of 3D-printed structures were enhanced by curing time. The initial low strength at day 1 can be attributed to microstructural defects and weaker interlayer bonds

often seen in freshly printed structures, as shown in Figure 4.40 [169, 287]. However, as the hydration process progressed and the cement matrix continued to cure, these weaknesses were mitigated, leading to enhanced compressive strength. Despite this improvement, the final compressive strength at 28 days (22 MPa) remained significantly lower than that of the monolithic structures (39.4 MPa). This suggested that while curing helps, the 3D printing process inherently introduces factors that limit the ultimate strength, such as weak layer interfaces and potential porosity within the printed layers. Tables 4.9 presents the compressive strength of 3D-printed structures.

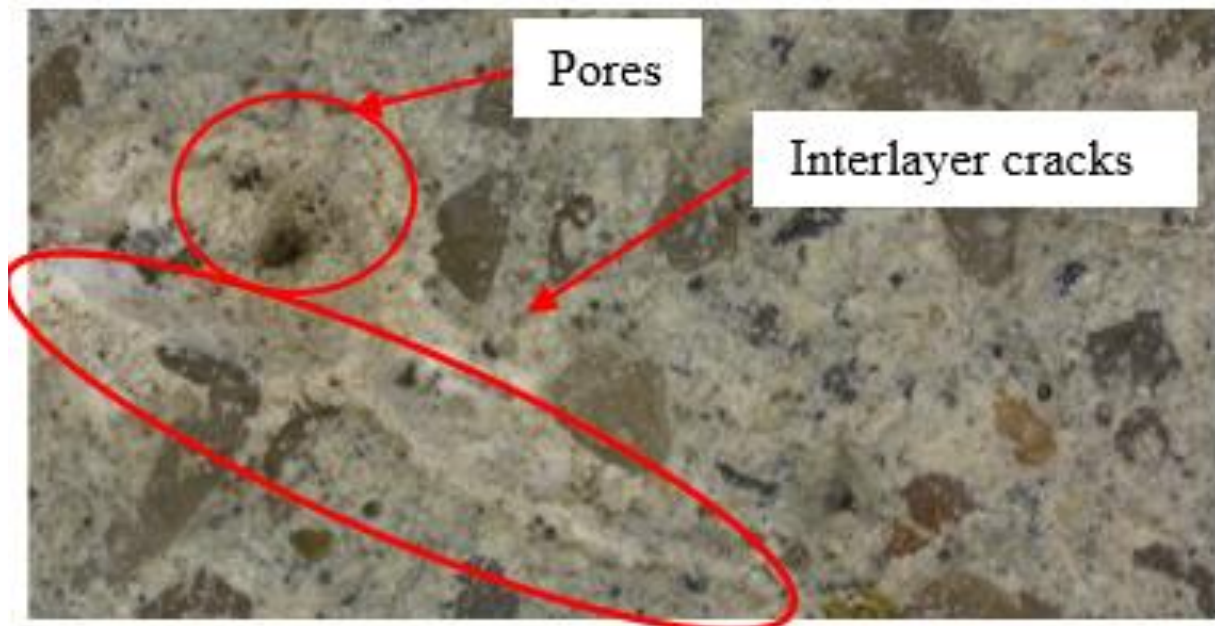


Figure 4.40. Microstructure defect

Table 4.9. Compressive strength of 3D printed structure.

Day	Load rate (MPa/s)	Load (kN)	Strength (MPa)	Mean strength	Standard deviation
1	0.20	28.60	1.70	2.1	0.46
		45.00	2.60		
		35.80	2.00		
7	0.20	242.20	14.10	12.2	2.10
		215.60	12.60		
		177.30	10.00		

		237.70	13.90		
	0.2	220.00	12.70	14.0	1.40
14		262.60	15.40		
		350.30	20.40		
	0.2	350.10	20.40	21.9	2.66
28		423.70	25.00		

#### 4.11.2. Analysis of monolithic structures

The monolithic structures consistently exhibited superior compressive strength compared to the 3D-printed structures throughout the curing period. The compressive strength at 1 day was 2.1 MPa, slightly higher than the 3D-printed structures. This marginal difference can be attributed to the more uniform material distribution and lack of layer interfaces in the monolithic structures. The compressive strength of the monolithic structure then increased, reaching 22.8 MPa at 7 days, 29.9 MPa at 14 days, and 39.4 MPa at 28 days. Table 4.10 presents the compressive strength result, showing the mean and standard deviation (SD) of structures after 28 days. These results highlight the effectiveness of the traditional casting method in achieving high material uniformity and strong internal cohesion, leading to superior mechanical properties. The monolithic structures benefited from a more continuous and homogeneous cement matrix, which facilitated better load distribution and resistance to compressive forces.

Table 4.10. Strength of Monolithic Structure.

Day	Load rate (MPa/s)	Load (kN)	Strength (MPa)	Mean strength	Standard deviation
		36.10	2.10		
	0.20	35.90	2.00	2.17	0.20
1		41.40	2.40		
		426.80	24.95		
	0.20	431.90	25.25	22.84	3.91
7		313.40	18.33		

		593.70	34.71		
	0.20	505.90	29.58	29.97	4.53
14		438.90	25.67		
		703.70	41.15		
	0.20	637.80	37.30	39.47	1.97
28		683.50	39.97		

#### 4.11.3. Comparative Analysis

The results revealed a significant disparity in compressive strength between 3D-printed and monolithic cement-based structures, highlighting the limitations of 3D printing technology for construction applications. The monolithic structures consistently demonstrated substantially higher compressive strength at all curing stages compared to the 3D-printed specimens. This performance discrepancy was primarily attributed to several factors. First, the 3D-printed structures exhibited inherent weaknesses at the interfaces between layers, known as interlayer bonding. These interlayer bonds were typically weaker than the bulk material, which contributed to a reduction in overall strength. Secondly, the monolithic structures benefited from more uniform material distribution. This homogeneity significantly enhanced their compressive strength. Furthermore, the layer-by-layer deposition method used in 3D printing introduced porosity and microstructural defects. These defects acted as stress concentrators, further diminishing the compressive strength of the 3D-printed structures. Additionally, while both sets of samples were cured under similar conditions, the initial state of the materials differed.

#### 4.11.4. Failure mode analysis

This study examined the failure modes of 3D-printed cement-based structures, focusing on the implications of the layer-by-layer deposition process. By comparing these structures to monolithic structures, the analysis provides insights into the potential weaknesses introduced by the 3D printing process. Figures 4.41a and b show the 3D-printed and monolithic structures that failed under compressive load on day 1, respectively.



Figure 4.41. Failed structure after 1 day of (a) 3D-printed and (b) monolithic structures

The failure characteristics of the 3D-printed and monolithic cement-based structures were distinct yet exhibited some similarities in their failure progression after 1 day of curing. In the early stages of the compression test, cracks propagated along the 3D-printed structures initiated at weak points along the top corner surface. These cracks then propagated vertically along the height of the structure, eventually forming continuous cracks that spanned the entire structure. As the load approached its peak, additional cracks developed within the printed layers, further propagating throughout the structure. Significant spalling of the surface material began, indicating the onset of severe structural deterioration. This spalling intensified as deformation increased, leading to a rapid decline in the load-bearing capacity of the structure. Ultimately, the 3D-printed specimens fractured along the interlayer interfaces, signalling complete structural failure across multiple surfaces.

The monolithic structure exhibited a similar failure progression, though it was more cohesive. Initial cracks formed and propagated vertically without the influence of layer interfaces. As the load increased, these cracks led to surface spalling, and the structure eventually fractured, which is typical of brittle failure in cement-based materials. The failure of both structures highlighted the influence of material age, with interlayer weaknesses in the 3D-printed structures playing a critical role in their failure.

After 28 days, the 3D-printed structure exhibited minimal cracking and limited spalling, as shown in Figure 4.42a. Similar to the structures tested on day 1, cracks propagated along the

top corners of the 3D-printed. These cracks then propagated vertically downwards along the entire structure. The difference between the structures tested on day 1 and day 28 was that there was limited crack generation and spalling from every side of the structure. The structure failed as the initial crack propagated. This suggested that the material properties had improved over time, particularly in interlayer bonding. The monolithic structure (Figure 4.42b), with its inherently stronger and more cohesive composition, demonstrated similar but superior damage resistance, minimal cracks and spalling.



Figure 4.42. Failed structure after 28 days of (a) 3D-printed and (b) monolithic structures

#### 4.11.5. Finite Element Analysis

Figure 4.43 shows a finite element simulation of a cement cube subjected to compressive loads. The colour-coded deformation map highlights the regions of maximum stress concentration, with red indicating the areas experiencing the greatest deformation.

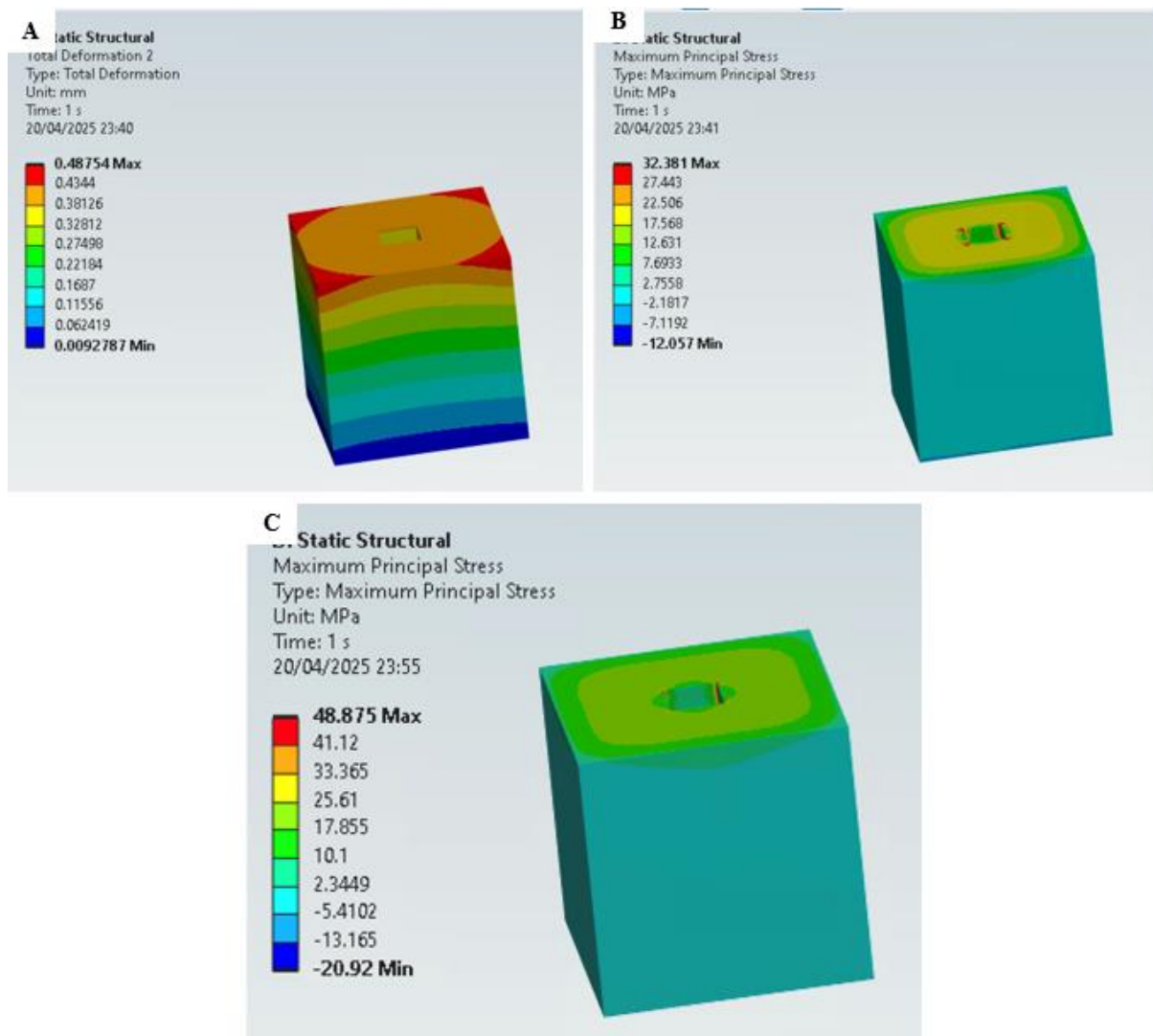


Figure 4.43. (a) Total deformation, (b) Maximum principal stress and (c) Mesh modified maximum principal stress

The simulation results clearly demonstrated the relationship between deformation, stress distribution, and the crack patterns observed in both the 3D-printed and monolithic cement structures. According to the total deformation plot, the maximum deformation measured was 0.48754 mm, occurring near the top surface and edges of the structure, particularly surrounding the cut-out region. The minimum deformation, recorded at 0.00928 mm, was observed near the bottom face, where the structure was fixed. These deformation zones correspond closely with the crack initiation regions observed in the physical specimens, suggesting that areas around the hole are highly vulnerable to displacement under axial compressive loading.

Further validation was provided by the stress analysis. With an initial mesh size of 5 mm, the maximum principal stress was recorded as 32.38 MPa, concentrated around the edges of the

cut-out. However, following mesh refinement to a 2 mm element size, the total deformation remained consistent, slightly decreasing to 0.48427 mm, indicating stable global behaviour. Notably, the maximum principal stress increased significantly to 48.86 MPa, as the finer mesh allowed for sharper resolution of stress gradients near geometric discontinuities. This rise in stress was expected, as a finer mesh better captures localized effects that coarser meshes tend to average out.

These stress concentrations, particularly around the cut-out edges, aligned with the physical crack formations seen in the experimental monolithic samples. The updated principal stress values also approached and exceeded the experimentally observed average compressive strength of 39.47 MPa, which is consistent with the nature of principal stress reflecting localized tensile stress, a common trigger for crack initiation in brittle materials like concrete. Overall, the FEA results strongly support the experimental findings and emphasize the importance of mesh refinement for accurate representation of failure-critical regions.

#### 4.11.6. Analysis of 3D-Printed Structures

The 3D printed structures demonstrated an increase in flexural strength over time, with recorded values of 0.03 at 1 day, 0.16 at 7 days, 0.21 at 14 days, and 0.25 MPa at 28 days as shown in Figure 4.44. The application of aluminium sulphate on the surface of these structures during printing enhanced their buildability by accelerating the setting process. This resulted in higher early age strength compared to conventional methods. However, the flexural strength development eventually aligns with more monolithic structures, indicating that the initial effects of the aluminium sulphate diminish as the curing process continues. Table 4.11 Presents the flexural strength of the 3D-printed structures.

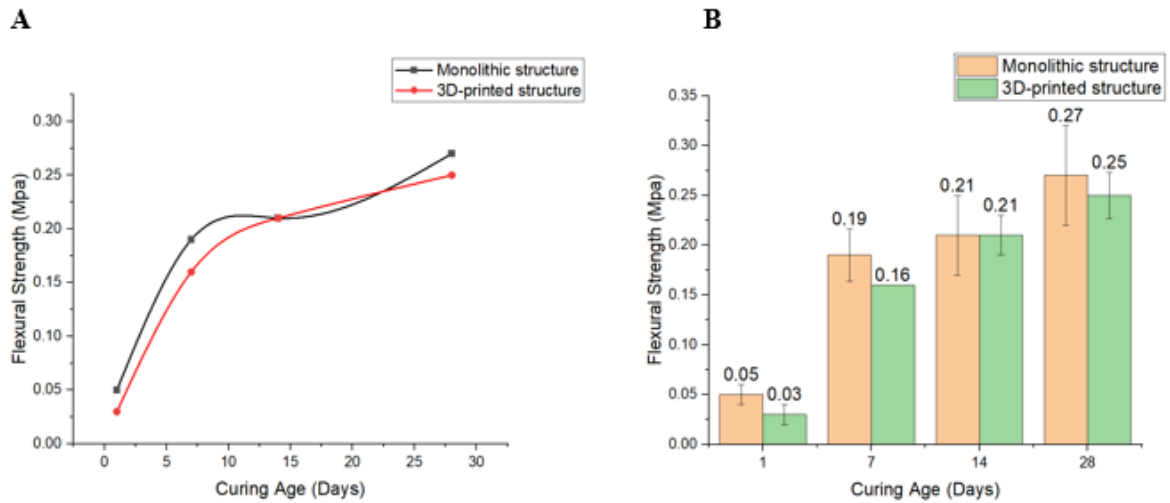


Figure 4.44. Flexural strength of 3D-printed structure versus monolithic structure

Table 4.11. Flexural strength of 3D-printed structure

Day	Load rate (MPa/s)	Load (kN)	Strength (MPa)	Mean strength	Standard deviation
1	200.00	1.34	0.03	0.03	0.01
		1.35	0.03		
		1.35	0.03		
7	200.00	6.23	0.16	0.16	0.00
		6.42	0.16		
		6.45	0.16		
14	200.00	7.89	0.20	0.21	0.02
		9.40	0.24		
		8.64	0.22		
28	200.00	10.45	0.26	0.25	0.02
		8.62	0.22		

---

10.33                      0.26

---

#### 4.11.7. Analysis of Monolithic Structures

Monolithic structures were constructed using a single pour of concrete, ensuring a homogenous material without layers, thus reducing the potential for weak interfaces. The flexural strength of these structures was recorded at 0.05 after 1 day, 0.19 after 7 days, 0.21 after 14 days, and 0.27 MPa after 28 days. Although the early-age strength gain was slower compared to the 3D printed structures, the monolithic structures achieved comparable strengths by 14 and 28 days. This indicates that the continuous curing process of the monolithic structure promotes uniform hydration and strength development. Table 4.12 Presents the flexural strength of the monolithic structures

Table 4.12. Flexural strength of Monolithic structure

Day	Load rate (MPa/s)	Load (kN)	Strength (MPa)	Mean strength	Standard deviation
1	200	2.40	0.06	0.05	0.02
		2.06	0.05		
		1.02	0.03		
7	200	7.55	0.18	0.19	0.01
		8.19	0.19		
		8.19	0.20		
14	200	7.13	0.17	0.21	0.03
		8.19	0.22		
		9.23	0.23		
28	200	8.37	0.21	0.27	0.05
		12.36	0.30		
		11.84	0.29		

#### 4.11.8. Comparative Analysis

The early-age flexural strength of the 3D-printed structures was initially lower than that of the monolithic structures, with a strength of 0.03 MPa compared to 0.05 MPa at 1 day. While aluminium sulphate was used to improve buildability and accelerate setting, its impact on flexural performance was not significant at this stage. However, by 7 days, both systems showed similar strength development, with monolithic structures slightly outperforming the printed ones. This trend continued through to 14 and 28 days, where both types of structures exhibited comparable flexural strength. The findings from this study suggest that, under the tested conditions, the 3D-printed elements demonstrated flexural strength comparable to that of monolithic structures at later ages.

#### 4.11.9. Fracture mode of concrete

This study evaluated the failure mode of 3D-printed and monolithic cement-based structures using a four-point bending test to assess their structural integrity under bending loads. The load was applied at two points along the span while the ends of the specimens were supported. The discussion focuses on the flexural failure process of the specimens at 1 and 28 days as shown in Figure 4.45.

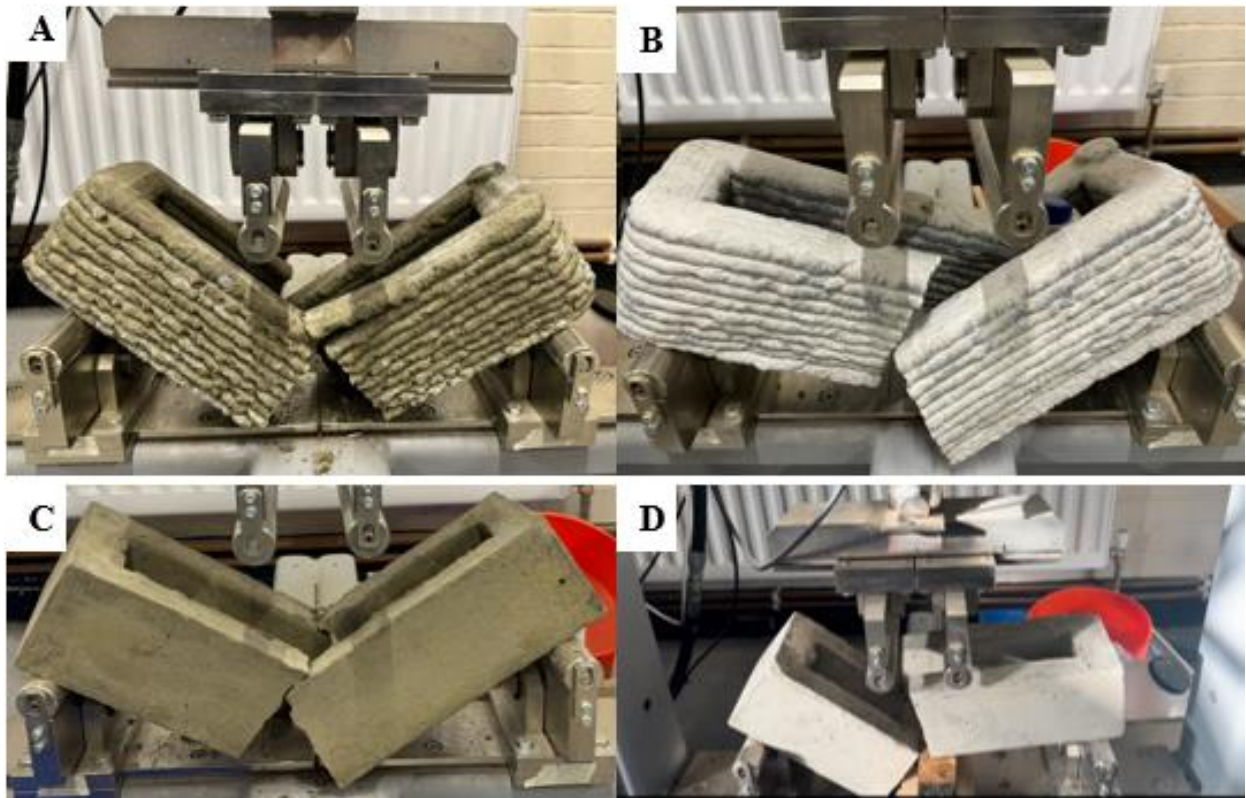


Figure 4.45. Failed structures of (a, b) 3D-printed and (c, d) monolithic structures at 1 and 28 days

The structures tested on days 1 and 28 exhibited brittle failure, characterised by a sudden fracture at the midspan, with the highest tensile stress. The fracture was initiated at the bottom of the specimens, where the tensile stresses were highest due to the bending moment applied during the test. The fracture propagated vertically through the cross-section, completely separating into two parts. As the load increased, the initial micro-cracks at the tensile surface coalesced into a visible crack, rapidly propagating upward through the cross-section of the specimen. This abrupt crack propagation progressed vertically towards the compressive side, leading to a complete fracture at the midspan. The crack paths were relatively straight and perpendicular to the layers, indicating that the failure was driven primarily by the tensile stress concentration at the bottom rather than by any inherent weakness between the 3D-printed layers. This behaviour aligns with the typical behaviour of any cement-based material, which is brittle and fails abruptly when their tensile strength is exceeded. Examination of the fracture surfaces revealed no significant plastic deformation, further confirming the brittle nature of the failure.

The monolithic structure exhibited similar failure mode and progression. Fractures were initiated at the bottom where tensile stress was highest, propagating vertically and causing the structures to split into two parts. The straight, perpendicular crack paths indicate that the failures were driven by tensile stress concentration rather than layer weaknesses, demonstrating comparable mechanical behaviour in both types of structures.

#### 4.11.10. Finite Element Analysis

The analysis of crack propagation in the concrete block under applied load demonstrated a clear pattern of fracture initiation and development as shown in Figure 4.46. Cracks originated at the points of load application, which were the regions of the highest stress concentration. These cracks then propagated upwards toward the support points. This behaviour was consistent with the expected failure mechanisms in concrete, which has high compressive strength but relatively low tensile capacity. The maximum deformation recorded in the simulation is approximately 13.124 mm, located at the mid-span, where the crack initiated.

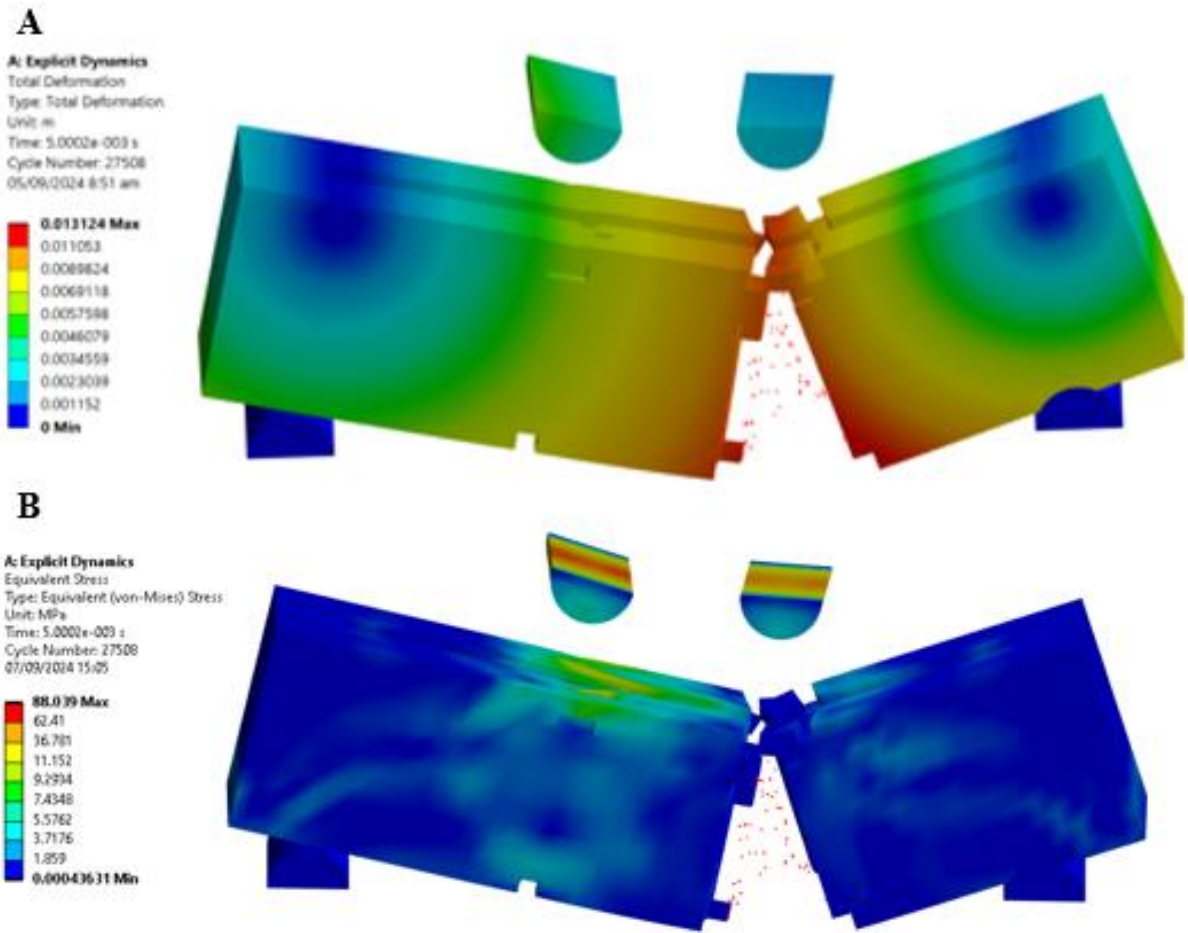
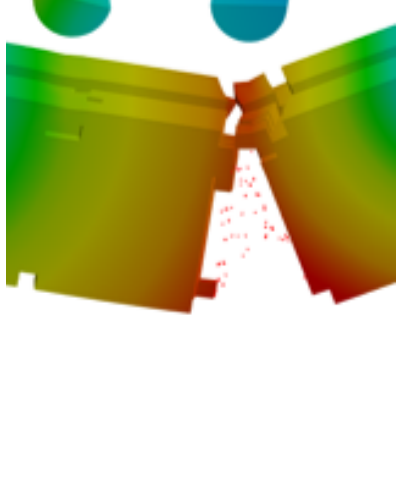
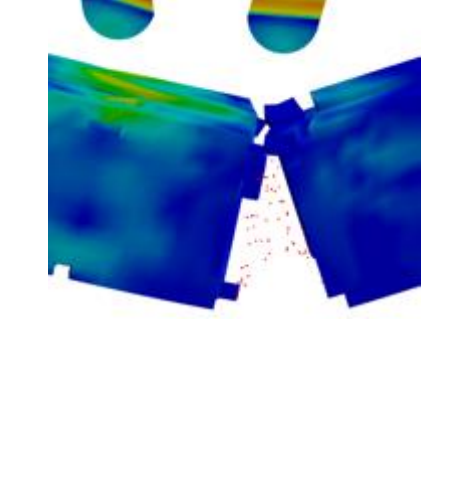


Figure 4.46. Deformation and stress contour of cement block

#### 4.11.11. Failure mode analysis

The failure modes observed in the simulation are consistent with the expected behaviour under a four-point bending scenario. Table 4.13 presents the result of crack propagation and stress distribution using FEA.

Table 4.13. Crack propagation and stress distribution.

<p><b>Crack Propagation:</b> The cracks primarily propagated upwards from the points of load application, leading to the eventual failure of the concrete block.</p>		<p><b>Stress Distribution:</b> The stress distribution indicated higher stress concentrations at the loading points, which correlates with the observed crack initiation.</p>	
--	---	---	---

The analysis of the concrete block under applied loading revealed a fracture pattern characteristic of bending failure in brittle materials such as concrete. Vertical cracks formed at the mid-span, indicating that the structure failed primarily due to tensile rupture induced by flexural action. The absence of diagonal cracks suggested that shear forces were not a dominant factor in the failure process. Crack propagation occurred symmetrically about the mid-span region, implying that the load was evenly distributed and the material exhibited uniform behaviour across its length. The simulation indicated that cracking began early during loading, highlighting the limited tensile resistance of the concrete. As the loading progressed at a controlled rate of 200 N/s, visible deformation increased steadily at the centre of the span until fracture initiated. The observed crack path followed a typical flexural failure mode, aligning closely with the failure patterns seen in both the 3D-printed and monolithic specimens. This consistency between experimental and numerical results confirms the accuracy of the model in predicting the structural response of the specimen under bending. Figure 4.47 illustrates the close agreement in crack formation across the three versions.



Figure 4.47. Failure modes in (a) FEA, (b) 3D-printed and (c) monolithic structures

#### 4.11.12. Effect of layer-by-layer deposition

The impact of layer-by-layer deposition on the failure modes of 3D-printed concrete structures was evident in the mechanical behaviour and fracture patterns observed during testing. The process introduced visible lines that, although not classified as cracks, influenced the stress distribution within the structure. These lines had the potential to initiate cracks, especially in areas where interlayer bonding was weaker than intralayer bonding. Since the 3D-printed structures were built in layers, the bonding between those layers had potential weaknesses as compared to that of the monolithic structure due to the lack of compaction, effect of several printing parameters like print and pump speed, layer height and thickness, nozzle dimensions and shape, inter and intralayer void, amongst many other factors as shown in Figure 4.48 [70, 200, 289]. The weak adhesion between layers may act as fault lines, causing interlayer failure when the structure is subjected to tension or shear forces.

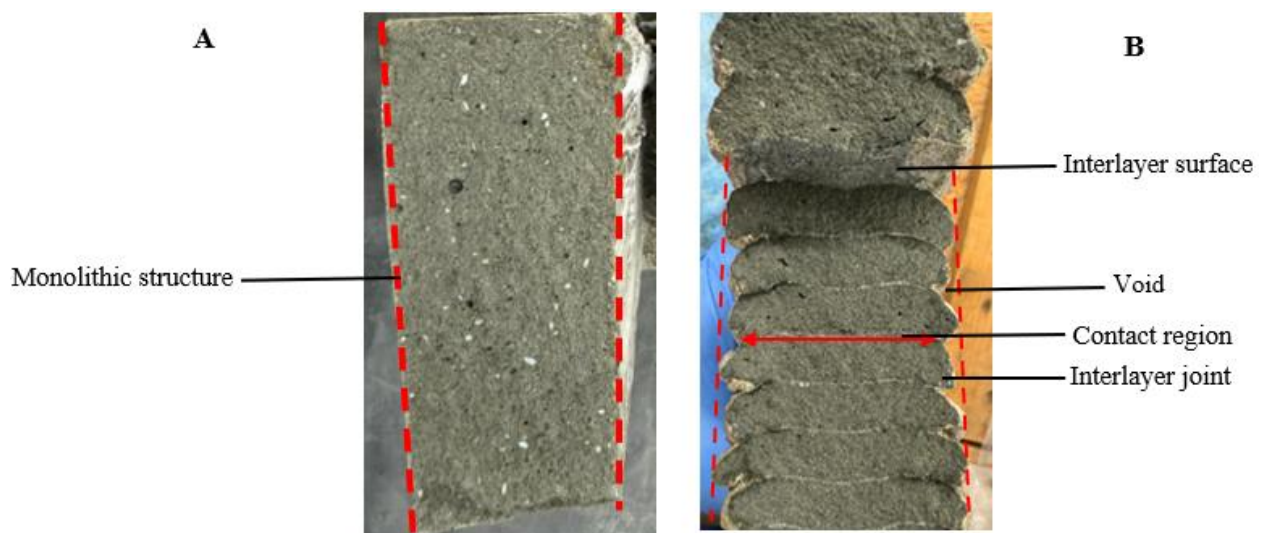


Figure 4.48. cross section of monolithic structure *versus* 3D-printed structure

Microscopic analysis revealed that the layer deposition process introduced porosity and voids at the interlayer joint, as shown in Figure 4.49. These voids acted as stress concentrators, initiating cracks under both compressive and tensile loads. Specimens with higher porosity exhibited more brittle failure modes, where cracks propagated quickly through the void-rich regions, leading to sudden catastrophic failure.

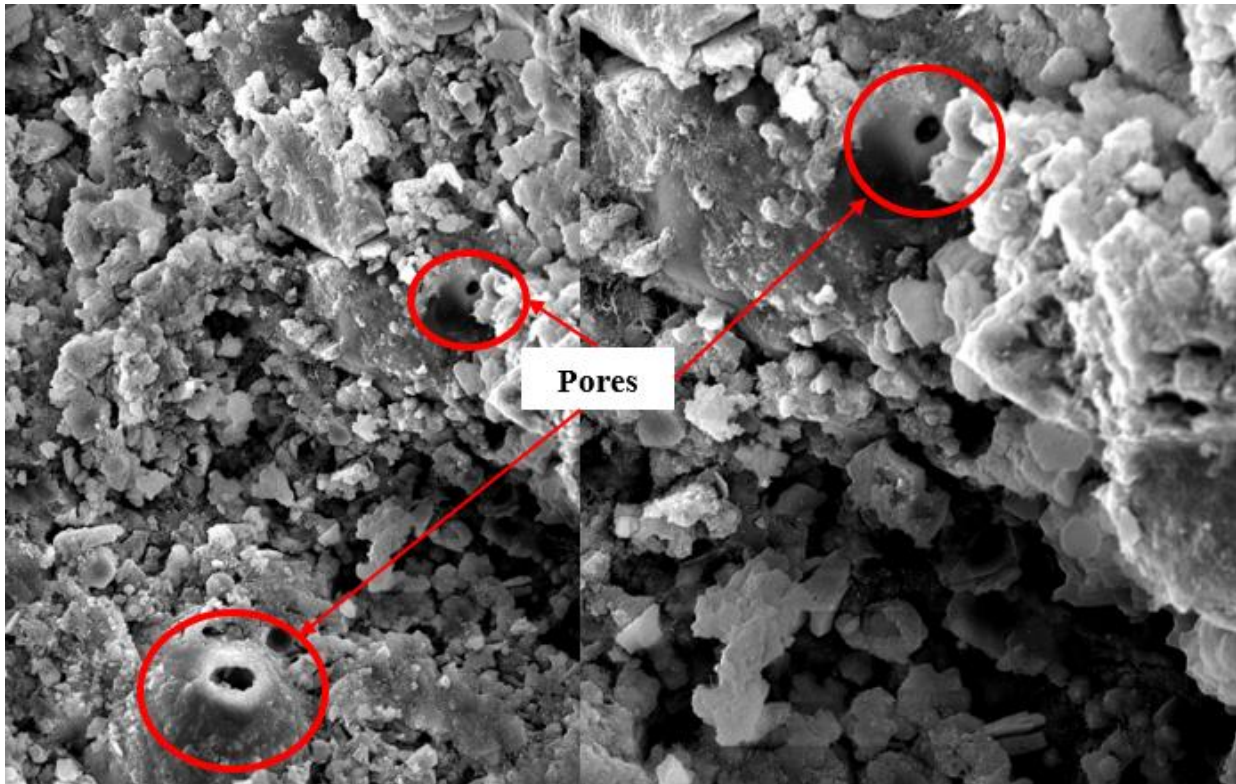


Figure 4.49. Microscopic analysis showing void

#### **4.12.Split tensile test**

This section examined how different concentrations of aluminium sulphate influenced the interlayer bonding performance of 3D-printed samples. Over a 28-day period, tensile strength development was observed, with graphical results displayed in Figure 4.50 showing the effects of various accelerator dosages.

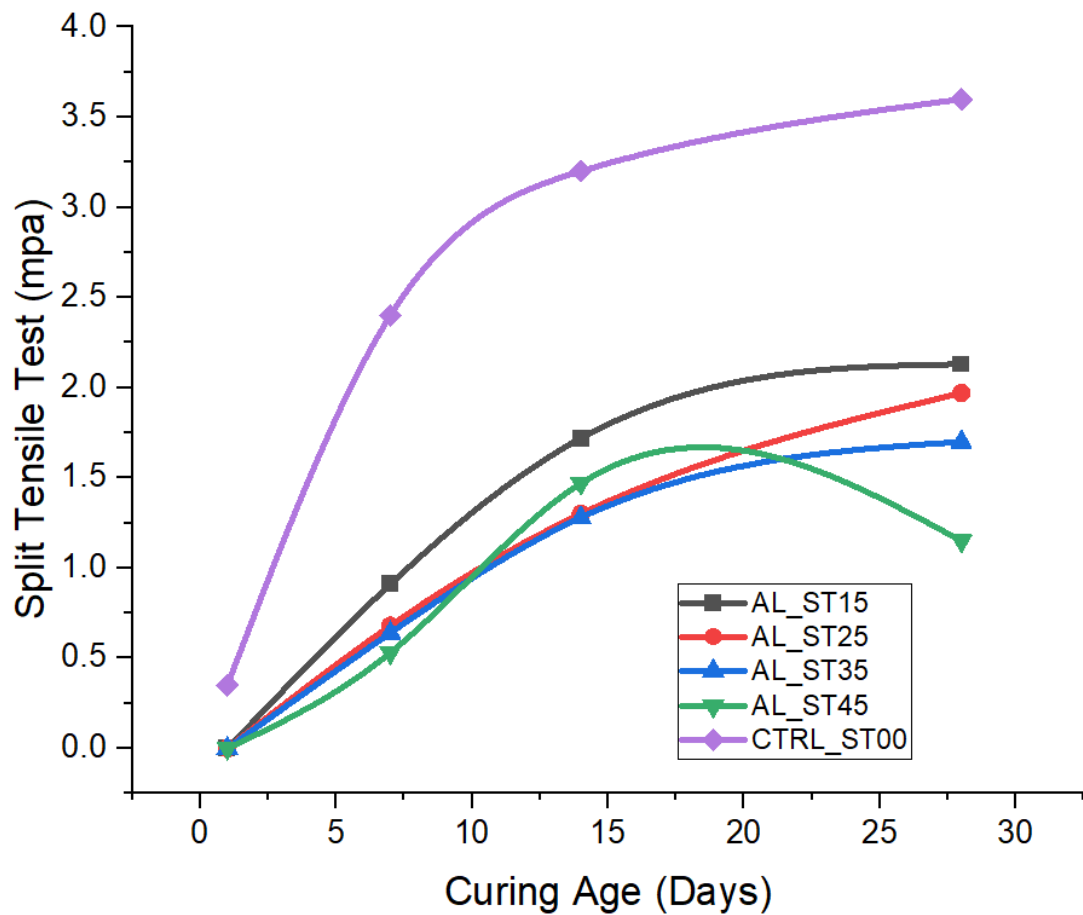


Figure 4.50. Split tensile strength of cement-based material with varying accelerator concentration

#### 4.12.1. Analysis of Split Tensile Strength Results for CTRL\_ST00

At day 1, the split tensile strength of the CTRL\_ST00 was relatively low at 0.35 MPa. This low initial strength was expected, given the early stage of the curing process. The cement matrix had not fully developed, and the bond between layers was still weak. This highlighted the initial weakness of 3D-printed structures, an important consideration for early-age performance. By day 7, the split tensile strength had increased significantly to 2.27 MPa, indicating substantial progress in the hydration process and the development of the cementitious matrix, leading to improved interlayer bonding. The 7 day mark often represented a critical phase in cement curing where substantial strength development occurred, and the results reflected this trend. At day 14, the split tensile strength further increased to 3.2 MPa. This continued improvement suggested that the 3D-printed structures benefited from ongoing hydration and curing. The

cement matrix became more cohesive, and the layers bonded more effectively. By 28 days, the split tensile strength reached 3.65 MPa, indicating that the material had achieved near-maximum strength. The final strength demonstrated that 3D-printed structures could achieve high levels of tensile strength.

#### 4.12.2. Comparative analysis of control sample *versus* accelerated samples

On Day 1, all of the accelerated samples, AL\_ST15, AL\_ST25, AL\_ST35, and AL\_ST45 exhibited 0 tensile strength, while the CTRL\_ST00 sample demonstrated a tensile strength of 0.34 MPa. This showed that the presence of the accelerator initially hindered the development of the interlayer bond strength, likely due to insufficient curing time for the chemical effects of the accelerator to take effect. This delay could be attributed to the accelerator hindering the natural hydration process, resulting in an incomplete or weak bond structure in the early stages. The control sample, in contrast, benefitted from natural hydration, which allowed for the gradual and consistent development of interlayer bonds. By Day 7, the control sample exhibited a significant increase in tensile strength, reaching 2.40 MPa. In comparison, the accelerated samples showed substantially lower tensile strengths, with AL\_ST15 at 0.91 MPa, AL\_ST25 at 0.68 MPa, AL\_ST35 at 0.64 MPa, and AL\_ST45 at 0.53 MPa. The trend observed here indicates an inverse relationship between the concentration of the accelerator and tensile strength: as the dosage increased, the strength decreased. This relationship suggests that higher concentrations introduced early-stage weaknesses, possibly due to the rapid and uneven bond formation that might have created brittle interlayer structures. Accelerated curing at higher concentrations could lead to premature hydration, resulting in microcracks or discontinuities that can weaken the interlayer bond. On Day 14, the control sample continued to outperform the accelerated samples, reaching a tensile strength of 3.2 MPa. Although the accelerated samples showed improvements compared to Day 7, they still lagged behind the control sample. AL\_ST15 achieved a tensile strength of 1.72 MPa, AL\_ST25 reached 1.3 MPa, AL\_ST35 was at 1.28 MPa, and AL\_ST45 reached 1.47 MPa. This pattern indicates that, while the strength of the accelerated samples had improved, it did not match the consistent bond development seen in the control sample. Additionally, the varying strengths among the accelerated samples indicate that the influence of the accelerator on curing and bond formation was complex, with non-linear interactions depending on dosage and distribution, possibly due to uneven spraying of the accelerator during application. By Day 28, the final tensile strength results highlighted

the long-term effects of using accelerators at different dosages. The CTRL\_ST00 achieved the highest strength at 3.65 MPa, indicating effective natural curing and strong interlayer bond development. The accelerated samples, however, continued to show lower strengths, with AL\_ST15 achieving 2.13 MPa, AL\_ST25 at 1.97 MPa, AL\_ST35 at 1.70 MPa, and AL\_ST45 at 1.15 MPa. The decrease in tensile strength with increasing accelerator dosage was significant, suggesting that the accelerators introduced persistent weaknesses that limited the development of strong interlayer bonds over time. Higher concentrations of the accelerator likely induced rapid early-stage hydration, which could have caused localised cold joints and disrupted the formation of a stable and uniform bond structure. Tables 4.14 – 4.18 presents the results of the split tensile test varying the accelerator dosage.

Table 4.14. Split tensile test of CTRL\_00

Day	Load rate (MPa/s)	Load (kN)	Strength (MPa)	Mean strength	Standard deviation
1	0.1	0.66	0.33	0.35	0.03
		0.76	0.38		
		0.71	0.35		
7	0.1	3.85	1.93	2.4	0.40
		5.31	2.66		
		5.16	2.58		
14	0.1	4.16	3.00	3.19	0.22
		6.27	3.14		
		6.89	3.44		
28	0.1	9.18	4.59	3.6	0.97
		7.37	3.69		
		5.31	2.66		

Table 4.15. Split tensile test of AL\_ST15

AL_ST15	Load rate (MPa)	Load (kN)	Strength (MPa)	Mean	Standard deviation
Day 1	0.1	0.00	0	0	0

Day 7	0.1	1.29	0.64	0.91	0.28
		2.43	1.20		
		1.83	0.91		
Day 14	0.1	2.61	1.31	1.72	0.37
		3.61	1.81		
		4.09	2.04		
Day 28	0.1	3.89	1.95	2.13	0.32
		3.87	1.94		
		5.00	2.50		

Table 4.16. Split tensile test of AL\_ST25

AL_ST25	Load rate (MPa)	Load (kN)	Strength (MPa)	Mean	Standard deviation
Day 1	0.1	0	0	0	0
Day 7	0.1	0.98	0.49	0.68	0.58
		2.68	1.34		
		0.46	0.23		
Day 14	0.1	2.59	1.29	1.3	0.20
		2.20	1.10		
		3.00	1.50		
Day 28	0.1	3.43	1.71	1.97	0.26
		4.44	2.22		
		3.99	2.00		

Table 4.17. Split tensile test of AL\_ST35

AL_ST35	Load rate (MPa)	Load (kN)	Strength (MPa)	Mean	Standard deviation
Day 1	0.1	0	0	0	0

Day 7	0.1	1.84	0.92	0.64	0.24
		1.05	0.52		
		0.97	0.48		
Day 14	0.1	2.74	1.37	1.28	0.65
		1.18	0.59		
		3.76	1.88		
Day 28	0.1	3.29	1.64	1.70	0.50
		4.48	2.24		
		2.48	1.24		

Table 4.18. Split tensile test of AL\_ST45

AL_ST45	Load rate (MPa)	Load (kN)	Strength (MPa)	Mean	Standard deviation
Day 1	0.1	0	0	0	0
Day 7	0.1	1.331	0.67	0.53	0.18
		1.187	0.59		
		0.647	0.32		
Day 14	0.1	3.235	1.62	1.47	0.17
		3.023	1.51		
		2.552	1.28		
Day 28	0.1	3.045	1.52	1.15	0.35
		1.689	0.84		
		2.173	1.09		

#### 4.12.3. Effect of aluminium sulphate on the interlayer bond strength

The integrity and durability of cement-based structures, particularly in 3D-printed applications, are highly dependent on the strength of the bonds formed between successive layers. Weaknesses in interlayer bond strength can significantly compromise the overall structural strength, leading to reduced tensile strength, increased susceptibility to cracking, and potential

failure under load [169, 170]. This section focused on identifying and understanding the factors that contributed to interlayer bond weakness, with a particular emphasis on the role of cold joints and the impact of the chemical accelerator used (aluminium sulphate) [43, 290] Figure 4.51 shows the split tensile test results of the cement-based samples. The CTRL\_ST00 samples, as compared to AL\_ST45, as they provided optimum buildability. The red circles highlight the presence of ettringite formation between the interlayers in the fractured zones, which becomes more visible as the accelerator dosage increases. The CTRL\_ST00 samples exhibit less visible ettringite formation.

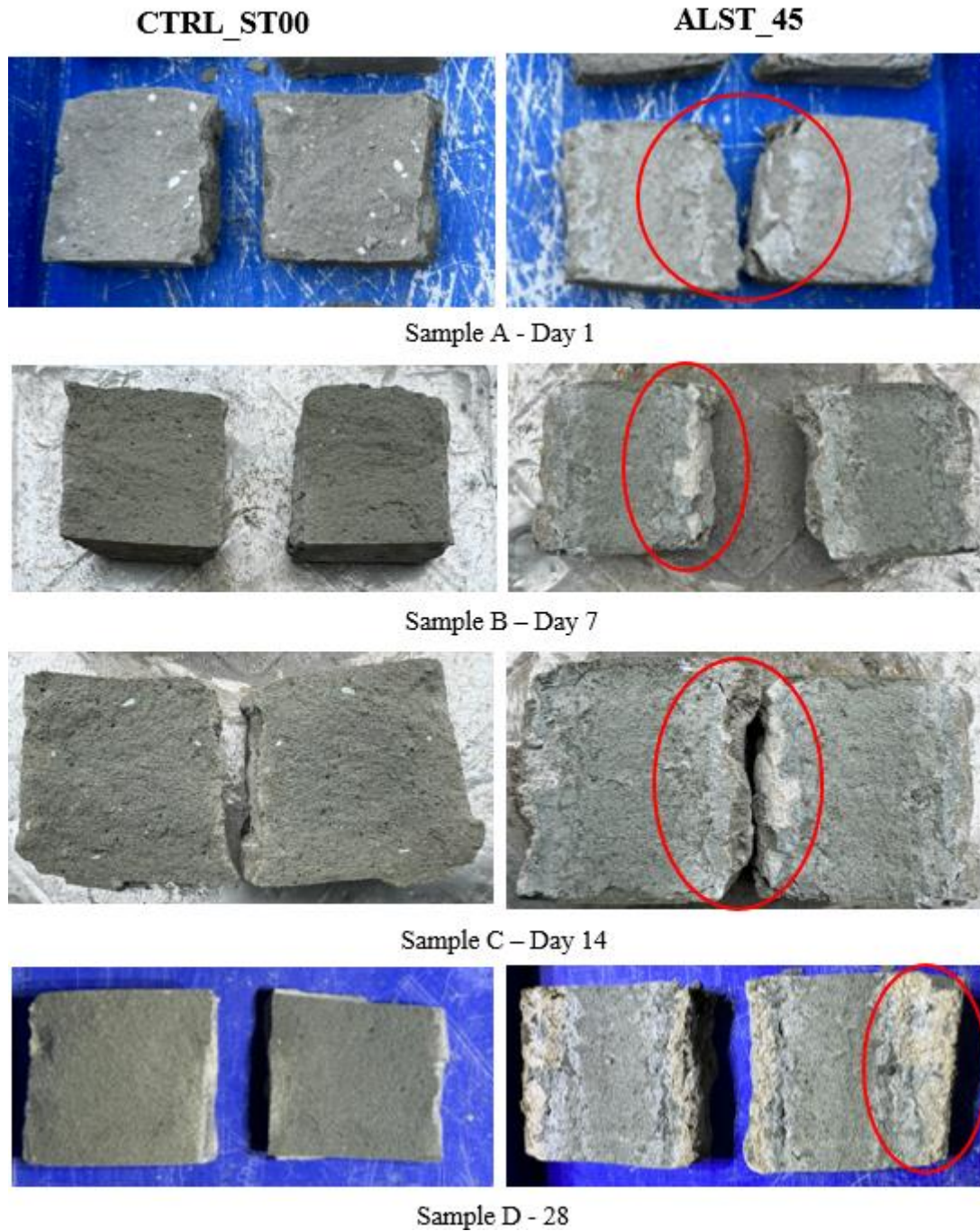


Figure 4.51. Split tensile failure of concrete with varying accelerator dosages

In the initial stages (Day 1), a whitish substance began to appear in between the split layers where aluminium sulphate was sprayed but is barely visible in Sample A, indicating that the formation of ettringite is still in its early stage. The reaction between sulphate ions from the aluminium sulphate and calcium aluminates in the cement paste initially forms needle-like

ettringite crystals. Because these crystals are small and not well developed, they do not create a noticeable expansion or disruption at the interface.

By Day 7 (Sample B), the whitish substance is more prominent, suggesting that ettringite crystals have grown larger and are beginning to exert pressure on the surrounding matrix. This is a crucial point where internal stresses start to develop at the interface, weakening of the interlayer bond. The increase in the visibility of the whitish substance is an indication of increased ettringite content, which reflects the ongoing sulphate attack.

By Day 14 (Sample C), the ettringite formation had increased, causing a more pronounced expansion at the interface. The whitish material is more apparent. This points to the accumulation of ettringite and possibly gypsum, which form under the influence of excessive sulphate ions. The expansive pressure generated by these crystallisations increases the stress concentration within the already weak interfacial transition zone (ITZ), resulting in larger and more visible cracks [291].

By Day 28 (Sample D), the whitish substance has become highly prominent and concentrated around the interlayer region. This marks the culmination of sustained sulphate reactions, where ettringite crystals have completely filled the available pore spaces and microcracks at the interface. The transformation of the initially formed ettringite into secondary phases, such as mono-sulphate or gypsum, can increase the structural instability, leading to complete detachment or spalling of layers. This explains why the interlayer bond strength decreases with increased aluminium sulphate concentration. The progressive increase in the visibility of the whitish substance is an indication of the long-term effects of excessive sulphate. This effect highlights the detrimental impact of using aluminium sulphate without proper control, as it accelerates the formation of expansive products, undermines the mechanical integrity of interlayer bonds, and promotes premature cracking and failure of the concrete structure. Thus, while aluminium sulphate might initially aid in setting and adhesion, its long-term consequences are deleterious, leading to loss of strength and durability due to excessive sulphate attack.

Figures 4.52 (a-d) show the microstructure of the 3D-printed structures on 1, 7, 14 and 28 days, respectively.

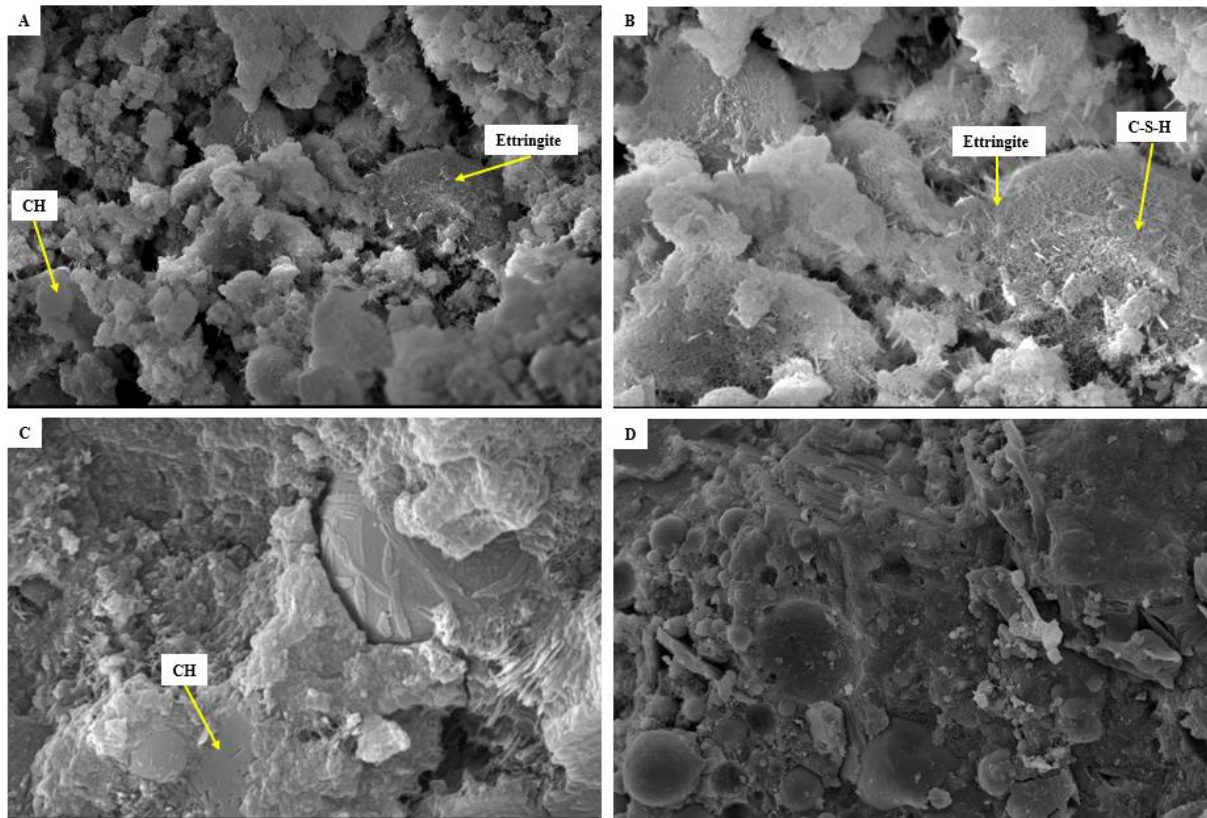


Figure 4.52. Microstructure of 3D-printed structure

#### 4.12.4. Reaction between water and cement

When Portland cement is mixed with water, the calcium sulphate and high-temperature calcium compounds begin to dissolve, causing the liquid phase to quickly become saturated with various ions, including calcium, sulphate, aluminate, and hydroxyl ions [291, 292]. This leads to the formation of needle-shaped crystals of calcium trisulfoaluminate hydrate, known as ettringite, within the first few minutes of hydration. As the process continues over the next few hours, larger prismatic crystals of calcium hydroxide and very small fibrous crystals of calcium silicate hydrates (C-S-H) begin to form, filling the spaces previously occupied by water and the dissolving cement particles. Depending on the alumina-to-sulphate ratio in the cement, high concentrations of sulphate can trigger a series of secondary reactions that result in the transformation of stable hydration products into less stable and more soluble phases. For instance, mono-sulphate, a hydration product that is typically stable in sulphate-free environments, can react with excess sulphate to form additional ettringite. This secondary ettringite formation leads to further expansion and cracking, perpetuating a cycle of

degradation that gradually weakens the structure. Figure 4.53 shows the micor-structure of a 3D-printed material.

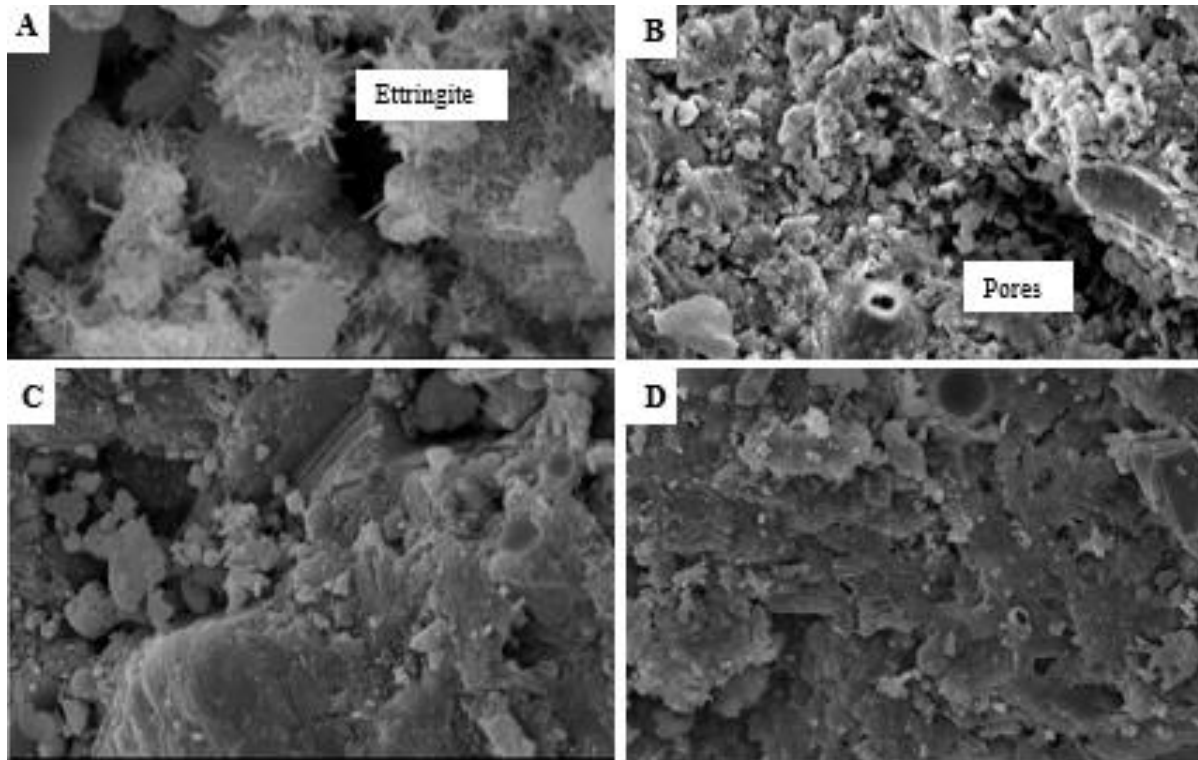


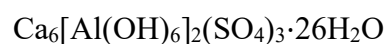
Figure 4.53. Micro-structure of 3D-printed material, (a)1 day, (b)7 days, (c)14 days, d) 28 days

#### 4.12.5. Reaction between aluminium sulphate and cement

When aluminium sulphate is sprayed onto the surface of cement, it provides sulphate ions that react with the aluminate phases, particularly tricalcium aluminate ( $C_3A$ ), leading to the formation of ettringite. The general chemical reaction for the formation of ettringite in the presence of sulphate ions and calcium aluminates in cement is:



Or



Or



Where;

C stands for CaO (calcium oxide)

A stands for Al<sub>2</sub>O<sub>3</sub> (alumina)

S̄ stands for SO<sub>3</sub> (sulphate)

H stands for H<sub>2</sub>O (water)

Ettringite is a needle-like crystalline structure that forms early in the hydration process and can be beneficial in moderate amounts, contributing to initial strength. However, excessive aluminium sulphate causes rapid and excessive ettringite formation, generating internal stresses within the cement matrix and causing external sulphate attack, leading to cold joints, as shown in Figure 4.54. The term external sulphate attack means a deterioration process that affects cement-based materials and other cementitious materials when they are exposed to sulphate ions from external sources. Cold joint occurs when the deposited layer cures due to the reaction before the next layer is deposited. This resulted in a weak bond between the layers, creating a potential plane of weakness.

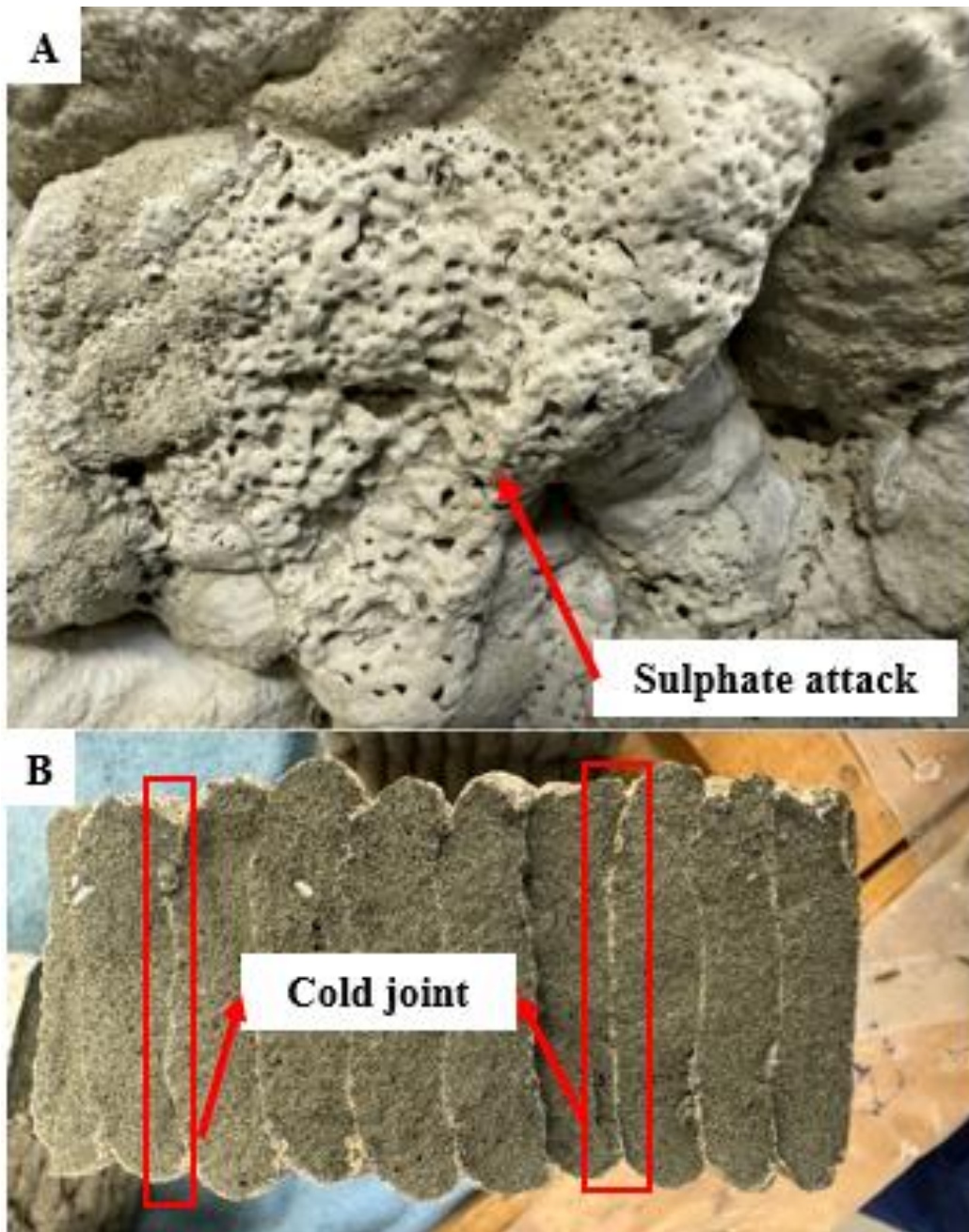


Figure 4.54. Cold joints and sulphate attach on3D-printed structure

As mentioned earlier, these internal stresses can lead to micro-cracks, weakening the tensile strength. The disruption of the cement matrix by excessive ettringite also creates irregularities, reducing the overall cohesion and tensile strength of the material. High concentrations of aluminium sulphate can cause rapid surface hardening. This leads to a strong outer layer but negatively affects tensile strength due to uneven hydration. This rapid curing can isolate the internal structure, resulting in incomplete hydration, which weakens the internal structure of the material. The hydration products formed under high sulphate concentrations may also bond

weakly, compromising the microstructure and reducing the ability of the material to withstand tensile forces. Aluminium sulphate at high concentrations also makes the cement matrix prone to micro-cracking and higher porosity. Excessive ettringite formation and rapid surface hydration contribute to more micro-voids, which act as stress points under tensile loading, leading to premature failure. The overall effect is reduced tensile strength, making the material more brittle and prone to failure.

If the sulphate concentration continues to increase, another phase known as gypsum can form. Gypsum formation is more detrimental than ettringite formation because it leads to a further expansion and an even more severe weakening of the concrete matrix. The presence of gypsum reduces the cohesion between hydrated cement phases, which results in a loss of strength and a softening of the matrix. Gypsum has a relatively low strength and higher solubility compared to other hydration products, making it a critical factor in the long-term deterioration of concrete exposed to excessive sulphates. Consequently, the cement-based material becomes more permeable and susceptible to other forms of chemical and physical attack, such as freeze-thaw cycles and chloride penetration.

The CNTR\_ST00 structures exhibited higher tensile strength due to balanced hydration. This allowed for the development of a strong, cohesive microstructure with controlled ettringite formation. Structures treated with aluminium sulphate showed a decrease in tensile strength as concentration increased, indicating that while aluminium sulphate accelerates hydration, it compromises tensile properties, especially at high concentrations. The interfacial zone (ITZ) between 2 layers in the 3D-printed structure is inherently weaker than a monolithic structure due to differences in hydration and microstructure continuity. The presence of aluminium sulphate can either mitigate or exacerbate these weaknesses depending on its impact on the microstructure. In particular, a well-controlled dosage may refine the microstructure by promoting the formation of fine, needle-like ettringite crystals that interlock effectively across the interface. Conversely, excessive use can disrupt the microstructural continuity, leading to larger voids and weakened contact surfaces.

Overall, the use of aluminium sulphate in the 3D printing of cement layers can have both positive and negative effects on interlayer bond strength. Its effectiveness largely depends on the balance between accelerating early strength development and avoiding excessive expansion that could cause internal cracking.

### 4.13. Summary

This chapter provided an in-depth analysis of the critical factors affecting the buildability, and mechanical performance of 3D-printed cement-based structures. Through extensive experimentation and engineering analysis, the research emphasised how key variables such as printing speed, layer height, and aluminium sulphate concentration influenced the quality and strength of 3D-printed structures.

The investigation revealed that printing speed was pivotal for achieving stable, well-bonded layers, with 20 mm/s identified as the optimal speed. At this rate, material deposition and setting time were balanced, leading to improved interlayer bonding and enabling the structure to maintain stability over multiple layers. Lower speeds, such as 10 mm/s led to excessive material deposition, resulting in nozzle clogging and poor surface finishes, while higher speeds of 80 mm/s compromised interlayer bonding due to insufficient settling time, causing weak adhesion and early collapse. Calculations using flow rate and buckling formulas highlighted the importance of matching material flow with printing speed, indicating that stability was best achieved when material flow, bonding strength, and deposition rates were in sync.

Layer height also significantly affected structural integrity. Smaller layer heights, such as 10 mm, facilitated greater interlayer contact, resulting in stronger adhesion and better stress distribution across layers, allowing structures to support more layers before failure. In contrast, larger layer heights reduced contact and bonding strength, inducing stress concentrations that led to premature structural failure. The findings from the study demonstrated that optimising layer height was crucial for minimising weak points within the structure and achieving better interlayer bond.

The role of aluminium sulphate used as an accelerator was also evaluated, showing that increased concentrations enhanced buildability by accelerating the setting process and adding stiffness to each layer. Higher concentrations, such as 45%, allowed for taller structures by supporting up to 14 stable layers with minimised height reduction under load. However, excessive sulphate led to cold joints and microcracks at interlayer zones due to rapid ettringite formation, which increased brittleness and reduced long-term tensile strength. These observations revealed that while aluminium sulphate aided in early structural stability, its concentration had to be carefully controlled to prevent long-term degradation from excessive sulphate attack.

Mechanical tests on 3D-printed and monolithic structures over a 28-day curing period revealed that monolithic structures attained higher compressive and flexural strengths due to their uniform material distribution and continuous curing process. Although aluminium sulphate enhanced early-age flexural strength in 3D-printed samples, both 3D-printed and monolithic structures exhibited comparable strength by the end of the curing period. This finding underscored the need for consistent curing and interlayer bonding to achieve durable 3D-printed structures.

## **Chapter 7: Conclusion and Recommendations**

---

# CHAPTER FIVE

## Conclusions

### 5. Introduction

This concluding chapter provides a general and detailed summary of the research conducted, aligned with the aims and objectives of this work.

#### 5.1. Process optimisation

- The research tackled the persistent issue of backpressure caused by the auger mixing mechanism, which led to material blockages. A major advancement was achieved through the removal of the auger and propeller mixers, which were replaced with a peristaltic pump and a uniquely angled 3 mm accelerator inlet. This design provided more precise control over the accelerator injection, eliminating backpressure and improving the consistency of material mixing a crucial step for ensuring homogeneity in printed cementitious materials.
- Additionally, the transition from manual to automated accelerator application represented another key advancement. Initially, the accelerator was applied manually between each printed layer, allowing greater control over setting times and ensuring the early strength of each layer. Building upon this manual approach, an automated application system was later developed, featuring a micro-nozzle attached to the extrusion head, which ensured consistent application without the need for human intervention. This automation contributed significantly to the structural integrity and buildability of the printed layers, enhancing the overall efficiency and reliability of the process.
- In terms of structural stability, the study addressed stress concentrations and layer deformations arising from inconsistent movement speeds along the x- and y-axes. By adjusting the robotic programming from OVRD to SPD mode, a uniform speed was maintained across all axes, which significantly reduced stress concentrations at layer intersections. This improvement highlighted the importance of precise movement

control in multi-axis 3D printing to minimise deformation and ensure structural integrity.

## **5.2. Effect of printing speed on buildability of 3D-printed small-scale structures**

The main findings of this investigation into the effect of printing speed on the buildability of small-scale 3D-printed concrete structures revealed distinct performance variations across different speeds. The following conclusions can be summarised:

- Sample B1, printed at a slow speed of 10 mm/s, demonstrated poor buildability with a layer thickness of 70 mm. This slower speed resulted in excessive material deposition, leading to localised buckling, nozzle blockage, and an undesirable surface finish. The accumulation of material caused clogging after only two layers, making this speed the least effective for maintaining structural stability and quality.
- Sample B2, printed at an optimised speed of 20 mm/s, achieved the best buildability with a layer thickness of 40 mm and supported up to 10 stable layers before failure. This speed facilitated a balanced interaction between deposition and setting time, ensuring strong inter-layer bonding and structural integrity. Consequently, this speed proved to be the most effective for achieving high buildability in the tested conditions.
- Sample B3, printed at 40 mm/s, produced 7 layers with a thinner layer thickness of 20 mm, although early deformation and reduced adhesion between layers were noticeable. The increased speed limited the material's settling time, reducing the overall buildability compared to Sample B2. Thus, while moderately effective, this speed did not support optimal inter-layer bonding.
- Sample B4, printed at the highest speed of 80 mm/s, achieved only five layers with a very thin layer thickness of 13 mm. This rapid speed did not allow sufficient time for the material to settle, resulting in major inconsistencies and poor inter-layer bonding, leading to early structural collapse.

### 5.3. Effect of layer height on 3D-printed small-scale structures

The investigation into the effect of layer height on the buildability of small-scale 3D-printed structures revealed significant performance differences across various layer heights, primarily due to the relationship between layer height, interlayer adhesion, and structural stability. The following conclusions can be summarised:

- Sample C1, with a layer height of 10 mm, exhibited the highest buildability, achieving ten layers before structural failure. This smaller layer height facilitated proper interlayer adhesion, contributing to the structural stability of the printed layers. A layer thickness of 40 mm indicated that the reduced height allowed for better material cohesion and stronger layer bonding, thus enhancing the overall buildability of the structure.
- Sample C2, printed with a layer height of 15 mm, managed to produce seven layers before experiencing structural failure. Although this increased height allowed for adequate interlayer adhesion, it was less effective than the smaller layer height of Sample C1. With a layer thickness of 30 mm, this height began to compromise material adhesion, resulting in a reduction in buildability due to weaker interlayer bonding.
- Sample C3, with a layer height of 20 mm and a layer thickness of 28 mm, printed only four layers before failure. The larger layer height contributed to insufficient interlayer adhesion, leading to a reduction in bond strength between layers. This occurred due to the decreased interfacial contact area and an increased likelihood of cold joints, which weakened structural integrity and heightened the risk of delamination and cracking.
- Sample C4, printed with a layer height of 25 mm, supported only three layers before structural failure occurred. This substantial layer height led to a nozzle distance too far from the previously deposited layer, resulting in uncontrolled extrusion and significant buildability challenges. A layer thickness of 20 mm reflected the excessive distance between nozzle and layer, causing weak interlayer bonding and inadequate structural support, leading to rapid structural failure.

Significantly, a layer height of 10 mm was found to be optimal, facilitating adequate interlayer bonding and allowing for the printing of ten layers before structural collapse. This finding

aligns with similar studies [5, 15], which established that smaller layer heights enhance material cohesion and layer bonding, thereby improving overall buildability and structural stability.

#### **5.4. Effect of aluminium sulphate on buildability of 3D-printed structures**

The experimental results demonstrated a clear positive correlation between aluminium sulphate concentration and the buildability of 3D-printed structures, with underlying mechanisms providing insights into this enhanced performance.

Both the CTRL\_ST00 and AL\_ST15 samples achieved 10 layers before structural failure. At these low concentrations, the accelerator was insufficient to promote rapid setting and early-age strength, limiting the structural support needed for successive layers. This baseline performance highlighted the limited buildability achievable without the reinforcing effects of higher aluminium sulphate levels.

Sample AL\_ST25 supported 11 layers before failure, showing slight improvement. This enhancement became more pronounced in AL\_ST35, achieving 13 layers. At these concentrations, aluminium sulphate effectively accelerated the setting process, allowing the lower layers to solidify more quickly and enhancing their load-bearing capacity. This gradual improvement increased buildability due to better initial layer bonding and reduced material deformation under the weight of additional layers.

Sample AL\_ST45 achieved the best results, supporting 14 layers without any compression before structural failure. The higher concentration provided rapid early-stage strength development, which prevented the lower layers from compressing under the weight of subsequent layers. This result is consistent with the effect of aluminium sulphate in accelerating the formation of ettringite, which enhances the stiffness and strength of cement-based materials.

The reduction in layer height before failure highlighted the effect of aluminium sulphate concentration on structural stability. The CTRL\_ST00 sample showed an 8% height reduction due to insufficient rigidity, while Samples AL\_ST15 and AL\_ST25 showed a reduced height compression of 6%, indicating moderate stiffness improvement. Sample AL\_ST35 had minimal height reduction at 2%, and Sample AL\_ST15 exhibited no compression, implying

that higher accelerator concentrations sufficiently reinforced the material's resistance to compaction.

## 5.5. Mechanical properties of 3D-printed structures

The experiment demonstrated a significant contrast in compressive strength development between 3D-printed and monolithic structures over the curing period.

### 5.5.1. Compressive strength

**3D-Printed Structures:** The compressive strength of the 3D-printed structures increased steadily, reaching 22 MPa at 28 days. This gradual improvement reflected the curing effect, where interlayer adhesion and material cohesion developed over time. The initial low strength (2 MPa on day 1) suggested that the 3D printing process introduced porosity and weaker layer interfaces, which restricted ultimate compressive strength. Even with curing, the final strength remained lower than that of the monolithic structures, indicating inherent limitations in the 3D printing process for achieving high structural integrity.

**Monolithic Structures:** The monolithic structures exhibited superior compressive strength at all curing stages, reaching 39.4 MPa at 28 days. This higher performance was attributed to the uniform material distribution and the absence of layer interfaces, which reduced potential stress concentrators and allowed for better load-bearing capacity. The continuous cement matrix in these structures enabled enhanced internal cohesion, leading to a more robust and consistent strength profile over time.

### 5.5.2. Flexural strength

The experiment demonstrated a notable progression in flexural strength for both 3D-printed and monolithic structures over a 28-day curing period, with distinct differences in their early-age strength development.

**3D-Printed Structures:** The flexural strength of the 3D-printed structures increased from 0.14 MPa on day 1 to 0.25 MPa at 28 days, as shown in Figure 7.17. The use of aluminium sulphate

on the surface enhanced early-age buildability, contributing to a higher initial flexural strength compared to conventional methods. This early strength gain indicated that the accelerator successfully facilitated rapid setting. However, as curing continued, the flexural strength of the 3D-printed structures began to align more closely with that of the monolithic structures, suggesting that the benefits of the aluminium sulphate diminished over time.

**Monolithic Structures:** Constructed as a single, homogeneous pour, the monolithic structures exhibited a slower initial flexural strength gain, starting at 0.04 MPa after 1 day and reaching 0.27 MPa by day 28. The absence of layers in the monolithic structures reduced the likelihood of weak interfaces, allowing for more uniform hydration and consistent strength development. By 14 and 28 days, the flexural strengths of both 3D-printed and monolithic structures were nearly comparable, indicating that the continuous curing process allowed the monolithic structures to achieve similar strength levels without the need for an accelerator.

### 5.5.3. Split tensile test

The results demonstrated a clear progression in split tensile strength for the control sample (CTRL\_ST00) over the 28-day curing period, with distinct effects observed in samples treated with varying accelerator dosages

**Control Sample (CTRL\_ST00):** The split tensile strength of the control sample increased consistently from 0.35 MPa on Day 1 to 3.65 MPa by Day 28. This gradual increase reflected the natural hydration and cohesive bond formation in the cement matrix, which facilitated steady strength development over time. The 7-day strength of 2.27 MPa marked a critical phase in the curing process, where substantial strength gains were evident due to enhanced interlayer bonding. By Day 28, the control sample demonstrated near-maximum tensile strength, indicating that natural curing enabled robust interlayer cohesion without premature setting effects.

**Accelerated Samples (AL\_ST15, AL\_ST25, AL\_ST35, AL\_ST45):** The addition of aluminium sulphate accelerators initially hindered the tensile strength of the 3D-printed samples. All accelerated samples displayed 0 tensile strength on Day 1, indicating that the accelerator delayed effective bond development at early stages. By Day 7, the tensile strength of the accelerated samples improved but remained significantly lower than the control, with an inverse relationship observed between accelerator concentration and tensile strength. For

example, AL\_ST15 reached 0.91 MPa, while AL\_ST45 was only 0.53 MPa. This trend suggested that higher concentrations of accelerator induced rapid, uneven hydration, which reduced the interlayer bonds.

**Long-Term Performance:** By Day 28, the control sample maintained superior tensile strength (3.65 MPa) compared to the accelerated samples, which ranged from 1.15 MPa (AL\_ST45) to 2.13 MPa (AL\_ST15). This consistent strength reduction with increasing accelerator dosage highlighted that higher concentrations led to persistent weaknesses in the interlayer bonds, likely due to premature hydration and the formation of localised cold joints. The accelerated curing process, while effective in promoting early setting, seemed to disrupt uniform bond development, ultimately compromising tensile strength.

## Summary

The research demonstrated that while 3D-printed cement structures showed significant improvements in buildability and early-age strength through optimised parameters like printing speed, layer height, and the use of aluminium sulphate as an accelerator, they still faced limitations in compressive, tensile, and flexural strength compared to monolithic structures. Optimal printing speed (20 mm/s) and layer height (10 mm) were critical in achieving the best structural stability and buildability. Higher concentrations of aluminium sulphate accelerated the setting and supported more layers, enhancing early buildability, but introduced long-term weaknesses at excessive dosages, reducing tensile strength and causing cold joints. Compressive and flexural strength improved over the curing period, with 3D-printed samples reaching 22 MPa in compressive strength and 0.25 MPa in flexural strength by day 28, yet remained below the monolithic structures, which achieved 39.4 MPa and 0.27 MPa, respectively. Failure modes indicated that 3D-printed structures experienced crack propagation along interlayer boundaries, emphasising the challenge of weak layer interfaces inherent to AM. These results highlighted the need for balanced parameter optimisation and careful application of accelerators to enhance structural integr

## 5.6. RECOMMENDATIONS FOR FUTURE WORKS

Building upon the insights from this thesis, several recommendations are proposed to advance the understanding and practical applications of robot-assisted 3D printing for cement-based structures. These recommendations address the need for scalability, material innovation, adaptive control, and resilience in diverse environmental conditions, with a view toward making 3D printing a viable solution for the construction industry.

Future studies could prioritise scale-up testing in real world scenarios to verify the performance of 3D-printed structures under actual construction conditions. Such testing would involve assessing factors like load-bearing capacity, durability, and structural stability, which are essential for large-scale deployment. Real world trials could reveal practical insights into the material and structural behaviour of 3D-printed elements when exposed to real building environments and load stresses.

Exploring new materials is essential for improving construction practices. Expanding the range of materials beyond cement, such as incorporating fibre-reinforced cement, geopolymers, concrete, and other sustainable options, could enhance tensile strength, interlayer bonding, and environmental sustainability. Sustainable alternatives like geopolymer concrete or recycled aggregates could help reduce carbon emissions, while fibre reinforcement could strengthen structures against cracking and other mechanical stresses.

To improve print quality and consistency, developing adaptive real-time control systems is recommended. These systems would employ sensors and feedback mechanisms to dynamically adjust printing parameters such as speed, layer height, and pressure during the process, thereby reducing defects and improving consistency. Machine learning algorithms could further enhance this adaptability, allowing the system to ‘learn’ optimal settings under varying conditions and material properties, minimising structural inconsistencies.

Finally, exploring the use of fibre-reinforced cement and nanomaterials could significantly enhance the structural integrity of 3D-printed structures. Fibres, such as basalt, polypropylene, or steel, could improve tensile strength and crack resistance, while nanomaterials, like carbon nanotubes, could strengthen interlayer bonding at a microstructural level. These materials could be particularly valuable in high-stress applications, enabling printed structures to withstand greater mechanical loads.

## **REFERENCES AND APPENDICES**

---

## References

- [1] F. Bos, R. Wolfs, Z. Ahmed, and T. Salet, "Additive manufacturing of concrete in construction: potentials and challenges of 3D concrete printing," *Virtual and Physical Prototyping*, vol. 11, no. 3, pp. 209-225, 2016/7// 2016, doi: 10.1080/17452759.2016.1209867.
- [2] Y. W. D. Tay, B. Panda, S. C. Paul, N. A. Noor Mohamed, M. J. Tan, and K. F. Leong, "3D printing trends in building and construction industry: a review," *Virtual and Physical Prototyping*, vol. 12, no. 3, pp. 261-276, 2017.
- [3] R. Duballet, O. Baverel, and J. Dirrenberger, "Classification of building systems for concrete 3D printing," *Automation in Construction*, vol. 83, pp. 247-258, 2017/11// 2017, doi: 10.1016/j.autcon.2017.08.018.
- [4] S. C. Paul, G. P. A. G. van Zijl, M. J. Tan, and I. Gibson, "A review of 3D concrete printing systems and materials properties: current status and future research prospects," *Rapid Prototyping Journal*, vol. 24, no. 4, pp. 784-798, 2018, doi: 10.1108/RPJ-09-2016-0154.
- [5] T. D. Ngo, A. Kashani, G. Imbalzano, K. T. Q. Nguyen, and D. Hui, "Additive manufacturing (3D printing): A review of materials, methods, applications and challenges," in *Composites Part B: Engineering* vol. 143, ed: Elsevier Ltd, 2018, pp. 172-196.
- [6] X. Zhang *et al.*, "Large-scale 3D printing by a team of mobile robots," *Automation in Construction*, vol. 95, pp. 98-106, 2018/11// 2018, doi: 10.1016/j.autcon.2018.08.004.
- [7] W. Gao *et al.*, "The status, challenges, and future of additive manufacturing in engineering," *CAD Computer Aided Design*, vol. 69, pp. 65-89, 2015/12// 2015, doi: 10.1016/j.cad.2015.04.001.
- [8] S. Ford and M. I. Despeisse, "Additive manufacturing and sustainability: an exploratory study of the advantages and challenges," *Journal of Cleaner Production*, vol. 137, pp. 1573-1587, 2016/11// 2016, doi: 10.1016/j.jclepro.2016.04.150.
- [9] M. A. Hossain, A. Zhumabekova, S. C. Paul, and J. R. Kim, "A review of 3D printing in construction and its impact on the labor market," in *Sustainability (Switzerland)* vol. 12, ed: MDPI AG, 2020, pp. 1-21.
- [10] Z. Li *et al.*, "Fresh and hardened properties of extrusion-based 3D-printed cementitious materials: A review," in *Sustainability (Switzerland)* vol. 12, ed: MDPI AG, 2020.
- [11] D. Crosthwaite, "The global construction market: a cross-sectional analysis," *Construction management and economics*, vol. 18, no. 5, pp. 619-627, 2000.
- [12] I. Horta, A. Camanho, J. Johnes, and G. Johnes, "Performance trends in the construction industry worldwide: an overview of the turn of the century," *Journal of productivity analysis*, vol. 39, pp. 89-99, 2013.
- [13] G. C. Expenditures. "Construction industry spending worldwide from 2014 to 2019, with forecasts from 2020 to 2035." <https://www.statista.com/statistics/788128/construction-spending-worldwide/> (accessed 9/04, 2023).

- [14] Sriram Changali , Azam Mohammad , and M. v. Nieuwland. "The construction productivity imperative." Mckinsey&Company. <https://www.mckinsey.com/capabilities/operations/our-insights/the-construction-productivity-imperative> (accessed 9/04, 2023).
- [15] D. Delgado Camacho *et al.*, "Applications of additive manufacturing in the construction industry â A forward-looking review," *Automation in Construction*, vol. 89, pp. 110-119, 2018/5// 2018, doi: 10.1016/j.autcon.2017.12.031.
- [16] J. Zhang, J. Wang, S. Dong, X. Yu, and B. Han, "A review of the current progress and application of 3D printed concrete," *Composites Part A: Applied Science and Manufacturing*, vol. 125, p. 105533, 2019.
- [17] H. Yang, J. K. Chung, Y. Chen, and Y. Li, "The cost calculation method of construction 3D printing aligned with internet of things," *EURASIP Journal on Wireless Communications and Networking*, vol. 2018, no. 1, pp. 1-9, 2018.
- [18] V. Mechtcherine, V. N. Nerella, F. Will, M. Näther, J. Otto, and M. Krause, "Large-scale digital concrete construction—CONPrint3D concept for on-site, monolithic 3D-printing," *Automation in construction*, vol. 107, p. 102933, 2019.
- [19] A. M. Jarkas, "Effect of buildability on labor productivity: a practical quantification approach," *Journal of Construction Engineering and Management*, vol. 142, no. 2, p. 06015002, 2016.
- [20] D. Proverbs, G. Holt, and P. Olomolaiye, "Productivity rates and construction methods for high rise concrete construction: a comparative evaluation of UK, German and French contractors," *Construction Management & Economics*, vol. 17, no. 1, pp. 45-52, 1999.
- [21] WBCDS. "The cement sustainable initiative." <https://www.wbcds.org/Sector-Projects/Cement-Sustainability-Initiative/Resources/CSI-Our-Agenda-for-Action> (accessed 26/05, 2023).
- [22] R. Allouzi, W. Al-Azhari, and R. Allouzi, "Conventional construction and 3D printing: A comparison study on material cost in Jordan," *Journal of Engineering*, vol. 2020, pp. 1-14, 2020.
- [23] I. AgustÃ--Juan and G. Habert, "Environmental design guidelines for digital fabrication," *Journal of Cleaner Production*, vol. 142, pp. 2780-2791, 2017/1// 2017, doi: 10.1016/j.jclepro.2016.10.190.
- [24] B. Nematollahi, M. Xia, and J. Sanjayan, "Current Progress of 3D Concrete Printing Technologies," 2017.
- [25] ManpowerGroup. "5 major challenges in the construction industry." <https://www.manpowergroup.co.uk/the-word-on-work/manpower-tech-expertise-5-major-challenges-construction-industry/> (accessed).
- [26] A. Alsharef, A. Ovid, S. M. J. Uddin, and A. Albert, *Biggest Challenges Facing the Construction Industry*. 2024, pp. 652-660.
- [27] H. a. s. Executive, "Health and safety statistics," ed, 2020.

- [28] H. a. S. Executive, "Construction statistics in Great Britain," 2023. [Online]. Available: <https://www.hse.gov.uk/statistics/assets/docs/construction.pdf>
- [29] T. Marchment, J. Sanjayan, and M. Xia, "Method of enhancing interlayer bond strength in construction scale 3D printing with mortar by effective bond area amplification," *Materials and Design*, vol. 169, 2019/5// 2019, doi: 10.1016/j.matdes.2019.107684.
- [30] M. Adaloudis and J. Bonnin Roca, "Sustainability tradeoffs in the adoption of 3D Concrete Printing in the construction industry," *Journal of Cleaner Production*, vol. 307, 2021/7// 2021, doi: 10.1016/j.jclepro.2021.127201.
- [31] V. Mechtcherine, V. N. Nerella, F. Will, M. N  tner, J. Otto, and M. Krause, "Large-scale digital concrete construction â CONPrint3D concept for on-site, monolithic 3D-printing," *Automation in Construction*, vol. 107, 2019/11// 2019, doi: 10.1016/j.autcon.2019.102933.
- [32] Y. Weng *et al.*, "Comparative economic, environmental and productivity assessment of a concrete bathroom unit fabricated through 3D printing and a precast approach," *Journal of Cleaner Production*, vol. 261, 2020/7// 2020, doi: 10.1016/j.jclepro.2020.121245.
- [33] Q. Shahzad, J. Shen, R. Naseem, Y. Yao, S. Waqar, and W. Liu, "Influence of phase change material on concrete behavior for construction 3D printing," *Construction and Building Materials*, vol. 309, 2021/11// 2021, doi: 10.1016/j.conbuildmat.2021.125121.
- [34] C. m. Gosselin *et al.*, "Large-scale 3D printing of ultra-high performance concrete-a new processing route for architects and builders," doi: 10.1016/j.matdes.2016.03.097.
- [35] S. Keating, "Beyond 3D printing: The new Dimensionsof additive fabrication," *Designing for emerging technologies: UX for genomics, robotics, and the internet of things*, vol. 379, 2014.
- [36] R. A. Buswell, R. C. Soar, A. G. Gibb, and A. Thorpe, "Freeform construction: mega-scale rapid manufacturing for construction," *Automation in construction*, vol. 16, no. 2, pp. 224-231, 2007.
- [37] D. Delgado Camacho *et al.*, "Applications of additive manufacturing in the construction industry â A forward-looking review," *Automation in Construction*, vol. 89, pp. 110-119, 2018/5// 2018, doi: 10.1016/j.autcon.2017.12.031.
- [38] A. Standard, "F2792. 2012 Standard terminology for additive manufacturing technologies, West Conshohocken, PA: ASTM International," See [www.astm.org](http://www.astm.org).(doi: 10.1520/F2792-12), 2012.
- [39] C. W. Hull, "Apparatus for production of three-dimensional objects by stereolithography," *United States Patent, Appl., No. 638905, Filed, 1984.*
- [40] Z. Pan, D. Si, J. Tao, and J. Xiao, "Compressive behavior of 3D printed concrete with different printing paths and concrete ages," *Case Studies in Construction Materials*, vol. 18, p. e01949, 2023.
- [41] T. T. Le *et al.*, "Hardened properties of high-performance printing concrete," *Cement and Concrete Research*, vol. 42, no. 3, pp. 558-566, 2012/3// 2012, doi: 10.1016/j.cemconres.2011.12.003.

- [42] Y. W. Tay *et al.*, "Processing and properties of construction materials for 3D printing," in *Materials Science Forum*, 2016, vol. 861: Trans Tech Publ, pp. 177-181.
- [43] B. Zareiyan and B. Khoshnevis, "Interlayer adhesion and strength of structures in Contour Crafting - Effects of aggregate size, extrusion rate, and layer thickness," *Automation in Construction*, vol. 81, pp. 112-121, 2017/9// 2017, doi: 10.1016/j.autcon.2017.06.013.
- [44] A. El Moumen, M. Tarfaoui, and K. Lafdi, "Additive manufacturing of polymer composites: Processing and modeling approaches," *Composites Part B: Engineering*, vol. 171, pp. 166-182, 2019/8// 2019, doi: 10.1016/j.compositesb.2019.04.029.
- [45] P. Urhal, A. Weightman, C. Diver, and P. Bartolo, "Robot assisted additive manufacturing: A review," *Robotics and Computer-Integrated Manufacturing*, vol. 59, pp. 335-345, 2019/10// 2019, doi: 10.1016/j.rcim.2019.05.005.
- [46] E. Uhlmann, A. Bergmann, R. Bolz, and W. Gridin, "Application of additive manufactured tungsten carbide tool electrodes in EDM," *Procedia CIRP*, vol. 68, pp. 86-90, 2018.
- [47] H. Bikas, P. Stavropoulos, and G. Chryssolouris, "Additive manufacturing methods and modelling approaches: a critical review," *The International Journal of Advanced Manufacturing Technology*, vol. 83, pp. 389-405, 2016.
- [48] B. P. Conner *et al.*, "Making sense of 3-D printing: Creating a map of additive manufacturing products and services," *Additive manufacturing*, vol. 1, pp. 64-76, 2014.
- [49] S. Derakhshanfar, R. Mbeleck, K. Xu, X. Zhang, W. Zhong, and M. Xing, "3D bioprinting for biomedical devices and tissue engineering: A review of recent trends and advances," *Bioactive materials*, vol. 3, no. 2, pp. 144-156, 2018.
- [50] S. Bose, D. Ke, H. Sahasrabudhe, and A. Bandyopadhyay, "Additive manufacturing of biomaterials," *Progress in materials science*, vol. 93, pp. 45-111, 2018.
- [51] C. L. Ventola, "Medical applications for 3D printing: current and projected uses," *Pharmacy and Therapeutics*, vol. 39, no. 10, p. 704, 2014.
- [52] J. C. Vasco, "Additive manufacturing for the automotive industry," in *Additive Manufacturing*: Elsevier, 2021, pp. 505-530.
- [53] I. Gibson, T. Kvan, and L. Wai Ming, "Rapid prototyping for architectural models," *Rapid prototyping journal*, vol. 8, no. 2, pp. 91-95, 2002.
- [54] J. I. Lipton, M. Cutler, F. Nigl, D. Cohen, and H. Lipson, "Additive manufacturing for the food industry," *Trends in food science & technology*, vol. 43, no. 1, pp. 114-123, 2015.
- [55] B. Berman, "3-D printing: The new industrial revolution," *Business Horizons*, vol. 55, no. 2, pp. 155-162, 2012/3// 2012, doi: 10.1016/j.bushor.2011.11.003.
- [56] A. K. Sood, R. K. Ohdar, and S. S. Mahapatra, "Parametric appraisal of mechanical property of fused deposition modelling processed parts," *Materials and Design*, vol. 31, no. 1, pp. 287-295, 2010/1// 2010, doi: 10.1016/j.matdes.2009.06.016.
- [57] J. M. Chacón, M. A. Caminero, E. García-Plaza, and P. J. Núñez, "Additive manufacturing of PLA structures using fused deposition modelling: Effect of process parameters on

- mechanical properties and their optimal selection," *Materials and Design*, vol. 124, pp. 143-157, 2017/6// 2017, doi: 10.1016/j.matdes.2017.03.065.
- [58] P. Anakhu, C. Bolu, A. Abioye, and J. Azeta, "Fused Deposition Modeling Printed Patterns for Sand Casting in a Nigerian Foundry: A Review Effects of Increasing Chitosan Nanofibre Volume Fraction on the Mechanical Property of Hydroxyapatite View project Material Selection View project Fused Deposition Modeling Printed Patterns for Sand Casting in a Nigerian Foundry: A Review," in "International Journal of Applied Engineering Research," 2018, vol. 13. [Online]. Available: <http://www.ripublication.com>
- [59] B. Khoshnevis, "AUTOMATED CONSTRUCTION BY CONTOUR CRAFTING-RELATED ROBOTICS AND INFORMATION TECHNOLOGIES," 2004, vol. 13. [Online]. Available: [www.calearth.org](http://www.calearth.org)
- [60] B. Khoshnevis, "Automated construction by contour crafting - Related robotics and information technologies," in *Automation in Construction*, 2004/1// 2004, vol. 13, 1 ed., pp. 5-19, doi: 10.1016/j.autcon.2003.08.012.
- [61] P. Bosscher, R. L. Williams, L. S. Bryson, and D. Castro-Lacouture, "Cable-suspended robotic contour crafting system," *Automation in Construction*, vol. 17, no. 1, pp. 45-55, 2007, doi: 10.1016/j.autcon.2007.02.011.
- [62] J. Zhang and B. Khoshnevis, "Optimal machine operation planning for construction by Contour Crafting," *Automation in Construction*, vol. 29, pp. 50-67, 2013/1// 2013, doi: 10.1016/j.autcon.2012.08.006.
- [63] H. Kwon, *Experimentation and analysis of contour crafting (CC) process using uncured ceramic materials*. University of Southern California, 2002.
- [64] H. Al Jassmi, F. Al Najjar, and A. H. I. Mourad, "Large-Scale 3D Printing: The Way Forward," in *IOP Conference Series: Materials Science and Engineering*, 2018/4// 2018, vol. 324: Institute of Physics Publishing, 1 ed., doi: 10.1088/1757-899X/324/1/012088.
- [65] E. Lloret *et al.*, "Complex concrete structures: Merging existing casting techniques with digital fabrication," *Computer-Aided Design*, vol. 60, pp. 40-49, 2015/03/01/ 2015, doi: <https://doi.org/10.1016/j.cad.2014.02.011>.
- [66] S. Neudecker *et al.*, "A New Robotic Spray Technology for Generative Manufacturing of Complex Concrete Structures Without Formwork," *Procedia CIRP*, vol. 43, pp. 333-338, 2016/01/01/ 2016, doi: <https://doi.org/10.1016/j.procir.2016.02.107>.
- [67] H. Kloft *et al.*, "Influence of process parameters on the interlayer bond strength of concrete elements additive manufactured by Shotcrete 3D Printing (SC3DP)," *Cement and Concrete Research*, vol. 134, p. 106078, 2020/08/01/ 2020, doi: <https://doi.org/10.1016/j.cemconres.2020.106078>.
- [68] I. Dressler, N. Freund, and D. Lowke, "The effect of accelerator dosage on fresh concrete properties and on interlayer strength in shotcrete 3D printing," *Materials*, vol. 13, no. 2, 2020/1// 2020, doi: 10.3390/ma13020374.
- [69] F. P. Bos *et al.*, "The realities of additively manufactured concrete structures in practice," *Cement and Concrete Research*, vol. 156, p. 106746, 2022/06/01/ 2022, doi: <https://doi.org/10.1016/j.cemconres.2022.106746>.

- [70] N. Zhang and J. Sanjayan, "Extrusion nozzle design and print parameter selections for 3D concrete printing," *Cement and Concrete Composites*, vol. 137, 2023/3// 2023, doi: 10.1016/j.cemconcomp.2023.104939.
- [71] J. M. Chacón, M. A. Caminero, E. García-Plaza, and P. J. Núñez, "Additive manufacturing of PLA structures using fused deposition modelling: Effect of process parameters on mechanical properties and their optimal selection," *Materials & Design*, vol. 124, pp. 143-157, 2017/06/15/ 2017, doi: <https://doi.org/10.1016/j.matdes.2017.03.065>.
- [72] B. Derby, "Printing and prototyping of tissues and scaffolds," *science*, vol. 338, no. 6109, pp. 921-926, 2012.
- [73] K. A. Seerden, N. Reis, J. R. Evans, P. S. Grant, J. W. Halloran, and B. Derby, "Ink-jet printing of wax-based alumina suspensions," *Journal of the American Ceramic Society*, vol. 84, no. 11, pp. 2514-2520, 2001.
- [74] J. Perelaer *et al.*, "Printed electronics: the challenges involved in printing devices, interconnects, and contacts based on inorganic materials," *Journal of Materials Chemistry*, vol. 20, no. 39, pp. 8446-8453, 2010.
- [75] N. Travitzky *et al.*, "Additive manufacturing of ceramic-based materials," *Advanced engineering materials*, vol. 16, no. 6, pp. 729-754, 2014.
- [76] Z. C. Eckel, C. Zhou, J. H. Martin, A. J. Jacobsen, W. B. Carter, and T. A. Schaedler, "Additive manufacturing of polymer-derived ceramics," *Science*, vol. 351, no. 6268, pp. 58-62, 2016.
- [77] X. Wang, M. Jiang, Z. Zhou, J. Gou, and D. Hui, "3D printing of polymer matrix composites: A review and prospective," *Composites Part B: Engineering*, vol. 110, pp. 442-458, 2017.
- [78] S. H. Huang, P. Liu, A. Mokasdar, and L. Hou, "Additive manufacturing and its societal impact: a literature review," *The International journal of advanced manufacturing technology*, vol. 67, pp. 1191-1203, 2013.
- [79] X. Tian, T. Liu, C. Yang, Q. Wang, and D. Li, "Interface and performance of 3D printed continuous carbon fiber reinforced PLA composites," *Composites Part A: Applied Science and Manufacturing*, vol. 88, pp. 198-205, 2016/9// 2016, doi: 10.1016/j.compositesa.2016.05.032.
- [80] H. Lee, C. H. J. Lim, M. J. Low, N. Tham, V. M. Murukeshan, and Y.-J. Kim, "Lasers in additive manufacturing: A review," *International Journal of Precision Engineering and Manufacturing-Green Technology*, vol. 4, pp. 307-322, 2017.
- [81] I. Gibson, D. Rosen, and B. Stucker, "Additive manufacturing technologies: 3D printing, rapid prototyping, and direct digital manufacturing," ed: Deakin University, 2015.
- [82] W. E. Frazier, "Metal Additive Manufacturing: A Review," *Journal of Materials Engineering and Performance*, vol. 23, no. 6, pp. 1917-1928, 2014/06/01 2014, doi: 10.1007/s11665-014-0958-z.
- [83] R. Lediga and D. Kruger, "Optimizing concrete mix design for application in 3D printing technology for the construction industry," in *Solid State Phenomena*, 2017, vol. 263 SSP: Trans Tech Publications Ltd, pp. 24-29, doi: 10.4028/[www.scientific.net/SSP.263.24](http://www.scientific.net/SSP.263.24).

- [84] T. T. Le, S. A. Austin, S. Lim, R. A. Buswell, A. G. F. Gibb, and T. Thorpe, "Mix design and fresh properties for high-performance printing concrete," *Materials and Structures/Materiaux et Constructions*, vol. 45, no. 8, pp. 1221-1232, 2012/8// 2012, doi: 10.1617/s11527-012-9828-z.
- [85] "Optimizing the Use of Fly Ash in Concrete."
- [86] G. Slavcheva, A. Levchenko, M. Shvedova, D. Karakchi-ogly, and D. Babenko, "Anisotropy in mechanical properties of 3D-printed layered concrete," *Magazine of Civil Engineering*, vol. 17, no. 3, p. 2, 2024.
- [87] G. Ma, Z. Li, and L. Wang, "Printable properties of cementitious material containing copper tailings for extrusion based 3D printing," *Construction and building materials*, vol. 162, pp. 613-627, 2018.
- [88] B. Panda, S. C. Paul, N. A. N. Mohamed, Y. W. D. Tay, and M. J. Tan, "Measurement of tensile bond strength of 3D printed geopolymers mortar," *Measurement*, vol. 113, pp. 108-116, 2018.
- [89] C. Joh, J. Lee, T. Q. Bui, J. Park, and I.-H. Yang, "Buildability and mechanical properties of 3D printed concrete," *Materials*, vol. 13, no. 21, p. 4919, 2020.
- [90] N. Shahrubudin, T. C. Lee, and R. Ramlan, "An overview on 3D printing technology: Technological, materials, and applications," in *Procedia Manufacturing*, 2019, vol. 35: Elsevier B.V., pp. 1286-1296, doi: 10.1016/j.promfg.2019.06.089.
- [91] C. Zhang *et al.*, "Mix design concepts for 3D printable concrete: A review," in *Cement and Concrete Composites* vol. 122, ed: Elsevier Ltd, 2021.
- [92] F. Hamidi and F. Aslani, "Additive manufacturing of cementitious composites: Materials, methods, potentials, and challenges," *Construction and Building Materials*, vol. 218, pp. 582-609, 2019/09/10/ 2019, doi: <https://doi.org/10.1016/j.conbuildmat.2019.05.140>.
- [93] B. Lu *et al.*, "A systematical review of 3D printable cementitious materials," *Construction and Building Materials*, vol. 207, pp. 477-490, 2019/05/20/ 2019, doi: <https://doi.org/10.1016/j.conbuildmat.2019.02.144>.
- [94] M. Chen, L. Li, Y. Zheng, P. Zhao, L. Lu, and X. Cheng, "Rheological and mechanical properties of admixtures modified 3D printing sulphoaluminate cementitious materials," *Construction and Building Materials*, vol. 189, pp. 601-611, 2018/11// 2018, doi: 10.1016/j.conbuildmat.2018.09.037.
- [95] M. Chen *et al.*, "Rheological parameters, thixotropy and creep of 3D-printed calcium sulfoaluminate cement composites modified by bentonite," *Composites Part B: Engineering*, vol. 186, p. 107821, 2020/04/01/ 2020, doi: <https://doi.org/10.1016/j.compositesb.2020.107821>.
- [96] N. Khalil, G. Aouad, K. El Cheikh, and S. Rémond, "Use of calcium sulfoaluminate cements for setting control of 3D-printing mortars," *Construction and Building Materials*, vol. 157, pp. 382-391, 2017.

- [97] B. Panda, S. C. Paul, L. J. Hui, Y. W. D. Tay, and M. J. Tan, "Additive manufacturing of geopolymer for sustainable built environment," *Journal of Cleaner Production*, vol. 167, pp. 281-288, 2017/11/20/ 2017, doi: <https://doi.org/10.1016/j.jclepro.2017.08.165>.
- [98] C. Sun, J. Xiang, M. Xu, Y. He, Z. Tong, and X. Cui, "3D extrusion free forming of geopolymer composites: Materials modification and processing optimization," *Journal of Cleaner Production*, vol. 258, p. 120986, 2020/06/10/ 2020, doi: <https://doi.org/10.1016/j.jclepro.2020.120986>.
- [99] A. V. Rahul and M. Santhanam, "Evaluating the printability of concretes containing lightweight coarse aggregates," *Cement and Concrete Composites*, vol. 109, p. 103570, 2020/05/01/ 2020, doi: <https://doi.org/10.1016/j.cemconcomp.2020.103570>.
- [100] T. Ding, J. Xiao, F. Qin, and Z. Duan, "Mechanical behavior of 3D printed mortar with recycled sand at early ages," *Construction and Building Materials*, vol. 248, p. 118654, 2020/07/10/ 2020, doi: <https://doi.org/10.1016/j.conbuildmat.2020.118654>.
- [101] Y. Han, Z. Yang, T. Ding, and J. Xiao, "Environmental and economic assessment on 3D printed buildings with recycled concrete," *Journal of Cleaner Production*, vol. 278, p. 123884, 2021/01/01/ 2021, doi: <https://doi.org/10.1016/j.jclepro.2020.123884>.
- [102] Y. Zhang, Y. Zhang, G. Liu, Y. Yang, M. Wu, and B. Pang, "Fresh properties of a novel 3D printing concrete ink," *Construction and Building Materials*, vol. 174, pp. 263-271, 2018/6// 2018, doi: 10.1016/j.conbuildmat.2018.04.115.
- [103] B. Panda, S. Ruan, C. Unluer, and M. J. Tan, "Investigation of the properties of alkali-activated slag mixes involving the use of nanoclay and nucleation seeds for 3D printing," *Composites Part B: Engineering*, vol. 186, p. 107826, 2020/04/01/ 2020, doi: <https://doi.org/10.1016/j.compositesb.2020.107826>.
- [104] J. Kruger, S. Zeranka, and G. van Zijl, "An ab initio approach for thixotropy characterisation of (nanoparticle-infused) 3D printable concrete," *Construction and Building Materials*, vol. 224, pp. 372-386, 2019/11/10/ 2019, doi: <https://doi.org/10.1016/j.conbuildmat.2019.07.078>.
- [105] Y. Chen *et al.*, "Improving printability of limestone-calcined clay-based cementitious materials by using viscosity-modifying admixture," *Cement and Concrete Research*, vol. 132, p. 106040, 2020/06/01/ 2020, doi: <https://doi.org/10.1016/j.cemconres.2020.106040>.
- [106] S. Michalopoulos, ""Printable profile of sustainable modified cementitious materials for additive manufacturing applications in digital construction"."
- [107] M. Aqel and D. K. Panesar, "Hydration kinetics and compressive strength of steam-cured cement pastes and mortars containing limestone filler," *Construction and Building Materials*, vol. 113, pp. 359-368, 2016/6// 2016, doi: 10.1016/j.conbuildmat.2016.03.031.
- [108] J. J. Brooks, M. A. Megat Johari, and M. Mazloom, "Composites Effect of admixtures on the setting times of high-strength concrete," in "Cement & Concrete Cement & Concrete Composites," 2000, vol. 22. [Online]. Available: [www.elsevier.com/locate/cemconcomp](http://www.elsevier.com/locate/cemconcomp)
- [109] Q. Shahzad, M. UmaÄ°R, and S. Waqar, "Bibliographic analysis on 3D printing in the building and construction industry: Printing systems, material properties, challenges, and future trends," *Journal of Sustainable Construction Materials and Technologies*, vol. 7, no. 3, pp. 198-220, 2022/9// 2022, doi: 10.47481/jscmt.1143239.

- [110] T. T. Le *et al.*, "Hardened properties of high-performance printing concrete," *Cement and Concrete Research*, vol. 42, no. 3, pp. 558-566, 2012.
- [111] M. Tramontin Souza *et al.*, "Role of chemical admixtures on 3D printed Portland cement: Assessing rheology and buildability," *Construction and Building Materials*, vol. 314, 2022/1// 2022, doi: 10.1016/j.conbuildmat.2021.125666.
- [112] L. Senff\*, D. Hotza, W. Repette, V. Ferreira, and J. Labrincha, "Rheological characterisation of cement pastes with nanosilica, silica fume and superplasticiser additions," *Advances in Applied Ceramics*, vol. 109, no. 4, pp. 213-218, 2010.
- [113] L. Senff, R. Modolo, A. S. Silva, V. Ferreira, D. Hotza, and J. Labrincha, "Influence of red mud addition on rheological behavior and hardened properties of mortars," *Construction and Building Materials*, vol. 65, pp. 84-91, 2014.
- [114] Z. Li *et al.*, "Fresh and hardened properties of extrusion-based 3D-printed cementitious materials: A review," in *Sustainability (Switzerland)* vol. 12, ed: MDPI AG, 2020.
- [115] C. Gosselin, R. Duballet, P. Roux, N. GaudilliÃ"re, J. Dirrenberger, and P. Morel, "Large-scale 3D printing of ultra-high performance concrete - a new processing route for architects and builders," *Materials and Design*, vol. 100, pp. 102-109, 2016/6// 2016, doi: 10.1016/j.matdes.2016.03.097.
- [116] C. Kan, M. Lan, L. Kong, and J. Yang, "Effect of aluminium sulfate on cement properties," in *Materials Science Forum*, 2013, vol. 743-744: Trans Tech Publications Ltd, pp. 285-291, doi: 10.4028/[www.scientific.net/MSF.743-744.285](http://www.scientific.net/MSF.743-744.285).
- [117] S. Bhattacharjee and M. Santhanam, "Enhancing Buildability of 3D Printable Concrete by Spraying of Accelerating Admixture on Surface," in *RILEM Bookseries*, vol. 28: Springer, 2020, pp. 13-22.
- [118] V. N. Nerella, M. A. B. Beigh, S. Fataei, and V. Mechtcherine, "Strain-based approach for measuring structural build-up of cement pastes in the context of digital construction," *Cement and Concrete Research*, vol. 115, pp. 530-544, 2019.
- [119] S. Kim, T. Kim, B. Kim, H.-d. Kim, J. Kim, and H. Lee, "Early hydration and hardening of OPC-CSA blends for cementitious structure of 3D printing," *Advances in Applied Ceramics*, vol. 119, no. 7, pp. 393-397, 2020.
- [120] D. Han and R. D. Ferron, "Effect of mixing method on microstructure and rheology of cement paste," *Construction and Building Materials*, vol. 93, pp. 278-288, 2015.
- [121] F.-J. Rubio-Hernández, "Rheological behavior of fresh cement pastes," *Fluids*, vol. 3, no. 4, p. 106, 2018.
- [122] S. Bhattacharjee and M. Santhanam, "Investigation on the effect of alkali-free aluminium sulfate based accelerator on the fresh properties of 3D printable concrete," *Cement and Concrete Composites*, vol. 130, p. 104521, 2022.
- [123] Y. W. D. Tay, G. H. A. Ting, Y. Qian, B. Panda, L. He, and M. J. Tan, "Time gap effect on bond strength of 3D-printed concrete," *Virtual and Physical Prototyping*, vol. 14, no. 1, pp. 104-113, 2019/1// 2019, doi: 10.1080/17452759.2018.1500420.

- [124] V. N. Nerella, S. Hempel, and V. Mechtcherine, "Effects of layer-interface properties on mechanical performance of concrete elements produced by extrusion-based 3D-printing," *Construction and Building Materials*, vol. 205, pp. 586-601, 2019.
- [125] B. Panda, N. A. Noor Mohamed, S. C. Paul, G. Bhagath Singh, M. J. Tan, and B. Šavija, "The effect of material fresh properties and process parameters on buildability and interlayer adhesion of 3D printed concrete," *Materials*, vol. 12, no. 13, p. 2149, 2019.
- [126] J. Zhong, G. X. Zhou, P. G. He, Z. H. Yang, and D. C. Jia, "3D printing strong and conductive geo-polymer nanocomposite structures modified by graphene oxide," *Carbon*, vol. 117, pp. 421-426, 2017/6// 2017, doi: 10.1016/j.carbon.2017.02.102.
- [127] A. Kazemian, X. Yuan, E. Cochran, and B. Khoshnevis, "Cementitious materials for construction-scale 3D printing: Laboratory testing of fresh printing mixture," *Construction and Building Materials*, vol. 145, pp. 639-647, 2017/8// 2017, doi: 10.1016/j.conbuildmat.2017.04.015.
- [128] Z. Jianchao, T. Zhang, M. Faried, and C. Wengang, "3D printing cement based ink, and it's application within the construction industry."
- [129] M. Hambach and D. Volkmer, "Properties of 3D-printed fiber-reinforced Portland cement paste," *Cement and Concrete Composites*, vol. 79, pp. 62-70, 2017/5// 2017, doi: 10.1016/j.cemconcomp.2017.02.001.
- [130] K. Rashid, T. Ueda, D. Zhang, K. Miyaguchi, and H. Nakai, "Experimental and analytical investigations on the behavior of interface between concrete and polymer cement mortar under hygrothermal conditions," *Construction and Building materials*, vol. 94, pp. 414-425, 2015.
- [131] Y. Weng, M. Li, D. Zhang, M. J. Tan, and S. Qian, "Investigation of interlayer adhesion of 3D printable cementitious material from the aspect of printing process," *Cement and Concrete Research*, vol. 143, p. 106386, 2021.
- [132] R. J. M. Wolfs, F. P. Bos, and T. A. M. Salet, "Hardened properties of 3D printed concrete: The influence of process parameters on interlayer adhesion," *Cement and Concrete Research*, vol. 119, pp. 132-140, 2019/5// 2019, doi: 10.1016/j.cemconres.2019.02.017.
- [133] J. G. Sanjayan, B. Nematollahi, M. Xia, and T. Marchment, "Effect of surface moisture on inter-layer strength of 3D printed concrete," *Construction and building materials*, vol. 172, pp. 468-475, 2018.
- [134] N. Roussel, "Rheological requirements for printable concretes," in *Cement and Concrete Research* vol. 112, ed: Elsevier Ltd, 2018, pp. 76-85.
- [135] P. Feng, X. Meng, J. F. Chen, and L. Ye, "Mechanical properties of structures 3D printed with cementitious powders," *Construction and Building Materials*, vol. 93, pp. 486-497, 2015/6// 2015, doi: 10.1016/j.conbuildmat.2015.05.132.
- [136] J. Kruger, S. Cho, S. Zeranka, C. Viljoen, and G. van Zijl, "3D concrete printer parameter optimisation for high rate digital construction avoiding plastic collapse," *Composites Part B: Engineering*, vol. 183, p. 107660, 2020.

- [137] V. C. Li *et al.*, "On the emergence of 3D printable Engineered, Strain Hardening Cementitious Composites (ECC/SHCC)," *Cement and Concrete Research*, vol. 132, p. 106038, 2020/06/01/ 2020, doi: <https://doi.org/10.1016/j.cemconres.2020.106038>.
- [138] H. Ogura, V. N. Nerella, and V. Mechtcherine, "Developing and Testing of Strain-Hardening Cement-Based Composites (SHCC) in the Context of 3D-Printing," *Materials*, vol. 11, no. 8, doi: 10.3390/ma11081375.
- [139] B. Zhu, J. Pan, B. Nematollahi, Z. Zhou, Y. Zhang, and J. Sanjayan, "Development of 3D printable engineered cementitious composites with ultra-high tensile ductility for digital construction," *Materials & Design*, vol. 181, p. 108088, 2019/11/05/ 2019, doi: <https://doi.org/10.1016/j.matdes.2019.108088>.
- [140] D. G. Soltan and V. C. Li, "A self-reinforced cementitious composite for building-scale 3D printing," *Cement and Concrete Composites*, vol. 90, pp. 1-13, 2018/07/01/ 2018, doi: <https://doi.org/10.1016/j.cemconcomp.2018.03.017>.
- [141] H. Alghamdi and N. Neithalath, "Synthesis and characterization of 3D-printable geopolymeric foams for thermally efficient building envelope materials," *Cement and Concrete Composites*, vol. 104, p. 103377, 2019/11/01/ 2019, doi: <https://doi.org/10.1016/j.cemconcomp.2019.103377>.
- [142] V. Markin, V. N. Nerella, C. Schröfl, G. Guseynova, and V. Mechtcherine, "Material Design and Performance Evaluation of Foam Concrete for Digital Fabrication," *Materials*, vol. 12, no. 15, doi: 10.3390/ma12152433.
- [143] D. Falliano, D. De Domenico, G. Ricciardi, and E. Gugliandolo, "3D-printable lightweight foamed concrete and comparison with classical foamed concrete in terms of fresh state properties and mechanical strength," *Construction and Building Materials*, vol. 254, p. 119271, 2020/09/10/ 2020, doi: <https://doi.org/10.1016/j.conbuildmat.2020.119271>.
- [144] H. Shen, X. Ye, G. Xu, L. Zhang, J. Qian, and J. Fu, "3D printing build orientation optimization for flexible support platform," *Rapid Prototyping Journal*, vol. 26, no. 1, pp. 59-72, 2020/1// 2020, doi: 10.1108/RPJ-09-2018-0252.
- [145] T. S. Rushing *et al.*, "Investigation of concrete mixtures for additive construction," *Rapid Prototyping Journal*, vol. 23, no. 1, pp. 74-80, 2017, doi: 10.1108/RPJ-09-2015-0124.
- [146] A. V. Rahul, M. Santhanam, H. Meena, and Z. Ghani, "3D printable concrete: Mixture design and test methods," *Cement and Concrete Composites*, vol. 97, pp. 13-23, 2019/03/01/ 2019, doi: <https://doi.org/10.1016/j.cemconcomp.2018.12.014>.
- [147] Y. Weng, B. Lu, M. Li, Z. Liu, M. J. Tan, and S. Qian, "Empirical models to predict rheological properties of fiber reinforced cementitious composites for 3D printing," *Construction and Building Materials*, vol. 189, pp. 676-685, 2018/11/20/ 2018, doi: <https://doi.org/10.1016/j.conbuildmat.2018.09.039>.
- [148] Z. Liu, M. Li, Y. Weng, T. N. Wong, and M. J. Tan, "Mixture Design Approach to optimize the rheological properties of the material used in 3D cementitious material printing," *Construction and Building Materials*, vol. 198, pp. 245-255, 2019/02/20/ 2019, doi: <https://doi.org/10.1016/j.conbuildmat.2018.11.252>.

- [149] V. Mechtcherine, V. N. Nerella, and K. Kasten, "Testing pumpability of concrete using Sliding Pipe Rheometer," *Construction and Building Materials*, vol. 53, pp. 312-323, 2014/02/28/ 2014, doi: <https://doi.org/10.1016/j.conbuildmat.2013.11.037>.
- [150] M. Choi, N. Roussel, Y. Kim, and J. Kim, "Lubrication layer properties during concrete pumping," *Cement and Concrete Research*, vol. 45, pp. 69-78, 2013/03/01/ 2013, doi: <https://doi.org/10.1016/j.cemconres.2012.11.001>.
- [151] Y. W. D. Tay, Y. Qian, and M. J. Tan, "Printability region for 3D concrete printing using slump and slump flow test," *Composites Part B: Engineering*, vol. 174, p. 106968, 2019/10/01/ 2019, doi: <https://doi.org/10.1016/j.compositesb.2019.106968>.
- [152] R. A. Buswell, W. R. Leal de Silva, S. Z. Jones, and J. Dirrenberger, "3D printing using concrete extrusion: A roadmap for research," in *Cement and Concrete Research* vol. 112, ed: Elsevier Ltd, 2018, pp. 37-49.
- [153] L. Anell, "Concrete 3d printer," 2015.
- [154] A. Perrot, D. Rangeard, and A. Pierre, "Structural built-up of cement-based materials used for 3D-printing extrusion techniques," *Materials and Structures/Materiaux et Constructions*, vol. 49, no. 4, pp. 1213-1220, 2016/4// 2016, doi: 10.1617/s11527-015-0571-0.
- [155] Z. Toutou, N. Roussel, and C. Lanos, "The squeezing test: a tool to identify firm cement-based material's rheological behaviour and evaluate their extrusion ability," *Cement and Concrete Research*, vol. 35, no. 10, pp. 1891-1899, 2005/10/01/ 2005, doi: <https://doi.org/10.1016/j.cemconres.2004.09.007>.
- [156] V. N. Nerella, M. Näther, A. Iqbal, M. Butler, and V. Mechtcherine, "Inline quantification of extrudability of cementitious materials for digital construction," *Cement and Concrete Composites*, vol. 95, pp. 260-270, 2019/01/01/ 2019, doi: <https://doi.org/10.1016/j.cemconcomp.2018.09.015>.
- [157] M. Rubio, M. Rubio, M. Sonebi, and S. Amziane, "Composite civil engineering structures View project Finite element modelling of thermal uniaxial creep of HPC View project EcoGRAFI Second International Conference on Bio-based Building Materials 3D PRINTING OF FIBRE CEMENT-BASED MATERIALS: FRESH AND RHEOLOGICAL PERFORMANCES," 2017. [Online]. Available: <https://www.researchgate.net/publication/338127120>
- [158] B. Panda and M. J. Tan, "Experimental study on mix proportion and fresh properties of fly ash based geopolymer for 3D concrete printing," *Ceramics International*, vol. 44, no. 9, pp. 10258-10265, 2018/06/15/ 2018, doi: <https://doi.org/10.1016/j.ceramint.2018.03.031>.
- [159] C. Zhang, Z. Hou, C. Chen, Y. Zhang, V. Mechtcherine, and Z. Sun, "Design of 3D printable concrete based on the relationship between flowability of cement paste and optimum aggregate content," *Cement and Concrete Composites*, vol. 104, p. 103406, 2019/11/01/ 2019, doi: <https://doi.org/10.1016/j.cemconcomp.2019.103406>.
- [160] B. Panda, S. Ruan, C. Unluer, and M. J. Tan, "Improving the 3D printability of high volume fly ash mixtures via the use of nano attapulgite clay," *Composites Part B: Engineering*, vol. 165, pp. 75-83, 2019/05/15/ 2019, doi: <https://doi.org/10.1016/j.compositesb.2018.11.109>.

- [161] Q. Yuan *et al.*, "A feasible method for measuring the buildability of fresh 3D printing mortar," *Construction and Building Materials*, vol. 227, p. 116600, 2019/12/10/ 2019, doi: <https://doi.org/10.1016/j.conbuildmat.2019.07.326>.
- [162] V. N. Nerella and V. Mechtcherine, "Studying the printability of fresh concrete for formwork-free concrete onsite 3D printing technology (CONPrint3D)," in *3D concrete printing technology*: Elsevier, 2019, pp. 333-347.
- [163] S. C. Paul, Y. W. D. Tay, B. Panda, and M. J. Tan, "Fresh and hardened properties of 3D printable cementitious materials for building and construction," *Archives of civil and mechanical engineering*, vol. 18, pp. 311-319, 2018.
- [164] B. Panda, S. C. Paul, and M. J. Tan, "Anisotropic mechanical performance of 3D printed fiber reinforced sustainable construction material," *Materials Letters*, vol. 209, pp. 146-149, 2017.
- [165] Y. Zhang, Y. Zhang, W. She, L. Yang, G. Liu, and Y. Yang, "Rheological and harden properties of the high-thixotropy 3D printing concrete," *Construction and Building Materials*, vol. 201, pp. 278-285, 2019.
- [166] F. P. Bos, Z. Y. Ahmed, R. J. Wolfs, and T. A. Salet, "3D printing concrete with reinforcement," in *High Tech Concrete: Where Technology and Engineering Meet: Proceedings of the 2017 fib Symposium, held in Maastricht, The Netherlands, June 12-14, 2017*, 2018: Springer, pp. 2484-2493.
- [167] G. Ma, N. M. Salman, L. Wang, and F. Wang, "A novel additive mortar leveraging internal curing for enhancing interlayer bonding of cementitious composite for 3D printing," *Construction and Building Materials*, vol. 244, p. 118305, 2020.
- [168] D. Asprone, F. Auricchio, C. Menna, and V. Mercuri, "3D printing of reinforced concrete elements: Technology and design approach," *Construction and building materials*, vol. 165, pp. 218-231, 2018.
- [169] E. Hosseini, M. Zakertabrizi, A. H. Korayem, and G. Xu, "A novel method to enhance the interlayer bonding of 3D printing concrete: An experimental and computational investigation," *Cement and Concrete Composites*, vol. 99, pp. 112-119, 2019.
- [170] B. Zareiyan and B. Khoshnevis, "Effects of interlocking on interlayer adhesion and strength of structures in 3D printing of concrete," *Automation in Construction*, vol. 83, pp. 212-221, 2017/11// 2017, doi: 10.1016/j.autcon.2017.08.019.
- [171] S. Al-Qutaifi, A. Nazari, and A. Bagheri, "Mechanical properties of layered geopolymer structures applicable in concrete 3D-printing," *Construction and Building Materials*, vol. 176, pp. 690-699, 2018.
- [172] H. Liu *et al.*, "Hardened properties of 3D printed concrete with recycled coarse aggregate," *Cement and Concrete Research*, vol. 159, p. 106868, 2022.
- [173] T. Ding, J. Xiao, S. Zou, and X. Zhou, "Anisotropic behavior in bending of 3D printed concrete reinforced with fibers," *Composite Structures*, vol. 254, p. 112808, 2020.
- [174] C. Liu *et al.*, "Anisotropic mechanical properties of extrusion-based 3D printed layered concrete," *Journal of Materials Science*, vol. 56, no. 30, pp. 16851-16864, 2021.

- [175] D. Heras Murcia, M. Genedy, and M. M. Reda Taha, "Examining the significance of infill printing pattern on the anisotropy of 3D printed concrete," *Construction and Building Materials*, vol. 262, pp. 120559-120559, 2020/11// 2020, doi: 10.1016/J.CONBUILDMAT.2020.120559.
- [176] Y. Yang, C. Wu, Z. Liu, H. Wang, and Q. Ren, "Mechanical anisotropy of ultra-high performance fibre-reinforced concrete for 3D printing," *Cement and Concrete Composites*, vol. 125, p. 104310, 2022.
- [177] K. Zhang, W. Lin, Q. Zhang, D. Wang, and S. Luo, "Evaluation of anisotropy and statistical parameters of compressive strength for 3D printed concrete," *Construction and Building Materials*, vol. 440, p. 137417, 2024.
- [178] P. Shakor, S. Nejadi, S. Sutjipto, G. Paul, and N. Gowripalan, "Effects of deposition velocity in the presence/absence of E6-glass fibre on extrusion-based 3D printed mortar," *Additive Manufacturing*, vol. 32, p. 101069, 2020.
- [179] P. Rossi and N. Harrouche, "Mix design and mechanical behaviour of some steel-fibre-reinforced concretes used in reinforced concrete structures," *Materials and Structures*, vol. 23, pp. 256-266, 1990.
- [180] T. Uygunoğlu, "Effect of fiber type and content on bleeding of steel fiber reinforced concrete," *Construction and Building Materials*, vol. 25, no. 2, pp. 766-772, 2011.
- [181] D. Falliano, D. De Domenico, G. Ricciardi, and E. Gugliandolo, "Compressive and flexural strength of fiber-reinforced foamed concrete: Effect of fiber content, curing conditions and dry density," *Construction and building materials*, vol. 198, pp. 479-493, 2019.
- [182] G. Fischer and V. C. Li, "Effect of fiber reinforcement on the response of structural members," *Engineering Fracture Mechanics*, vol. 74, no. 1-2, pp. 258-272, 2007.
- [183] A. T. Abdelrazik and K. H. Khayat, "Effect of fiber characteristics on fresh properties of fiber-reinforced concrete with adapted rheology," *Construction and Building Materials*, vol. 230, p. 116852, 2020.
- [184] G. Ma, J. Zhang, L. Wang, Z. Li, and J. Sun, "Mechanical characterization of 3D printed anisotropic cementitious material by the electromechanical transducer," *Smart Materials and Structures*, vol. 27, no. 7, p. 075036, 2018.
- [185] G. Ma, Z. Li, L. Wang, F. Wang, and J. Sanjayan, "Mechanical anisotropy of aligned fiber reinforced composite for extrusion-based 3D printing," *Construction and Building Materials*, vol. 202, pp. 770-783, 2019.
- [186] B. G. Compton and J. A. Lewis, "3D-printing of lightweight cellular composites," *Advanced materials*, vol. 26, no. 34, pp. 5930-5935, 2014.
- [187] M. Hambach, H. Möller, T. Neumann, and D. Volkmer, "Portland cement paste with aligned carbon fibers exhibiting exceptionally high flexural strength (> 100 MPa)," *Cement and Concrete Research*, vol. 89, pp. 80-86, 2016.
- [188] S. Austin, P. Robins, and Y. Pan, "Tensile bond testing of concrete repairs," *Materials and structures*, vol. 28, pp. 249-259, 1995.

- [189] S. Austin, P. Robins, and Y. Pan, "Shear bond testing of concrete repairs," *Cement and concrete research*, vol. 29, no. 7, pp. 1067-1076, 1999.
- [190] E. N. Julio, F. A. Branco, and V. t. D. Silva, "Concrete-to-concrete bond strength. Influence of the roughness of the substrate surface," *Construction and building materials*, vol. 18, no. 9, pp. 675-681, 2004.
- [191] M.-G. Lee, Y.-C. Wang, and C.-T. Chiu, "A preliminary study of reactive powder concrete as a new repair material," *Construction and building materials*, vol. 21, no. 1, pp. 182-189, 2007.
- [192] E. K. Tschegg, M. Ingruber, C. H. Surberg, and F. Munger, "Factors influencing fracture behavior of old-new concrete bonds," *Materials Journal*, vol. 97, no. 4, pp. 447-453, 2000.
- [193] S. Austin and P. Robins, "Development of patch test to study behaviour of shallow concrete patch repairs," *Magazine of Concrete Research*, vol. 45, no. 164, pp. 221-229, 1993.
- [194] A. Momayez, M. Ehsani, A. Ramezani-pour, and H. Rajaie, "Comparison of methods for evaluating bond strength between concrete substrate and repair materials," *Cement and concrete research*, vol. 35, no. 4, pp. 748-757, 2005.
- [195] A. D. Espeche and J. León, "Estimation of bond strength envelopes for old-to-new concrete interfaces based on a cylinder splitting test," *Construction and building materials*, vol. 25, no. 3, pp. 1222-1235, 2011.
- [196] H. Beushausen and M. G. Alexander, "Bond strength development between concretes of different ages," *Magazine of concrete research*, vol. 60, no. 1, pp. 65-74, 2008.
- [197] T. Lan, S. Yang, M. Wang, M. Xu, S. Cheng, and Z. Chen, "Prediction of interfacial tensile bond strength in 3D printed concrete based on a closed-form fracture model," *Journal of Building Engineering*, vol. 70, p. 106411, 2023/07/01/ 2023, doi: <https://doi.org/10.1016/j.jobe.2023.106411>.
- [198] G. M. Moelich, J. Kruger, and R. Combrinck, "Modelling the interlayer bond strength of 3D printed concrete with surface moisture," *Cement and Concrete Research*, vol. 150, p. 106559, 2021.
- [199] T. Wangler *et al.*, "Digital Concrete: Opportunities and Challenges," *RILEM Technical Letters*, vol. 1, pp. 67-67, 2016/10// 2016, doi: 10.21809/rilemtechlett.2016.16.
- [200] J. Van Der Putten, G. De Schutter, and K. Van Tittelboom, "The effect of print parameters on the (micro)structure of 3D printed cementitious materials," in *RILEM Bookseries*, vol. 19: Springer Netherlands, 2019, pp. 234-244.
- [201] V. Mechtcherine, "MICRO-AND MACROSCOPIC INVESTIGATIONS ON THE INTERFACE BETWEEN LAYERS OF 3D-PRINTED CEMENTITIOUS ELEMENTS," 2017. [Online]. Available: <https://www.researchgate.net/publication/319504633>
- [202] A. c. institute. "Shrinkage-Compensating Concrete." [https://www.concrete.org/store/productdetail.aspx?ItemID=22321&Format=PROTECTED\\_PDF&Language=English&Units=US\\_AND\\_METRIC&gad\\_source=1&gclid=Cj0KCQjwGL-3BhDnARIsAL6KZ690SZwVDjhEu8Wxh8Hq7JIHcKXVMcyX0obvc40Q3XSY-7kHGHswZcaAr4WEALw\\_wcB](https://www.concrete.org/store/productdetail.aspx?ItemID=22321&Format=PROTECTED_PDF&Language=English&Units=US_AND_METRIC&gad_source=1&gclid=Cj0KCQjwGL-3BhDnARIsAL6KZ690SZwVDjhEu8Wxh8Hq7JIHcKXVMcyX0obvc40Q3XSY-7kHGHswZcaAr4WEALw_wcB) (accessed).

- [203] G. S. Slavcheva, "Drying and shrinkage of cement paste for 3D printable concrete," *IOP Conference Series: Materials Science and Engineering*, vol. 481, no. 1, p. 012043, 2019/02/01 2019, doi: 10.1088/1757-899X/481/1/012043.
- [204] S. Markin, R. Combrinck, and V. Mechtcherine, "Specifics of plastic shrinkage in 3D-printed concrete elements," *Cement and Concrete Research*, vol. 184, p. 107512, 2024/10/01/ 2024, doi: <https://doi.org/10.1016/j.cemconres.2024.107512>.
- [205] M. Nodehi, F. Aguayo, S. E. Nodehi, A. Gholampour, T. Ozbakkaloglu, and O. Gencel, "Durability properties of 3D printed concrete (3DPC)," *Automation in Construction*, vol. 142, pp. 104479-104479, 2022/10// 2022, doi: 10.1016/J.AUTCON.2022.104479.
- [206] A. V. Rahul, M. K. Mohan, G. De Schutter, and K. Van Tittelboom, "3D printable concrete with natural and recycled coarse aggregates: Rheological, mechanical and shrinkage behaviour," *Cement and Concrete Composites*, vol. 125, p. 104311, 2022/01/01/ 2022, doi: <https://doi.org/10.1016/j.cemconcomp.2021.104311>.
- [207] K. Federowicz, M. Kaszyńska, A. Zieliński, and M. Hoffmann, "Effect of Curing Methods on Shrinkage Development in 3D-Printed Concrete," *Materials*, vol. 13, no. 11, p. 2590, 2020.
- [208] G. Markovski, M. ÄteÄtez, C. University, D. e. BijediÄž, i. Mostar, and M. Å ahinagiÄž- IsoviÄž, "Shrinkage strain of concrete-causes and types Deformacije skupljanja betona-uzroci i vrste," 666.97.03.001.8.
- [209] N. Gaudillière *et al.*, "Chapter 3 - Building Applications Using Lost Formworks Obtained Through Large-Scale Additive Manufacturing of Ultra-High-Performance Concrete," in *3D Concrete Printing Technology*, J. G. Sanjayan, A. Nazari, and B. Nematollahi Eds.: Butterworth-Heinemann, 2019, pp. 37-58.
- [210] G. De Schutter, K. Lesage, V. Mechtcherine, V. N. Nerella, G. Habert, and I. Agusti-Juan, "Vision of 3D printing with concrete — Technical, economic and environmental potentials," *Cement and Concrete Research*, vol. 112, pp. 25-36, 2018/10/01/ 2018, doi: <https://doi.org/10.1016/j.cemconres.2018.06.001>.
- [211] J. H. Lim, B. Panda, and Q. C. Pham, "Improving flexural characteristics of 3D printed geopolymer composites with in-process steel cable reinforcement," *Construction and Building Materials*, vol. 178, pp. 32-41, 2018/7// 2018, doi: 10.1016/j.conbuildmat.2018.05.010.
- [212] M. J. Bassan de Moraes, E. Y. Nagata, A. J. Felício Peres Duran, and J. A. Rossignolo, "Alkali activated materials applied in 3D printing construction: A review," *Heliyon*, vol. 10, no. 5, p. e26696, 2024/03/15/ 2024, doi: <https://doi.org/10.1016/j.heliyon.2024.e26696>.
- [213] B. Panda, Y. W. D. Tay, S. C. Paul, and M. J. Tan, "Current challenges and future potential of 3D concrete printing: Aktuelle Herausforderungen und Zukunftspotenziale des 3D-Druckens bei Beton," *Materialwissenschaft und Werkstofftechnik*, vol. 49, no. 5, pp. 666-673, 2018.
- [214] Y. Chen *et al.*, "Effect of printing parameters on interlayer bond strength of 3D printed limestone-calcined clay-based cementitious materials: An experimental and numerical study," *Construction and Building Materials*, vol. 262, p. 120094, 2020.
- [215] Y. Chen, S. He, Y. Gan, O. Çopuroğlu, F. Veer, and E. Schlangen, "A review of printing strategies, sustainable cementitious materials and characterization methods in the context

- of extrusion-based 3D concrete printing," *Journal of Building Engineering*, vol. 45, p. 103599, 2022.
- [216] Y. W. D. Tay, M. Y. Li, and M. J. Tan, "Effect of printing parameters in 3D concrete printing: Printing region and support structures," *Journal of Materials Processing Technology*, vol. 271, pp. 261-270, 2019/09/01/ 2019, doi: <https://doi.org/10.1016/j.jmatprotec.2019.04.007>.
- [217] C.-H. Ko, "Constraints and limitations of concrete 3D printing in architecture," *Journal of Engineering, Design and Technology*, vol. 20, no. 5, pp. 1334-1348, 2022.
- [218] R. B. A. S. SALEH, "Exploration of the advancements and potential of 3DCP," ed.
- [219] R. Krishna *et al.*, "Design And Implementation Of A Robotic Arm Based On Haptic Technology," in "International Journal of Engineering Research and Applications (IJERA)," vol. 2. [Online]. Available: [www.ijera.com](http://www.ijera.com)
- [220] J.-Q. Xuan and S.-H. Xu, "Review on kinematics calibration technology of serial robots," *International journal of precision engineering and manufacturing*, vol. 15, pp. 1759-1774, 2014.
- [221] J. Fleischer, V. Schulze, J. Burtscher, and S. Dosch, "Robot-based guiding of extrusion profiles-increase of guiding accuracy by considering the temperature-dependent effects," *Procedia CIRP*, vol. 18, pp. 21-26, 2014.
- [222] I. Daniyan, K. Mpofu, B. Ramatsetse, and A. Adeodu, "Design and simulation of a robotic arm for manufacturing operations in the railcar industry," in *Procedia Manufacturing*, 2020, vol. 51: Elsevier B.V., pp. 67-72, doi: 10.1016/j.promfg.2020.10.011.
- [223] J. Olawale, A. Oludele, A. Ayodele, and N. M. Alejandro, "Development of a microcontroller based robotic arm," in *Proceedings of the 2007 Computer Science and IT Education Conference*, 2007, pp. 549-557.
- [224] M. Slamani, S. Gauthier, and J.-F. Chatelain, "A study of the combined effects of machining parameters on cutting force components during high speed robotic trimming of CFRPs," *Measurement*, vol. 59, pp. 268-283, 2015.
- [225] M. F. Zaeh and O. Roesch, "Improvement of the machining accuracy of milling robots," *Production Engineering*, vol. 8, pp. 737-744, 2014.
- [226] L. Wang, A. Mohammed, and M. Onori, "Remote robotic assembly guided by 3D models linking to a real robot," *CIRP annals*, vol. 63, no. 1, pp. 1-4, 2014.
- [227] C. Pupăză, G. Constantin, and Ș. NEGRILĂ, "Computer aided engineering of industrial robots," *Proceedings in Manufacturing Systems*, vol. 9, no. 2, pp. 87-92, 2014.
- [228] K. Alexopoulos, D. Mavrikios, and G. Chryssolouris, "ErgoToolkit: an ergonomic analysis tool in a virtual manufacturing environment," *International journal of computer integrated manufacturing*, vol. 26, no. 5, pp. 440-452, 2013.
- [229] P. Kah, M. Shrestha, E. Hiltunen, and J. Martikainen, "Robotic arc welding sensors and programming in industrial applications," *International Journal of Mechanical and Materials Engineering*, vol. 10, pp. 1-16, 2015.

- [230] S. Ong, J. Chong, and A. Nee, "A novel AR-based robot programming and path planning methodology," *Robotics and Computer-Integrated Manufacturing*, vol. 26, no. 3, pp. 240-249, 2010.
- [231] M. Bugday and M. Karali, "Design optimization of industrial robot arm to minimize redundant weight," *Engineering Science and Technology, an International Journal*, vol. 22, no. 1, pp. 346-352, 2019.
- [232] J. Brüning, B. Denkena, M.-A. Dittrich, and H.-S. Park, "Simulation based planning of machining processes with industrial robots," *Procedia Manufacturing*, vol. 6, pp. 17-24, 2016.
- [233] B. Denkena, B. Bergmann, and T. Lepper, "Design and optimization of a machining robot," *Procedia Manufacturing*, vol. 14, pp. 89-96, 2017.
- [234] N. Papakostas, K. Alexopoulos, and A. Kopanakis, "Integrating digital manufacturing and simulation tools in the assembly design process: A cooperating robots cell case," *CIRP Journal of Manufacturing Science and Technology*, vol. 4, no. 1, pp. 96-100, 2011/01/01/ 2011, doi: <https://doi.org/10.1016/j.cirpj.2011.06.016>.
- [235] P. Tsarouchi *et al.*, "Robotized Assembly Process Using Dual Arm Robot," *Procedia CIRP*, vol. 23, pp. 47-52, 2014/01/01/ 2014, doi: <https://doi.org/10.1016/j.procir.2014.10.078>.
- [236] S. Makris, G. Michalos, A. Eytan, and G. Chryssolouris, "Cooperating Robots for Reconfigurable Assembly Operations: Review and Challenges," *Procedia CIRP*, vol. 3, pp. 346-351, 2012/01/01/ 2012, doi: <https://doi.org/10.1016/j.procir.2012.07.060>.
- [237] G. Michalos, S. Makris, P. Tsarouchi, T. Guasch, D. Kontovrakis, and G. Chryssolouris, "Design considerations for safe human-robot collaborative workplaces," *Procedia CirP*, vol. 37, pp. 248-253, 2015.
- [238] M. K. Mohan, A. V. Rahul, G. De Schutter, and K. Van Tittelboom, "Extrusion-based concrete 3D printing from a material perspective: A state-of-the-art review," *Cement and Concrete Composites*, vol. 115, p. 103855, 2021/01/01/ 2021, doi: <https://doi.org/10.1016/j.cemconcomp.2020.103855>.
- [239] T. Marchment and J. Sanjayan, "Mesh reinforcing method for 3D Concrete Printing," *Automation in Construction*, vol. 109, p. 102992, 2020/01/01/ 2020, doi: <https://doi.org/10.1016/j.autcon.2019.102992>.
- [240] D. Lowke, E. Dini, A. Perrot, D. Weger, C. Gehlen, and B. Dillenburger, "Particle-bed 3D printing in concrete construction – Possibilities and challenges," *Cement and Concrete Research*, vol. 112, pp. 50-65, 2018/10/01/ 2018, doi: <https://doi.org/10.1016/j.cemconres.2018.05.018>.
- [241] P. Stavropoulos, P. Foteinopoulos, A. Papacharalampopoulos, and H. Bikas, "Addressing the challenges for the industrial application of additive manufacturing: Towards a hybrid solution," *International Journal of Lightweight Materials and Manufacture*, vol. 1, no. 3, pp. 157-168, 2018/9// 2018, doi: 10.1016/j.ijlmm.2018.07.002.
- [242] S. G. Bilal, J. Duarte, and S. Nazarian, "Large-Scale Additive Manufacturing of Concrete Using a 6-Axis Robotic Arm for Autonomous Habitat Construction Modeling the impact of urban features on COVID-19 spreading in US cities View project Generative and responsive

design system View project." [Online]. Available:  
<https://www.researchgate.net/publication/341451084>

- [243] J. Mueller and K. Shea, "THE EFFECT OF BUILD ORIENTATION ON THE MECHANICAL PROPERTIES IN INKJET 3D PRINTING."
- [244] A. Puzatova, P. Shakor, V. Laghi, and M. Dmitrieva, "Large-Scale 3D Printing for Construction Application by Means of Robotic Arm and Gantry 3D Printer: A Review," *Buildings*, vol. 12, no. 11, pp. 2023-2023, 2022/11// 2022, doi: 10.3390/buildings12112023.
- [245] N. Labonnote, A. Rånquist, B. Manum, and P. Rånther, "Additive construction: State-of-the-art, challenges and opportunities," in *Automation in Construction* vol. 72, ed: Elsevier B.V., 2016, pp. 347-366.
- [246] W. Wu, W. Ye, Z. Wu, P. Geng, Y. Wang, and J. Zhao, "Influence of layer thickness, raster angle, deformation temperature and recovery temperature on the shape-memory effect of 3D-printed polylactic acid samples," *Materials*, vol. 10, no. 8, 2017/8// 2017, doi: 10.3390/ma10080970.
- [247] A. W. Gebisa and H. G. Lemu, "Investigating effects of Fused-deposition modeling (FDM) processing parameters on flexural properties of ULTEM 9085 using designed experiment," *Materials*, vol. 11, no. 4, 2018/3// 2018, doi: 10.3390/ma11040500.
- [248] W. Lao, Y. W. D. Tay, D. Quirin, and M. J. Tan, "The effect of nozzle shapes on the compactness and strength of structures printed by additive manufacturing of concrete," in *Proceedings of the International Conference on Progress in Additive Manufacturing*, 2018, vol. 2018-May: Pro-AM, pp. 80-86, doi: 10.25341/D4V01X.
- [249] Y. Zhang, Z. Jiang, Y. Zhu, J. Zhang, Q. Ren, and T. Huang, "Effects of redispersible polymer powders on the structural build-up of 3D printing cement paste with and without hydroxypropyl methylcellulose," *Construction and Building Materials*, vol. 267, p. 120551, 2021/01/18/ 2021, doi: <https://doi.org/10.1016/j.conbuildmat.2020.120551>.
- [250] S. B. Singh, P. Munjal, and N. Thammishetti, "Role of water/cement ratio on strength development of cement mortar," *Journal of Building Engineering*, vol. 4, pp. 94-100, 2015/12/01/ 2015, doi: <https://doi.org/10.1016/j.jobbe.2015.09.003>.
- [251] Y. Ji, Yun, T. Kyeong, Jeong, Donghoon, and Lee, "Development of 3D Concrete Extrusion Nozzle for Producing Free-form Concrete Panels," in "Turkish Journal of Computer and Mathematics Education," 2021, vol. 12.
- [252] K. Manikandan, X. Jiang, A. A. Singh, B. Li, and H. Qin, "Effects of nozzle geometries on 3D printing of clay constructs: Quantifying contour deviation and mechanical properties," 2020, vol. 48: Elsevier B.V., pp. 678-683, doi: 10.1016/j.promfg.2020.05.160.
- [253] B. Zareiyan and B. Khoshnevis, "Effects of mixture ingredients on extrudability of concrete in Contour Crafting," *Rapid Prototyping Journal*, vol. 24, no. 4, pp. 722-730, 2018, doi: 10.1108/RPJ-01-2017-0006.
- [254] L. Yang, S. M. E. Sepasgozar, S. Shirowzhan, A. Kashani, and D. Edwards, "Nozzle criteria for enhancing extrudability, buildability and interlayer bonding in 3D printing concrete," *Automation in Construction*, vol. 146, p. 104671, 2023/02/01/ 2023, doi: <https://doi.org/10.1016/j.autcon.2022.104671>.

- [255] N. Roussel, J. Spangenberg, J. Wallevik, and R. Wolfs, "Numerical simulations of concrete processing: From standard formative casting to additive manufacturing," *Cement and Concrete Research*, vol. 135, p. 106075, 2020.
- [256] W. Lao, M. Li, T. N. Wong, M. J. Tan, and T. Tjahjowidodo, "Improving surface finish quality in extrusion-based 3D concrete printing using machine learning-based extrudate geometry control," *Virtual and Physical Prototyping*, vol. 15, no. 2, pp. 178-193, 2020.
- [257] Z. Liu, M. Li, Y. W. D. Tay, Y. Weng, T. N. Wong, and M. J. Tan, "Rotation nozzle and numerical simulation of mass distribution at corners in 3D cementitious material printing," *Additive Manufacturing*, vol. 34, p. 101190, 2020.
- [258] Z. Liu, M. Li, Y. Weng, Y. Qian, T. N. Wong, and M. J. Tan, "Modelling and parameter optimization for filament deformation in 3D cementitious material printing using support vector machine," *Composites Part B: Engineering*, vol. 193, p. 108018, 2020.
- [259] R. J. Wolfs, F. P. Bos, E. C. Van Strien, and T. A. Salet, "A real-time height measurement and feedback system for 3D concrete printing," in *High Tech Concrete: Where Technology and Engineering Meet: Proceedings of the 2017 fib Symposium, held in Maastricht, The Netherlands, June 12-14, 2017*, 2018: Springer, pp. 2474-2483.
- [260] P. Shakor, S. Nejadi, and G. Paul, "A study into the effect of different nozzles shapes and fibre-reinforcement in 3D printed mortar," *Materials*, vol. 12, no. 10, 2019, doi: 10.3390/MA12101708.
- [261] X. Li, R. Zhou, W. Yao, and X. Fan, "Flow characteristic of highly underexpanded jets from various nozzle geometries," *Applied Thermal Engineering*, vol. 125, pp. 240-253, 2017.
- [262] T. T. Le, S. A. Austin, S. Lim, R. A. Buswell, A. G. Gibb, and T. Thorpe, "Mix design and fresh properties for high-performance printing concrete," *Materials and structures*, vol. 45, pp. 1221-1232, 2012.
- [263] J. Xu, L. Ding, L. Cai, L. Zhang, H. Luo, and W. Qin, "Volume-forming 3D concrete printing using a variable-size square nozzle," *Automation in construction*, vol. 104, pp. 95-106, 2019.
- [264] G. Bai, L. Wang, G. Ma, J. Sanjayan, and M. Bai, "3D printing eco-friendly concrete containing under-utilised and waste solids as aggregates," *Cement and Concrete Composites*, vol. 120, p. 104037, 2021.
- [265] R. Comminal, W. R. L. da Silva, T. J. Andersen, H. Stang, and J. Spangenberg, "Modelling of 3D concrete printing based on computational fluid dynamics," *Cement and Concrete Research*, vol. 138, p. 106256, 2020.
- [266] S. Muthukrishnan, S. Ramakrishnan, and J. Sanjayan, "Effect of microwave heating on interlayer bonding and buildability of geopolymers 3D concrete printing," *Construction and building materials*, vol. 265, p. 120786, 2020.
- [267] P. Bridge, "What is deionized water," ed, 2019.
- [268] MitsubishiElectric. "Vertical Type Robot." <https://www.mitsubishielectric.com/fa/products/rbt/robot/pmerit/vertical/index.html> (accessed 25/05, 2023).

- [269] M. Calì, "Stress Concentration Factors in loaded strips and bars," 2020.
- [270] Soroto. "Forced action mixers." <https://www.soroto.com/products/forced-action-mixers> (accessed).
- [271] MarkhamSheffield. "About Us." <https://www.markham-sheffield.co.uk/about/> (accessed 08/12/2023, 2023).
- [272] Tapflo. "Progressive Cavity Pump Guide." Tapflo (tapflopumps.co.uk) (accessed 08/12/2023, 2023).
- [273] Festo. "Pinch valves VZQA." [https://media.festo.com/media/203938\\_documentation.pdf](https://media.festo.com/media/203938_documentation.pdf) (accessed).
- [274] F. c. LTD. <https://www.fluidcontrols.co.uk/how-solenoid-valves-work/> (accessed 2024).
- [275] A. Das, Y. Song, S. Mantellato, T. Wangler, D. A. Lange, and R. J. Flatt, "Effect of processing on the air void system of 3D printed concrete," *Cement and Concrete Research*, vol. 156, p. 106789, 2022/06/01/ 2022, doi: <https://doi.org/10.1016/j.cemconres.2022.106789>.
- [276] N. Roussel and P. Coussot, "'Fifty-cent rheometer' for yield stress measurements: From slump to spreading flow," *Journal of Rheology*, vol. 49, no. 3, pp. 705-718, 2005, doi: 10.1122/1.1879041.
- [277] A. R. Krishnaraja and K. V. Guru, "3D Printing Concrete: A Review," *IOP Conference Series: Materials Science and Engineering*, vol. 1055, no. 1, pp. 012033-012033, 2021/2// 2021, doi: 10.1088/1757-899x/1055/1/012033.
- [278] S. Seyedreza Zaribaf Juan Murcia Delso Aratz GarcÃ-a Llona, "Analysis of interlayer bond in 3D printed concrete Ingeniería Estructural i de la ConstrucciÃ³n."
- [279] M. Papachristoforou, V. Mitsopoulos, and M. Stefanidou, "Evaluation of workability parameters in 3D printing concrete," *Procedia Structural Integrity*, vol. 10, pp. 155-162, 2018/01/01/ 2018, doi: <https://doi.org/10.1016/j.prostr.2018.09.023>.
- [280] O. Disu, S. Ismail, L. Wood, A. Chrysanthou, and A. Kanellopoulos, "Design and development of a small-scale cement-based 3D printing robot extrusion nozzle," *MATEC Web of Conferences*, vol. 401, 08/27 2024, doi: 10.1051/mateconf/202440102014.
- [281] V. Mechtcherine *et al.*, "Extrusion-based additive manufacturing with cement-based materials – Production steps, processes, and their underlying physics: A review," *Cement and Concrete Research*, vol. 132, p. 106037, 2020/06/01/ 2020, doi: <https://doi.org/10.1016/j.cemconres.2020.106037>.
- [282] L. Shao *et al.*, "A new strategy to enhance 3D printability of cement-based materials: In-situ polymerization," *Additive Manufacturing*, vol. 89, p. 104299, 2024/06/05/ 2024, doi: <https://doi.org/10.1016/j.addma.2024.104299>.
- [283] C. D. Lawrence, "Sulphate attack on concrete," *Magazine of concrete Research*, vol. 42, no. 153, pp. 249-264, 1990.

- [284] J. Forero, J. de Brito, L. Evangelista, and C. H. Pereira, "Mechanical and fracture properties of concrete with recycled concrete aggregates treated with acids and addition of aluminium sulphate," *Construction and Building Materials*, vol. 447, p. 137947, 2024.
- [285] L. G. Briendl *et al.*, "Early hydration of cementitious systems accelerated by aluminium sulphate: Effect of fine limestone," *Cement and Concrete Research*, vol. 134, p. 106069, 2020.
- [286] A. S. J. Suiker, R. J. M. Wolfs, S. M. Lucas, and T. A. M. Salet, "Elastic buckling and plastic collapse during 3D concrete printing," *Cement and Concrete Research*, vol. 135, p. 106016, 2020/09/01/ 2020, doi: <https://doi.org/10.1016/j.cemconres.2020.106016>.
- [287] G. M. Moelich, J. Kruger, and R. Combrinck, "Plastic shrinkage cracking in 3D printed concrete," *Composites Part B: Engineering*, vol. 200, p. 108313, 2020.
- [288] J. Liu, S. Li, C. Gunasekara, K. Fox, and P. Tran, "3D-printed concrete with recycled glass: Effect of glass gradation on flexural strength and microstructure," *Construction and Building Materials*, vol. 314, 2022/1// 2022, doi: 10.1016/j.conbuildmat.2021.125561.
- [289] M. T. Souza, I. M. Ferreira, E. n. Guzi de Moraes, L. Senff, and A. P. Novaes de Oliveira, "3D printed concrete for large-scale buildings: An overview of rheology, printing parameters, chemical admixtures, reinforcements, and economic and environmental prospects," in *Journal of Building Engineering* vol. 32, ed: Elsevier Ltd, 2020.
- [290] J. G. da Silveira Júnior *et al.*, "Influence of Time Gap on the Buildability of Cement Mixtures Designed for 3D Printing," *Buildings*, vol. 14, no. 4, p. 1070, 2024.
- [291] K. p. Mehta and M. Paulo J. M, *Concrete microstructure, properties and materials* United States: McGraw-Hill, 2006.
- [292] S. M. V. Anand and S. K. Agarwala, *Concrete Technology: Theory and Practice*. India, 2023.

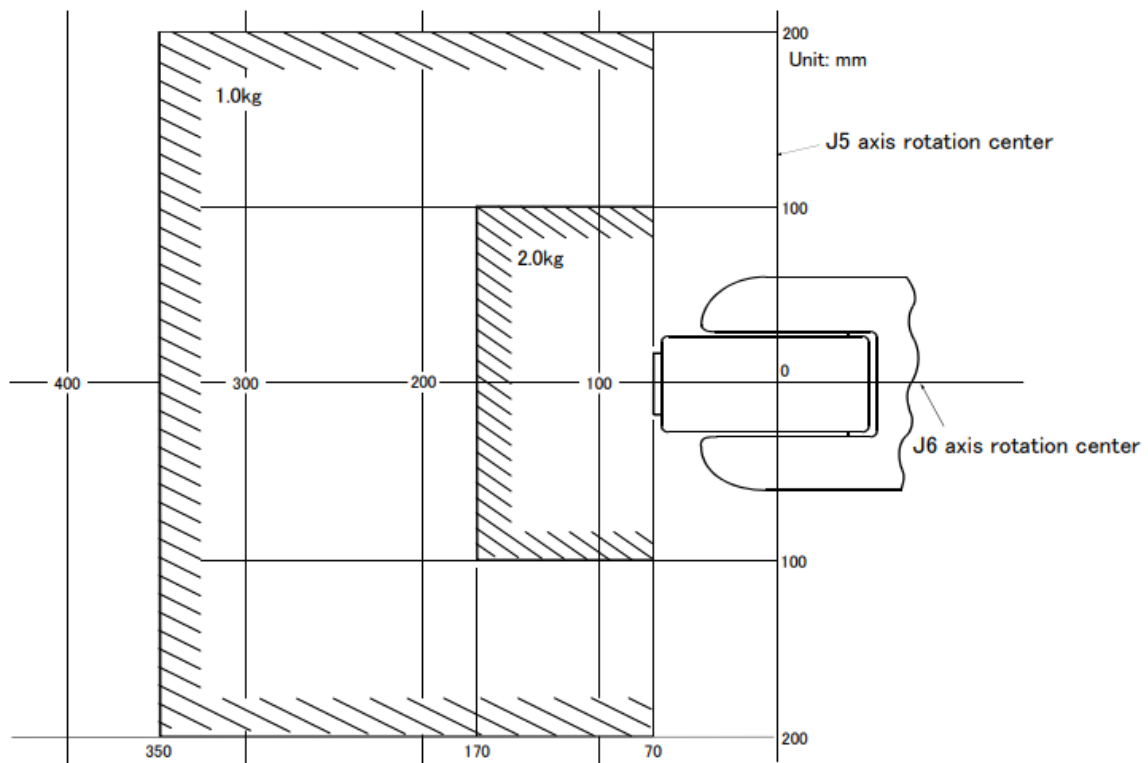
# APPENDICES

## APPENDICES A

### A1. Robot mass capacity

The mass capacity of the robot was expressed solely in terms of mass. When selecting a robot or designing tooling, it was important to note that the eccentric load would have had some restrictions for tooling or works of similar mass. The following issues were considered when selecting a robot or designing the tooling [268]:

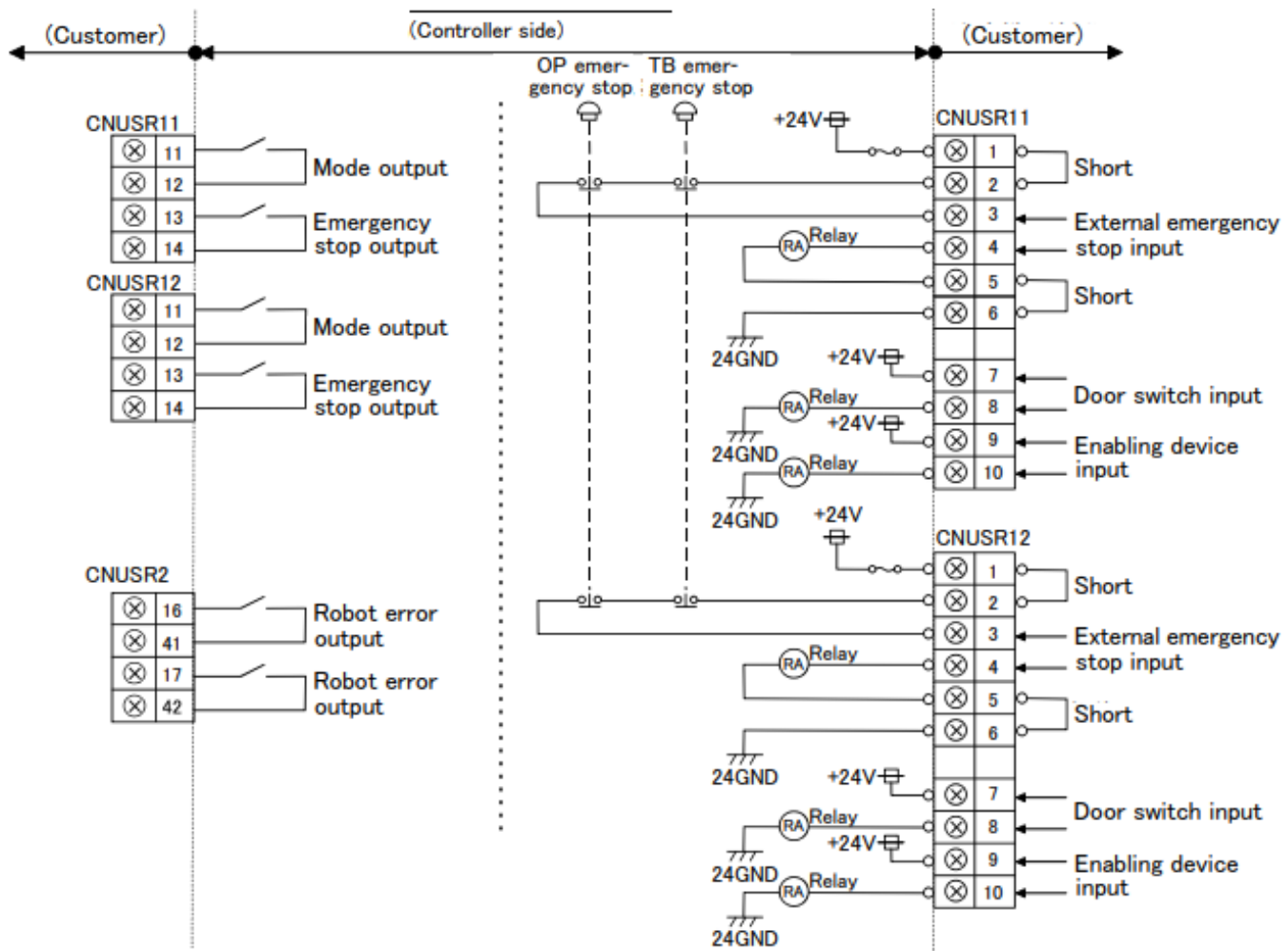
1. Figure A.1 was used as a reference when designing the tooling because it showed an accurate distribution dimension of the centroid in the case of a relatively small volume.
2. When selecting tooling, it was ideal that the values be less than or equal to the smaller of the tolerable moment or tolerable inertia.
3. The tool was designed so that the moment did not exceed the allowable moment, even if the load was a force rather than a mass.



A 1. Position of center of gravity for loads [268]

## A2. Technical instruction for wiring the external emergency stop connection

Figure A.2 shows the technical wiring procedure for the emergency stop and the security door switches (micro switches).



A 2. Internal circuit structure [268]

### A3. Cost analysis of materials

The following materials presented in Table A3.1 were purchased for the manufacturing of security enclosure.

#### A3. 1. Cost analysis of materials used to manufacture the robot security enclosure

S.N	Item	company	Quantity	Rate (£)	Total amount (£)
1	Polycarbonate sheets	ThePlasticShop	4	199.18	796.72
2	Aluminium angle	RS Component	4	58.42	233.70
	Stainless steel hinge	Rs Component	6	13.07	78.42
3	Marine plywood	Travis Perkins	2	87.66	175.32
4	Micro switch	RS Component	2	29.42	58.54
5	Emergency button	RS Component	1	42	42
6	Electrical wires	RS Component	Nil	Approx. 10	10
7	Pinch valve	RS Component	1	85	85
8	Solenoid valve	RS Component	1	40	40
9	Pressure gauge	RS Component	1	20	20
	<b>Total</b>	-	-	-	<b>1539.7</b>
<b>The following spare parts were provided by the University of Hertfordshire</b>					
10	Red steel table	-	-	-	-
11	Aluminium for gantry system	-	-	-	-

## **APPENDIX B**

### **B1. Mitsubishi electric certifications**

The follows certificates shown in Figures B1 and B2 were achieved after attending a Mitsubishi electric robot programming and maintenance course, sponsored by the university of Hertfordshire.



This is to certify that

**Oluwatimilehin Abdulwahab Disu**  
of

**University of Hertfordshire**

Has attended the  
Mitsubishi Automation Systems Training Course for

**Robot Programming**

Completion Date: 21/09/2022

Course Tutor: **Muhammad Khan**



Note:

By attending the above training course, you have started to build the skill set and knowledge base required to take a Mitsubishi Certified Engineers Exam in the above subject.



ASD ITD 080 03 F

B 1. Mitsubishi electric training on robot programming



This is to certify that

Oluwatimilehin Abdulwahab Disu  
of

**University of Hertfordshire**

Has attended the  
Mitsubishi Automation Systems Training Course for

**Robot Servicing**

Completion Date: 22/09/2022

Course Tutor: Steve Case



Note:  
By attending the above training course, you have started to build the skill set and knowledge base required to take a Mitsubishi Certified Engineers Exam in the above subject.



ASD ITD 080 03 F

B 2. Mitsubishi electric training on robot maintenance

# APPENDIX C

## Standard Operating Procedure

### Robot System

#### C1. Safe Start Procedure

1. Adhere to procedures or systems in place for risk assessment, COSHH, personal protective equipment (PPE) and other relevant safety regulations.
2. Check that all the teach pendant/computer equipment is correctly connected, and is in a safe and usable working condition (such as cable undamaged, safely routed and tested)
3. Place yourself in a location safely outside the robot arm's operating zone.
4. Ensure all of the emergency stop buttons are in the run position (not pressed).
5. Turn on the robot control unit and the computer. Once the controller has booted, the green light on the indicator beacon should be lit to indicate arm power is on and there are no errors. If there are no errors proceed to step number 7
6. If the robot reports an error at startup (red light flashing on indicator beacon and audible alarm, make sure all of the emergency stop buttons are in the run position (not pressed) and press RESET on the front of the robot controller. If there is still an error, call a technician in room JHE205 (ext. 24628).
7. Launch the RT ToolBox 3 software on the PC and connect robot.
8. Open the robot program you want to run and produce industrial robot control programs, in the appropriate formats, containing all the relevant and necessary data for the engineering activity to be carried out. Ensure that the correct process input/output and control data to produce the program is obtained and checked for currency and validity. FAILURE TO DO SO COULD RESULT IN PERSONAL INJURY OR DAMAGE OF THE ROBOT.
9. Determine an operational sequence that avoids wasted robot arm movements and tool/accessory changes and make sure that codes and other references used in the programs are applicable to the type of controller used.

10. Run the program by making sure the software is in an online mode before pressing the START button. Keep your hand on the emergency stop button until the robot has successfully completed one program cycle and be prepared to quickly stop the robot if it looks like it will collide with any object.

## C2. Safe Working Procedure

1. Adhere to procedures or systems in place for risk assessment, COSHH, personal protective equipment (PPE) and other relevant safety regulations.
2. The operator should only access the robot arm's working space when the robot controller is turned off.
3. When operating the robot arm always have an emergency stop button close at hand in case the robot needs to be immediately stopped. This can be the emergency stop button on the teach pendant, the emergency stop button on the front of the control unit, or the emergency stop button located at the front of the enclosure.
4. Run a dry test of the robot program to ensure its accuracy before passing materials through.
5. Ensure that the robot enclosure is closed during operation to prevent cement splashes.

## C3. Safe Stopping Procedure

1. To stop the robot in an emergency, push one of the emergency stop buttons located on the teach pendant, the front of the control unit or the front of the enclosure.
2. For a controlled shut down of the robot, allow the program to finish normally or push the STOP button on the front of the controller to stop the program execution. Then turn off the robot using switch located on the front of the controller and shut down the computer.

## C4. Accident / injury response

Report all minor cuts and bruises to the Technical Staff.

### In the Case of Critical Injuries

1. Shutdown equipment and secure the area to prevent further injury.
2. Immediately arrange for medical and emergency assistance.

3. Apply first aid as required.

## C5. Equipment Malfunction

In the event of an equipment malfunction, (unexpected motion, non-resettable robot errors, abnormal sounds, etc.) shut the robot off using the switch on the front of the controller and immediately contact the Technical Staff

## **APPENDIX C2**

### **Standard Operating Procedure**

#### **3D Printed Cement Robotic Arm Rig**

A minimum of two people are required for any time this rig is to be used, more are highly recommended due to the risks, labor and clean up required over a long period of hours, which can be reduced with more help. Only authorized people are allowed to work the rig itself and helpers for cleaning are only brought in once the machine has completed running. Due to the nature of cement the cleaning must happen immediately after testing to prevent it hardening and damaging equipment.

#### **C2.1 Initial steps**

Checks for cement pump, robotic arm & it's enclosure. These are necessary to be completed before any cement mixing is undertaken to prevent waste of material. If any fails on the checks are found the activity must be halted until resolved and cannot be continued until relevant technicians are satisfied. They must be made by only these authorized persons:

#### **C2.2. Checklist:**

##### **C2.2.1 Cement Pump**

- Hopper is clear of all debris.
- Self-lubricating fluid is open (pointing at number 1-12), 0 is closed.
- The lubricant is not empty or out of date.
- Transformer and power cables are undamaged, dry and PAT tested.
- Positioned appropriately far from the robotic arm enclosure but close enough for pipework to not be a trip hazard.

- Pressurized tubing is connected securely.
- All hoses connected between the pump and robotic arm are fastened, secured or out of the way of risk of injuring someone.
- Check the pressure washer is working and in place for cleaning at the end of testing.

### **C2.2.2 Robotic arm**

- All pipework is clear of debris and undamaged with no cracks.
- Pipework is securely fastened to connectors.
- Electrical wires are undamaged, dry and PAT tested.
- All functionality of the robotic arm is checked, and locks are correctly aligned.
- Emergency stop buttons are operational.
- Enclosure hatch door is installed properly, lock is secure.

Once these checks are carried out and there are no fails then the cement mixing can begin. (Measurement of materials can be undertaken before the checks if deemed necessary but cannot be mixed)

## **C2.3 Standard Operating Procedure**

### **Cement Pump**

To prepare the cement pump for supplying the robotic arm is must first be filled with product for the Archimedes screw to feed the robotic arm properly, the following steps must be undertaken before printing can occur.

Mix a small amount of mixture with water to ensure pipes are filled with material, have large bin / container to collect this material. Switch the pump on in manual mode and slowly fill the hopper with the watered-down cement.

SOP:

1. Once the machine is connected, press the ON/OFF button (A), the warning light lights up.
2. Connect the product hose to the machine and place the lance, without the nozzle.
3. Do not plug the connector of the lance on the machine.
4. Open the lance.
5. Set the flowrate on 4 with the potentiometer (B)
6. Switch the (C) button to MANU (manual) to check that the machine is working properly.
7. Switch back the (C) button to the AUTO (AUTOMATIC) position.
8. Prepare a mixture of your product very diluted with water and pour it into the tank/hopper.
9. Switch back (C) to the MANU position.
10. Wait until the mixture flows regularly to the lance and make it pour into a bucket.
11. Before the tank is completely emptied of the mixture, pour some product into the tank.
12. Remove the lance.
13. Connect the hose to the T junction.
14. Control the flow with the robotic program

Once the mix is ready it is transported to the robotic arm enclosure area and can be filled into the cement pump hopper.

## Printing

The pump will now feed the two pipes that the cement pump has been connected to, the feedback pipe and the robotic arm feed pipe. This is to reduce the pressure and control the material being delivered to the robot arm for printing. The time for printing is limited to an hour after the water was first added to the cement back in the mixing part of the initial phase before the cement will start to harden and damage the equipment.

Acrylic sheets or trays can be quickly moved into the printing area for new / different print designs.

### End of print

Once the printing has finished

- Excess material within the pump is delivered to a bin.
- Once material cannot be seen in the hopper/tank and is no longer being delivered regularly the pump and robotic arm can be switched off and unplugged.
- With care separate the pipes from their connectors looking out for cement still inside that can dribble out.
- Take these pipes and the pump to the outside back of the barn for washing with the pressure washer.
- Any material inside the pipe connected to the robotic arm, which is not removable (unless being replaced), is removed by pouring small amounts of water down it from above and collected in a small bin taking care to not splash the robotic arm.
- Each hosepipe is placed on the floor outside with one end in a large bin and the other inserted with the pressure washer and filled until runs clear with water.
- The cement pump is also cleaned with the pressure washer taking care not to splash the control box at the back of the pump.
- All parts are placed safely to dry until next use.
- All bins filled with cement are taken to the cement dump and monitored what level it is at for replacing.

## **APPENDIX D**

### **Risk assessment**

Risk assessment is a very integral section of the health and safety management plan. It helped to raise awareness of risk and danger. Figure D1 to D16 shows the risk associated to this research.

School/SBU/ Department:

SPECS/Civil Engineering

Assessor Name:

Date:

ACTIVITY TITLE/DESCRIPTION:

Robot 3D printing of cementitious material

GENERAL

IDENTIFY HAZARDS	WHO COULD BE HARMED & HOW		EVALUATE THE RISK AND DECIDE ON CONTROLS		RECORD YOUR FINDINGS AND IMPLEMENT THEM	
<p><b>Hazards associated with the activity/task/Event?</b>  <i>What are the significant hazards with the potential to cause harm?</i>                      Review the activity, location &amp; people involved. Check equipment or manufacturer instructions. Check UH, Sector or HSE guidance.</p>	<p><b>Who could be harmed?</b>  <i>Who is at risk from harm:</i> Students, Staff, Visitors and/or Contractors?</p>	<p><b>How could they be harmed?</b>  <i>Types of injury:</i> Major or Minor Injuries from Lifting/Handling, Slips/Trips/Falls or Ill Health Effects.</p>	<p><b>How would you rate the level of risk?</b>                      Risk = Likelihood X Consequence:                      High   Medium   Low</p>	<p><b>What controls are currently in place and what further action is necessary to reduce the risk?</b>  <i>What is already in place to reduce the likelihood of harm and/or impact of harm occurring?</i>  <i>What further actions or additional controls are required to reduce the remaining risk?</i></p>	<p><b>Remaining Actions?</b>                      Actions by Who and by When?</p>	<p><b>Actions Completed ?</b>                      Completed (Y/N)</p>
Travelling to and from campus – (risk of transmission if in close proximity to other people.)	Staff, Student, Visitor	Possible exposure to virus.	High	<ul style="list-style-type: none"> <li>Alternative to public transport - Walking</li> <li>Minimise number of journeys</li> <li>Recommend face coverings if possible</li> <li>Hand washing immediately when onsite</li> </ul>	All people visiting the campus should try walking, use car or bike instead of public transport and minimise number of work journeys whenever possible.	Yes
Contracting or spreading coronavirus by not washing hands or not washing them adequately	Staff, Student, Visitor	Covid 19 infection	Medium	<ul style="list-style-type: none"> <li>Follow the government guidance on cleaning, hygiene and sanitiser.</li> <li>Provision of hand sanitiser where hand washing is impossible.</li> </ul>	Wash <u>you</u> hands always and only come on campus when necessary.	Yes
Risk of acquiring or transmitting infection in lab or workshop.	Staff, Student, Visitor	Ill health.	Medium	<ul style="list-style-type: none"> <li>Sink and hand sanitisers have been provided</li> <li>Scheduled lab practise (one person at a time)</li> <li>Following the government guidance on social distancing and proper hygiene.</li> <li>Use PPE when necessary</li> </ul>	Student and staff should only use labs when necessary and must follow all necessary precautions.  Works should also be scheduled in the lab to reduce contact.	Yes

Review Date:		Signed/Reviewed by Supervisor	
--------------	--	-------------------------------	--

School/SBU/ Department: SPECS/Civil Engineering

Assessor Name:

Date:

ACTIVITY TITLE/DESCRIPTION:

Robot 3D printing of cementitious material

IDENTIFY HAZARDS	WHO COULD BE HARMED & HOW		EVALUATE THE RISK AND DECIDE ON CONTROLS		RECORD YOUR FINDINGS AND IMPLEMENT THEM	
<b>Hazards associated with the activity/task/Event?</b> <i>What are the significant hazards with the potential to cause harm?</i> Review the activity, location & people involved. Check equipment or manufacturer instructions. Check UH, Sector or HSE guidance.	<b>Who could be harmed?</b> <i>Who is at risk from harm:</i> Students, Staff, Visitors and/or Contractors?	<b>How could they be harmed?</b> <i>Types of injury:</i> Major or Minor injuries from Lifting/Handling, Slips/Trips/Falls or ill Health Effects.	<b>How would you rate the level of risk?</b> Risk = Likelihood X Consequence: High   Medium   Low	<b>What controls are currently in place and what further action is necessary to reduce the risk?</b> <i>What is already in place to reduce the likelihood of harm and/or impact of harm occurring?</i> <i>What further actions or additional controls are required to reduce the remaining risk?</i>	<b>Remaining Actions?</b> Actions by Who and by When?	<b>Actions Completed?</b> Completed (Y/N)
Equipment failure	Staff, Student, Visitor	Injuries sustained by equipment failure. If catastrophic can result in death.	High	<ul style="list-style-type: none"> <li>Proper supervision has been provided.</li> <li>Any defect in appliance should be reported immediately and suitably labelled.</li> <li>Proper maintenance, safety test and servicing of electrical appliance should be carried out.</li> <li>First aid must be ready to be administered by a member of staff or the security team.</li> </ul>	All Technical staff must ensure that all equipment is checked as well as serviced at all times.  All equipment to undergo an annual thorough examination	yes
Disposal of contaminated items including PPE	Staff, Student, Visitor	Exposure to virus	High	<ul style="list-style-type: none"> <li>Dustbins are stationed visibly and properly labelled for disposal of waste such as items used for cleaning, food and PPE.</li> <li>Person hygiene of lab coat is necessary as it should be used by just one person at a time.</li> <li>Practise good hygiene when wearing and taking off lap coat and other PPE.</li> </ul>	Students and staff should ensure proper disposal of waste product to avoid contact from others.	Yes

Review Date:		Signed/Reviewed by Supervisor	
--------------	--	-------------------------------	--

School/SBU/ Department: SPECS/Civil Engineering

Assessor Name:

Date:

ACTIVITY TITLE/DESCRIPTION:

Robot 3D printing of cementitious material

Robot, Cement pump and mixer (F103)

IDENTIFY HAZARDS	WHO COULD BE HARMED & HOW		EVALUATE THE RISK AND DECIDE ON CONTROLS		RECORD YOUR FINDINGS AND IMPLEMENT THEM	
Hazards associated with the activity/task/Event? <i>What are the significant hazards with the potential to cause harm?</i> Check – Manufacturer’s Instructions. Check – UH, Sector or HSE guidance.	Who could be harmed? <i>Who is at risk from harm:</i> Students, Staff, Visitors and/or Contractors?	How could they be harmed? <i>Types of injury: Major or Minor injuries from Lifting/Handling, Slips/Trips/Falls or Ill Health Effects.</i>	What controls are currently in place/available to reduce the risk? <i>Current control measures:</i> Engineering Controls, Safe Operating Procedures, Local Rules, Training or Supervision.	What further action is necessary? <i>Actions/additional controls required to reduce the remaining risks.</i>	Remaining Actions? <i>Actions by Who and by When?</i>	Actions Completed? <i>Completed (Y/N)</i>
<b>Electric shocks (Electrocution)</b> All tools that use electricity	Staff, Student, Visitor	<ul style="list-style-type: none"> <li>Naked wire could lead to electrocution or burns caused by incorrect use of equipment or faulty equipment.</li> <li>Tangling wires could lead to trips and falls.</li> </ul>	<ul style="list-style-type: none"> <li>Proper maintenance, safety test and servicing of electrical appliance is PAT tested in accordance with University of Hertfordshire Regulation.</li> <li>Electrical cables and plugs are visible to inspect possible damage.</li> <li>Adequate trainings for all users on how to use PPE and how to use tools safely.</li> <li>Read manufacturers manual for proper installation guide.</li> </ul>	None	Risk assessment training online by user.  Staffs should ensure that the equipment is properly maintained.	yes
<b>Burning</b> Use of tools that contain heated elements	Students, Staff	Major injury could occur as a result of burns from hot tips/ hot air, swarf or filing and molten substances.	<ul style="list-style-type: none"> <li>Staff or student making use of any equipment that has the capacity to cause burns will be trained prior to the first use including the use of PPE.</li> <li>Coolants will be used where necessary to reduce heat and friction.</li> </ul>	None	Staff or student making use of the equipment will be trained prior to the first use including the use of PPE.	

Review Date:		Signed/Reviewed by Supervisor	
--------------	--	-------------------------------	--

School/SBU/ Department: SPECS/Civil Engineering

Assessor Name:

Date:

ACTIVITY TITLE/DESCRIPTION:

Robot 3D printing of cementitious material

IDENTIFY HAZARDS	WHO COULD BE HARMED & HOW		EVALUATE THE RISK AND DECIDE ON CONTROLS		RECORD YOUR FINDINGS AND IMPLEMENT THEM	
<p>Hazards associated with the activity/task/Event?</p> <p><i>What are the significant hazards with the potential to cause harm?</i></p> <p>Check – Manufacturer’s instructions. Check – UH, Sector or HSE guidance.</p>	<p>Who could be harmed?</p> <p><i>Who is at risk from harm:</i> Students, Staff, Visitors and/or Contractors?</p>	<p>How could they be harmed?</p> <p><i>Types of injury: Major or Minor injuries from Lifting/Handling, Slips/Trips/Falls or Ill Health Effects.</i></p>	<p>What controls are currently in place/available to reduce the risk?</p> <p><i>Current control measures:</i> Engineering Controls, Safe Operating Procedures, Local Rules, Training or Supervision.</p>	<p>What further action is necessary?</p> <p><i>Actions/additional controls required to reduce the remaining risks.</i></p>	<p>Remaining Actions?</p> <p>Actions by <b>Who</b> and by <b>When</b>?</p>	<p>Actions Completed?</p> <p>Completed (Y/N)</p>
			<ul style="list-style-type: none"> <li>• Proper maintenance, safety test and servicing of electrical appliance will only be carried out by a technician in accordance with the manufacturer’s guidelines.</li> <li>• All users will be made aware of the potential danger of mis-using PPE or not using tools correctly</li> </ul>			
<p><b>Contact injury</b></p>	<p>Staff, Student, Visitor</p>	<p>Component malfunctions, Unpredicted movements or programming errors can lead to serious injury.</p>	<ul style="list-style-type: none"> <li>• Robot is securely placed and fastened on a flat surface to avoid slippage.</li> <li>• Safety equipment will always be used.</li> <li>• Stay at a safe distance from the robot arm whilst in operation.</li> </ul>	<p>None</p>	<p>Staff or student making use of the equipment will be trained prior to the first use including the use of PPE.</p>	
<p><b>Fumes/dust/harmful particles</b></p> <p>Use of tools that emit fumes, dust or other harmful particles, such as 3D printers, cement pump and mixers.</p>	<p>Students, Staff, visitor</p>	<p>Inhalation could trigger Irritations, coughing, sneezing, asthma attack, hay fever, respiratory issues and many more illnesses.</p>	<ul style="list-style-type: none"> <li>• Allow of adequate ventilation when equipment is being used, with adequate extraction systems in place.</li> <li>• Staff or student making use of any equipment that has the capacity to emit fumes will be trained prior to the first use</li> </ul>	<p>None</p>	<p>Staff or student making use of the equipment will be trained prior to the first use including the use of PPE.</p>	

Review Date:

Signed/Reviewed by Supervisor

D 4. Risk assessment 4 of 16

School/SBU/ Department: SPECS/Civil Engineering

Assessor Name:

Date:

ACTIVITY TITLE/DESCRIPTION:

Robot 3D printing of cementitious material

IDENTIFY HAZARDS	WHO COULD BE HARMED & HOW		EVALUATE THE RISK AND DECIDE ON CONTROLS		RECORD YOUR FINDINGS AND IMPLEMENT THEM	
Hazards associated with the activity/task/Event? <i>What are the significant hazards with the potential to cause harm?</i> <i>Check – Manufacturer’s Instructions.</i> <i>Check – UH, Sector or HSE guidance.</i>	Who could be harmed? <i>Who is at risk from harm:</i> <i>Students, Staff, Visitors and/or Contractors?</i>	How could they be harmed? <i>Types of injury: Major or Minor Injuries from Lifting/Handling, Slips/Trips/Falls or Ill Health Effects.</i>	What controls are currently in place/available to reduce the risk? <i>Current control measures: Engineering Controls, Safe Operating Procedures, Local Rules, Training or Supervision.</i>	What further action is necessary? <i>Actions/additional controls required to reduce the remaining risks.</i>	Remaining Actions? <i>Actions by Who and by When?</i>	Actions Completed? <i>Completed (Y/N)</i>
			including adequate training on the use of PPE.			
<b>Crushing, Trapping or Pinching</b> All tools, including hand tools, robot joints, cement pump and mixer	Student, Staff	Without proper precautions, body parts can get trapped in between robot arms and other peripheral equipment which could lead to bruising and contact from heavy machinery.	<ul style="list-style-type: none"> <li>Robots is being used by only authorised persons (Student and Staff).</li> <li>Yellow and black safety tapes are used to define “Safe Working Zones”.</li> <li>Safe code of working practise must be read and understood by robot user.</li> <li>Long hair will be tied up during operation and loose-fitting clothing will be made secure or removed if applicable.</li> <li>Safety equipment will be used at all times.</li> </ul>	None	Staff or student making use of the equipment will be trained prior to the first use including the use of PPE.	
<b>Sharp tools/blades or object</b> The robot nozzle has the tendency to be sharp. The edges of the polycarbonate edges could potentially be sharp.	Students, staff, visitors	Major injury such as laceration, punctures and abrasion could occur due to incorrect	<ul style="list-style-type: none"> <li>Users to receive adequate safety training before using the tools, which also includes the use of PPE.</li> </ul>	None	Staff or student making use of the equipment will be trained prior to the	

Review Date:

Signed/Reviewed by Supervisor

School/SBU/ Department: SPECS/Civil Engineering

Assessor Name:

Date:

ACTIVITY TITLE/DESCRIPTION:

Robot 3D printing of cementitious material

IDENTIFY HAZARDS	WHO COULD BE HARMED & HOW	EVALUATE THE RISK AND DECIDE ON CONTROLS		RECORD YOUR FINDINGS AND IMPLEMENT THEM		
<p>Hazards associated with the activity/task/Event?  <i>What are the significant hazards with the potential to cause harm?</i>                      Check – Manufacturer’s Instructions.                      Check – UH, Sector or HSE guidance.</p>	<p>Who could be harmed?  <i>Who is at risk from harm:</i>                      Students, Staff, Visitors and/or Contractors?</p>	<p>How could they be harmed?  <i>Types of injury: Major or Minor injuries from Lifting/Handling, Slips/Trips/Falls or Ill Health Effects.</i></p>	<p>What controls are currently in place/available to reduce the risk?  <i>Current control measures:</i>                      Engineering Controls, Safe Operating Procedures, Local Rules, Training or Supervision.</p>	<p>What further action is necessary?  <i>Actions/additional controls required to reduce the remaining risks.</i></p>	<p>Remaining Actions?                      Actions by Who and by When?</p>	<p>Actions Completed?                      Completed (Y/N)</p>
		use of tools or mishandling of tools.	•Only trained technical will carry out maintenance on the machinery.		first use including the use of PPE.	
<p><b>Moving Parts/entanglements/entrapment</b>                      The use of all tools that have moving parts, such as 3D printers, cement pump and mixers.</p>	Students, Staff	<ul style="list-style-type: none"> <li>•Major injuries could occur as a result of entangled hair, clothing or other materials.</li> <li>•Fingers could get bruised.</li> <li>•Skin damage could occur from burns from hot tips and molten substances</li> </ul>	<ul style="list-style-type: none"> <li>•Adequate training for user of the equipment on how to use PPE</li> <li>• All Jewry must be removed, long hairs tied, and long cloths tucked in.</li> <li>•Users are instructed not to put their hands inside the machine while they are in operation.</li> </ul>	None	Staff or student making use of the equipment will be trained prior to the first use including the use of PPE.	
<p><b>Striking/kickback</b>                      All equipment operated electrically with exposed moving components.</p>	Students, Staff	A sudden forcefully recoil known as "kickback" could occur which could throw workpieces around violently.	<ul style="list-style-type: none"> <li>•Equipment is held firmly by use of bolt and nuts.</li> <li>•All users will be trained on my to safely use equipment and how to use PPE appropriately.</li> <li>•Risk assessment training should be done to give proper understanding on what to do and what not to do when a fault/emergency occurs.</li> </ul>	Risk assessment training online by user	Staff or student making use of the equipment will be trained prior to the first use including the use of PPE.	Yes

Review Date:		Signed/Reviewed by Supervisor	
--------------	--	-------------------------------	--

School/SBU/ Department: SPECS/Civil Engineering

Assessor Name:

Date:

ACTIVITY TITLE/DESCRIPTION:

Robot 3D printing of cementitious material

IDENTIFY HAZARDS	WHO COULD BE HARMED & HOW	EVALUATE THE RISK AND DECIDE ON CONTROLS		RECORD YOUR FINDINGS AND IMPLEMENT THEM		
<p>Hazards associated with the activity/task/Event?  <i>What are the significant hazards with the potential to cause harm?</i>                      Check – Manufacturer’s instructions.                      Check – UH, Sector or HSE guidance.</p>	<p>Who could be harmed?  <i>Who is at risk from harm:</i>                      Students, Staff, Visitors and/or Contractors?</p>	<p>How could they be harmed?  <i>Types of injury: Major or Minor injuries from Lifting/Handling, Slips/Trips/Falls or Ill Health Effects.</i></p>	<p>What controls are currently in place/available to reduce the risk?  <i>Current control measures:</i>                      Engineering Controls, Safe Operating Procedures, Local Rules, Training or Supervision.</p>	<p>What further action is necessary?  <i>Actions/additional controls required to reduce the remaining risks.</i></p>	<p>Remaining Actions?                      Actions by Who and by When?</p>	<p>Actions Completed?                      Completed (Y/N)</p>
			<ul style="list-style-type: none"> <li>Ensure the user is protected from moving parts by means of guards and safety devices.</li> </ul>			
<b>Improper installation</b>	Students, Staff	If the device is incorrectly setup, serious hazard may occur in the future due to variance from the original design.	<ul style="list-style-type: none"> <li>Proper understanding of device manual will be carried out prior to installation.</li> <li>Device is held securely to avoid it tripping off.</li> </ul>	<ul style="list-style-type: none"> <li>Allow visibility of electrical cables and plugs to enable rapid detection of possible damage.</li> </ul>	Staffs should ensure that the equipment is properly maintained.	
<b>Noise</b>	Staff, Students, Visitors	Temporary hearing loss or damage	<ul style="list-style-type: none"> <li>It is mandatory that all users wear PPE such as ear defenders if necessary to reduce the risk.</li> </ul>	None	Staff or student making use of the equipment will be trained prior to the first use including the use of PPE.	
<b>Damaged tools</b>	Students, Staff	Major injuries as a result of damaged tools.	<ul style="list-style-type: none"> <li>Staffs should ensure that the equipment is properly maintained.</li> <li>Damaged tools should be reported to staff immediately and well labelled to prevent use from other users.</li> </ul>	None	None	

Review Date:		Signed/Reviewed by Supervisor	
--------------	--	-------------------------------	--

School/SBU/  
Department:

SPECS/Civil Engineering

Assessor Name:

Date:

ACTIVITY TITLE/DESCRIPTION:

Robot 3D printing of cementitious material

IDENTIFY HAZARDS	WHO COULD BE HARMED & HOW		EVALUATE THE RISK AND DECIDE ON CONTROLS		RECORD YOUR FINDINGS AND IMPLEMENT THEM	
Hazards associated with the activity/task/Event? <i>What are the significant hazards with the potential to cause harm?</i> Check – Manufacturer's instructions. Check – UH, Sector or HSE guidance.	Who could be harmed? <i>Who is at risk from harm:</i> Students, Staff, Visitors and/or Contractors?	How could they be harmed? <i>Types of injury:</i> Major or Minor injuries from Lifting/Handling, Slips/Trips/Falls or Ill Health Effects.	What controls are currently in place/available to reduce the risk? <i>Current control measures:</i> Engineering Controls, Safe Operating Procedures, Local Rules, Training or Supervision.	What further action is necessary? <i>Actions/additional controls required to reduce the remaining risks.</i>	Remaining Actions? <i>Actions by Who and by When?</i>	Actions Completed? <i>Completed (Y/N)</i>
Human error/ Control error	Students, Staff	General human error occurs daily, such as over confidence or lack of technical knowledge.  Miss-handling of the robot arm which could lead to severe injury.	<ul style="list-style-type: none"> <li>Users must read and understand the operator manual.</li> <li>Proper training on programming and robot operations will be carried out.</li> <li>Safety equipment will be used at all times.</li> </ul>	None	Staff or student making use of the equipment will be trained prior to the first use including the use of PPE.	
Unauthorized access	Students, Staff, Visitor	Any unauthorized person who is unfamiliar with the safety hardware and gains access to the device could be seriously injured.	<ul style="list-style-type: none"> <li>Security measures have been put in place to prevent unauthorized access.</li> </ul>	None	Staff must ensure proper security measure is in place at all times.	
Environmental sources	Any person in the immediate area, while the robotic arm is in operation	Freezing temperature could lead to slippery surfaces and hot temperature could lead to overheating of the robotic arm which could lead to a fire outbreak.	<ul style="list-style-type: none"> <li>Ensure the device is covered when not in use to prevent dust particles and adverse effect of temperature.</li> </ul>	<ul style="list-style-type: none"> <li>Undertake an environmental awareness course. (Uhasco)</li> </ul>	Environmental awareness training by user.	yes

Review Date:		Signed/Reviewed by Supervisor	
--------------	--	-------------------------------	--

School/SBU/ Department: SPECS/Civil Engineering

Assessor Name:

Date:

ACTIVITY TITLE/DESCRIPTION:

Robot 3D printing of cementitious material

IDENTIFY HAZARDS	WHO COULD BE HARMED & HOW		EVALUATE THE RISK AND DECIDE ON CONTROLS		RECORD YOUR FINDINGS AND IMPLEMENT THEM	
<p>Hazards associated with the activity/task/Event?  <i>What are the significant hazards with the potential to cause harm?</i>                      Check – Manufacturer’s instructions.                      Check – UH, Sector or HSE guidance.</p>	<p>Who could be harmed?  <i>Who is at risk from harm:</i>                      Students, Staff, Visitors and/or Contractors?</p>	<p>How could they be harmed?  <i>Types of injury: Major or Minor Injuries from Lifting/Handling, Slips/Trips/Falls or Ill Health Effects.</i></p>	<p>What controls are currently in place/available to reduce the risk?  <i>Current control measures:</i>                      Engineering Controls, Safe Operating Procedures, Local Rules, Training or Supervision.</p>	<p>What further action is necessary?  <i>Actions/additional controls required to reduce the remaining risks.</i></p>	<p>Remaining Actions?                      Actions by Who and by When?</p>	<p>Actions Completed?                      Completed (Y/N)</p>
<p><b>Mechanical Hazard</b>                      All tools that have not been tested or fastened properly</p>	<p>Students, Staff</p>	<p>Potential hazard due to failure in mechanical parts, Injuries sustained by equipment failure. If catastrophic can result in death.</p> <p>Collision, pinch points</p>	<ul style="list-style-type: none"> <li>•Newly manufactured parts would undergo the required strength and durability test.</li> <li>•Adequate distance will be given when testing parts for the first time.</li> <li>•Press emergency switch in case of equipment failure.</li> <li>•All body parts will be kept out of path when in operation.</li> <li>•Protective gears such as lab coats and safety glasses will be put on at all times.</li> </ul>	<p>None</p>	<p>None</p>	
<p><b>Material spillage from robot, cement mixer or pump</b></p>	<p>Students, Staff</p>	<ul style="list-style-type: none"> <li>•Concrete burns to the skin can occur in the event of material spillage. Refer to COSHH assessment for details of hazards associated with cement and additives.</li> </ul>	<ul style="list-style-type: none"> <li>•Ensure the robot enclosure is closed at all times to prevent material spillage.</li> <li>•All moving parts on the concrete pump and mixer are fully guarded</li> <li>•Adequate training for user of the equipment on how to use PPE</li> </ul>	<p>Refer to COSHH assessment for details of hazards associated with cement and additives.</p>	<p>Staff or student making use of the equipment will be trained prior to the first use including the use of PPE.</p>	

Review Date:	Signed/Reviewed by Supervisor
--------------	-------------------------------

School/SBU/ Department: SPECS/Civil Engineering

Assessor Name:

Date:

ACTIVITY TITLE/DESCRIPTION:

Robot 3D printing of cementitious material

IDENTIFY HAZARDS	WHO COULD BE HARMED & HOW		EVALUATE THE RISK AND DECIDE ON CONTROLS		RECORD YOUR FINDINGS AND IMPLEMENT THEM	
<p>Hazards associated with the activity/task/Event?  <i>What are the significant hazards with the potential to cause harm?</i>                      Check – Manufacturer’s instructions.                      Check – UH, Sector or HSE guidance.</p>	<p>Who could be harmed?  <i>Who is at risk from harm:</i>                      Students, Staff, Visitors and/or Contractors?</p>	<p>How could they be harmed?  <i>Types of injury: Major or Minor injuries from Lifting/Handling, Slips/Trips/Falls or ill Health Effects.</i></p>	<p>What controls are currently in place/available to reduce the risk?  <i>Current control measures:</i>                      Engineering Controls, Safe Operating Procedures, Local Rules, Training or Supervision.</p>	<p>What further action is necessary?  <i>Actions/additional controls required to reduce the remaining risks.</i></p>	<p>Remaining Actions?                      Actions by Who and by When?</p>	<p>Actions Completed?                      Completed (Y/N)</p>
			<p>•Provision of and washing facilities on site.</p>			
<p><b>High pressure concrete and aggregate going into eyes, face or any exposed skin due to standing or working in front of end hose/robot nozzle, or opening up pipe joints when pumping</b></p>	<p>Students, Staff, Visitors</p>	<p>Skin reaction may occur due to cement splashes. If the pipe explodes. Refer to COSHH assessment for details of hazards associated with cement and additives.</p>	<p>Under no circumstances would any unauthorised personnel be allowed to open the pipeline.</p> <p>Staff or student making use of the equipment will be trained prior to the first use including the use of PPE.</p>	<p>All unnecessary personnel including the general public should be kept well away from the concreting area.</p> <p>Pipe seals to be maintained correctly.</p> <p>Concrete level in the hopper should be checked correctly</p>	<p>Staff or student making use of the equipment will be trained prior to the first use including the use of PPE.</p>	
<p><b>Potential blockages at start or restart of pump</b></p>	<p>Students, Staff</p>	<p>Skin and eye reaction may occur due to cement splashes. Refer to COSHH assessment for details of hazards associated with cement and additives.</p>	<p>Student and staffs are required to remain clear of the suspended hose at each start or restart of the pump until smooth flow has been achieved.</p>	<p>None</p>	<p>None</p>	

Review Date:		Signed/Reviewed by Supervisor	
--------------	--	-------------------------------	--

School/SBU/ Department: SPECS/Civil Engineering

Assessor Name:

Date:

ACTIVITY TITLE/DESCRIPTION:

Robot 3D printing of cementitious material

IDENTIFY HAZARDS	WHO COULD BE HARMED & HOW		EVALUATE THE RISK AND DECIDE ON CONTROLS		RECORD YOUR FINDINGS AND IMPLEMENT THEM	
<p>Hazards associated with the activity/task/Event?  <i>What are the significant hazards with the potential to cause harm?</i>                      Check – Manufacturer’s instructions.                      Check – UH, Sector or HSE guidance.</p>	<p>Who could be harmed?  <i>Who is at risk from harm:</i>                      Students, Staff, Visitors and/or Contractors?</p>	<p>How could they be harmed?  <i>Types of injury: Major or Minor injuries from Lifting/Handling, Slips/Trips/Falls or Ill Health Effects.</i></p>	<p>What controls are currently in place/available to reduce the risk?  <i>Current control measures:</i>                      Engineering Controls, Safe Operating Procedures, Local Rules, Training or Supervision.</p>	<p>What further action is necessary?  <i>Actions/additional controls required to reduce the remaining risks.</i></p>	<p>Remaining Actions?                      Actions by Who and by When?</p>	<p>Actions Completed?                      Completed (Y/N)</p>
Bursting of pipelines/hoses under pressure	Students, Staff, and visitors	Loud explosion could lead to hearing difficulty or damage  Small parts could fly around which could lead to serious bodily injury  Exposure to cementitious material that can lead to skin irritation and if gotten in the eyes could cause damage.	Only pipes, hoses, clips of sufficient safety rating shall be used.  All manufactured fittings are securely fastened using bolts and nuts.	Wear and damage shall be monitored by student, staffs and supervisors and checked during scheduled services. Excessively damaged/worn components shall be withdrawn	Staff or student making use of the equipment will be trained prior to the first use including the use of PPE.	
Forceful ejection of air/concrete from the end of the pipeline.	Students, Staff, and visitors	Small parts could fly around which could lead to serious bodily injury  Exposure to cementitious material that can lead to skin irritation and if gotten in the eyes could cause damage.	Pipe jointing seals shall be clean and in good order.  Concrete level in the pump hopper must be maintained at the required level to ensure air is not pumped into the pipe system	None	Staff or student making use of the equipment will be trained prior to the first use including the use of PPE.	

Review Date:		Signed/Reviewed by Supervisor	
--------------	--	-------------------------------	--

RISK ASSESSMENT – TASK ANALYSIS		Page 12 of 1	
School/SBU/ Department:	SPECS/Civil Engineering	Assessor Name:	
		Date:	
ACTIVITY TITLE/DESCRIPTION:		Robot 3D printing of cementitious material	

IDENTIFY HAZARDS	WHO COULD BE HARMED & HOW		EVALUATE THE RISK AND DECIDE ON CONTROLS		RECORD YOUR FINDINGS AND IMPLEMENT THEM	
<p>Hazards associated with the activity/task/Event?</p> <p><i>What are the significant hazards with the potential to cause harm?</i></p> <p><i>Check – Manufacturer’s Instructions.</i></p> <p><i>Check – UH, Sector or HSE guidance.</i></p>	<p>Who could be harmed?</p> <p><i>Who is at risk from harm:</i></p> <p>Students, Staff, Visitors and/or Contractors?</p>	<p>How could they be harmed?</p> <p><i>Types of injury: Major or Minor injuries from Lifting/Handling, Slips/Trips/Falls or Ill Health Effects.</i></p>	<p>What controls are currently in place/available to reduce the risk?</p> <p><i>Current control measures: Engineering Controls, Safe Operating Procedures, Local Rules, Training or Supervision.</i></p>	<p>What further action is necessary?</p> <p><i>Actions/additional controls required to reduce the remaining risks.</i></p>	<p>Remaining Actions?</p> <p><i>Actions by Who and by When?</i></p>	<p>Actions Completed?</p> <p><i>Completed (Y/N)</i></p>
<p><b>Pipeline cleaning with Pressurised water - pressurised release/ejection of sponge ball/ concrete/water/air</b></p>	<p>Students, Staff, and visitors</p>	<p>Eye injuries, burns, cuts, or wounds due to high water pressure</p>	<p>A separated and access restricted area has been provided for the cleaning of the material conveying pipes.</p> <p>The pressure washer lance should never be pointed at Others</p> <p>PPE required for normal use is safety goggles, waterproof clothing</p> <p>When hosing, the area is cordoned off so that pedestrians do not stray into area</p>	<p>Technical staffs should be aware that major injury from a pressure washer jet might appear minor at first and that treatment should not be delayed</p>	<p>Staff or student making use of the equipment will be trained prior to the first use including the use of PPE.</p>	
<p><b>Pump &amp; Hopper Cleaning</b></p>	<p>Students, Staff</p>	<p>Entanglement, crushing and amputation hazards in a concrete hopper and pumping machine</p>	<p>The concrete pump and mixer would be cleaned under the supervision of technical staffs</p> <p>Where cleaning involves entering the equipment the equipment should be shut down.</p>	<p>Ensure that the extruder is thoroughly cleaned; this can be done by putting the pump into reverse and spraying water down the delivery neck on the outside of the hopper.</p>	<p>Staff or student making use of the equipment will be trained prior to the first use including the use of PPE.</p>	

Review Date:		Signed/Reviewed by Supervisor	
--------------	--	-------------------------------	--

School/SBU/ Department: SPECS/Civil Engineering

Assessor Name:

Date:

ACTIVITY TITLE/DESCRIPTION:

Robot 3D printing of cementitious material

IDENTIFY HAZARDS	WHO COULD BE HARMED & HOW		EVALUATE THE RISK AND DECIDE ON CONTROLS		RECORD YOUR FINDINGS AND IMPLEMENT THEM	
Hazards associated with the activity/task/Event? <i>What are the significant hazards with the potential to cause harm?</i> Check – Manufacturer's instructions. Check – UH, Sector or HSE guidance.	Who could be harmed? <i>Who is at risk from harm:</i> Students, Staff, Visitors and/or Contractors?	How could they be harmed? <i>Types of injury: Major or Minor injuries from Lifting/Handling, Slips/Trips/Falls or Ill Health Effects.</i>	What controls are currently in place/available to reduce the risk? <i>Current control measures:</i> Engineering Controls, Safe Operating Procedures, Local Rules, Training or Supervision.	What further action is necessary? <i>Actions/additional controls required to reduce the remaining risks.</i>	Remaining Actions? <i>Actions by Who and by When?</i>	Actions Completed? <i>Completed (Y/N)</i>
			Cleaning shall only be done when there is another person in the immediate vicinity to <u>provide assistance</u> if required.			
Mixer falling over when in operation	Students, Staff	Skin reaction may occur due to cement spillage. Refer to COSHH assessment for details of hazards associated with cement and additives.  Equipment might fall on body parts which may lead so serious bodily injury.	Ensure the mixer is stable and wheels are braced	None	Staff or student making use of the equipment will be trained prior to the first use including the use of PPE.	
Misbehaviour and Misuse of Lab tools	Students, Staff, Visitors	Major injuries could occur.	•Every Lab user is mandated to ensure general workplace behaviour is maintained.	None	None	

Review Date:		Signed/Reviewed by Supervisor	
--------------	--	-------------------------------	--

School/SBU/ Department: SPECS/Civil Engineering

Assessor Name:

Date:

ACTIVITY TITLE/DESCRIPTION:

Robot 3D printing of cementitious material

IDENTIFY HAZARDS	WHO COULD BE HARMED & HOW		EVALUATE THE RISK AND DECIDE ON CONTROLS		RECORD YOUR FINDINGS AND IMPLEMENT THEM	
<p>Hazards associated with the activity/task/Event?  <i>What are the significant hazards with the potential to cause harm?</i>                      Check – Manufacturer’s instructions.                      Check – UH, Sector or HSE guidance.</p>	<p>Who could be harmed?  <i>Who is at risk from harm:</i>                      Students, Staff, Visitors and/or Contractors?</p>	<p>How could they be harmed?  <i>Types of injury: Major or Minor injuries from Lifting/Handling, Slips/Trips/Falls or Ill Health Effects.</i></p>	<p>What controls are currently in place/available to reduce the risk?  <i>Current control measures: Engineering Controls, Safe Operating Procedures, Local Rules, Training or Supervision.</i></p>	<p>What further action is necessary?  <i>Actions/additional controls required to reduce the remaining risks.</i></p>	<p>Remaining Actions?                      Actions by Who and by When?</p>	<p>Actions Completed?                      Completed (Y/N)</p>
<p><b>Slip and Trips</b>                      A heavy fall due to presence of dust or wet surfaces</p>	<p>Student, Staff, Visitor</p>	<p>Rough, wet, or dusty surfaces could lead to a heavy fall which could lead to a minor or major injury.</p> <p>Wet environment could lead to electrocution and damage to appliance.</p>	<ul style="list-style-type: none"> <li>•Work area kept clear of obstructions.</li> <li>•Proper lighting at workspace.</li> <li>•No defect to floor or surfaces.</li> <li>•Prevent Spillage and put-up caution sign immediately.</li> <li>• Staff or students should ensure that the general workshop practices are maintained.</li> </ul>	<p>None</p>	<p>Risk assessment training online by user.</p>	<p>yes</p>
<p><b>Flying Particles</b>                      Use of tools with the capacity to emit particles</p>	<p>Student, Staff, Visitor</p>	<p>Inhalation could trigger Irritations, coughing, sneezing, asthma attack, hay fever, respiratory issues and many more illnesses.</p> <p>Major damage to the eyes as a result of splinters, ejected</p>	<p>Staff or student making use of the equipment will be trained prior to the first use including the use of PPE.</p>	<p>None</p>	<p>Staff or student making use of the equipment will be trained prior to the first use including the use of PPE.</p>	

Review Date:		Signed/Reviewed by Supervisor	
--------------	--	-------------------------------	--

School/SBU/ Department: SPECS/Civil Engineering

Assessor Name:

Date:

ACTIVITY TITLE/DESCRIPTION:

Robot 3D printing of cementitious material

IDENTIFY HAZARDS	WHO COULD BE HARMED & HOW		EVALUATE THE RISK AND DECIDE ON CONTROLS		RECORD YOUR FINDINGS AND IMPLEMENT THEM	
Hazards associated with the activity/task/Event? <i>What are the significant hazards with the potential to cause harm? Check – Manufacturer's instructions. Check – UH, Sector or HSE guidance.</i>	Who could be harmed? <i>Who is at risk from harm: Students, Staff, Visitors and/or Contractors?</i>	How could they be harmed? <i>Types of injury: Major or Minor Injuries from Lifting/Handling, Slips/Trips/Falls or Ill Health Effects.</i>	What controls are currently in place/available to reduce the risk? <i>Current control measures: Engineering Controls, Safe Operating Procedures, Local Rules, Training or Supervision.</i>	What further action is necessary? <i>Actions/additional controls required to reduce the remaining risks.</i>	Remaining Actions? <i>Actions by Who and by When?</i>	Actions Completed? <i>Completed (Y/N)</i>
		materials or parts breaking off.				
<b>Fire</b> All electrically operated power tools	Students, Staff, Visitors	In the case of robot overheating, this could lead to a fire outbreak.	<ul style="list-style-type: none"> <li>Equipment is switched off when not in use.</li> <li>Presence of functional fire alarm.</li> <li>Empty cardboard boxes are kept away as they are easily flammable.</li> </ul>	All electrical equipment must pass a safety test.  Technicians must be familiar with fire routine procedures.  Pass a fire awareness course ( <a href="#">Ihasco</a> )	Fire awareness training by user.	yes
<b>Lone working</b>	Students, Staff	Student or staff is working alone, therefore they are unable to call for help when needed.	<ul style="list-style-type: none"> <li>Students and staffs are mandated to follow the required working practise to reduce the risk of getting harmed.</li> </ul>	None	None	
<b>Transmission of covid-19 from tools, equipment and use of the laboratory</b>	Students, Staff, Visitor	Ill health due to virus	<ul style="list-style-type: none"> <li>Social distancing rules would be followed, and hand sanitising stations have been provided</li> <li>Equipment/tools will be cleaned before and after use.</li> <li>Students will be allocated time slots in the lab to prevent overcrowding.</li> </ul>	Follow government and university guidance on covid 19.  Clean tools before and after usage.	Staffs should ensure that the necessary cleaning materials are provided at all times.	

Review Date:		Signed/Reviewed by Supervisor	
--------------	--	-------------------------------	--

School/SBU/ Department:	SPECS/Civil Engineering	Assessor Name:	
		Date:	

ACTIVITY TITLE/DESCRIPTION:	Robot 3D printing of cementitious material
-----------------------------	--

IDENTIFY HAZARDS	WHO COULD BE HARMED & HOW	EVALUATE THE RISK AND DECIDE ON CONTROLS		RECORD YOUR FINDINGS AND IMPLEMENT THEM		
<b>Hazards associated with the activity/task/Event?</b> <i>What are the significant hazards with the potential to cause harm?</i> Check – Manufacturer’s instructions. Check – UH, Sector or HSE guidance.	<b>Who could be harmed?</b> <i>Who is at risk from harm:</i> Students, Staff, Visitors and/or Contractors?	<b>How could they be harmed?</b> <i>Types of injury: Major or Minor injuries from Lifting/Handling, Slips/Trips/Falls or Ill Health Effects.</i>	<b>What controls are currently in place/available to reduce the risk?</b> <i>Current control measures:</i> Engineering Controls, Safe Operating Procedures, Local Rules, Training or Supervision.	<b>What further action is necessary?</b> <i>Actions/additional controls required to reduce the remaining risks.</i>	<b>Remaining Actions?</b> Actions by Who and by When?	<b>Actions Completed?</b> Completed (Y/N)
<b>Health hazard</b> A state of feeling unwell	Students, Staff	<ul style="list-style-type: none"> <li>• Major injury could occur which could lead to death from misuse of machine due to ill health.</li> </ul>	<ul style="list-style-type: none"> <li>• proper advice and mental health counselling from the student centre</li> <li>• Don't use the lab is you feel unwell.</li> </ul>	Seek medical attention if you feel unwell.	None	

D 16. Risk assessment 16 of 16